Volume 69C
Number 1
Jan.–Mar. 1965

Engineering and Instrumentation

U.S. DEPARTMENT OF COMMERCE

SECTION C

JOURNAL OF RESEARCH

NATIONAL BUREAU OF STANDARDS

Journal of Research

of the

National Bureau of Standards

C. Engineering and Instrumentation

JAN.–MAR. • 1965

VOLUME • 69C

NUMBER • 1

Editor: Martin Greenspan

Associate Editors: G. F. Montgomery, Thomas N. Flynn

Publication dates:
Feb. 15, May 15, Aug. 15, Nov. 15, 1965

JOURNAL OF RESEARCH

The National Bureau of Standards Journal of Research reports research and development in the fields of activity shown at right. Also included from time to time are survey articles on topics closely related to the Bureau's scientific and technical program.

The Journal is published in four separate sections as follows:

A. Physics and Chemistry

Contains papers of interest primarily to scientists working in these fields. Issued six times a year. Annual subscription: domestic, $4.00; foreign, $4.75. Single copy, 70¢.

B. Mathematics and Mathematical Physics

Presents studies and compilations designed mainly for the mathematician and the theoretical physicist. Issued Quarterly. Annual subscription: domestic, $2.25; foreign, $2.75. Single copy, 75¢.

C. Engineering and Instrumentation

Reports research and development results of interest chiefly to the engineer and the applied scientist. Issued Quarterly. Annual subscription: domestic, $2.25; foreign, $2.75. Single copy, 75¢.

D. Radio Science (formerly Radio Propagation)

Published in cooperation with U.S. National Committee of URSI. Presents papers in radio propagation, communications, and radio science generally. Issued monthly. Annual subscription: domestic, $9.00; foreign, $11.50. Single copy, $1.00.

The National Bureau of Standards is a principal focal point in the Federal Government for assuring maximum application of the physical and engineering sciences to the advancement of technology in industry and commerce. Its responsibilities include development and maintenance of the national standards of measurement, and the provisions of means for making measurements consistent with those standards; determination of physical constants and properties of materials; development of methods for testing materials, mechanisms, and structures, and making such tests as may be necessary, particularly for government agencies; cooperation in the establishment of standard practices for incorporation in codes and specifications; advisory service to government agencies on scientific and technical problems; invention and development of devices to serve special needs of the Government; assistance to industry, business, and consumers in the development and acceptance of commercial standards and simplified trade practice recommendations; administration of programs in cooperation with United States business groups and standards organizations for the development of international standards of practice; and maintenance of a clearinghouse for the collection and dissemination of scientific, technical, and engineering information.

Institute for Basic Standards. Electricity. Metrology. Heat. Radiation Physics. Mechanics. Applied Mathematics. Atomic Physics. Physical Chemistry. Laboratory Astrophysics.* Radio Standards Laboratory: Radio Standards Physics; Radio Standards Engineering.** Office of Standard Reference Data.

Institute for Materials Research. Analytical Chemistry. Polymers. Metallurgy. Inorganic Materials. Reactor Radiations. Cryogenics.** Office of Standard Reference Materials.

Central Radio Propagation Laboratory.** Ionosphere Research and Propagation. Troposphere and Space Communications. Radio Systems. Upper Atmosphere and Space Physics.

Institute for Applied Technology. Textiles and Apparel Technology Center. Building Research. Industrial Equipment. Information Technology. Performance Test Development. Instrumentation. Transport Systems. Office of Technical Services. Office of Weights and Measures. Office of Engineering Standards. Office of Industrial Services.

*NBS Group, Joint Institute for Laboratory Astrophysics at the University of Colorado.
**Located at Boulder, Colo.

U.S. DEPARTMENT OF COMMERCE
Luther H. Hodges, Secretary
NATIONAL BUREAU OF STANDARDS
A. V. Astin Director

Order all publications from the Superintendent of Documents
U.S. Government Printing Office, Washington, D.C., 20402.

Use of funds for printing this publication approved by the Director of the Bureau of the Budget (June 19, 1961).

JOURNAL OF RESEARCH of the National Bureau of Standards—C. Engineering and Instrumentation
Vol. 69C, No. 1, January-March 1965

Two Picnometers of Increased Convenience and Precision

Arnold Johnson*

(Received 1 June 1964)

Two picnometer designs that provide increased convenience and precision in the determination of the density of liquids are discussed. Both designs provide ready access to the capillary tubes and reservoir area, thus facilitating the removal of excess liquid and setting of the liquid level. The standard deviation of a series of calibrations with water using the earlier of these devices, the Collett picnometer, was 0.001 ml to 0.002 ml over the range 5 to 70 °C; with a Collett picnometer recently modified by the author and presently usable only above room temperature, the standard deviation was 0.0002 ml to 0.0005 ml over the range 40 to 50 °C. (The weighing procedure used to calibrate the author's picnometer differed from that used with the Collett picnometer.) These data apply to picnometers of 50 to 70 ml internal volume.

Many picnometers are inconvenient to use in that a great deal of time and care must be taken in the cleaning and drying of the surface of the overflow region after the contents have been brought to the desired temperature.[1] Two picnometers have been developed which provide ready access to the overflow region. The ease of manipulation and inherent precision of these designs when used as described in this paper have been established through a series of calibrations with air-free water.[2]

The earlier (1950) of these two designs, that of C. T. Collett, is shown in figure 1. While the reservoir of this picnometer is more readily accessible than that of most conventional picnometers, some difficulty is experienced, especially with viscous liquids, in cleaning and drying the reservoir. The Collett design was therefore modified by the author (1961), as shown in figure 2, a removable reservoir being used. With a removable reservoir the capillary tubes can easily be wiped clean (using solvents, if necessary) after the reservoir has been slipped off, and the possibility of solvents entering the capillaries is greatly reduced. The Collett picnometer has been successfully used, in normal practice, from 5 to 70 °C. The author's picnometer is limited to use above room temperature, no provision being made at present for retaining the liquid that would expand upon a temperature rise.

Borosilicate glass was used in the construction of both picnometers, careful annealing, followed by aging for several months, being necessary to insure dimensional stability. The top of the inside of the body of both picnometers was streamlined to diminish the possibility of bubbles becoming entrapped during filling. The glass at the junctions of the tubes on the inside of the reservoir of the Collett picnometer was smoothly rounded to facilitate cleaning and the top surfaces of the capillary tubes of both picnometers were ground to make the tubes equal in height.

A reservoir for the author's picnometer can be made from a rubber stopper by working a cork borer part way into the stopper (a No. 6½ rubber stopper and a 1 in. diam. borer were used in this work), turning inside-out the rubber on the outside and cutting across the cylinder of rubber exposed in the center. The holes for the capillary tubes are then cut through the remainder of the stopper, as shown in figure 2. The usual rubber stoppers work well with water and many other liquids; other flexible materials may be used with liquids that are contaminated by the usual rubber stoppers.

The manipulations of each of the picnometers, i.e., cleaning, filling, and weighing, were almost identical both for the calibration of the instrument and for its use in determining the density of a liquid.

The Collett picnometer was prepared for use by careful cleaning. The interior was blown dry with air that had been passed successively through sulfuric acid and calcium chloride. The exterior was first wiped with cheesecloth soaked in ethanol and then wiped with lens tissue. The clean picnometer was then exposed to ions created by a polonium strip to remove external electrostatic charges.

The picnometer and its cap were then suspended below one pan of a balance, a similar counterpoise picnometer of nearly equal mass and volume being suspended from the other pan. The use of a counterpoise picnometer reduces the number of measurements and simplifies calculations.[3] A metallic counterpoise weight was put on the pan holding the counterpoise picnometer, and mass standards were added to the other pan to achieve a balance.

The picnometer was filled through a funnel which was attached by a short piece of plastic tubing to the glass tube extending into the interior, the latter being necessary to prevent direct loss of liquid out the other capillary during vacuum filling. Enough liquid was added to the reservoir to cover the tubes.

With the ground glass stopper in place, the picnometer was immersed in a water bath so that the surface of the water was slightly below the top of

*Present address: David Taylor Model Basin, code 755, Washington, D.C.

[1] For example, see some of the picnometers illustrated in NBS Circ. 487 (Mar. 1950) Density of Solids and Liquids, P. Hidnert and E. L. Peffer, and reprinted in Vol. II of NBS Handbook 77, p. 659/1.

[2] The density of water was taken from NBS Circular 19, Standard Density and Volumetric Tables. The table on page 47 was used for determinations below 41 °C. In using the table on page 46 for the determinations above 41 °C, values were assumed exact to 7 decimal places.

[3] Simplification of calculations in routine density and volumetric determinations, C. T. Collett, J. Res. NBS **52**, 201 (April 1954) RP 2489.

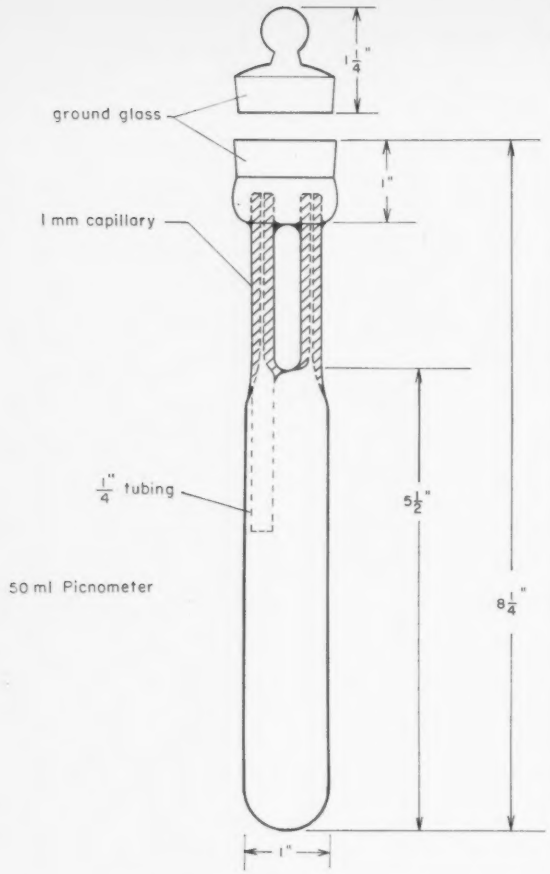

FIGURE 1. *Collett picnometer.*

the reservoir. The bath can be controlled to within ± 0.002 °C at 25 °C; the ability to control decreases gradually to about ± 0.004 °C at 70 °C.

After the picnometer and contents attained the temperature of the bath, most of the liquid in the reservoir was removed with a syringe. Small absorbent swabs were used to clean and dry the reservior and to set the liquid level even with the top of the capillary tubes. The picnometer was then removed from the bath and externally recleaned and reexposed to a polonium strip as before. It was put back on the balance and mass standards were removed from its pan until a balance was achieved. Barometric pressure, temperature, and relative humidity were recorded at the time of the final weighing to permit calculation of the air density to be used in buoyancy corrections.

During the calibration of the author's picnometer, the procedures were similar to those described except for weighing. The method of weighing using a counterpoise picnometer, although decreasing the number of measurements and simplifying the calculations, is a substitution weighing in which

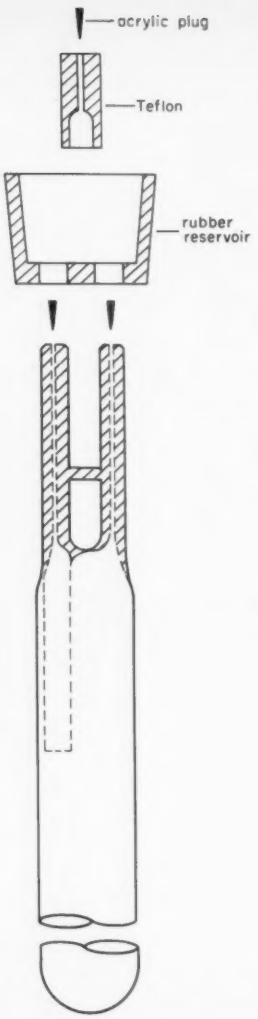

FIGURE 2. *Author's picnometer.*

several hours pass between the first and second halves of the weighing. As the rest point of a balance can change with time, this delay may lead to errors. To avoid these errors, no counterpoise picnometer was used when calibrating the author's picnometers. A substitution weighing with a minimum delay between each half of the weighing was used to determine the mass of the empty picnometer. The same procedure was followed to determine the mass of the picnometer and its contents after being filled. Buoyancy corrections were applied in both weighings.

After determining the mass of the empty picnometer, the rubber reservoir was slipped over the capillary tubes, and the picnometer was filled in the same manner as the Collett picnometer. In the temperature bath a plastic cover rested lightly on top of the reservoir. When thermal equilibrium

was reached, most of the liquid was removed from the reservoir by a syringe, the liquid level in the capillaries was set, the picnometer was quickly removed and the body of the picnometer was immersed in cool water. The liquid rapidly retreated down the capillaries, and small tapered plugs (in this work, drawn from 1/16 in. diam. rods of acrylic plastic), whose mass had been separately determined, were inserted tightly into the tubes. The rubber reservoir was carefully removed and the picnometer was cleaned, exposed to a polonium strip, and weighed as previously described.

To demonstrate that the acrylic plugs kept the evaporation loss to within the precision of the balance during the time required for the weighing, the filled picnometer was weighed three times over a period of about 2 hr during the calibration. Statistical tests indicated that during this period no detectable loss of mass occurred. Over extended periods, however, some evaporation can take place, with up to a milligram being lost overnight. (A few overnight tests of the Collett picnometer indicated a somewhat greater mass loss. However, the rate was such that during the relatively short period required for cleaning and weighing, the total loss was of no consequence.)

For a period of 10 or 15 min after each cleaning, the picnometers, empty or filled, increased in mass by about 1 mg. This increase in mass was assumed to be moisture being readsorbed onto the surface of the picnometer. Weighings of the picnometer, empty or filled, were performed at least 30 min after the picnometer had been cleaned, ionized, and suspended from the pan of the balance.

At 50 °C and above, the procedure with the author's picnometer was modified to reduce evaporation from the capillaries. While the picnometer was still in the bath, and after one tube had had its liquid level set, a Teflon cylinder (see fig. 2) with a small hole in the top was slipped over this tube, and a tapered acrylic plug loosely fitted into the hole. The other tube was similarly capped after its liquid level had been set. The picnometer was then removed from the bath and immersed in cool water, the Teflon cylinders removed, and the capillaries plugged as before.

For work with both picnometers at about 50 °C or above, it is necessary with some liquids, especially water, to inhibit the formation of bubbles. This was done by having the liquid in the picnometer at a temperature higher than that of the bath at the time of immersion. (By using this technique, one set of Collett picnometers has recently been calibrated successfully at the National Bureau of Standards to as high as 85 °C.)

Recent tests indicated that interior electrostatic charges, created by the passage of dry air, can lead to slight inaccuracies in the determination of the mass of an empty picnometer. Apparent changes of up to 1 mg occurred when using air passed through sulfuric acid and calcium chloride; when super-dry nitrogen was used the change was 2 mg or more. The use of a counterpoise picnometer during the calibration of the Collett picnometer before the importance of internal electrostatic charges was fully realized provided a possible additional source of error.

TABLE 1. *Results of the calibration of the picnometers*

Picnometer designation	Nominal capacity	Temperature or range of temperature at which calibrated	Standard deviation [a]	Degrees of freedom
		Collett		
	ml	*°C*	*ml*	
52	50	5–70	0.0016	22
53	50	5–70	.0015	22
55	50	5–70	.0010	22
56	50	5–70	.0014	22
(52, 53, 55, 56)	50	40–50	[b].0011	20
71	70	5–70	.0013	22
72	70	5–70	.0015	22
73	70	5–70	.0021	23
74	70	5–70	.0017	22
		Johnson		
S	65	40	.00024	25
151	50	40	.00023	22
151	50	45	.00045	8
151	50	50	.00030	13
151	50	40–50	[b].00031	44
152	50	40	.00016	10
153	50	40	[c].00048	10

[a] Standard deviations over temperature intervals computed from the residuals of a least squares fit of a straight line to the data.
[b] Pooled estimate of standard deviations.
[c] Tops of capillary tubes hemispherically shaped.

The experimental results in the calibration of the author's picnometer did not indicate the same weighing problem mentioned above when the picnometer was filled with water. Assuming electrostatic charges to have been on the interior surface, they were conducted away during the filling through the stream of water between the picnometer and the flask from which water was being poured.

A vacuum drying technique in which the picnometer was maintained at a pressure of about 5 mm of Hg for at least 3 hr at room temperature was tried. (Ionization of the air inside the picnometer did not seem practical with these picnometers because of the capillary entrances.) After removal from the vacuum the picnometer was weighed. Successive weighings sometimes indicated that the mass was increasing; however, successive weighings on the following day always indicated that the mass had become constant to within the precision of the balance. The gain in mass was probably due to the readsorption of vapors and gases which had been lost under vacuum; therefore, it would appear to be advisable to perform weighings of the empty picnometer, externally cleaned and exposed to a polonium strip as usual, on the day following removal from the vacuum.

Table 1 shows the standard deviations achieved in calibration at different temperatures with picnometers representing both designs.[4] The small standard deviations achieved with the author's picnometer may be the result of one or more of the following considerations: (1) the feature of a removable reservoir, (2) the different weighing procedures used (delayed substitution with Collett picnometer, immediate substitution with the author's picnometer) and, (3) the weighing problem which

[4] The standard deviations over temperature intervals were computed from the residuals of at least squares fit of a straight line to the data points. The calibrations of both picnometers were performed over a period of time which lasted from several weeks to several months.

appeared to be created by electrostatic charges inside an empty air-dried picnometer.

The Collett design has been in continuous use at the National Bureau of Standards for over 10 years in the determination of the density of submitted samples. Examples of the reproducibility obtained using Collett picnometers are listed in table 2. In general, the reproducibility is not as good for volatile liquids as for the nonvolatile, as would be expected. The author's picnometer is rather new and has yet to be tested with liquids other than water.

TABLE 2. *Results of density determinations with the Collett picnometer*

Name or description of submitted sample	Nominal temperature range	Density (to 2 decimal places) at center of temperature range	Standard deviation [a]	Degrees of freedom
	°C	g/ml	g/ml	
Rapeseed oil	10–20	0.91	0.000006	10
Octoil S [b]	20–30	.91	.000004	10
N-Oil [b]	55–65	.86	.000014	6
Manometer fluid	20–35	2.86	.000305	8
Manometer fluid	27–38	1.23	.000086	7
Chloroform	22–28	1.48	.001577	12
Toluene	16–32	0.86	.000058	10
Silicone fluid	65–75	.93	.000022	8
2-ethylhexane	15–25	.83	.000032	4
Ethanol	18–29	.81	.000024	7
Sea water	4	1.03	[c] .000046	20

[a] Standard deviations over temperature intervals computed from the residuals of a least squares fit of a straight line to the data.

[b] NBS standard viscosity sample. A description of all NBS standard materials can be found in Misc. Publ. 241, Standard Materials, available from the Superintendent of Documents, U.S. Government Printing Office, Washington, D.C., 20402.

[c] Pooled estimate of standard deviation based on 10 samples.

Two Collett picnometers have recently been recalibrated at temperatures above room temperature using tapered acrylic plugs and Teflon cylinders to reduce evaporation at 50 °C and above, and using the counterpoise picnometer method of weighing. The standard deviations obtained were comparable to those for the Collett picnometer listed in table 1.

A modification that was tried recently, and which seems promising, is the use of capillary tubes that have a ground hemispherically shaped top. With water, at least, the menisci are practically self-setting, since during the experiment no wiping of the capillary tubes was performed (see last item in table 1). Another possible modification is the use of fused quartz to decrease thermal expansion and the inclusion of a radioactive material in the quartz to eliminate electrostatic charges.

The advantages of the removable reservoir of the author's picnometer can be better evaluated through density determination of different types of liquids after the calibration has been extended over a wider temperature range. For use below room temperature, it will be necessary to provide expansion chambers, perhaps made of Teflon, that will attach to the top of each capillary tube, the reservoir then being removed by destruction. A removable reservoir will greatly reduce the problem of drying condensation when the picnometer is used below the dew point.

The author expresses his appreciation to C. T. Collett for many helpful discussions and to William Gallagher for techniques and data on the Collett picnometer.

(Paper 69C1–178)

JOURNAL OF RESEARCH of the National Bureau of Standards—C. Engineering and Instrumentation
Vol. 69C, No. 1, January–March 1965

Construction of a Michelson Interferometer for Fourier Spectroscopy

Howard N. Rundle*

(June 29, 1964)

The properties of the method employing a double beam interferometer for Fourier spectroscopy are briefly presented. A Michelson interferometer is described which is suitable for use in Fourier spectroscopy in the 1 to 10 micron region. The instrument can be used at any resolving power up to about 10^5.

1. Introduction

Michelson [1,2][1] showed the usefulness of the interferometer that bears his name. He showed that the intensity of the light measured at the output of his device is the Fourier transform of the incident optical spectra. Lord Rayleigh [3] showed how the observation of the visibility of the fringes could give the spectral profile of a symmetrical line. With the development of infrared detectors, Rubens and Wood [4] measured an "interferogram" and calculated a spectrum from this. The interferogram is the output measured from a Michelson interferometer.

Because of the availability of modern computers, this method has recently been revived [5,6, and 7]. Connes [8] has presented a detailed theory of the complete method. The following presents a brief outline of the properties of the method, and a description of an instrument with design criteria.

2. Properties of the Method

Figure 1 shows a schematic of a Michelson interferometer. Light from an extended source is collimated by lens L_1. The separating plate, S.P., has a reflectance and transmission of one-half and the reflected light from mirrors M_1 and M_2 is recombined by S.P., thereby forming circular fringes which are focused by lens L_2 at the exit aperture. This aperture isolates the central fringe and a detector then detects the resultant intensity called the interferogram, $I(\delta)$, where δ is the path difference $2(d_2-d_1)n$; and n is the index of refraction. The fringes of such a double beam interferometer are described by

$$F(\delta)=B\cos^2(\pi\sigma_0\delta)$$

$$=\frac{B}{2}[1+\cos(2\pi\sigma_0\delta)] \qquad (1)$$

where B is the intensity of the incident monochromatic radiation of wavenumber σ_0. If a spectrum $B(\sigma)$ is incident on the interferometer, instead of a monochromatic spectrum, the interferogram is given by the sum of many such fringes or

$$I(\delta)=\int_0^\infty B(\sigma)\cos(2\pi\sigma\delta)d\sigma, \qquad (2)$$

where the d-c term is dropped. That is, $I(\delta)$ is the cosine transform of the incident spectra.

The interferogram, $I(\delta)$, is measured as a function of δ and the spectrum $B(\sigma)$ is given by

$$B(\sigma)=\int_0^\infty I(\delta)\cos 2\pi\sigma\delta d\delta. \qquad (3)$$

Since it is physically possible to vary δ from 0 to only δ_M, one calculates

$$B'(\sigma)=\int_0^{\delta_M} I(\delta)\cos 2\pi\sigma\delta d\delta$$

which may be written as

$$B'(\sigma)=\int_0^\infty A(\delta)I(\delta)\cos 2\pi\sigma\delta d\delta \qquad (4)$$

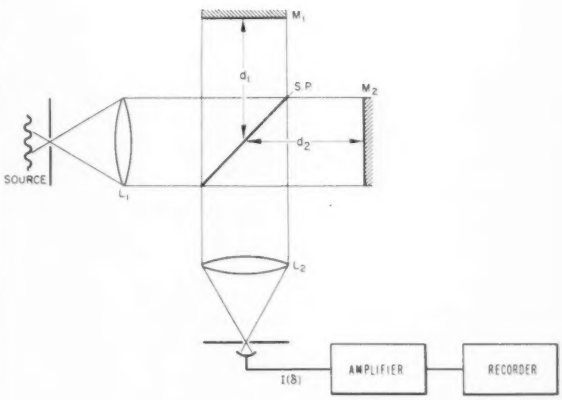

FIGURE 1. *Michelson inteferometer*

* Department of Physics, University of Saskatchewan, Saskatchewan, Canada.
[1] Figures in brackets indicate the literature references at the end of this paper.

where

$$A(\delta)=\begin{cases}\alpha(\delta), 0\leq\delta\leq\delta_M\\ 0 \text{ elsewhere.}\end{cases}$$

$\alpha(\delta)$ can be taken as unity, but it is desirable to introduce a function for apodization. $B'(\sigma)$ is an approximation to the actual incident spectrum $B(\sigma)$ and can be calculated by an analog or digital method. The analog methods are useful for low resolving power (less than 1000) and at present digital methods must be used for higher resolving powers.

In an actual interferometer, flux is measured which implies that there are off-axis rays defining an angular field of solid angle Ω. If these off-axis rays are considered [8],

$$B'(\sigma)=\frac{\Omega}{4\pi}\left[\overline{B\left(\frac{\sigma}{1-\frac{\Omega}{4\pi}}\right)}+\overline{B\left(\frac{-\sigma}{1-\frac{\Omega}{4\pi}}\right)}\right]*T_c\{A(\delta)\} \quad (5)$$

where $\bar{B}$ signifies the value obtained when B is smeared over a width of $\frac{\sigma\Omega}{2\pi}$; i.e., $\bar{B}$ is the convolution of B with a slit or rectangle of unit height and width $\frac{\sigma\Omega}{2\pi}$. "$*$" stands for the convolution product and $T_c\{A(\delta)\}$ is the cosine transform of $A(\delta)$ or

$$T_c\{A(\delta)\}=T_c[\alpha(\delta)]*\left\{\delta_M\frac{\sin 2\pi\sigma\delta_M}{2\pi\sigma\delta_M}\right\}. \quad (6)$$

As $B(\sigma)$ is smeared over a slit of width $\frac{\Omega\sigma}{2\pi}$, the resolution limit is $\Delta\sigma=\frac{\sigma\Omega}{2\pi}$; or if R_t is the theoretical resolving power,

$$\Omega R_t=2\pi. \quad (7)$$

From (6), the half width of $\frac{\sin 2\pi\delta_M\sigma}{2\pi\delta_M\sigma}$ is $\frac{1}{2\delta_M}$. Therefore, if $\alpha(\delta)=1$, an optimum condition results if the resolution limit is also given by

$$\Delta\sigma=\frac{1}{2\delta_M}. \quad (8)$$

If $\alpha(\delta)\neq 1$, but is some function chosen to reduce the feet of $\frac{\sin 2\pi\delta_M\sigma}{2\pi\delta_M\sigma}$, i.e., apodization is performed [8], then the half width of the apodized function (6) is close to $\frac{1}{\delta_M}$, *i.e.*,

$$\Delta\sigma=\frac{1}{\delta_M}. \quad (9)$$

Equations (7) and (8) or (9) determine the maximum path difference and the output aperture diameter which are to be used. It should be noted that the theoretical resolving power R_t is reduced to about $0.7R_t$ when (7) and (8) or (9) are considered.

In the above discussion, single-sided transforms have been used (i.e., integration from 0 to ∞). In this method, $I(\delta)$ is measured from 0 to δ_M, and the assumption is made that if $I(\delta)$ was measured from 0 to $-\delta_M$, the same result would be obtained. This is true only if the zero path difference occurs at the same place for all wave numbers. If this is not the case, one must know this phase shift (as it is called) and use it to find the zero path difference for each wave number. The same result can be accomplished by measuring $I(\delta)$ from $-\delta_M$ to 0 and to $+\delta_M$. Then double-sided transforms (i.e., integration from $-\infty$ to $+\infty$) are used. The same conclusions as stated in this section are obtained.

It is useful to point out some of the properties of the method. If $B'(\sigma)$ is calculated from an interferogram that is digitized at every step h of δ, one must assume that $h\leq\frac{1}{2\sigma_M}$ where the incident spectra is nonzero in the region from 0 to σ_M only.

However, when noise is present, h must be smaller yet. In fact, if an R.C. time constant τ is employed, then for the best signal to noise in $B'(\sigma)$, $h\approx\tau$ [8], where h is measured in seconds and the spectra is a function of frequency. In all the previous discussion, the path difference δ can be replaced by time t and the wave number σ can be replaced by frequency ν. When $h=\tau$, the spectral range in frequency units is from 0 to $\frac{1}{2\pi\tau}$.

A calculation of the signal-to-noise ratio obtained in the calculated spectra is complicated and the exact theory is not fully understood. However, the case when one is observing a monochromatic line only, has been presented [8]. In general, the signal-to-noise of the calculated spectra is

$$\left(\frac{S}{N}\right)_{\text{spectra}}\propto\beta\sqrt{\frac{T}{\xi}} \quad (10)$$

where T is the total time for one scan, β is the amplitude of the observed spectral element, and ξ is the noise amplitude.

In the case of a scanning instrument (i.e., spectrometer or Fabry-Perot)

$$\left(\frac{S}{N}\right)'_{\text{spectra}}\propto\beta\sqrt{\frac{T}{M\xi}} \quad (11)$$

where the time $\frac{T}{M}$ is spent measuring each of the M spectral elements. Hence, if ξ is independent of the amount of incident radiation on the detector, as is the case for present day infrared detectors, the gain in the signal-to-noise which is realized with the interferometer is $\sqrt{M}$ over that of a scanning instrument of the same light-gathering power, resolution, and detector. This gain is often referred to as "Fellgett's Advantage" since he was the first to point out this gain [5 and 6]. This is the only reason

for building such an instrument and can be a powerful reason for weak sources.

In the case where the noise from the detector is due to signal photons (as for the photomultiplier tubes in the visible) then ξ is proportional to the square root of the incident radiation and the same signal-to-noise is obtained from the interferometer and above equivalent scanning instrument. The Michelson interferometer should not be used for general applications in this region.

A comparison of the usefulness of the Michelson interferometer with other interference techniques is presented by Jacquinot [9].

3. Construction and Design of a Michelson Interferometer

3.1. General Description

It has been shown that a Michelson interferometer is useful in the infrared for obtaining optical spectra. Such an instrument has been built and will now be described. Figure 2 shows the optical and electronic layout. Several plane mirrors which only change the direction of the light beam, are omitted and focusing mirrors are shown as equivalent lenses for simplicity. The instrument was built to be used in the 3 to 4 μ region with a detector of lead sulfide or lead selenide. The maximum path difference available is about 80 cm and the aperture is 8 cm diam. The instrument was evacuated so that the index of refraction would be unity for all wavelengths. The source was imaged by spherical mirror F_1 onto the entrance aperture. Off-axis parabolic mirror F_2 collimates the light for the interferometer. The separating and compensating plates are mounted together for convenience. One arm of the interferometer has mirror M_1 and the other arm has a cube corner, C.C., and mirror M_2. The cube corner slides on machined ways and has the property that light rays enter and leave it in parallel paths regardless of the cube corner's orientation. Its motion is controlled by a hydraulic system.

Off-axis parabolic mirror F_3 focuses the fringes onto the exit aperture behind which sits the detector. The mirror F_3, the output aperture, and the detector, are at liquid nitrogen temperatures. The mirror M_3 is half-silvered and is used for introducing into the interferometer light of wavelength 5461 Å from a mercury lamp for the purpose of alinement. A high intensity mercury lamp is used for the coarse adjustments, and a monoisotopic mercury lamp excited by a microtherm unit and cooled by blowing air, is used for the fine adjustments. Mirror M_3, is slid to one side when the source is observed. An interference filter can be placed at the entrance aperture or at the exit aperture if a cold filter is desired. Radiation from the source is chopped at 640 c/s for discrimination against radiation emitted by the

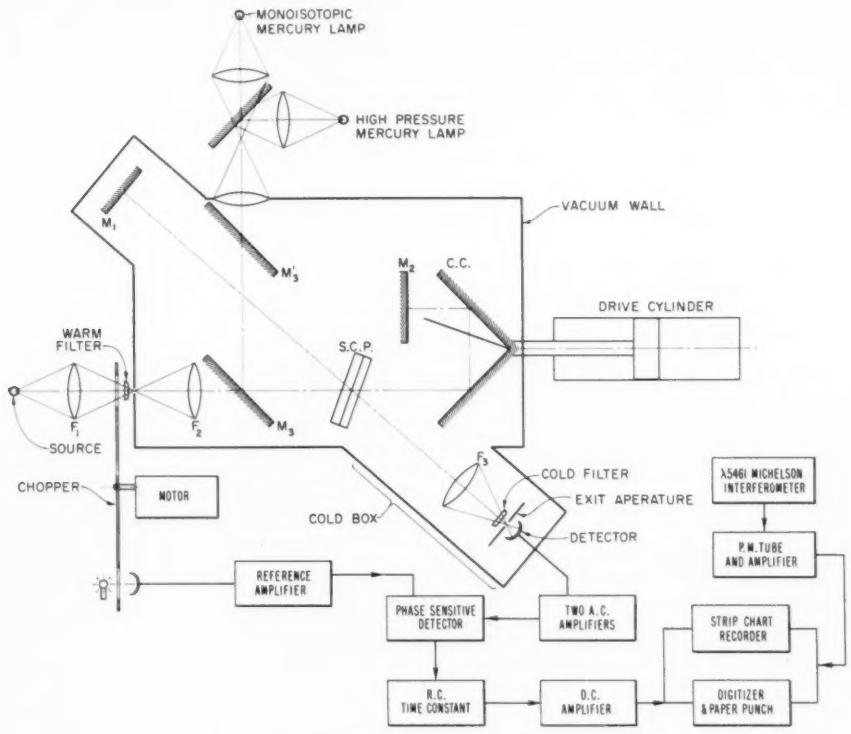

FIGURE 2. *A schematic of the constructed Michelson interferometer.*

optical components. The chopped interferogram is amplified and detected in a phase sensitive detector, the reference being derived from the chopper. A d-c amplifier supplies the correct signal voltages for the digitizer-paper punch unit and for the strip chart recorder. Care is taken that the only phase shifts in the electronics is in the R-C time constant after the phase sensitive detector.

Another Michelson interferometer is used to measure the path difference which has the cube corner as a common element with the main interferometer. This second interferometer is situated below the first interferometer. The 5461 Å line from the previously mentioned monoisotopic mercury lamp is used. Thus, this becomes a reference wavenumber or frequency. The fringes are detected by a photomultiplier and are used to tell the digitizer when to take a reading. These reference fringes are also recorded on the strip chart recorder. A similar technique was first used by Connes and Gush [10] and is now employed by many people, e.g., Gebbie, Habell, and Middleton [11]. Some of the more interesting design details will now be pointed out.

3.2. Cube Corner

The design employing one cube corner in a Michelson interferometer was first suggested by Murty [12]. The design of using one cube corner, instead of two, is superior, as pointed out by Murty, due to the elimination of large lateral shifts of the fringes when the cube corner moves. The small fringe shifts present when one solid cube corner is used, are eliminated with a front surface cube corner. The tolerances required on the cube corner angles were calculated assuming that the misalinement of the wave front upon reflection from the cube corner should be less than or equal to $\lambda/8$. The result is that

$$\frac{\Phi\Delta}{\lambda}\leq 10^{-5} \tag{12}$$

where λ is in microns, Δ is the maximum excursion in centimeters of the bumps on the slide or ways, and Φ is the maximum error in radians of the cube corner angles. This formula applies to a cube corner 5 in. to 10 in. on one side. If $\Delta=10^{-2}$ cm, $\Phi=\frac{10^{-3}}{3}$ radians, and $\lambda=\frac{1}{2}\mu$, $\Delta\Phi/\lambda=10^{-5}$. Therefore, the tolerance required on the 90° angles of the cube corner is less than 1 min of arc. The cube corner consists of three front surface mirrors glued together at angles of 90° to a tolerance of 1 sec of arc. Thus, almost any kind of machined ways can be used. Roller bearings sliding on stock steel rods were employed. The steel ways were situated in a plane containing the cube corner apex to minimize the rolling motion of the cube corner when it moves. The optical polish of the cube corner mirrors is limited by warpage of the plates when glued. It is suggested that optically contacting the surfaces should be superior, although more expensive. This technique was successfully used [13] for making a hollow cube of fused silica.

3.3. Cube Corner Drive System

The function of the hydraulic drive is to provide a smooth motion of the apex of the cube corner in one direction at a velocity of about 2×10^{-5} cm/sec. Both the long and short term stability of the drive are important as it is necessary to have the phase shifts for one wave number constant during a scan. The phase shifts in an electronic filter are, of course, a function of frequency. In general, a nut and screw gives a good long term stability but a poorer short term stability, while a hydraulic system is capable of a good short and long term stability. Figure 3 shows a schematic of the hydraulic system and is similar to one employed by Ameer and Benesch [14]. The 500 lb weight supplies a constant pressure of 1000 lb/in.^{2} to the system. In the drive cylinder, there is more force pushing in the forward direction than in the opposite direction, hence the cube corner moves. The rate at which it moves is determined by the dimensions of the hypodermic tubing placed in the hydraulic circuit. Using Poiseuille's law of flow of liquid through a tube, it can be shown that the velocity of the cube corner is

$$V=\frac{\pi}{8\eta}\frac{r^4}{l}\frac{PA_2-F}{(A_1)^2} \tag{13}$$

where η is the viscosity of the fluid, r and l are the radius and length, respectively, of the hypodermic tubing. P is the pressure (1000 lb/in.^{2}). A_1 and A_2 are the area of the drive cylinder piston and of the rod, respectively. F is the net force resulting from friction on the cube corner ways and in the drive cylinder rod seals. This frictional force will oscillate between the static and kinetic case due to the slow motion. In (13) only η and F can vary; the other quantities are rigidly fixed. Hence, upon

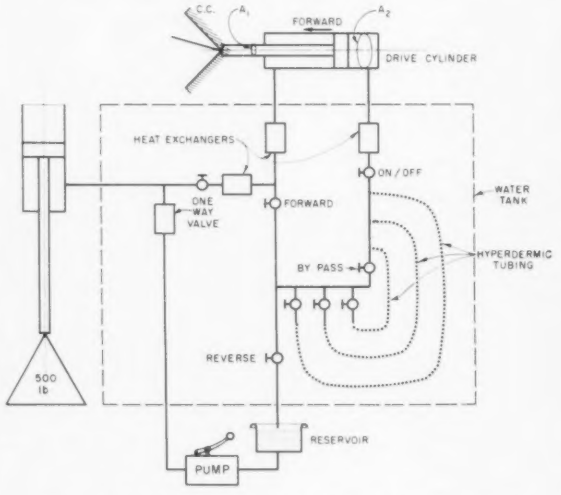

FIGURE 3. *A schematic of the hydraulic drive system.* The cube corner, c.c., can move in the forward or reverse directions.

differentiation (13) becomes

$$-\frac{dV}{V}=\frac{d\eta}{\eta}+\frac{dF}{PA_2-F}. \tag{14}$$

Equation (14) shows that if the percentage change of the cube corner velocity is to be a minimum two conditions should be met. They are: (a) $F<<PA_2$ and (b) $\frac{d\eta}{\eta}$ be a minimum. Now PA_2 is 750 lb and F is one or two orders of magnitude less. This is the main reason for using a high pressure in the system. The frictional forces and thereby dF can also be reduced if air bearings are used; then P can be lower, resulting in an elegant and simple hydraulic system. Such a system has been built by Stroke [15 and 16], but would be difficult to incorporate in the Michelson interferometer in a vacuum. A hydraulic fluid was used which has a viscosity of about 50 cP at 70 °F and $\frac{d\eta}{dt}\frac{1}{\eta}$ of about 0.04/°F. Thus, for the velocity of the cube corner to be constant to 4 percent, the oil should have a constant temperature to 1 °F. This is accomplished by placing the components of the system in a water bath and allowing oil which flows into these components to first pass through a heat exchanger which consists of a coil of tubing in the water bath. The large heat capacity of the water is sufficient to keep the temperature of the oil to better than 1 °F over the time of one scan; if a silicon oil was used, $\frac{d\eta}{dt}\frac{1}{\eta}$ would be about 0.01/°F.

3.4. Mounting of the Optical Components

The interferometer is supported on small rubber inner tubes inflated to about 4 or 5 lb/in^2. The mass of the instrument was intentionally made large for further stability from vibrations. The weight of the instrument is about 1000 lb. Each individual optical component is mounted by a type of ball joint and three adjusting screws, one of which is spring-loaded. The ball of the ball joint is a nut, which is tightened on a screw for mechanical stability. This type of adjustment constitutes the coarse adjustment and is illustrated in figure 4.

The fine adjustment of the parallelism of the interferometer plates (for the infrared and visible fringes) is made by tilting mirror M_1. This mirror has a coarse adjustment on its base plate and the mirror itself is supported on a shaft with a groove cut in it. Two springs placed 90° from each other relative to the center of the mirror are pulled to bend the shaft at its groove. A d-c motor turns a screw which pulls the springs. The mirrors M_1 and M_2 are flat to $\lambda/20$ in the visible. The separating and compensating plates are made of calcium fluoride with dielectric coatings on the separating plate. They are used at an incidence angle of 20° to conserve their size. Their polish is to $\lambda/3$ in the visible, their thicknesses are to 0.0005 in. or better, and the parallelism of the plates is to 3 sec of arc.

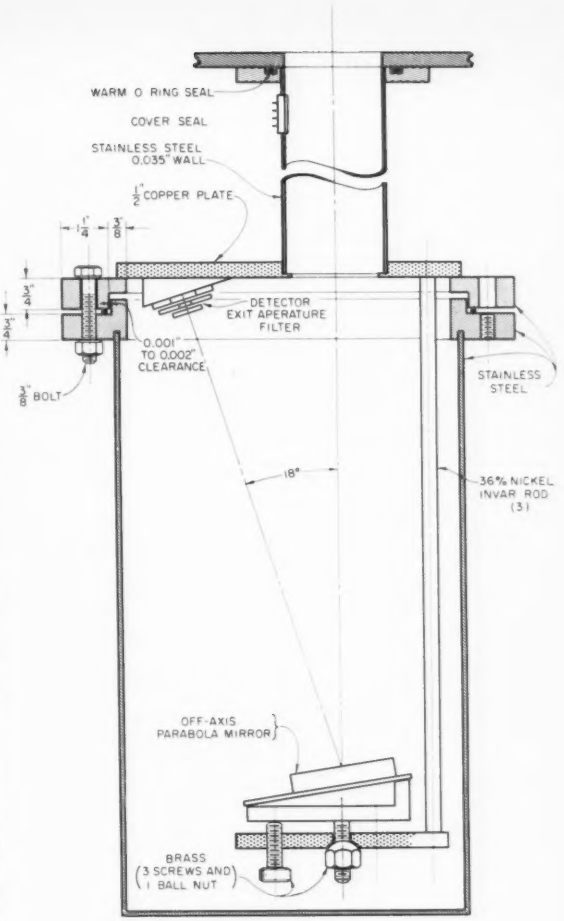

FIGURE 4. *A schematic of the "cold box."*

3.5. Cold Box

It was decided to use a lead selenide or lead sulfide cell cooled to liquid nitrogen temperatures as a detector. It was then simple to cool the exit aperture, interference filter, and the focusing mirror F_3 of figure 2. Figure 4 shows the design. Liquid nitrogen covers the ½ in. copper plate which cools the attached detector, exit aperture, and filter. The off-axis parabolic mirror F_3 of figure 2, is cooled mainly by radiation. The position of this mirror is kept fixed with respect to the detector as the contraction of the brass mounting and invar support rods are equal. Any tilting of the cold box is prevented by metal-to-metal contact at the warm O-ring seal. The cold O-ring seal employs a ⅛ in. O-ring with an i.d. about ¾ in. undersize. It is of 60 or 70 durometer and is compressed to ⅓ of its thickness by 3,000 to 4,000 lb/in. compression supplied by ⅜ in. bolts spaced every 2 in. The O-ring surfaces should allow for the resulting flow of the O-ring and have a finish

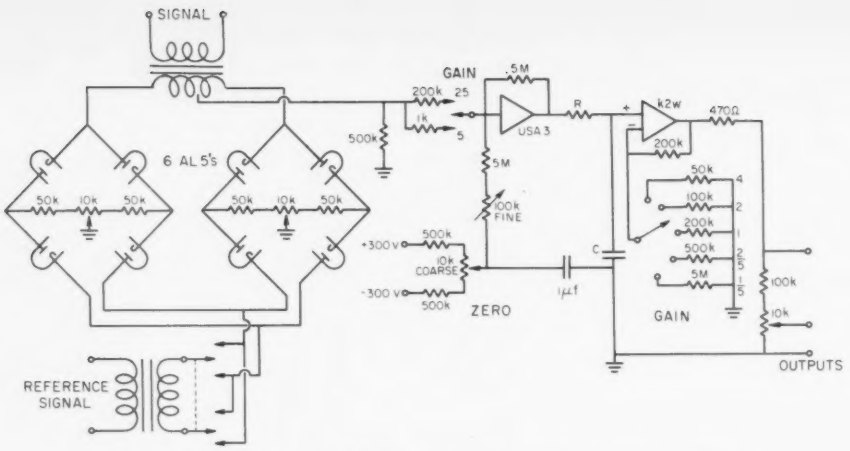

FIGURE 5. *A schematic of the phase sensitive detector and d-c amplifier.*

of 32 to 64 μ in. One O-ring should be used only once or twice and the flanges and O-ring should be degreased with chlorothene.

3.6. Electronics

The chopped interferogram is amplified and detected by the conventional a-c amplifier and phase sensitive detector method, commonly called a lock-in amplifier. Two a-c amplifiers are used, the first being a low level preamplifier which is mounted on the interferometer itself for shock mounting and elimination of pickup in long cables. The available gain is 10^3 to 10^5. The signal and reference to the phase sensitive detectors are fed from cathode followers. Figure 5 shows the circuit of the phase sensitive detector, time constant, and d-c amplifier. The d-c amplifier employs operational amplifiers. A chopper stabilized amplifier supplies the required stability and a differential input operational amplifier supplies a high input impedance to the time constant. The signal required for the digitizer is about 0 to -10 V. The photomultiplier and amplifier circuit for detecting the green fringes is similar to a design by Hunten [17]. This signal is used to order the digitizer to read and is also displayed on the strip chart recorder.

4. Performance

Figure 6 shows an interferogram obtained with a globar as source, a cold broadband filter, and a lead selenide detector. The globar was operated at a very low level (3 V across the 1.6 Ω globar) and the filter was a narrow band filter at 3.63 μ which suffered a permanent deteriation when cooled to liquid nitrogen temperatures. The resultant incident spectra consisted of two broadbands, one at 4 μ and the other at 6 μ, with bandwidths of 1.5 μ and 0.8 μ, respectively. The interferometer has a good response to the 4 μ band, but very little response to the 6 μ band, due to the separating plate. The reference mercury fringes are also shown and had a frequency of about 2 c/s. A time constant of 0.03 sec was used for the interferogram so that electronic phase shifts were not present. The interferogram demonstrates the following:

(1) The instrument has excellent mechanical stability from interfering vibrations.

(2) The stability of the cube corner drive is good.

(3) The problem of phase shifts does not appear to be serious as the interferogram is symmetrical about a narrow zero order fringe. As the incident spectra had a large band width of 1.5 μ, any serious phase shifts would certainly have shown up.

The first two properties were forcibly demonstrated by observing on an oscilloscope the Lisajous figure made from an audio oscillator and the mercury

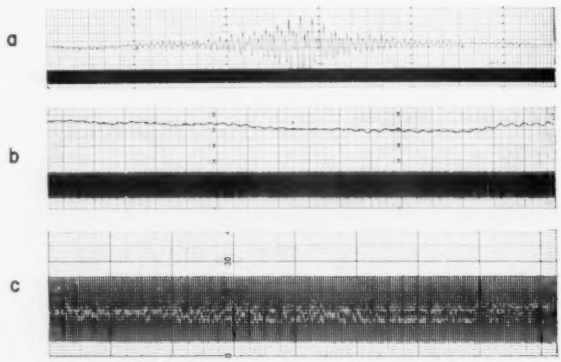

FIGURE 6. *The interferogram obtained with the interferometer from a spectral band at 4 μ with a bandwidth of about 1.5 μ.*

a. Shows the interferogram around the position where the path difference is zero. It can be seen that the interferogram is symmetrical about the zero order fringe.
b. Shows a portion of the interferogram at about 1 mm path difference.
c. Shows a portion of the mercury reference fringes. The scale on figures b and c are expanded by a factor of 2 and 4, respectively, over figure a.

fringe signal at about 20 c/s. There was very little motion of this figure over, say, a minute. However, there was a slow drift in the fringe signal frequency which amounted to about 5 percent in 5 min and 10 percent in 30 min. If this drift is serious, it may be possible to reduce it by simply continued operation of the hydraulic system, as there may still be some air in the system. A controlling mechanism could also be built to lock the signal frequency to some reference.

5. Conclusion

A Michelson interferometer with excellent mechanical stability and with an unusual drive system has been built and tested. Apparently, the hydraulic system gives a superior drive to the drive obtained from an expensive screw and nut with the exception of the long term stability.

Interferograms can now be obtained and recorded. The problems of calculating the spectra have not been completed, but involves solving the problem of obtaining a working relationship between the interferometer and computer, and possibly of improving the long term stability of the drive system.

This work was performed at the National Bureau of Standards under the supervision of David M. Gates for the USAF, Contract No. PRO 63–507.

The author would like to acknowledge the excellent machine work of P. F. Biddle and J. H. McCarron. Acknowledgements are due to R. H. Kropschot and D. H. Weitzel for advice on the cryogenic design of the cold box, and K. F. Nefflon for suggestions on some aspects of the interferometer design.

(Paper 69C1–179)

6. References

[1] Michelson, A. (1891), Visibility of interference-fringes in the focus of a telescope, Phil. Mag. **31,** 256.

[2] Michelson, A. (1892), On the application of interference methods to spectroscopic measurements II, Phil. Mag. **34,** 280.

[3] Rayleigh, Lord (1892), On the interference bands of approximately homogeneous light; in a letter to Prof. A. Michelson, Phil. Mag. **34,** 407.

[4] Rubens, H., and R. W. Wood (1911), Focal isolation of long heatwaves, Phil. Mag. **21,** 249.

[5] Fellgett, P. (1951), The theory of infra-red sensitivities and its application to investigations of stellar radiation in the near infra-red, Thesis (Cambridge University).

[6] Fellgett, P. (1958), A propos de la théorie du spectromètre interférentiel multiplex, J. Phys. Radium **19,** 237.

[7] Jacquinot, P. (1958), Caractéres communs aux nouvelles méthodes de spectroscopie interférentielle; facteur de mérite, J. Phys. Radium **19,** 223.

[8] Connes, J. (1961), Recherches sur la spectroscopie par transformation de Fourier, Rev. d'Optique **40,** 45–78, 116–140, 171–190, 231–265.

[9] Jacquinot, P. (1960), New developments in interference spectroscopy, Rept. Progr. Phys. **23,** 267.

[10] Connes, J., and H. P. Gush (1959), Spectroscopie du ciel nocturne dans l'infrarouge par transformation de Fourier; J. Phys. Radium **20,** 915.

[11] Gebbie, H. A., K. J. Hubell, and S. P. Middleton (1961), Michelson interferometers for spectrophotometry in the near infra-red region, Optical Instruments Conference London (1961).

[12] Murty, M. V. R. K. (1960), Modification of Michelson interferometer using only one cube-corner prism, J. Opt. Soc. Am. **50,** 83.

[13] Cook, A. H. (1961), Precise measurements of the density of mercury at 20° C, Phil. Trans. Roy. Soc. London (A) **254,** 125.

[14] Ameer, G. A. and W. M. Benesch (1961), Interferometrically controlled hydraulic wavelength drive, J. Opt. Soc. Am. **51,** 303.

[15] Stroke, G. W. (1958), Systems interférentiels a miroirs en mouvement continu et detection photo électrique, J. Phys. Radium **19,** 415.

[16] Stroke, G. W. (1963), Interferometric method of velocity of light measurement, Appl. Opt. **5,** 481.

[17] Hunten, D. M. (1953), A rapid-scanning auroral spectrometer, Can. J. Phys. **31,** 681.

JOURNAL OF RESEARCH of the National Bureau of Standards—C. Engineering and Instrumentation
Vol. 69C, No. 1, January–March 1965

The National Bureau of Standards Gas Thermometer II. Measurement of Capacitance to a Grounded Surface With a Transformer Ratio-Arm Bridge

L. A. Guildner and R. E. Edsinger

(September 4, 1964)

A modification of the conventional transformer ratio-arm capacitance bridge was made to measure the values of three-lead capacitors having one of the plates grounded. With this ground point it is necessary to use triaxial cable with solid shields. A troublesome capacitance coupling between the primary and secondary shields of the transformer was neutralized by means which still enable one to attain the extremely high precision and accuracy characteristic of this type of bridge. The modified bridge was developed initially for highly accurate determinations of the locations of the grounded mercury menisci of the National Bureau of Standards precision manometer. Other applications are readily thought of and one interesting example is presented.

1. Introduction

In the last decade, one of the important developments in the field of metrology is the recognition of the value of transformer ratio-arm bridges using 3-lead capacitors. [1,2,3,4].[1] This system can measure capacitance without including parasitic lead effects, and is capable of such accuracy for a computable 1 pF capacitor, [6,7], that it is used to check the U.S. standards of the electrical units. Not only is the bridge system essentially simple, but it has a special elegance in the ability to produce voltages in ratios which are very precisely the turns ratios of the transformer secondary windings. Thus a decade system or any other ratio of integral numbers within the limits of a practical number of turns may readily be established.

When conditions permit, both plates of the capacitors are isolated and the bridge is grounded at the junction of the ratio-arm secondary windings. However, under a variety of conditions it is at least very inconvenient, if not impossible, to prevent one of the plates of the capacitor from being grounded. In particular, many opportunities arise for computing very small distances or changes of distances from capacitance measurements, where the object under observation is grounded.

This paper presents the modifications for changing the ground connection from the center-tap of the ratio-arms of the bridge to the capacitance plates on the other side of the detector. This involves a more elaborate, double-shielding arrangement, and a means of overcoming a capacitance coupling in the transformer.

[1] Figures in brackets indicate the literature references at the end of this paper.

2. Transformer Ratio-Arm Capacitance Bridge

Figure 1 is a simplified schematic of the modified bridge, without the primary windings. There are two segments of the secondary windings for the ratio

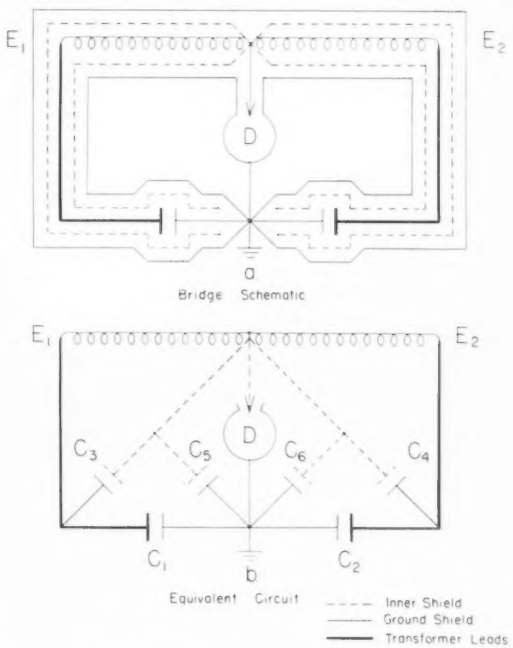

FIGURE 1. *Bridge schematic.*

arms and the active elements of two three-lead capacitors, C_1 and C_2, for the other arms. A high impedance detector, D, is connected from the center tap of the secondary windings to the grounded midpoint of the two capacitors. An inner shield, indicated in figure 1 by the dashed line, connects with the center-tap of the secondary windings and encloses the secondary windings and the capacitors. The capacitances, C_3 and C_4, between this shield and the transformer leads, are shunts which load both the leads and the ratio-arms, but are not detected as part of the measured capacitance. These capacitances are kept small external to the transformer and of approximately equal value so that the voltage drop in the lead of either secondary ratio arm, because of this additional loading, is less than 1 part in 10^7, and is partially compensated as well by a similar shunting capacitance on the lead of the other ratio arm. An outer shield connected to the grounded midpoint between the two capacitors is necessary to reduce noise pickup by the system. As shown in figure 1, the capacitances, C_5 and C_6, between this ground shield and the inner shield, shunt the detector and directly affect its sensitivity. To minimize this detector shunting capacitance, the ground shield is kept at as large a distance as possible from the inner shield.

The special construction of the transformer gives two voltages at E_1 and E_2, opposite in phase and of a fixed voltage ratio within a part per million of the turns ratio. This is accomplished by the use of tightly coupled secondary turns wound on a large toroidal core of high permeability tape. The two secondary windings are identical copper helices, constructed so as to have large cross section and low resistance and interleaved to sample very nearly the same flux along the core. The low resistance and leakage inductance of each secondary winding assure adequate voltage constancy at E_1 and E_2 when C_3 does not vary from C_4 by more than 1000 pF.

The properties of 3-lead capacitors [5,6] made it possible to define precisely small changes of capacitance (1×10^{-5} pF) in this system. The bridge circuit, shown in figure 1, eliminates the detection of parasitic capacitance, so that additional capacitors can be switched into the circuit in parallel with a reproducible and calculable effect.

Most components of the bridge were placed in a large metal enclosure at ground potential. Triaxial cable or a double shielding arrangement was necessary for each bridge element, such as a measuring probe, outside of the shielded enclosure. The use of a solid inner shield was found to be necessary to eliminate errors caused by the detection of parasitic capacitance.

3. Transformer Design and Construction

The specific design of the transformer with secondary windings in the ratio of 1 to 1, is based on a suggestion by R. D. Cutkosky.[2] An additional tap gives a second ratio of 4 to 3.

The transformer is operated at a frequency of 1000 Hz with 40 V on the primary, which gives approximately 12 V across the secondary windings in series.

The primary winding consists of 132 turns of AWG No. 15 copper wire, closely and evenly spaced around the core of the transformer. To be sure of uniformity of spacing, a second Nylon form milled with grooves to receive the primary winding, was made to fit around the Nylon case of the core. One end of the primary was soldered to a smaller, more flexible wire which was placed around the outer circumference of the core in the direction opposite to the advance of the windings in order to compensate for the single turn effect caused by the advance of the main windings around the core. The core of the transformer is a toroid of 0.002 in. thick Supermalloy [3] tape with an outer Nylon case 4.5 in. o.d., 3 in. i.d., and 1.5 in. high.

The bridge arrangement necessitates the use of two electrostatic shields between the primary and secondary windings. (See fig. 2.) These shields are part of the inner and ground shields referred to in the discussion of the bridge. Part of the ground shield encloses the primary windings and part of the inner shield encloses the secondary windings. That part of the ground shield enclosing the primary windings is in the shape of a toroidal cup of $\frac{1}{16}$ in. thick copper. A top cover to complete the shield is screwed to the outer circumference. A small gap in the shield, centered on the inside, prevents a shorted turn around the core of the transformer. A threaded ring, TR, attached to the shield on the top side of the gap can be moved up or down by rotation to change the "effective" gap position. Melamine sheet of 0.015 in. thickness is used as insulation between the primary windings and this shield. The need for the adjustable gap position will be explained later.

Each of the two secondary windings was constructed of 20 pieces of 0.025 in. thick copper sheet, machined in circular form, 5.5 in. o.d. and 3.5 in. i.d. The pieces were cut on a radius, properly oriented on a jig, and butt silver soldered to one another to form a helix. Two approximately identical secondary windings of 20 turns apiece were then, in effect, screwed together and insulated from one another by the insertion of 0.0075 in. thick Teflon sheets. Small flexible wires were used to make the connections from the windings to the BNC terminals mounted on the (enclosing) inner shield.

That part of the inner shield enclosing the secondary windings was assembled from 14 different copper pieces. They were accurately machined so they would fit tightly together with a steplike gap at the center of one side and located to be at about the same level as the gap of the primary shield. Four machined Nylon spacers were used to insulate the inner shield from the ground shield and to hold it in a stable position. The form and placement of the inner shield allowed comparatively little surface area close to the ground shield and thus the detector shunting capacitance was minimized.

[2] Electricity Division, National Bureau of Standards.

[3] Arnold Engineering Company, Marengo, Ill.

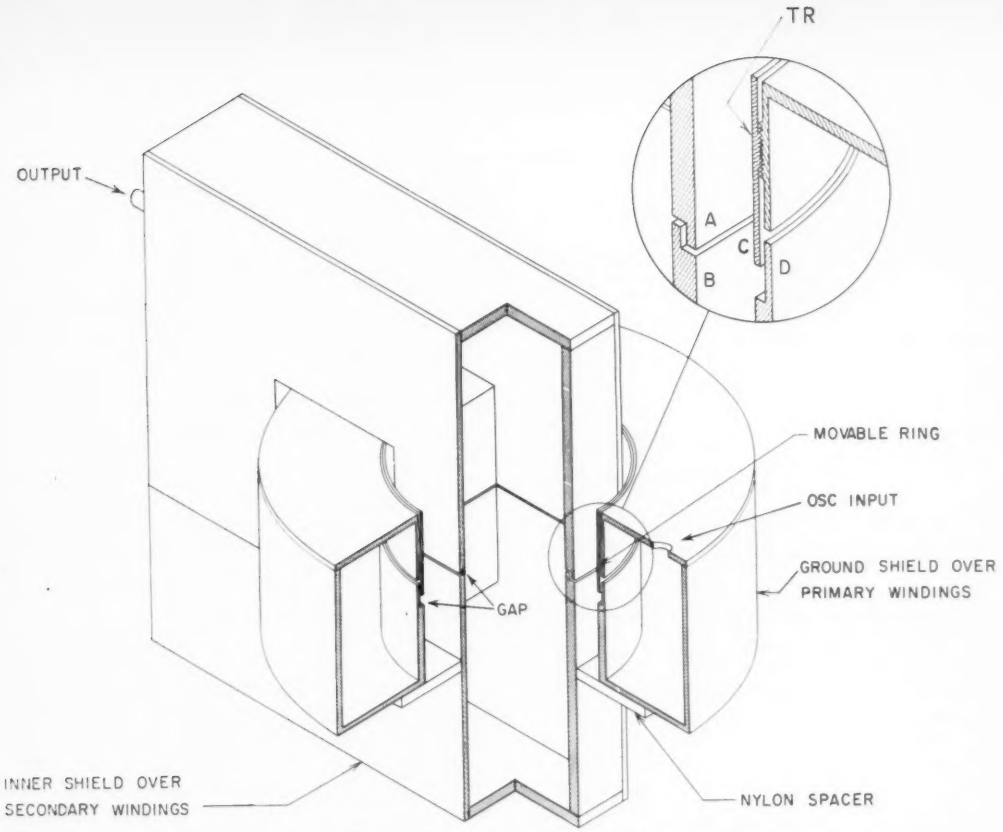

FIGURE 2. *Transformer illustration.*

4. Bridge Unbalance Due to Shield Arrangement

Since both shields make one turn through the core of the transformer, the detector, connected across the shields, is influenced by the induced voltages on the shields. In the design being discussed the voltage across the gap of each shield is approximately 0.8 percent of the primary voltage. A current path is provided through the detector by capacitances between the secondary shield and the primary shield or ground. This can be explained further by reference to figures 2 and 3, which represent a sectional view showing the core, the primary shield and the secondary shield of the transformer and the equivalent electrical circuit. The windings are not shown and for the following discussion are not considered except to assume that the primary is providing flux to the core. When a positive voltage is induced at A (secondary) and C (primary), a negative voltage exists at B (secondary) and D (primary). The gap in each shield limits the current circulating within the shield. Because of equal voltage between A and C and between B and D, only those capacitances between A and D and between B and C are important. A difference in the value of these capacitances creates a net current through the detector. A provision to reduce the current flow to zero by adjustment of these capacitances was made by the construction of a threaded ring attached to the inner wall of the primary shield.

The location of both gaps at the center of the core provides symmetry and reduces the effect of capacitance to the surroundings.

5. Capacitance and Conductance Balance

In almost all a-c bridges, means must be provided to balance out the resistive component of the system as well as the capacitive component in order to obtain a true null. This is accomplished by switching into one arm of the bridge or the other a conductive balance control (see fig. 4) to balance the excess resistive component in the adjacent arm of the bridge. The construction of a network to obtain a small voltage in phase with the voltage E, is described by Thompson [6] and others. An adaptation of this circuit has been made with only the components needed for operation at 1 kHz. A decade-switched, tapped inductor connected across one secondary winding or the other acts as a voltage divider. The line from the tapped inductor is con-

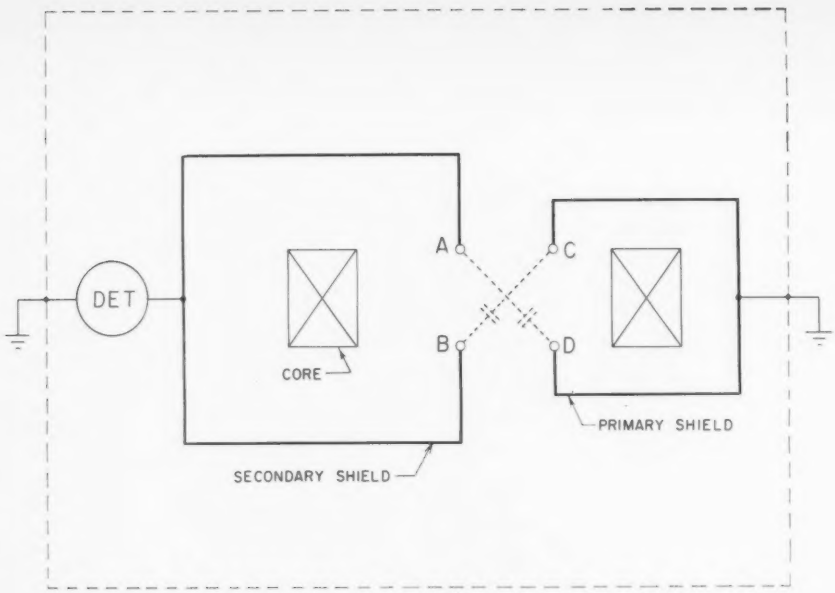

FIGURE 3. *Shield arrangement.*

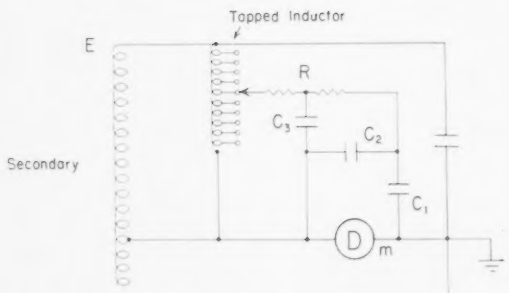

FIGURE 4. *Conductive balance control.*

nected to a "T" network consisting of a resistance with a midpoint connection and several capacitors. The values of R and C_1, C_2, and C_3 are selected to produce a small voltage of correct magnitude and phase at the input to the detector. In effect the reactance of the combination of C_1 C_2 in parallel is small compared to R and the voltage at *m* due to this network is nearly in phase with voltage, *E*. It is made almost, if not exactly equal in phase by the small capacitance at C_3.

6. Shielded Switch

To switch capacitors into or out of the bridge either singly or in combination, a modification to provide the proper shielding was made of a standard Leeds and Northrup 12-position silver contact rotary switch.

Figure 5 shows the terminals around the circumference of the switch laid out in the plane of the paper for ease of illustration. The heavy dark line, around the switch represents the inner shield, enclosing the entire switch.

The two portions of the shield represented by the horizontal lines were machined from brass to replace the original sections of the switch. Connections from the various switch terminals were made to BNC receptacles mounted through the shield. The common terminals R_1 and R_2 were connected to one of the ratio arms, and common terminal L was connected to the other ratio arm. Only 6 positions were used and certain brushes which connect some of the single terminals to a common terminal were relocated 180 deg from the normal position.

Each position of the switch allows the connection of one or two of five different capacitance elements into one arm of the bridge at the same time connecting one or two of the remaining capacitance elements into the other arm. Any elements not being used are connected to the shield so that their presence will not influence the balance point by parasitic capacitance. The lower portion of the switch is an arrangement to short out the input to the detector while going from one switch position to another.

7. Operation of Bridge

The ratio of the secondary voltages of the transformer used in the configuration described by Thompson is equal to the turns ratio within 1 or 2 parts in 10^7. The modified bridge configuration loses this desirable feature because of the voltage produced on the secondary shield.

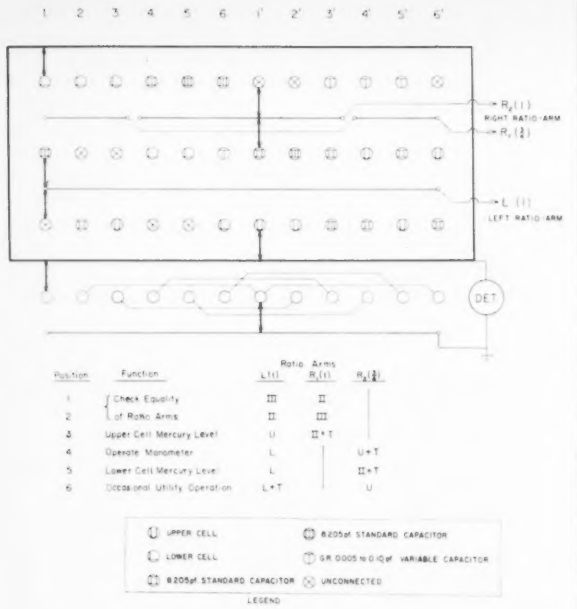

FIGURE 5. *Coaxial switch.*

Equality of the secondary voltages is tested by switching the ground point to the center tap of the secondary windings, so that the detectible effect of the shield capacitances is eliminated. For equal ratio arm voltages two nominally equal and highly stable standard capacitors [4] are then placed in the arms of the bridge. The capacitance value of one is decreased to be equal within 1×10^{-5} pF of the value of the other by removal of a small area of the plate of the capacitor. A check of both the equality of the ratio arms and the equality of the capacitors is made by interchanging the capacitors in the arms.

The two equal standard capacitors are then used in the two equal arms of the modified arrangement and the movable inner ring of the primary shield is adjusted until null is again observed.

The complete detection system of the bridge and other components is illustrated in the block diagram of figure 6. If desired, the output signal of the phase detector can be used for automatic control purposes.

Performance of the particular system described, over a period of several months, indicates that the standard capacitors have remained equal in value (within 1×10^{-5} pF), and the shield cross capacitances have not changed sufficiently to introduce a significant error.

[4] The values of the standard capacitors were made to be 8.205 pF. These capacitors were made from disks of high quality fused silica with a gold film evaporated onto polished surfaces to produce the plates and guard.

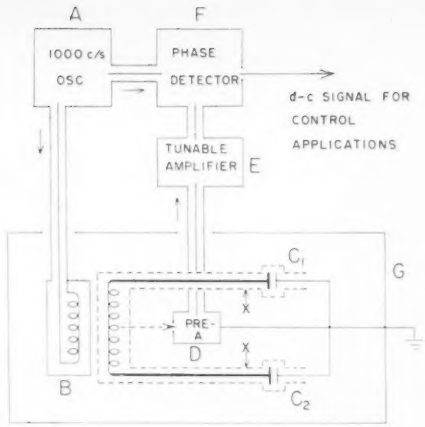

FIGURE 6. *Block diagram of system.*

8. Determination of Probe or Cell Capacitance Constant

In applications involving use of this bridge to determine the change of position of a grounded object, it is necessary to know the relation for the capacitance between the capacitance probe and the object. One may measure the mechanical dimensions of the capacitance detecting plate, shield ring, and reference object, and calculate capacitance versus the distance of separation of the reference object from the probe. Accuracy of the result is limited to the exactness of the capacitance equation available for the configuration used and the accuracy by which the mechanical dimensions of the probe can be measured. Exact equations are not available for the capacitance of some probe configurations. In these cases, a graphical relaxation method [8] of determining the potential field and thereby the capacitance can be used.

9. Applications

One application of the modified bridge is its use in a precision mercury manometer. In normal operation, the upper cell (see fig. 7) of the manometer is in one arm of the bridge and the lower cell is in the other. A 3-lead adjustable trimmer capacitor is in parallel with the lower cell. At "zero level" with both cells evacuated, the plate-to-mercury capacitance is not exactly the same in the two cells because of small differences in level of the plates, and differences in the mechanical configuration of the plate-guard assembly. This is compensated for by the trimmer. Subsequently the upper cell is wrung to the top of a column of gage blocks. When the pressure is such as to reestablish bridge null, the difference between separation of the upper cell mercury meniscus from its plate and the separation of the lower cell mercury meniscus from its plate

is the same as zero level. Therefore the height of the column of mercury supported by the pressure in the lower cell is equal to the additional length of gage blocks placed between the upper cell and the base. Since the separation of the mercury from the plate is probably not exactly the same in the two cells, an error may result if the amount of the separation changes. The mercury level is adjusted so that the capacitance in the upper cell corresponds to about 800 μ separation and the lower cell separation at bridge null is not more than 1 μ different. So long as the separation in the upper cell does not vary more than 2 μ, the bridge null corresponds to the same pressure within 5 mμ. The total error in the pressure contributed by the detection system is in the millimicron range.

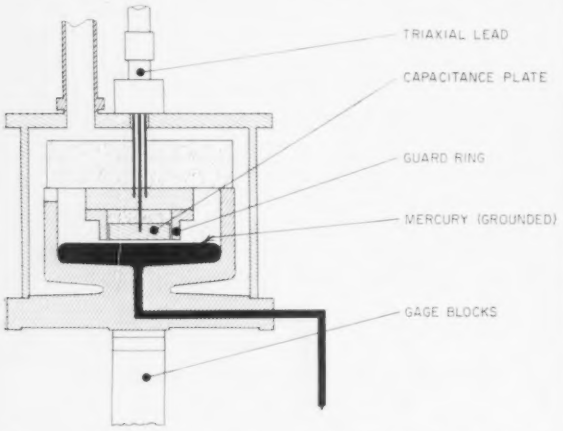

FIGURE 7. *Mercury meniscus and capacitance unit of manometer.*

A second application for the modified bridge is illustrated by the determination of the inside diameter of a long metal tube, nominally 0.8 mm. It is desired that the uncertainty in the inside diameter not exceed 6 x 10^{-5} cm. As shown in figure 8, a small probe, 0.75 mm in diameter and 1 mm long, properly insulated and centered by air flow, is moved along the length of the tube to sense the capacitance with relation to the position of the probe. Other probes of 2 and 3 mm length and of the same diameter are used, so that capacitance "end effects" can be eliminated. It is especially convenient that the measured tube can be grounded, because the tube itself then serves as a shield for the rest of the system.

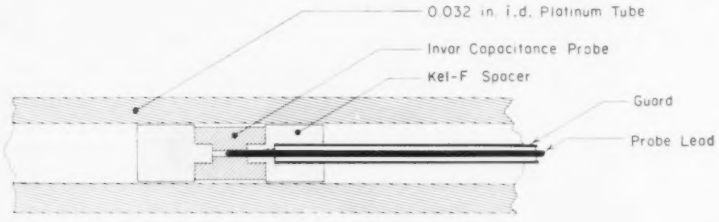

FIGURE 8. *Small capacitance probe.*

10. References

[1] A. D. Blumlein, British Patent No. 323037.
[2] H. A. M. Clark and P. B. Vanderlyn, Pro. Inst. Elec. Eng. **96,** 365 (1949).
[3] C. W. Oakley and J. G. Yates, Proc. Elect. Eng. **101,** 91 (1954).
[4] C. H. Young, Bell Lab. Record **24,** 433 (1946).
[5] F. K. Harris, Electrical Measurements, p. 682 (John Wiley and Sons, Inc., New York, N.Y., 1952).
[6] A. M. Thompson, Inst. Rad. Eng. Trans. on Instrumentation **I–7,** 245 (1958).
[7] M. C. McGregor, J. F. Hersh, R. D. Cutkosky, F. K. Harris, and F. R. Kotter, Inst. Rad. Eng. Trans. on Instrumentation **I–7,** 253 (1958).
[8] D. N. de G. Allen, Relaxation Methods (McGraw-Hill Book Co., Inc., New York, 1954).

(Paper 69C1-180)

JOURNAL OF RESEARCH of the National Bureau of Standards—C. Engineering and Instrumentation
Vol. 69C, No. 1, January-March 1965

An Adiabatic Calorimeter for the Range, 10 to 360 °K

K. F. Sterrett,[1] D. H. Blackburn, A. B. Bestul, S. S. Chang, and J. Horman

(July 21, 1964)

A low temperature adiabatic calorimeter and cryostat assembly is described for measuring heat capacities in the temperature range 10 to 360 °K. A combination of Dewar and tank system is used as refrigerant containers. The temperature of the adiabatic shield is automatically controlled to within a millidegree of that of the calorimeter vessel. This apparatus offers facilities for rapid cooling to about 50 °K and long term adiabatic control for conditioning of a sample and, thus, is especially suitable for measurements on glass, where long equilibration time is sometimes involved.

Data on the empty calorimeter vessel and on the Calorimetry Conference standard sample of synthetic sapphire are presented as a measure of the precision and the accuracy of the apparatus.

1. Introduction

A new adiabatic calorimeter and cryostat assembly with an automatic shield control has been constructed to determine heat capacity and glass transition data for various inorganic and organic glasses from 10 to 360 °K. This paper describes in detail the design and operation of this low temperature calorimeter assembly and presents an experimental evaluation of its precision and accuracy.

Although the general calorimetric design is similar to that of a number of authors [1–4],[2] the sample vessel used in this apparatus has been constructed especially for measurements on glass. Hence, the adiabatic shield and automatic shield control [5] designs were chosen for (a) versatility in producing a desired thermal history of the glass sample, and (b) reliability over long periods of continuous operation necessary for studying "kinetic effects" associated with the glass transition. Older work [6,7] on the heat capacity of glasses at low temperatures in the transition region has mostly relied upon the use of isothermal calorimetry combined with manual operating procedures.

To evaluate the reproducibility and to estimate the accuracy of this apparatus, heat capacity measurements were performed on the empty sample vessel and on the Calorimetry Conference standard α-Al_2O_3 sample [8]. Previous work on samples of the same material were reported by Furukawa, Douglas, McCoskey, and Ginnings [8] of the Heat Division, by Morrison and Patterson [9], and by Edwards and Kington [10]. Kerr, Johnston, and Hallett [11] also made measurements on a synthetic sapphire similar in origin to our standard.

[1] Present address: Northrup Space Laboratories, Hawthorne, Calif.
[2] Figures in brackets indicate the literature references at the end of this paper.

2. Description of the Apparatus

2.1. Calorimeter and Cryostat Assembly

a. Sample Vessel

The 150 ml cylindrical sample vessel (fig. 1) was constructed with 0.015 in. copper sides, a 0.010 in. copper top and a 0.020 in. Monel bottom. The Monel bottom was silver soldered to the central copper reentrant well and to the copper cylinder which forms the outside of the vessel. A false 0.010 in. copper bottom held insulated binding posts for the heater and thermometer leads and was soldered with indium-tin eutectic to the vessel below

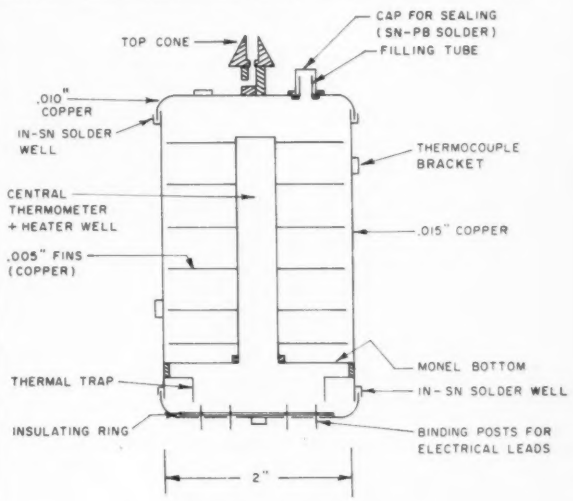

FIGURE 1. *Sample vessel.*

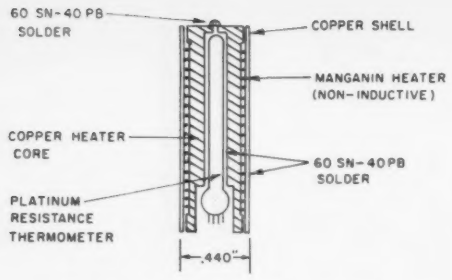

FIGURE 2. *Central well components.*

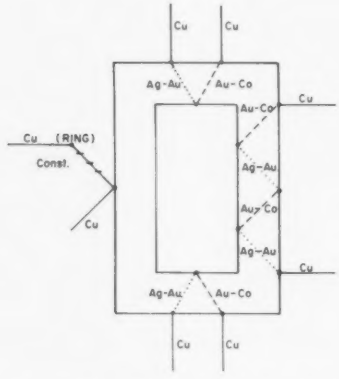

FIGURE 3. *Thermocouple schematic.*

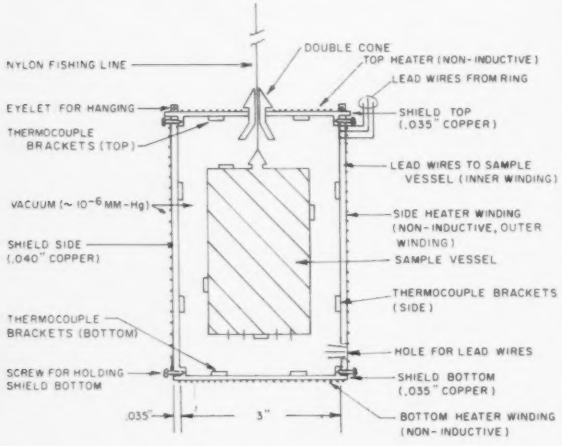

FIGURE 4. *Detail of adiabatic shield (showing sample vessel in measuring position).*

the Monel bottom. The top was designed to be soldered in place with this indium-tin eutectic after the vessel was packed with a sample. The entire sample vessel was gold-plated to minimize heat exchange by radiation. Six removable gold-plated fins, 0.005 in. thick × 0.500 in. i.d. × 1⅞ in. o.d., with raised edges and half-circle shaped holes and flaps were spring fitted to the central reentrant well in order to provide faster distribution of heat throughout the sample.

The central reentrant well components (fig. 2) contained a 25-ohm platinum resistance thermometer and a 180-ohm heater. The platinum resistance thermometer was an encapsulated four-lead, strain-free type described by Southard and Milner [12].

The heater consisted of #34 AWG [3] single cotton and enamel (S.C.E.) insulated manganin wire wound noninductively on a copper spool and insulated with several coats of G.E. #1696 high temperature varnish. The varnish was baked overnight at 150 °C after each application. The electrical leads from the thermometer and heater ran from the central well to the thermal trap, where they were wound around twice in 0.008 in. grooves. The winding was held in good thermal contact in the grooves with G.E. #7031 varnish. This winding prevented heat leakage along the leads during and immediately after a heating period when thermal gradients exist within the sample vessel. The leads then were connected to the binding posts mentioned above.

The central well components (fig. 2) were assembled using 60 tin-40 lead solder. The small hole at the top of the copper heater core, which let air escape during assembly of the thermometer into the core, was closed with a plug of the same solder. The assembly was then soldered within the central reentrant well of the sample vessel.

Two small U-shaped brackets were silver soldered to the side of the sample vessel. One junction of a multiple-junction difference thermopile used for controlling the adiabatic shield (fig. 3) was inserted into each bracket and was held by small copper wedges. Similar brackets were mounted on the top and false bottom. The junctions were electrically insulated from the copper sample vessel by mica "sandwiches." This type of mounting and insulation was described by R. B. Scott et al. [13].

A 60° cone was silver soldered at the center of the sample vessel top. This cone anchored the nylon suspension and also made thermal contact through the double adiabatic-shield cone to the helium tank when the sample vessel was cooled to liquid helium temperatures.

To aid in the distribution of heat, helium gas was introduced into the sample vessel at a slight overpressure through a 3/16 in. o.d. copper tubing which was soft-soldered to a tube fitting at the top of the sample vessel. The tubing was pinched off and sealed immediately with a drop of soft solder.

b. Adiabatic Shield and Control Thermocouples

The adiabatic shield (fig. 4) consisted of a 0.035 in. thick, 5.5 in. long copper can, gold plated. It was cylindrical with flat ends surrounding the sample vessel. The top and bottom were firmly attached to the side by means of two 56 screws. When the shield was in measuring position, it was suspended

[3] Hereafter, the numeral preceded by the # mark denotes the American wire gage number.

by three nylon lines attached to eyelets on the shield top. A 60° double cone which was an integral part of the top provided thermal contact between the sample vessel and the liquid helium tank as described above.

Differential thermocouples (fig. 3) between the calorimeter vessel and shield in conjunction with three independently controlled electrical heaters wound on the top, side, and bottom of the shield enabled the maintaining of the shield at the temperature of the sample vessel. Four thermocouple brackets were soft-soldered to the interior of the side, two to the top, and two to the bottom. The thermocouple junctions were attached to these brackets as described in the previous section.

The differential thermocouple consisted of two or more (Ag+0.37 at. percent Au) versus (Au+2.1 at. percent Co) junctions. This choice of thermocouple gave a greater thermoelectric power at low temperatures than a (Cu) versus (Constantan) thermocouple [14]. To keep the thermal conductivity low, especially at low temperatures, the silver alloy was used instead of (Cu) between the shield and sample vessel. The thermoelectric power of this "normal" silver is approximately the same as that of (Cu). All junctions were welded with a condenser discharge type welder.

The heater on the side shield was noninductively wound in a series of 0.012 in. spiral grooves machined in the side shield. It consisted of about 500 ohms of #30 S.C.E. Constantan wire which was thermally bonded to the metal with G.E. #7031 varnish. A layer of aluminum foil was placed over the heater to reduce heat loss by radiation. Beneath this heater thirty #34 copper lead wires and two #34 Constantan thermocouple wires were bonded to the side shield in another set of 0.008 in. grooves. These lead wires wrapped around the shield six times and passed into the interior through a hole near the bottom.

The heaters on the top and bottom shield consisted of about 125 ohms of #30 S.C.E. Constantan wire which was noninductively wound into a disk. A special coil winder was built to produce this flat winding. The flat coil was transferred to the copper shield top and then was varnished into place with G.E. #7031.

c. Floating Ring

Thirty-two #36 Formvar, double silk insulated copper wires were wound and varnished on a 1 in. wide $\times 2\frac{3}{4}$ in. diam. copper ring. These lead wires came from the helium tank where they were equilibrated at the helium tank temperature, to the ring where a 150 ohm noninductive #34 Constantan heater was used at temperatures above 200 °K to bring them to the temperature of the adiabatic shield. A single junction Cu versus Constantan thermocouple on the side shield (fig. 4) and a similar thermocouple junction on the ring sensed the temperature difference.

The floating ring was thermally insulated from the helium tank by three 1 in. long $\times \frac{3}{16}$ in. diam. plastic spacers. Each spacer also held one end of a nylon line which supported the adiabatic shield in the measuring position. An insulating ring attached to the copper floating ring contained 32 copper binding posts which connected the leads from the adiabatic shield to those from the floating ring.

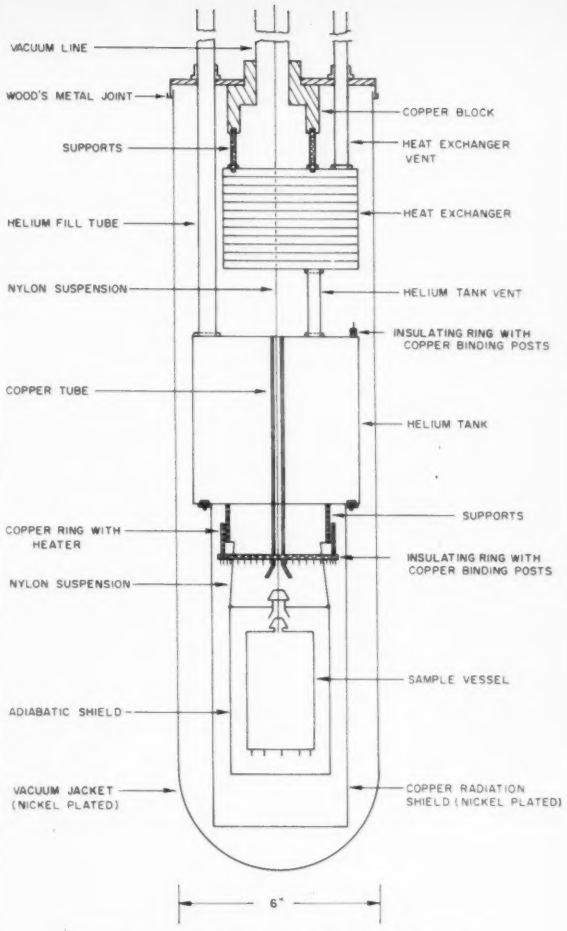

FIGURE 5. *Low temperature adiabatic calorimeter.*

d. Helium Tank and Radiation Shield

The internal coolant container (fig. 5—helium tank) held liquid helium or liquid nitrogen, depending upon the temperature range desired. By pumping on the coolant through the 0.5 in. diam. $\times$ 0.010 in. wall Monel "fill" tube while the $\frac{3}{8}$ in. diam. $\times$ 0.004 in. wall Monel vent tube was closed, temperatures can be obtained below the normal boiling points of liquid helium and liquid nitrogen.

The tank was constructed from 0.040 in. wall copper and was 5 in. long $\times$ 5 in. diam. Thirty-two #36 copper wires were wrapped six times around the tank in 0.008 in. grooves. The leads were varnished in these grooves and were connected to copper binding posts mounted in a plastic strip at the top of the tank. This procedure assured thermal equilib-

rium of the leads at the tank temperature to prevent heat from leaking to the floating ring and adiabatic shield assembly.

Six 10-32 threaded studs at the bottom of the helium tank were used to hold a nickel-plated copper radiation shield, 8.5 in. long × 4 in. diam. × 0.015 in. wall. The thirty-two #36 wires which were varnished to the helium tank entered the radiation shield through a small slot and then wrapped around the floating ring.

A ½ in. diam. × 1/16 in. wall copper tube with a 60° cone at the lower end extended from the top of the helium tank to 2 in. below the bottom of the helium tank. This 60° cone provided thermal contact to the shield and the sample vessel through the operation of the mechanical heat switch described in section 2.1.h.

A 3/32 in. o.d. × 0.015 in. wall Monel tube (not shown in fig. 5) led from the top of the helium tank to outside the cryostat. This tube served as a pressure measuring line when the pressure above the refrigerant was lower than atmospheric.

e. Heat Exchanger

When liquid helium was used as the coolant, the "boil-off" helium gas passed through the vent tube (fig. 5) to the interior of a 1/16 in. wall × 4 in. o.d. copper can containing ten copper fins, 0.010 in. thick × 3.75 in. o.d. × 2 in. i.d. These fins were soft soldered to the interior walls of the can. Around the outside of this can thirty-two #34 copper leads were wrapped and varnished with G.E. #7031 in 0.010 in. grooves. This design equilibrated the leads at a temperature somewhere between the boiling point of helium and the temperature of the nitrogen bath surrounding the vacuum jacket. It reduced the heat leak along the leads to the helium tank and thus served to diminish the liquid helium "boil-off" rate. This heat exchanger is similar to the "helium economizer" described by Westrum et al. [1].

f. Copper Block

A copper block, 2.5 in. diam., shown in figure 5, was silver soldered to the top flange of the brass vacuum jacket. Thirty-two #34 copper lead wires came down the vacuum line to this block where they were thermally bonded using G.E. #7031 varnish. This equilibration of the leads at the outer bath temperature minimized heat leakage along the leads from room temperature to the components inside the vacuum jacket.

Bundles of leads of about 12 in. length formed a full turn of loose helix between two adjacent components inside the vacuum jacket; namely, between the adiabatic shield and the binding posts on the floating ring, the ring and the helium tank, the binding posts on the tank and the heat exchanger, and the exchanger and the copper block.

g. Vacuum Jacket

A 24 in. long x 6 in. diam. x 1/16 in. wall nickel-plated, brass tube with a hemispherical spun bottom surrounded the components mentioned above. The spun bottom was silver soldered to the tube. The top of this tube was soldered with Wood's metal to a flange which held the interior parts. A vacuum of 1–3 x 10^{-6} mm Hg was maintained when desired for heat insulation within the brass tube.

h. Windlass and Mechanical Heat Switch

The internal bellows assembly from a ¾ in. Veeco high vacuum valve was employed as a convenient and compact windlass which caused contact between the 60° mating cones on the helium tank, adiabatic shield and sample vessel. This mechanical heat switch provided thermal contact between the sample vessel and the helium tank without using helium gas to destroy the insulating vacuum.

The valve assembly consisted of a sylphon bellows, an O-ring bonnet seal and an adjustment screw for raising and lowering the bellows. The effective length of the bellows was doubled by passing the sample vessel suspension over a pulley mounted on the plunger and then tying the suspension to an eyelet at the top of the heat exchanger.

i. Nitrogen Dewar

A 36 in. long x 8¼ in. i.d. stainless steel Dewar held in a brass container surrounded the vacuum jacket. The brass can was counterweighted so that it could slide easily on steel elevator rails. An O-ring was used at the top of this can as a vacuum seal.

2.2. External Electrical Equipment

a. Calorimeter Heater and Thermometer Circuits

The resistance of the platinum thermometer was determined by measuring the potential drop across and the current passing through the thermometer. A Rubicon #2773 Double Six-Dial Thermofree potentiometer calibrated by the Electricity Division was used to observe the potential across the thermometer on one set of its dials. The other set was used to measure the potential drop across a standard resistor in series with the thermometer. The double potentiometer was also used to measure the electrical energy dissipated by the heater during heating periods by observing the potential drop across the heater and that across a standard resistor in series with it. Voltage dividers made of standard resistors were used to reduce the voltage to within the range of the potentiometer (0.1111110 V). The balance indicating instrument was a Rubicon #3550 photoelectric galvanometer, the output of which was observed on a 25–0–25 microammeter connected in series in a resistance network to provide suitable overall sensitivity.

b. Interval Timer

The NBS standard frequency line supplied 60 cycles at 2 V which was amplified to 110 V to power the interval timer. The clutch of the timer was energized from the 110 V a-c general laboratory supply by the same switch that supplied power to the calorimeter heater.

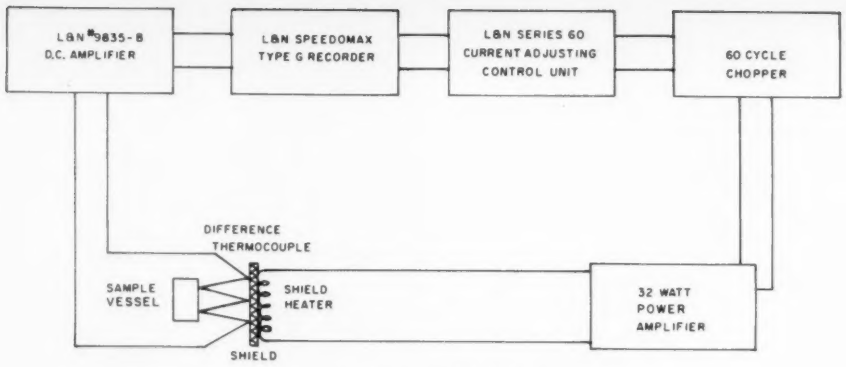

FIGURE 6. *Automatic shield control.*

c. Automatic Shield and Floating Ring Control Circuits

The automatic adiabatic shield control was similar to that used by the Heat Division [5]. It consisted of the thermocouple arrangement described earlier, three each of Leeds & Northrup 9835–B d-c amplifiers, Speedomax G recorders and Series 60 C.A.T. control units. In each channel the control signal generated by the C.A.T. unit was converted into ac by a 60-cycle chopper before feeding into a 32-W power amplifier from which power for heating the corresponding shield was generated (fig. 6). The deviation of shield temperature from the control point was usually within about 0.001 to 0.002°. Temperature differences in the order of 0.005 to 0.01° occurred momentarily at the beginning and the end of a heating period. The momentary departure from zero at "on" and "off" was so small that no correction for the heat input was necessary.

The floating ring was controlled manually with a box-type galvanometer as the indicator and with 110 V a-c variable transformers supplying heater power.

2.3. Vacuum Systems

Three vacuum systems were used with the calorimeter. They provided vacuum of 1–3 x 10^{-6} mm Hg for heat insulation, means for reducing the temperature of the refrigerants in the Dewar and in the helium tank, and the ability to fill the space in the vacuum jacket with helium heat exchange gas to cool the sample vessel when helium was used as refrigerant.

3. Temperature Scale

The platinum resistance thermometer was calibrated by the Temperature Physics Section of the Heat Division, above 90 °K in accordance with the International Practical Temperature Scale of 1948 [15] and between 10° and 90 °K with the NBS–1955 provisional scale, which is maintained by a set of platinum resistance thermometers which had been compared with a helium-gas thermometer. This provisional scale is 0.01° lower than the NBS–1939 scale [16].

4. Measurement Procedures

In both the α-Al_2O_3 and the empty sample vessel determinations a small quantity of helium gas was sealed in the sample vessel to shorten the internal thermal equilibration time. The sealed vessel was then checked for leaks with a helium mass spectrograph and hung in place in the cryostat with nylon fishing line. Thermocouples, electrical leads, radiation shield, and outer vacuum jacket were attached before the apparatus was cooled to the desired Dewar bath temperature with 10 to 20 cm Hg helium exchange gas in the vacuum jacket. After equilibration at the Dewar bath temperature the exchange gas was pumped out and heat capacity determinations were begun.

A special cooling procedure was used for the liquid helium range determinations; namely, (1) precooling with solid nitrogen around the vacuum jacket, (2) restoration of high vacuum within the vacuum jacket, (3) raising of the windlass to provide thermal contact between sample vessel, adiabatic shield and helium tank, (4) filling helium tank with liquid helium, (5) waiting a few hours for equilibration at 4 °K, and (6) lowering the windlass to obtain thermal insulation. The supply of liquid helium from one filling of the helium tank was sufficient for cooling and about 15 hr of experimental determinations.

5. Heat Capacity Measurements

Heat capacities of the empty sample vessel and of the vessel loaded with sapphire sample were determined from 10 to 360 °K. The results were tabulated in tables 1 and 2, respectively. Data represented were corrected for curvature. The correction was, in general, less than 0.1 percent of the apparent heat capacity. The temperature rise per heating interval was about 1 to 4° below 30 °K, 4 to 6° from 30 to 80 °K, and 5 to 9° above 80 °K.

The observed heat capacity data were fitted by means of least squares to an equation with Debye and Einstein terms programmed by the Heat Measurements Section [17]. Deviations of data

TABLE 1. *Principal experimental data for the heat capacity of the empty sample vessel*

C_p	T	ΔT
	Series I	
J/deg	°*K*	°*K*
72.174	302.129	4.761
72.400	306.994	4.934
72.643	311.917	4.911
	Series II	
19.899	52.043	5.994
23.782	57.549	5.018
26.970	62.296	4.427
30.188	67.353	5.673
33.397	72.753	5.126
36.208	77.680	4.727
38.589	82.258	4.432
38.953	82.900	6.735
42.070	89.379	6.226
42.037	89.276	7.265
44.903	96.302	6.787
47.396	102.904	6.418
49.526	109.177	6.129
51.396	115.189	5.896
53.041	120.989	5.704
54.543	126.609	5.537
52.685	119.735	6.201
	Series III	
0.3920	10.546	1.049
.6657	13.468	4.452
1.1732	16.997	2.531
1.6305	19.214	1.820
2.1121	21.110	1.911
2.8698	23.534	2.883
3.9794	26.469	2.945
5.5982	29.990	4.071
7.8032	34.066	4.056
10.334	38.110	4.021
13.439	42.817	5.385
17.041	47.988	4.950
21.150	53.834	6.741
	Series IV	
0.3979	10.735	1.548
.5289	12.289	1.533
.6971	13.864	1.505
.9058	15.392	1.517
1.1565	16.898	1.467
1.4477	18.388	1.471
1.7874	19.873	1.474
2.3313	21.862	2.467
3.1493	24.346	2.482
4.1300	26.836	2.479
5.3848	29.577	2.986
6.9580	32.573	2.978
8.7349	35.609	3.082
10.647	38.643	2.978
12.979	42.152	3.959
15.714	46.111	3.957
18.515	50.078	3.977
21.313	54.062	3.990
24.076	58.054	3.990
	Series V	
23.409	57.093	3.972
26.135	61.066	3.976
28.750	65.036	3.963
31.208	69.019	4.002
34.102	73.983	5.927
37.420	79.951	6.006
40.468	85.936	5.963
46.480	100.394	5.456
48.472	106.036	5.828
50.388	111.924	5.948
52.195	117.948	6.100
53.894	124.503	6.008
55.304	129.877	5.687
56.614	135.697	5.951
59.015	147.609	6.217
60.095	154.008	6.435
61.099	160.510	6.567
62.053	167.074	6.560
63.743	180.180	6.514
64.496	186.951	7.029
65.203	193.929	6.932
65.898	200.934	7.078

TABLE 1. *Principal experimental data for the heat capacity of the empty sample vessel*—Continued

C_p	T	ΔT
	Series VI	
J/deg	°*K*	°*K*
63.781	181.111	7.319
65.362	196.145	8.280
66.827	212.509	8.087
67.518	220.551	7.999
68.095	228.513	7.925
68.664	236.397	7.852
	Series VII	
62.903	174.541	8.794
63.981	183.262	8.648
64.919	191.843	8.515
65.761	200.301	8.396
66.511	208.643	8.292
67.209	216.600	7.987
67.741	224.553	7.918
68.318	232.429	7.843
	Series VIII	
68.978	243.327	7.395
69.559	250.689	7.326
69.972	257.989	7.272
70.429	265.234	7.217
70.766	272.428	7.171
71.169	279.573	7.121
69.394	246.974	4.768
69.745	251.706	4.741
70.049	256.437	4.714
70.418	261.141	4.686
70.814	271.719	4.627
71.020	276.343	4.610
	Series IX	
72.544	310.048	5.537
72.877	315.549	5.505
72.919	321.055	5.497
73.383	326.524	5.457
72.628	313.204	5.491
72.997	318.668	5.458
73.055	324.127	5.446
73.505	329.271	5.391
73.634	335.150	5.372
73.874	339.533	5.349
	Series X	
72.455	307.322	5.410
72.655	312.725	5.384
	Series XI	
71.202	281.346	5.526
71.431	286.898	5.501
71.743	292.381	5.473
72.123	297.472	5.421
72.223	302.888	5.408
72.474	307.981	5.365
72.682	313.665	5.400
73.007	319.058	5.371
73.153	325.117	5.355
73.350	329.782	5.335
73.551	335.117	5.314
73.730	340.468	5.378
73.965	346.128	5.883
74.182	352.139	6.150
74.446	358.505	6.538

TABLE 2. *Heat capacity data for sample vessel containing synthetic sapphire sample*

T	ΔT	$C_{p\ total}$	$C_p\ Al_2O_3$
		Series I	
°K	°K	J/deg	J/deg/mole
10.908	1.553	0.4123	0.010
12.554	1.939	.5743	.019
16.613	2.628	1.172	.041
20.606	5.358	2.122	.078
25.456	4.349	3.861	.153
30.449	5.631	6.346	.272
36.793	7.050	10.504	.515
42.775	4.912	15.134	.864
47.765	5.071	19.418	1.267
52.831	5.063	24.059	1.807
		Series II	
61.852	4.849	32.766	3.071
63.953	3.850	34.850	3.429
67.952	4.153	38.824	4.173
72.016	3.598	42.918	5.019
79.084	3.066	50.166	6.682
82.068	2.899	53.225	7.756
85.474	6.076	56.766	8.375
90.695	2.469	62.126	9.921
		Series III	
76.972	4.757	47.939	6.128
81.864	5.029	52.979	7.381
84.823	6.101	56.105	8.228
90.311	2.580	61.753	9.819
116.260	1.780	88.326	18.595
118.022	1.742	90.226	19.313
		Series IV	
96.546	5.061	68.067	11.71
102.199	6.244	73.881	13.57
108.197	5.747	79.994	15.63
113.743	5.340	85.829	17.70
119.886	6.943	92.097	20.00
126.580	6.442	98.942	22.59
133.229	6.876	105.55	25.17
139.889	6.444	112.27	27.88
146.889	7.566	119.15	30.70
154.230	7.115	126.28	33.74

TABLE 2. *Heat capacity data for sample vessel containing synthetic sapphire sample*—Continued

T	ΔT	$C_{p\ total}$	$C_p\ Al_2O_3$
		Series V	
°K	°K	J/deg	J/deg/mole
154.837	6.985	126.88	33.96
162.007	7.354	133.55	36.79
169.569	7.783	140.08	39.83
177.166	7.405	147.28	42.75
184.408	7.073	153.53	45.51
191.346	6.796	159.43	48.14
198.666	7.839	165.17	50.70
206.352	7.534	171.20	53.42
213.751	7.264	176.90	56.00
221.771	8.767	182.48	58.53
238.598	8.189	193.99	63.80
		Series VI	
205.015	4.258	170.30	53.01
211.700	9.106	175.22	55.23
220.632	8.775	181.57	58.10
229.248	8.473	187.52	60.82
237.578	8.207	193.35	63.49
245.660	7.972	198.53	65.86
266.072	8.277	210.58	71.35
274.230	8.069	215.13	73.50
282.280	7.873	219.44	75.49
289.906	7.700	223.21	77.22
297.546	7.547	226.81	78.87
		Series VII	
242.519	8.941	196.71	65.04
249.961	9.493	200.70	66.84
259.270	9.203	206.54	69.54
266.884	6.077	210.72	71.45
260.867	8.409	207.39	69.92
269.134	8.194	212.43	72.15
277.198	8.005	216.67	74.20
286.847	8.558	221.59	76.47
		Series VIII	
308.929	6.985	231.78	81.15
315.828	6.895	235.39	82.84
322.649	6.820	238.05	84.06
336.049	6.652	243.60	86.62
340.584	6.650	245.23	87.37
347.161	6.569	247.30	88.31
353.623	6.468	250.16	89.65

points from the equation were shown in figures 7 and 8 for the empty vessel and the loaded vessel, respectively. The deviations were, in general, confined within the envelope formed by the solid lines representing 0.1 percent of the observed heat capacity. The larger deviations near 90 °K probably resulted from the imperfection of the two temperature scales used.

A peritectic decomposition of the γ-phase of indium-tin alloy was proposed to occur below 80 °C, although no thermal effect for the reaction was found [18]. No thermal anomaly was observed in the heat capacity measurements.

Molal heat capacity values for α-Al_2O_3 were also listed in table 2. The Calorimetry Conference standard synthetic sapphire sample weighing 199.913 g (in vacuo) was used. The molecular weight (1961) of alumina was taken as 101.9612. Adjustments were made for the differences in the amount of helium, copper, and solders used between the measurements of the empty and of the loaded vessel.

Deviations of the observed heat capacity values of $\alpha-Al_2O_3$ from those of Furukawa et al., are shown in figure 9. The heat capacity of the empty sample vessel represented 95 to 85 percent of the total heat capacity of the loaded vessel from 10 to 50 °K, 85 to 65 percent from 50 to 100 °K, 65 to 40 percent from 100 to 200 °K, and from 40 to 30 percent from 200 to 360 °K. Hence deviations below 50 °K were not shown due to the unfavorable contribution from the empty vessel. The dash-line represented molal heat capacity values derived from the two equations with Debye and Einstein terms for the empty and the loaded vessel. The values at rounded temperatures were listed in table 3. Deviation of this curve from the data of Furukawa et al., varied between zero to +0.08 percent for the temperature range from 100 to 360 °K. From 100 to 50 °K, the deviation was of the order of 0.2 to 0.4 percent, and from 50 to 10 °K, 2 to 10 percent. Hence, with estimated uncertainty of 0.1 percent in the measurement of the total heat capacity (figs. 7 and 8), the agreement between the smoothed observed heat capacity and that of Furukawa et al., was remarkable. If the sample vessel were loaded with an appropriate amount of a typical glass, e.g., vitreous sodium tetraborate [19], the precision and accuracy should be markedly improved due to the more favorable

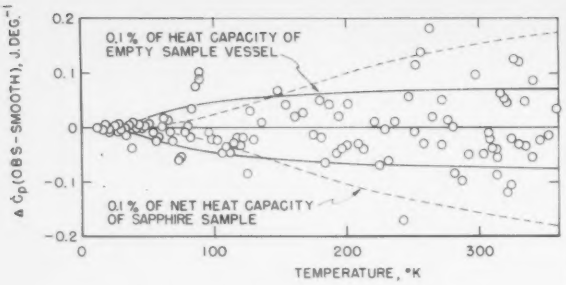

FIGURE 7. *Heat capacity of empty sample vessel, deviations of experimental data from a smooth curve.*

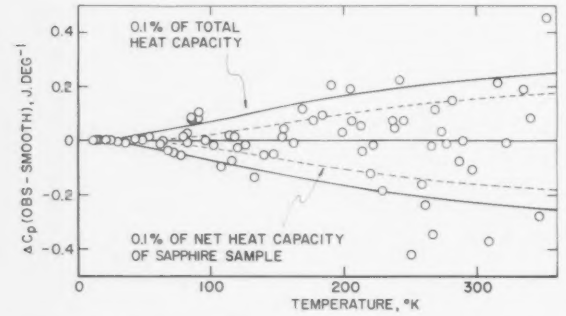

FIGURE 8. *Heat capacity of loaded sample vessel, deviations of experimental data from a smooth curve.*

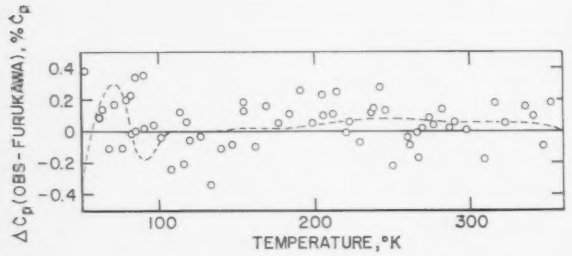

FIGURE 9. *Deviation of observed heat capacity of synthetic sapphire from the data of Furukawa et al.* [8]

contribution from the empty sample vessel toward the total heat capacity of the loaded vessel.

It was found that the EMF selector switch of the double potentiometer was of the "make-before-break" type, such that during the switching operation a shunt of very low resistance was effectively put across either the thermometer or the heater during temperature or power measurements respectively. Thus, a portion of the experimental error might be attributed to either the resulting upsetting of the steady-state of the thermometer current or inaccuracy in the evaluation of energy input. In some of the later runs of the loaded calorimeter vessel, by means of a different voltage divider arrangement, this type of error was minimized in the power measurement. However, these data points showed

TABLE 3. *Heat capacities of synthetic sapphire*

T	C_p	T	C_p
°K	J/deg/mole	°K	J/deg/mole
10	0.010	190	47.54
20	.067	200	51.16
30	.246	210	54.63
40	.674	220	57.96
50	1.487	230	61.14
60	2.782	240	64.18
70	4.595	250	67.07
80	6.904	260	69.81
90	9.670	270	72.42
100	12.83	280	74.89
110	16.32	290	77.23
120	20.06	300	79.45
130	23.96	310	81.56
140	27.96	320	83.55
150	31.99	330	85.44
160	36.00	340	87.22
170	39.94	350	88.92
180	43.80	360	90.52

scattering of the same order as the others. Hence, the deviation produced by the usual fast switching operation of the double potentiometer was assumed to be less than 0.1 percent. Nevertheless, experimental error resulting from this source could be completely eliminated by changing the switching arrangements to a "break-before-make" type [20]. Other possible sources of systematic error are being investigated.

6. References

[1] E. F. Westrum, Jr., J. B. Hatcher, and D. W. Osborne, J. Chem. Phys. **21,** 419 (1953).
[2] R. A. Ruehrwein and H. M. Huffman, J. Am. Chem. Soc. **65,** 1620 (1943).
[3] H. M. Huffman, Chem. Rev. **40,** 1 (1947).
[4] T. M. Dauphinee, D. K. C. McDonald, and H. Preston-Thomas, Proc. Roy. Soc. **221A,** 167 (1954).
[5] G. T. Furukawa and M. L. Reilly, publication pending.
[6] G. E. Gibson and W. F. Giauque, J. Am. Chem. Soc. **45,** 93 (1923).
[7] G. S. Parks, S. B. Thomas, and D. W. Light, J. Chem. Phys. **4,** 64 (1936).
[8] G. T. Furukawa, T. B. Douglas, R. E. McCoskey, and D. C. Ginnings, J. Res. NBS **57,** 67 (1956) RP2694.
[9] J. A. Morrison and D. Patterson, Trans. Faraday Soc. **52,** 764 (1956).
[10] J. W. Edwards and G. L. Kington, Trans. Faraday Soc. **58,** 1313 (1962).
[11] E. C. Kerr, H. L. Johnston, and N. C. Hallett, J. Am. Chem. Soc. **72,** 4740 (1950).
[12] J. C. Southard and R. T. Milner, J. Am. Chem. Soc. **55,** 4384 (1933).
[13] R. B. Scott, C. H. Meyers, R. D. Rands, Jr., F. G. Brickwedde, and N. Bekkedahl, J. Res. NBS **35,** 39 (1945).
[14] R. L. Powell, M. D. Bunch and R. J. Corruccini, Cryogenics **1,** 139 (1961).
[15] H. F. Stimson, J. Res. NBS **65A,** (Phys. and Chem.) No. 3, 139 (1961).
[16] H. J. Hoge and F. G. Brickwedde, BS J. Res. **22,** 351 (1939).
[17] G. T. Furukawa and M. L. Reilly, publication pending.
[18] F. N. Rhines, W. M. Urquhart and H. R. Hoge, Trans. Am. Soc. Metals **39,** 69 (1947).
[19] E. F. Westrum, Jr., and G. Grenier, J. Am. Chem. Soc. **79,** 1799 (1957).
[20] G. T. Furukawa and S. S. Chang (to be published).

(Paper 69C1–181)

JOURNAL OF RESEARCH of the National Bureau of Standards—C. Engineering and Instrumentation
Vol. 69C, No. 1, January-March 1965

A Rugged Null-Type Pressure Transducer of High Reproducibility for Accurate Gas Phase PVT Measurements*

Meyer Waxman and William T. Chen

(July 31, 1964)

A rugged and highly reproducible null-type transducer for accurately determining the equilibrium pressure between a Burnett PVT apparatus for gases and a counterbalancing pressure system is described. The transducer, closely coupled to the PVT sample volume, is used at temperatures from 0 to 175 °C and over the pressure range 4 to 250 atm. The transducer basically consists of a metallic diaphragm as the pressure responsive element, a stable capacitance sensor for detecting minute deflections of the diaphragm, and spherical concave backing surfaces with a sagitta of 0.001 in. and a chord of 0.937 in. for supporting the diaphragm against excessive pressure imbalances. The diaphragm is 0.001 in. thick, plane and circular with an effective deflection diameter of 0.937 in., and prestressed to reduce appreciably inelastic factors. The reproducibility of the null after the transducer has been subjected to unidirectional pressure overloads as large as 135 atm is within ±0.1 mm Hg. For pressure imbalances less than 1 atm and transducer pressures of 1 atm or less, the reproducibility is within 9×10^{-3} mm Hg, which is the equivalent resolution of the capacitance circuitry. The maximum uncertainty in the null for transducer pressures varying from 4 to 250 atm is, respectively, 0.003 to 0.00004 percent. The maximum uncertainty in the constancy of the transducer volume is 7×10^{-5} cm³ and contributes a maximum error of 0.0003 percent in the constancy of the sample PVT volume. General requirements, design considerations, and factors which limit the reproducibility of the transducer null are discussed. Detailed performance data at 25 °C are given.

1. Introduction

In an experimental PVT program for corrosive gases being conducted at the National Bureau of Standards, the coupling of the sample volume to the pressure-measuring instrumentation presented several problems. Ideally, the coupling should not affect the accuracy of the pressure measurements and should confine the gas to the sample volume. Correcting for the effect of extraneous volumes introduced through the coupling is difficult, and can result in significant errors, particularly if the temperatures of the extraneous volumes are lower than the temperature of the sample volume. In addition, the corrosive nature of the gases makes it desirable to isolate the gas from the pressure-measuring instrumentation so as to prevent possible chemical reaction of the gas with materials usually used in pressure gages. These general requirements suggested the use of a null-type transducer closely coupled to the sample volume and utilizing a circular plane or corrugated diaphragm as the gas separator and also as the pressure-responsive element [1, 2, 3].[1] If the transducer is thermostated at the temperature of the sample volume, the extraneous volume introduced, particularly if small, should have a negligible effect on the evaluation and constancy of the sample volume.

In the projected application of the transducer, the pressure of the sample gas acting on one side of the diaphragm is counterbalanced by an auxiliary gas system whose pressure is measured by a piston gage or a manometer. A pressure imbalance across the diaphragm deflects it, and this deflection is detected on the counterbalancing side of the diaphragm by an electrical capacitance method.

The first application of the transducer was to be in a Burnett apparatus [4] which imposed additional requirements. Through this apparatus, isotherms are derived for experimental pressures from 4 to 250 atm and over the temperature range 0 to 175 °C. The required precision of the pressure measurements was 1 part in 30,000, which is equivalent to 0.1 mm Hg for a gage pressure of 3 atm. The Burnett procedure consists of an iterative process of expanding the gas from a sample chamber into a previously evacuated auxiliary chamber. Pressure measurements are made before and after each expansion with a suitable time allowance for equilibration. If a diaphragm with the required sensitivity is used, the step-wise expansion results in a pressure imbalance many times greater than the elastic-pressure range of the diaphragm, whether plane or corrugated. Thus, the deflection of the diaphragm has to be limited, as excessive pressure imbalances would stretch it beyond its elastic limit, resulting in rupture or adverse effects on the reproducibility of the diaphragm null position.

At the time this problem was being considered, a survey of the available literature did not disclose a design or instrument that would satisfy the requirements discussed above. Thus the design of transducer prototypes was considered for both the plane and corrugated types of diaphragm transducer.

*This work was supported in part by the Division of Research, Atomic Energy Commission.

[1] Figures in brackets indicate the literature references at the end of this paper.

The reproducibility of the diaphragm null position for both types is affected by the elasticity of the diaphragm material and the stress anisotropy in the diaphragm. In the plane diaphragm, localized stresses or buckled areas can result in snap-action characteristics ("oil-canning") of the diaphragm, that is, with a changing pressure, the diaphragm has a sudden and discontinuous change of deflection. The shape, magnitude, and pressure characteristics associated with this deflection may vary considerably. Stress anisotropy can originate in the blank material or develop when the plane diaphragm is clamped to effect its pressure seal. The adverse effects of this anisotropy on performance can be eliminated or reduced appreciably by radial prestressing of the diaphragm. In the corrugated diaphragm, stress anisotropy in the blank material is eliminated in the forming and heat treatment process, and that introduced from the clamping process has generally a negligible effect on the performance of the diaphragm.

For the corrugated type of diaphragm, its protection against excessive pressure imbalances (overload protection) can be accomplished in one direction with the die used in forming the diaphragm as a backing plate. The fabrication of a backing plate for the opposite direction is considered to be difficult but not insurmountable. For the plane type of diaphragm, spherical concave backing plates can be fabricated to the approximate configuration of the diaphragm for a specified deflection [5]. A capacitance sensor for detecting minute deflections of the diaphragm can be fabricated as part of the backing plate for both types [5].

In addition to the overload protection feature, other important design considerations are the pressure-deflection characteristics, particularly the sensitivity at the diaphragm null position, and the elastic-pressure range. In a plane diaphragm with its edge completely fixed, the pressure-deflection characteristics depend on the magnitude of the radial prestressing. If the prestressing and the central deflections are small, the pressure-deflection relationship is that of a thin disk with the effect of prestressing included [6]. If the prestressing is increased sufficiently, however, the bending stress in the diaphragm becomes negligible relative to the applied radial stress, and the diaphragm characteristics can be considered as approximating those of a membrane. The pressure-deflection characteristics of the corrugated type of diaphragm have been evaluated in terms of the mechanical properties of the diaphragm material, its thickness, and its geometry, such as the spacing, depth, and number of convolutions [7, 8]. For small deflections of either type of diaphragm fabricated from the same material and having the same thickness and free diameter, the maximum sensitivity obtainable is greater for the plane type than it is for the corrugated type.

The development of transducer prototypes had as its objective the attainment of an easily fabricated design that satisfied the specified requirements. Because of previous experience with the plane type, it

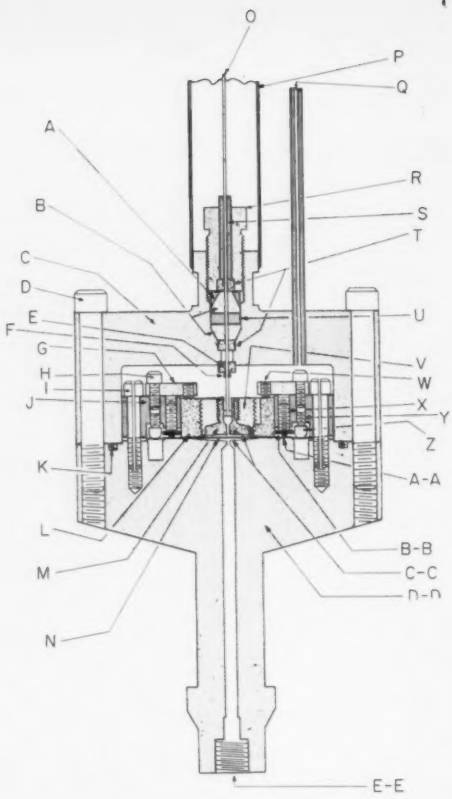

FIGURE 1. *Cross section of transducer model II.*

A. Follower, steel
B. Extrusion rings, lava stone
C. Top, nickel
D. Clamping bolts for pressure seal K
E. Ring, ceramic
F. Electrode stop, silver brazed bead
G. Clamping ring for capacitance sensor assembly, nickel
H. Inner clamping screws for clamping ring G
I. Outer clamping screws for clamping ring J
J. Clamping ring
K. V-ring, Teflon-coated Monel
L. Capacitor housing, nickel
M. Capacitor plate, nickel
N. Diaphragm, Monel
O. Capacitor lead, drill rod
P. Electrical and oil shield, Monel
Q. Counterbalancing gas inlet tube, nickel
R. Packing gland nut, steel
S. Electrical insulating sleeve, Teflon
T. Extrusion rings, ceramic
U. Packing ring, Teflon
V. Epoxy cement (insulator)
W. Thrust screws for clamping capacitance sensor assembly
X. Thrust screws for diaphragm pressure seal A-A
Y. Thrust screws for stressing diaphragm N
Z. Stressing ring, nickel
A-A. Diaphragm seal
B-B. Diaphragm sealing ring, ridge height—0.003 in., tool steel—50 RC
C-C. Diaphragm backing surfaces
D-D. Base
E-E. Sample gas port

was selected for the basic design of the transducer. Two models based on this design were fabricated. The second model, II, is shown in figure 1 with exploded views in figures 2, 3, and 4. In the first and earlier model, preferred initially for its smaller o.d., the pressure characteristics satisfied the requirements; however, the pressure seals were not effective over the required temperature range of 0 to 175 °C. The second model, fabricated after the first was thoroughly tested, was comparatively easier to fabricate and to seal effectively. This model has proven to be quite satisfactory and it is currently being used.

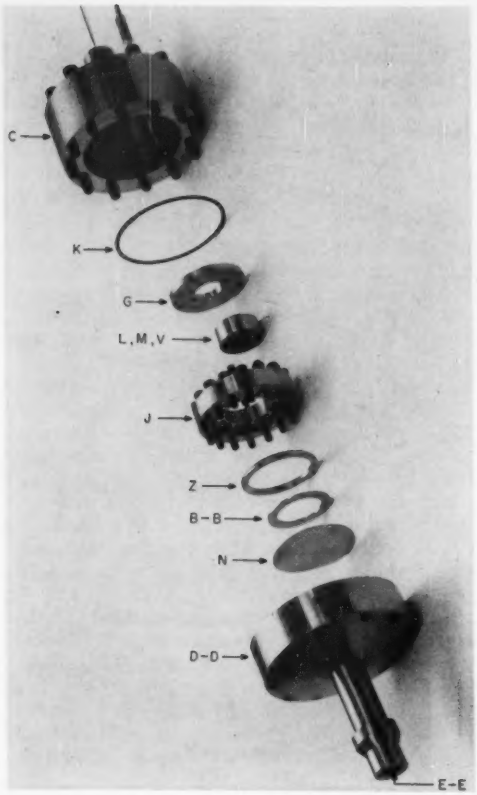

FIGURE 2. *Exploded view of transducer.*

See figure 1 legend.

2. Description and Installation of Components

2.1. Transducer

The model II transducer (see fig. 1) basically consists of the prestressed diaphragm N as the pressure responsive element, the capacitance sensor assembly (L, M, and V) for detecting deflections of the diaphragm, and the diaphragm backing surfaces C–C incorporated as part both of the base D–D and of the capacitance sensor assembly. This assembly is clamped in position by the use of the thrust screws W and the clamping ring G, which is first clamped to the clamping ring J by means of the inner clamping screws H. The clamping force exerted on this latter clamping ring (J) through the tightening of the outer clamping screws I is considerably greater than that of the total opposing thrust forces developed in stressing the diaphragm, effecting the diaphragm pressure seal, and clamping the capacitance sensor assembly. The base and the top C clamped together through the use of the clamping bolts D constitute the pressure housing which is designed to withstand pressures up to 500 atm without excessive deformation. The external pressure seals consist of the

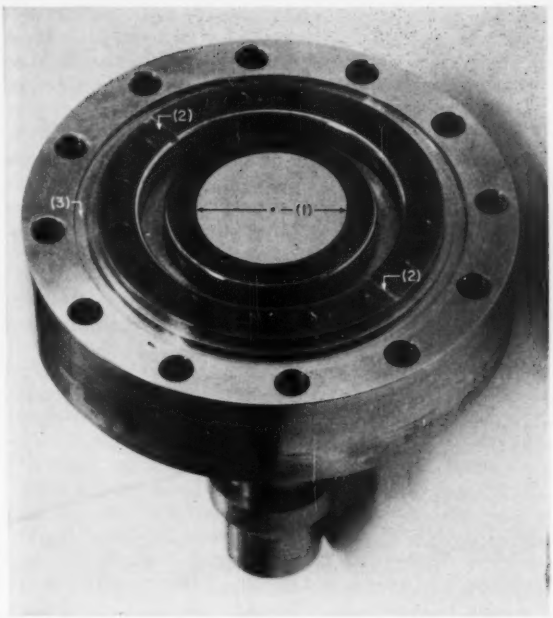

FIGURE 3. *Base of transducer showing (1) spherical concave backing surface, (2) grooves to facilitate pressure equilibrium, and (3) groove for the v-ring pressure seal.*

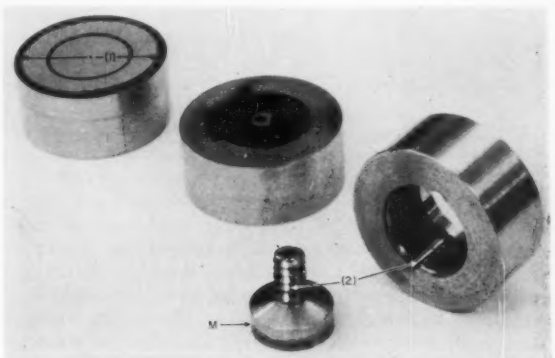

FIGURE 4. *Three views of capacitance sensor assembly (L, M, V) showing (1) spherical concave backing surface, and (2) threaded and slotted bonding surfaces to enhance the mechanical support of the capacitor plate.*

v-ring K clamped between the top and the base, and the Teflon packing ring U which is compressed for sealing the capacitor lead O. The lower reduced section of the base is designed for coupling the transducer to a Burnett apparatus [4]. The sample gas inlet is through the port E–E to the bottom side of the diaphragm, and the counterbalancing gas inlet is through the tube Q to the top side of the diaphragm. To facilitate the equilibrium of gas pressure on the top side, there is an axial hole in each of the outer clamping screws and two grooves

between the v-ring circular groove and the circular groove beneath the stressing ring (see fig. 3). Most of the transducer components are fabricated from commercial grade A nickel to resist gas corrosion.

2.2. Capacitance Sensor Assembly and Detector

A deflection of the diaphragm is detected electrically by a corresponding change of the capacitance between the capacitor plate M and the diaphragm (see fig. 1). The capacitor plate is electrically insulated and mechanically supported by the epoxy cement V between the capacitor plate and the capacitor housing L. This capacitance sensor assembly is positioned and clamped after the diaphragm has been installed.

The capacitance sensor assembly is designed so that it is fabricated easily and yet provides adequate mechanical support for the capacitor plate without introducing an excessive residual capacitance. The mechanical support is derived primarily from (1) the strength of the adhesive bond between the epoxy cement and the metallic components and (2) the shear strength of the epoxy cement in the threaded and slotted regions of the capacitor plate and the capacitor housing (see fig. 4). The adhesive bond alone is not sufficient to provide the necessary mechanical support. The threads and slots provide, respectively, translational and rotational support of the capacitor plate. The latter support is necessary for the final lathe machining of the assembly. The epoxy cement retains its physical stability up to 225 °C and has a temperature coefficient of expansion of 15×10^{-6} per °C, comparable to that of the capacitor housing and capacitor plate fabricated from nickel. The residual capacitance of this assembly is 10 pF.

The transducer capacitance, consisting of the residual capacitance and that between the capacitor plate and the diaphragm, constitutes one arm of a capacitance bridge. The bridge also has a variable capacitance arm, and two large and nearly equal capacitance ratio arms. The capacitor plate is coupled via the capacitor lead to a double shielded coaxial cable connected to the bridge. The effect of variations in cable capacitance on the bridge balance is reduced appreciably by shunting the capacitance between the inner shield and the central lead across a ratio capacitor. The capacitance between the inner shield and the outer shield at ground potential is shunted across the output of the bridge, and variations in it affect only slightly the sensitivity of the bridge circuit. A deflection of the diaphragm unbalances the capacitance bridge. The unbalanced signal is amplified, phase detected, and indicated on a 100–0–100 microammeter. The capacitance stability of the bridge circuitry exclusive of the transducer is 0.03 pF, which is the minimum change of capacitance detectable with the bridge voltage (0.4V) and the amplification being used. The potential difference between the diaphragm and the capacitor plate is sufficiently small for the effect of the associated electrostatic attraction to be negligible in the performance of the transducer.

2.3. Diaphragm Backing Surfaces

Diaphragm displacement is limited on each side by both the plane and spherical concave backing surfaces which were optically lapped. The nominal values of the sagitta and the chord of the spherical concave backing surface are 0.001 in. and 0.937 in., respectively (the corresponding radius of curvature is 9.2 ft). This chord is the effective diameter of the diaphragm area in which deflections can occur. The 0.001 in. central separation results in a capacitance of 49 pF between the capacitor plate and the diaphragm. Closer spacing may cause electrical shorting of the capacitor plate since minute dimples develop in the diaphragm after some usage. For pressure imbalances greater than the equivalent of 0.001 in. central deflection of the diaphragm, the diaphragm is supported by a backing surface and the diaphragm stresses remain within the elastic limits. The magnitude of permissible pressure imbalance is governed by both the rigidity of the backing surfaces and the stress developed in the unsupported sector of the diaphragm (central 0.014 in. diameter) when it is deflected against a backing surface. The pressure imbalance which the capacitor plate will support without affecting significantly the transducer performance is generally limited to 5 atm, although it has been exceeded a few times by a factor of 3 to 8. The pressure imbalance applied against the base can be considerably greater and has at times been as great as 135 atm.

2.4. Pressure Seals

In model I, the seal consisting of a toroidal copper ring clamped between the top and the base leaked above 150 °C, even though considerable clamping force was exerted on the ring. The difference in the temperature coefficient of expansion between the metals of the seal or the plastic flow of the copper ring may have been the cause for the leakage. In model II, a commercial Teflon-coated Monel v-ring (K) replaces the copper ring and has proven to be very satisfactory. The transducer can be disassembled and assembled many times and the same seal is still effective for the operating range of pressures and temperatures. In the application of the v-type of seal, the v-ring is compressed slightly by the clamping of the base to the top to produce a line-contact with both surfaces bearing on it. The sealing process is then enhanced by the internal pressure acting against the inner surface of the v-ring.

The diaphragm seal A–A which isolates the sample gas from the counterbalancing gas is effected by the thrust of the diaphragm sealing ring B–B against the diaphragm and the base. This thrust, obtained by tightening thrust screws X, must be sufficient to deform either the sealing surface of the diaphragm or that of the base. The method used for testing this seal is to overpressure the transducer on the top side and check for gas leakage on the bottom side by means of an accumulative technique with a commercial leak detector.

Different commercial seals basically similar to the seal used in model II (fig. 1, A, B, T, U) were tried for the capacitor lead seal. Generally these leaked when either Teflon or lava stone was used as the packing material. Teflon is more effective than lava stone for sealing in this type of seal; however, the Teflon must be supported completely. If a minute unsupported area exists, the Teflon extrudes through this area at about 150 °C for the maximum operating pressures. In the capacitor lead seal (model II), the Teflon packing ring is backed completely by lava stone extrusion rings B, and these in turn are backed by ceramic extrusion rings T. There is a clearance of about ± 0.002 in. on the o.d. and i.d. of the ceramic extrusion rings. A slight tightening of the packing gland nut R which bears against this sealing assembly is sufficient to obtain a seal. A bead F, silver brazed on the capacitor lead, and bearing against the ceramic ring E, acts as a stop for the capacitor lead and prevents it from being blown out.

2.5. Installation of the Diaphragm

Initially, the subassembly consisting of the clamping ring (J), stressing ring Z, diaphragm sealing ring (B–B), and the diaphragm (N), is positioned concentric with the axis of the base (D–D) after which the clamping ring (J) is clamped firmly to the base. This clamping adequately holds the edge of the diaphragm between the clamping ring and the base, and allows for radial stressing of the diaphragm without slippage at the outer edge. The stressing, accomplished by tightening the thrust screws Y against the stressing ring (which in turn exerts a thrust on an annulus of the diaphragm), draws the diaphragm downward over the rounded corners of the groove beneath the stressing ring. The thrust screws (consisting of eight 4–40 cap set screws) require only a very gentle torque to provide the necessary stressing thrust.

Before effecting the diaphragm seal, the diaphragm is stressed slightly by tightening all the thrust screws to remove generalized distortions. Localized distortions are usually eliminated by the additional tightening of the appropriate thrust screws. Distorted sectors can readily be detected from any movement caused by gentle pressure on the diaphragm at small selected areas over the plane part of the backing surface. Clamping of the diaphragm to effect its seal generally results in severe distortion of the diaphragm, particularly if slight distortions already exist in the diaphragm blank. These distortions are eliminated, or the subsequent adverse effects are reduced appreciably, by gradually and intermittently increasing the clamping pressure and adjusting the diaphragm stress on a selected area basis. This method results in a highly reproducible null position of the diaphragm and eliminates the adverse effects discussed in section 1.

2.6. Fabrication of the Diaphragm

The diaphragm, 1.90 in. in diameter and 0.001 in. thick, is fabricated from rolled Monel sheet stock, 0.001 in. thick and 4 in. wide. Different fabricating techniques, such as cutting with scissors, punching, and lathe machining, were tried. Of these, the machining technique developed fewer distortions in the diaphragm and proved most expedient. Several diaphragms should be prepared at one time. In this operation, about 20 square blanks separated from each other by 0.004 in. thick paper, and clamped together between expendable pressure plates mounted in a lathe, are machined to the required diameter. Approximately 25 percent of each lot is thus obtained relatively free of dimples or distorted areas and is therefore acceptable as diaphragms.

3. Performance

Early in the experimental use of the transducer there was concern with hysteresis of the diaphragm or other effects such as "oil-canning" which could affect the null position of the diaphragm. This problem is circumvented by confining any pressure overloading greater than a few atmospheres to the direction of the base, and overloading slightly the diaphragm towards the base prior to the final balancing of the gas pressures on both sides of the diaphragm. This procedure of using the unidirectional pressure behavior of the diaphragm eliminates or reduces appreciably the effect of bidirectional differences, if any, on the null position of the diaphragm.

Since the magnitude of the radial prestressing of the diaphragm varies from one diaphragm installation to another, the associated pressure imbalance versus bridge imbalance characteristics will vary also. In figure 5, a pressure imbalance versus Δ (bridge balance) graph, obtained at 25 °C and 1 atm, is shown for each of two diaphragm installations, one having the maximum sensitivity (diaphragm 1) and the other, the minimum sensitivity (diaphragm 2) encountered to date. By means of these graphs and a 0.03 pF capacitance bridge resolution, the transducer resolution for the null condition is 9×10^{-3} and 3×10^{-3} mm Hg, respectively, for diaphragms 1 and 2. This resolution is equivalent to an average diaphragm deflection over the capacitor plate of 5×10^{-7} in. (1×10^{-5} mm). The pressure range for which the deflection of the diaphragm is not restrained by either of the backing surfaces is generally about ± 1 cm Hg. This range is sufficient to counterbalance conveniently and accurately the sample gas pressure for pressures up to 250 atm [4].

The transducer null is affected by temperature and pressure changes. Experiments, in a special test rig, independent of the transducer indicated that this effect manifests itself primarily as a positional change of the *capacitor plate* relative to the diaphragm. It was found that a temperature change from 22 to 110 °C would change the transducer

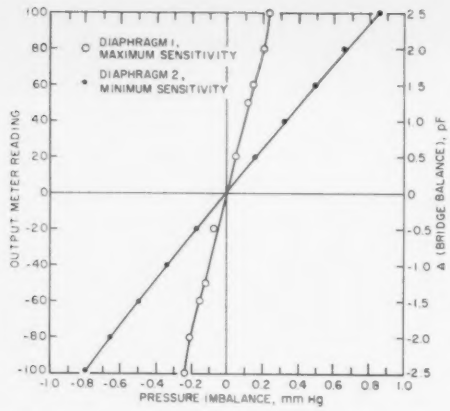

FIGURE 5. *Pressure-deflection characteristics of the transducer (obtained at 25 °C and 1 atm).*

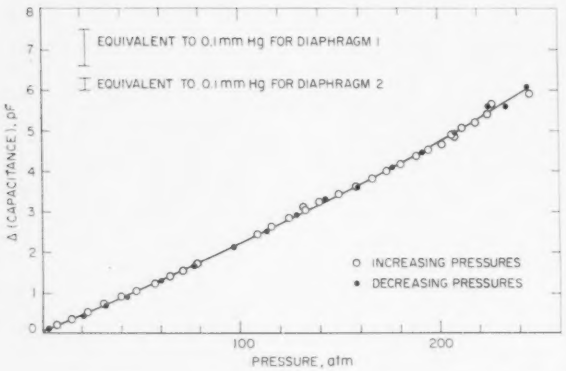
EQUIVALENT TO 0.1 mm Hg FOR DIAPHRAGM 1
EQUIVALENT TO 0.1 mm Hg FOR DIAPHRAGM 2
Δ (CAPACITANCE), pF
O INCREASING PRESSURES
• DECREASING PRESSURES
PRESSURE, atm

FIGURE 6. *Pressure effect on transducer capacitance for null condition (obtained at 25 °C)*

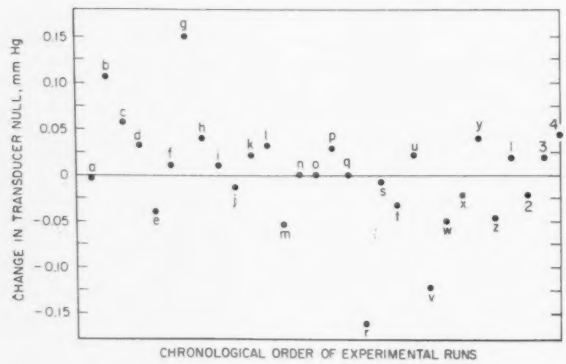

FIGURE 7. *Stability of transducer null (obtained at 25 °C and 1 atm).*

See table 1 for identification of the points.

null at 1 atm by the equivalent of 1.4 pF. For an isothermal application as mentioned in section 1, the temperature variation is within ±0.01 °C and results in a maximum pressure error of 5×10^{-5} mm Hg. This variation is smaller by a factor of two hundred than the detectable minimum pressure imbalance. An investigation of the pressure effect from 22 to 200 °C indicated that this effect can be determined to within ±0.1 mm Hg. Pressure effects on the transducer null are compensated by changing the bridge balance according to a typical calibration graph (obtained at 25 °C) as shown in figure 6. This graph was obtained with both sides of the transducer connected to a common gas source.

In the experimental procedure used with the Burnett apparatus, the transducer null at 1 atm is checked after the completion of the lower pressure measurements at the end of an experimental run. Stability test results (obtained at 25 °C), accumulated over a period of 4 months for different gases on the sample side of the diaphragm, are shown in figure 7. The changes can be attributed to pressure overloading, which may change the null positions of both the diaphragm and the capacitor plate. The occasional changes outside of the range ±0.1 mm Hg may be the result of excessive pressure imbalance against the capacitance sensor assembly. For present pressure measurements below 15 atm, the measurements are corrected for the pressure change in the transducer null obtained after the completion of an experimental run, when this change is greater

TABLE 1. *Experimental runs showing data used for points in figure 7*

Point	Maximum transducer pressure	Maximum pressure imbalance against the base	Sample gas
	atm	*atm*	
a	46	21	He
b	136	57	Ar
c	36	15	He
d	186	82	Ar
e	190	82	Ar
f	238	105	Ar
g	235	107	He
h	208	94	He
i	207	82	He
j	216	100	He
k	158	71	He
l	235	(*)	Ar
m	238	105	Ar
n	207	88	Ar
o	170	73	Ar
p	47	21	He
q	200	100	BF_3
r	232	129	BF_3
s	173	75	BF_3
t	46	21	He
u	47	21	He
v	144	54	BF_3
w	120	38	BF_3
x	130	45	BF_3
y	214	113	BF_3
z	125	41	BF_3
1	157	34	BF_3
2	190	64	BF_3
3	27	12	He
4	27	12	He

*run discontinued.

than 0.0014 percent. For pressure measurements above 15 atm, this correction is not made as its effect in the Burnett method becomes small compared to other errors.

Some experimental pressure measurements with the transducer have been made at or below 1 atm. At the completion of these measurements, the transducer null at 1 atm was checked and the offset from the null was found to be of the same magnitude as the equivalent resolution of the capacitance bridge (about the equivalent of 9×10^{-3} mm Hg).

The volume enclosed by the diaphragm and the spherical concave backing surface of the base is part of the sample volume [4]. Therefore, an uncertainty in the diaphragm null position must be considered as it affects the constancy of the sample volume. The volume of either concave enclosure is 0.006 cm^3 which, in the Burnett apparatus, represents 0.02 percent of the sample volume. An uncertainty in the diaphragm null position equivalent to 0.1 mm Hg would change the enclosure volume by a maximum of 7×10^{-5} cm^3, or about 0.0003 percent of the sample volume. In the Burnett method [4] the effect of this volume uncertainty is negligible compared to that of errors in the pressure measurements obtained with the piston gage.

The authors express their appreciation to Philomain Dery and Hans Mend for their skilled fabrication of the instrument and to Miss P. Naecker for her editorial advice.

3. References

[1] E. S. Burnett, Compressibility determinations without volume measurements, J. App. Mech. **58,** A136–140 (1936).

[2] D. White and J. Hilsenrath, Pressure-sensitive diaphragm type null detector, Rev. Sci. Instr. **29,** 648–651 (1958).

[3] A. Michels, T. Wassenaar, and Th. N. Zwietering, The experimental determination of the equation of state data of gases at temperatures between 0 °C and −180 °C, Physica **XVIII,** No. 1, 67–74 (1952).

[4] M. Waxman, W. T. Chen, and J. Hilsenrath, A Burnett apparatus for compressibility measurements on corrosive gases for pressures to 240 atm and temperatures from 0 to 175 °C (to be published).

[5] H. F. Stimson, Precision Resistance Thermometry and Fixed Points, American Institute of Physics, Temperature, Its Measurement and Control in Science and Industry (Reinhold Publishing Corporation, New York, 1955), Vol. **II,** 166–167.

[6] A. A. Griffin, The theory of pressure capsules, British A. R. C., R and M No. 1136 (1927).

[7] W. A. Wildhack, R. F. Dressler, and E. C. Lloyd, Investigations of the properties of corrugated diaphragms, Trans. Am. Soc. Mech. Engrs. **79,** 65–82 (1957).

[8] F. B. Newell, Diaphragm Characteristics, Design and Terminology (ASME, New York, 1958).

(Paper 69C1–182)

JOURNAL OF RESEARCH of the National Bureau of Standards—C. Engineering and Instrumentation
Vol. 69C, No. 1, January–March 1965

Detection and Damping of Thermal-Acoustic Oscillations in Low-Temperature Measurements

David A. Ditmars and George T. Furukawa

(June 8, 1964)

The spontaneous thermal-acoustic oscillations in nonisothermal columns of helium, hydrogen, nitrogen, argon, and oxygen gas have been investigated. The pressure fluctuations were measured with a barium titanate transducer and the particle displacements observed by a smoke technique. The observed pressure oscillations were often nonsymmetrical and of sufficient amplitude to indicate the necessity for a nonlinear approach in a theoretical treatment of the oscillations. An adjustable "Helmholtz resonator" attached at the warm end of the oscillating column was found to damp completely the oscillations and eliminate the energy transfer which they caused.

1. Introduction

Spontaneous pressure oscillations in gaseous columns, along which there is a temperature gradient, often hamper cryogenic work. An excellent review of this oscillation phenomenon has been given by Wexler [6].[1] While there are at least three reports of such oscillations having been used to advantage [1,2,3], they are most often undesirable. They can introduce errors in vapor-pressure measurements and sometimes make the measurements impossible to obtain [1,4]. Frequently, the oscillations cause a large uncontrollable energy transfer from hot to cold regions, making calorimetric measurements difficult or impossible.

Experience gained with a calorimeter at the National Bureau of Standards confirmed Wexler's observation [6] that the energy transfer due to gas oscillation from the room temperature region to the 4 °K region can be as much as 1000 times greater than the energy transfer by thermal conduction. It was decided to investigate the possibility of damping the oscillations by some device added externally.

Experiments with a simple auxiliary apparatus showed this solution to be promising. This apparatus was then used to investigate further the factors affecting the cause and suppression of the oscillations. In the course of this investigation, an adjustable "Helmholtz resonator" attached at the warm column end proved to be a reliable and effective damper.

2. Apparatus

The auxiliary apparatus shown in figure 1 consists basically of a tube T extending down into a Dewar containing a cryogenic liquid boiling at atmospheric pressure. The lower end of the tube T was always open and the upper end was closed by a pressure transducer and a device used to suppress the gaseous oscillations.

The Dewar, of two-liter capacity, was generally used with less than a liter of liquid. When the liquid was helium, the Dewar was immersed in a liquid nitrogen bath.

Temperatures along the tube T were occasionally measured with thermocouples. Typical temperature gradients along the tube ranged from 1 to 2 °C per mm when the Dewar contained 1 liter of liquid. The only means of changing the temperature gradient along the tube was to add or withdraw cryogenic liquid in the Dewar, keeping the same apparatus dimensions.

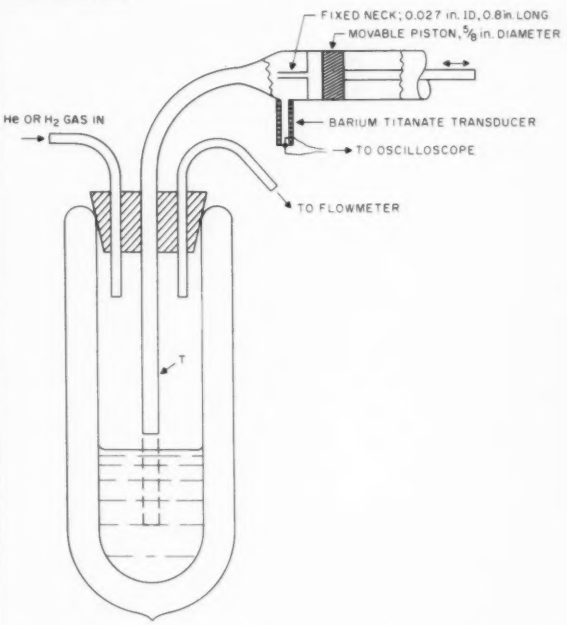

FIGURE 1. *Auxiliary apparatus for studying thermal-acoustic oscillations.*

[1] Figures in brackets indicate the literature references at the end of this paper.

A barium titanate tube, cemented onto the upper end of T, served as a pressure transducer. This transducer (2 in. long, ⅜ in. o.d. with a 1/16 in. wall) was silvered on the inside and outside and polarized through the wall thickness. A static pressure calibration showed that the transducer had a sensitivity of 7 mV/torr[2] differential pressure across its walls. This potential was measured with a vibrating reed electrometer and was a linear function of pressure in the range covered, 0 to 30 torr. The sensitivity should be independent of frequency at the low frequencies involved in these experiments (less than 60 Hz). The transducer output was fed directly to a sensitive oscilloscope. Because of the low impedance of the oscilloscope, the trace, at low frequencies (2 to 10 Hz), represented more nearly the time derivative of the average pressure fluctuations inside the transducer than the pressure itself. Additional circuitry or a dynamic calibration of the transducer-oscilloscope system would be necessary to interpret the trace directly as a pressure at low frequencies.

Some direct visual observations of the wave motion were made when T was a glass tube by introducing a smoke of finely divided TiO_2 particles into the tube. In the case of oscillations over liquid helium, that part of the energy dissipated in the liquid by the oscillating gas column was measured by passing the gas evolved from the Dewar through a flowmeter.

Pressure and net mass flow of gas in the tube were not controlled in these experiments. The mean pressure in the tube was always within a few torr of atmospheric and the net gas flow in the tube was zero. This is not to imply that oscillations occur only under these conditions. For instance, in the calorimeter referred to above, oscillations have been detected at pressures below 400 torr and also in tubes through which a net helium gas flow existed.

3. Results

3.1. Generation and Observation of Oscillations

The literature contains only references to oscillations in helium or hydrogen gas columns over baths of liquid helium or hydrogen, respectively. The present work has shown the phenomenon to be of a more general nature. For instance, gaseous columns can also be made to oscillate over baths of liquid nitrogen or oxygen. Columns of helium, hydrogen, nitrogen, argon, or oxygen gas were readily made to oscillate over a liquid oxygen bath. Evaporation caused by oscillation energy transfer to nitrogen or oxygen baths in the present experiments was small and could not be distinguished from evaporation due to other sources of heat leak to the baths. Two conditions had to be met, however, for the oscillations to occur with the higher temperature baths: (a) The open tube end had to extend several tube diameters beneath the bath surface, and (b) the Dewar volume above the surface had to be flooded with helium or hydrogen gas. This

[2] 1 torr = 1/760 normal atmosphere = 133.322 N/m².

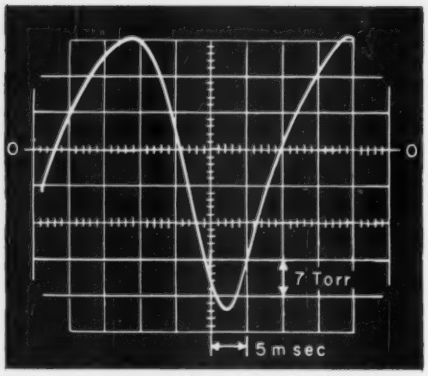

FIGURE 2. *Pressure oscillation at closed end of He gas column.*
Open end 1.5 cm above liquid He surface. "O" indicates sweep position without oscillation.

is in distinction to helium or hydrogen gas columns which oscillate in tubes whose open end is either above or below the surface of a liquid helium or hydrogen bath respectively. Probably the most important effect of the flooding was the increase in the surface heat-transfer coefficient [14] at the exterior tube wall. This also altered the bath composition and the tube temperature gradient. Experiments performed, in which these latter effects were eliminated or produced independently of any change in the heat transfer coefficient, showed that helium or hydrogen gas had to be present for oscillations to be sustained.

To obtain a column of a gas other than that of the bath species, the tube T, removed from the Dewar, was first flushed by introducing the desired gas through an opening in the upper tube end. The tube was then lowered into the Dewar until its lower (open) end was beneath the bath surface and the gas flow gradually reduced to zero. This procedure was followed, for instance, to obtain a column of helium gas above liquid nitrogen. The amplitude and period of the ensuing oscillation were recorded as soon as they reached stable values in order to minimize the effect of contamination of the helium gas column with nitrogen. The observed frequency was always several times that of a nitrogen gas column oscillating under the same condition—as much as eight times in one instance. By way of comparison, a similar gas column resonating in its lowest acoustic mode with helium would normally exhibit a frequency which is about three times that when resonating with nitrogen in the same mode. A helium column oscillating with the open tube end below the bath surface displayed approximately equal frequencies with baths of helium or nitrogen though the amplitude over the helium bath was several times that over the nitrogen bath.

At low amplitudes the pressure oscillations appeared sinusoidal, but with either increasing amplitude or increasing temperature gradient, a nonsymmetrical distortion appeared (fig. 2). The time between a pressure maximum and the following pressure minimum exceeded half the period.

Using the smoke technique referred to above, observations were made with a glass tube of 2 mm i.d. and 0.8 mm wall thickness, containing a nitrogen gas column oscillating at about 5 Hz over a liquid nitrogen bath. No displacement nodes were observed other than at the closed end. The displacement amplitude of the smoke particles increased monotonically along the tube length and was as great as ± 8 mm near the open (cold) tube end. The amplitude of this oscillation was 5 to 10 times less than typical amplitudes of helium gas oscillations over liquid helium in which a large energy transfer occurred. When direct observation of the liquid meniscus in the tube T was possible (i.e., with glass tubes), the mean position of the meniscus was below the bath level, indicating a net positive pressure within the tube during oscillation.

3.2. Damping the Oscillations

Reported attempts to damp or eliminate thermal-acoustic oscillations fall into three main categories:

(1) Changes in apparatus geometry such as employing tubes of greater diameter or closing tubes at the cold end when possible [2,7].

(2) Insertion of objects such as wire, wire mesh or knotted threads into the oscillating column [5,8,13].

(3) Thermal isolation of the oscillating column [2,4]. None of these methods was practical to apply to the calorimeter referred to above. It was possible to control the oscillations in the auxiliary apparatus (fig. 1) at any desired amplitude or to eliminate them completely with an adjustable Helmholtz resonator attached at the warm end of the oscillating column. The same technique permitted the control of the oscillations in the calorimeter. The effect of the resonator dimensions on its efficiency as a damper was then investigated using the auxiliary apparatus.

Resonator neck diameters from 0.014 in. to 0.058 in. and lengths up to 2 in. were tried. The neck dimensions were found to be critical and the best results were obtained with the neck dimensions indicated in figure 1. Necks whose diameters or lengths varied from the indicated neck dimensions by as little as a factor of two provided poor damping. Oscillations in helium and nitrogen gas columns ranging in frequency from 2 to 60 Hz and causing heat leaks of up to 7 W were successfully damped with the resonator. A typical set of damping curves obtained for helium gas oscillating over liquid helium is given in figure 3. The distance of the tube end above the liquid surface was kept constant along any curve. Larger values of the relative pressure amplitude correspond to lesser values for this distance. These curves varied considerably in shape with different oscillating gas columns and different neck dimensions. They exhibited, however, the common characteristic of a continual decrease in pressure amplitude (and associated energy transfer) with increasing piston extension.

Piston extensions up to three times the minimum length required for complete damping were investigated and in no instance did the oscillation ever reappear. No correlation was discovered between

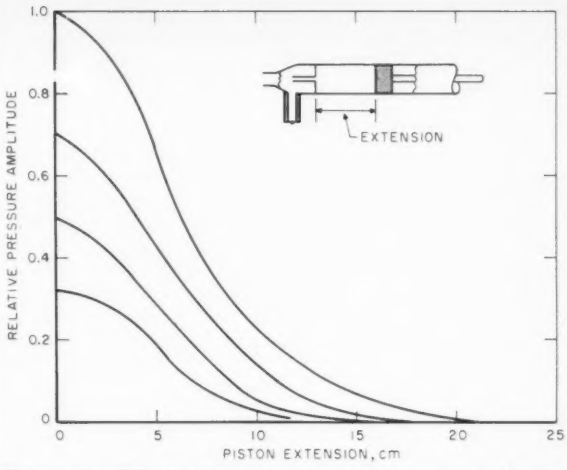

FIGURE 3. *Effect of piston extension on pressure amplitude.*
Pressure amplitude increased by decreasing distance between cold tube end and liquid surface.

the piston diameter and the minimum piston extension required to damp an oscillation of given amplitude; neither was the natural acoustic frequency of the damper related in any obvious way to its effectiveness as a damper. Piston diameters from 3/8 in. to 1 in. have been used successfully at extensions not exceeding 50 cm to damp oscillations in the entire amplitude and frequency range attainable in the auxiliary apparatus with the combinations of gas columns and liquid baths mentioned earlier.

The damper illustrated in figure 1, together with the oscillating column, constitutes a variable volume system. Equivalent results were also obtained by fixing the position of the piston and moving the neck assembly. In this case, the neck was mounted on a thin piston which was attached to a rod extending through a seal in the fixed piston.

In one series of experiments a porous tissue plug was substituted for the neck assembly. The damping of some oscillations was possible with this arrangement.

4. Discussion

The neck assembly is the vital part of the damper shown in figure 1. Since oscillations cannot be sustained in a tube open at the warm end, one could, in principle, attach a large closed volume onto the end of any tube to simulate an open end condition and thus damp the oscillations without use of the neck assembly. In practice, the volume required is often rather large and cumbersome. Damper experiments performed with the neck assembly removed have shown that the volume changes alone caused by retraction of the piston have little effect on the oscillation amplitude.

The resonator damper has several advantages. No modification of apparatus design in the cold region and no obstruction in the oscillating tube is required. This is an important consideration if a pumping tube is oscillating. Connections can be

provided so that the damper can be removed and it can be designed to be vacuum or pressure tight if the gas column is oscillating at a mean pressure considerably different from atmospheric. In the application to the above calorimeter, the piston was designed to be vacuum tight.

The coupling between the damper and oscillating system is not fully understood. Several workers [9,10] have investigated the nonlinear impedance of a Helmholtz resonator at large amplitudes and have tried to correlate it with energy dissipation in vortices near the resonator neck. The flow pattern near the neck of a damper used in the present experiments was observed by the smoke technique and appeared to be a pulsating jet similar to those described in [9].

A number of variables, probably not all independent of one another, determine whether or not a given system will perform sustained oscillations and if so, what the wave form and associated energy transfer will be. With a given temperature distribution throughout the system, the essential requirements seem to be that the gas column have a diameter small enough (usually less than ½ in.), that the cold tube end be open to a volume whose characteristic dimensions are large compared to the tube diameter, that the warm end be terminated with a high acoustic impedance, and that the tube be in good thermal contact with its surroundings. This contact need not be due to a conducting gas but can be provided by metal contact with heat sources or sinks along the tube length as was observed in the above calorimeter.

Kramers [15] has attempted to treat the gas oscillations analytically assuming small amplitudes of vibration. This linear approach did not account for the observed phenomena, a result which is plausible considering the oscillation amplitudes encountered in the present work. The possible existence of such oscillating states of a thermal system has been treated in some detail from an energy standpoint by Milne [11]. Milne's theory predicts periodic fluctuations with just the asymmetry observed in these experiments. Squire [12] has speculated that the occurrence of the Boyle temperature in the oscillating column may play a role in initiating the oscillations. Since a column of helium gas readily oscillates over liquid nitrogen, this evidently need not be a decisive role.

Since thermal-acoustic oscillations so often hamper low temperature experiments, the need for a fuller understanding of them is great. It is felt that an apparatus specifically designed to reproduce known temperature gradients would be valuable in future experimental investigation.

5. References

[1] K. W. Taconis, J. J. M. Beenakker, A. O. C. Nier, and L. T. Aldrich, Physica **15,** 733 (1949).
[2] J. R. Clement, Proc. 1954 Cryogenic Engineering Conf. (1954).
[3] D. Ter Harr, Proc. Paris Conference on Low Temperature Physics, p. 347 (1955). (See appended discussion.)
[4] F. E. Hoare and J. E. Zimmerman, Rev. Sci. Instr. **30,** 184 (1959).
[5] O. V. Lounasmaa, Ann. Univ. Turku, **A1,** No. 39 (1959).
[6] A. Wexler; in F. E. Hoare, L. C. Jackson, and N. Kurti (Eds.), Experimental Cryophysics, p. 155 (Butterworths, London, 1961).
[7] A. Van Itterbeek and W. H. Keesom, Comm. Leiden 209C.
[8] R. B. Scott, Cryogenic Engineering, p. 118 (D. Van Nostrand Co., Inc., 1959).
[9] U. Ingård and S. Labate, J. Acoust. Soc. Am. **30,** 211 (1950).
[10] F. Barthel, Frequenz **12,** 72 (1958).
[11] E. A. Milne, Quart. Journ. of App. Math. **4,** 258 (1933).
[12] C. F. Squire, Low Temperature Physics, p. 23 (McGraw-Hill Book Co., Inc., New York, N.Y., 1953).
[13] H. Plumb, private communication.
[14] M. Jakob, Heat Transfer, **I** (John Wiley & Sons, Inc., New York, N.Y., 1949).
[15] H. A. Kramers, Physica **15,** 971 (1949).

(Paper 69C1–183)

JOURNAL OF RESEARCH of the National Bureau of Standards—C. Engineering and Instrumentation
Vol. 69C, No. 1, January-March 1965

NBS Free-Air Chamber for Measurement of 10 to 60 kV X Rays

P. J. Lamperti and H. O. Wyckoff

(September 30, 1964)

Constructional details of the National Bureau of Standards' new free-air chamber for the measurement of 10 to 60 kV x rays in roentgens are given. The results of the comparisons of the new chamber with the National Bureau of Standards' "low" energy standard in their overlapping range are included. The two standard chambers, on the average, agreed to within 0.3 percent. The maximum uncertainties in the correction factors used for the comparison measurements are examined and their sum is compared with the results obtained for the chamber comparisons. An estimate is also made of the maximum uncertainty, about 1.3 percent, of an exposure rate determination to be expected when using the 10 to 60 kV chamber to measure 10 to 15 kV x rays.

1. Introduction

The National Bureau of Standards has constructed a free-air chamber standard, similar to the one designed by Greening [1960], for the measurement of 10 to 60 kV x rays in roentgens. Greening tested the performance of this chamber by comparing the calibrations obtained with it and those obtained at the U.K. National Physical Laboratory for two types of thimble chambers. The results of the comparisons were in good agreement for x rays generated below 55 kV except for the calibration at 37 kV where the difference between the two calibrations amounted to 2.6 percent.

The present paper gives constructional details of the new NBS chamber. It also gives the values of correction factors which are needed to correct for defects in its realization of the roentgen as well as results of comparative measurements made with the new chamber and with an older one previously described by Ritz [1960]. Uncertainties in the correction factors are examined and their sum is compared with the results obtained for the chamber comparison. In addition an estimate is made of the inaccuracy of a measurement of 10 to 15 kV x rays using the new chamber.

2. Apparatus

Major pieces of equipment used in this investigation included two x-ray sources, two free-air ionization chambers, a radiation monitor, and ionization current measuring systems.

2.1. New Chamber for 10 to 60 kV X Rays

Two cross-sectional views of the new NBS 10 to 60 kV chamber are shown in figures 1A and 1B. Most of the construction of this chamber is straightforward but one needs to take special precautions with the guard and collector plate combination and with tests of the diaphragm and exit apertures. Special care is required with the collector-guard plate system in order to assure that the length of the collecting region is well known. The plate system was machined as a unit until no point on the collector was as far as 0.0001 cm from the plane of the guard plate. According to a previous report [Wyckoff and Attix, 1957] lack of coplanarity of 0.0001 cm could cause an error in the collected ionization of less than 0.05 percent.

To reduce the possibility of differences in contact potential between the collector and guard plate, they were both coated with a thin layer of colloidal graphite. This coating did not change the measured ionization, indicating that this precaution was actually unnecessary.

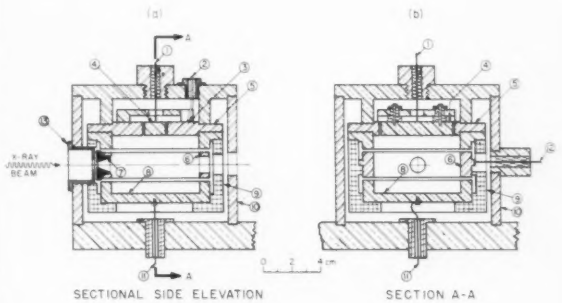

FIGURE 1A and 1B. *Schematic cross-sectional views of 10 to 60 kV free-air chamber.*

To test the influence of the exit and entrance apertures on the collecting field in the region of the collector, x-ray measurements were made with different size apertures. Entrance apertures of 1 and 5 mm and exit apertures of 4.2 and 13.1 mm diam were used. A monitor chamber located in the beam behind the 10 to 60 kV chamber measured the radiation passing through the 10 to 60 kV chamber. The ratio of the ionization obtained in the 10 to 60 kV chamber to that obtained in the monitor was independent of the aperture size, at least to the imprecision of measurement which had a standard deviation of about 0.12 percent. It thus appeared that neither the entrance nor the exit aperture diameter had an influence of as much as 0.12 percent on the field in the collecting region.

2.2. Chamber for 20 to 100 kV X Rays

The NBS chamber for measurement of 20 to 100 kV x rays, already described by Ritz [1960], has 3 different collectors of 1, 3, and 7 cm width, respectively. Ritz reported that the exposure measured with the 1 cm collector differed from that obtained by the 7 cm collector by as much as 0.3 percent at the softer radiation qualities. At the present time the 1 cm collector plate produces too low an ionization current compared to that of the other 2 collectors by as much as 0.9 percent. Subsequent studies appear to indicate that the large opening in the guard strips (2 cm diam) for the beam and the proximity of the guard strips and grounded box causes distortion of the electric field in the vicinity of the 1 cm collector. Therefore, for the present comparisons only the 3 and 7 cm collectors are used. Table 1 gives the important dimensions of the two free-air chambers.

TABLE 1. *Important dimensions of free-air chambers*

Description of dimension	Chamber	
	20–100 kV	10–60 kV
Plate separation.....cm	9.0	4.0
Plate height.....cm	9.0	5.0
Collector width.....cm	7.003$_5$ 3.023$_5$	1.014$_8$
Diaphragm aperture diameter.....cm	0.501$_6$	0.499$_7$
Air absorption path length.....cm	[a] 12.73$_9$ [b] 7.72$_6$	3.90$_2$

[a] Airpath length when using 7 cm wide collector.
[b] Airpath length when using 3 cm wide collector.

2.3. X-Ray Sources

Two x-ray sources, *a* and *b*, were used for the comparison. Each had a constant potential generator, a projected focal spot size of 1.5 mm × 1.5 mm and a beryllium window of 0.25 mm thickness. The radiation from source *b* was highly stabilized, but source *a* was not well stabilized so that a monitor was required with this source. This monitor was located in the beam about 150 cm from the focal spot, that is, after the beam had passed through a free-air chamber. In this position it did not add to the filtration of the measured beam and was not subject to heating by the x-ray tube. However, the area of the beam striking the monitor was dependent upon the size of the entrance aperture of the free-air chamber.

The chambers could be positioned reproducibly in the beam. Each chamber was adjusted for proper alinement in each beam and the alinement was finally checked radiographically. For a comparison, the distance between the x-ray focal spot and the defining plane of the aperture was adjusted so that it was the same for both chambers. This was indicated by a cathetometer capable of indicating differences of ±0.005 cm. Nominal distances of approximately 60 and 100 cm were used with source *a*, 36 and 66 cm with source *b*.

2.4. Monitor Chamber

The monitor chamber used with source *a* was the flat cavity ionization chamber described by Attix, DeLaVergne, and Ritz [1958] with a front and rear wall of 1.6-mm thick carbon and a colloidal-graphite-coated plastic membrane between these walls as a collector. The collecting volume had a larger cross-sectional area than the x-ray beam so its response was proportional to the area of the limiting aperture of the free-air chamber. Thus the ratio of the response of the free-air chamber to that of the monitor was independent of the free-air chamber aperture area.

2.5. Ionization Current Measuring System

All ionization-current measurements were made with a Townsend balance circuit using a capacitor, a potentiometer as a precision potential source, a vibrating reed electrometer as a null indicator, and a precision chronometer to indicate the duration of measurement. With such a technique the current is the product of the capacitance and the rate of voltage buildup.

3. Comparison Procedure

For each comparison, separate ionization measurements were made with one chamber, then with the other and finally again with the first chamber in the beam at the same nominal distance from the source. Two to eight comparisons were made at each quality of radiation listed in table 2. A collecting potential for each chamber was used which would give a lack of saturation of less than 0.03 percent (as indicated by the plots of the type given by Scott and Greening, 1961, 1963) at all exposure rates used.

Air pressures were obtained for each exposure from a barometer believed to have a systematic error of no greater than ±0.1 percent and to have a reading error of less than ±0.02 percent. Temperatures in the chambers were determined with thermometers installed in the 20 to 100 kV chamber and in the monitor chamber and either a thermometer or a thermistor device placed in the collecting volume of the 10 to 60 kV chamber before and after each set

TABLE 2. *Typical factors used in the comparison*

kV	Added filter (mm Al)	HVL (mm Al)	$\frac{(K_a)_R}{(K_a)_G}$	$\frac{(K_s)_R}{(K_s)_G}$	$\frac{(100-K_e+K_{sc})_G}{(100-K_e+K_{sc})_R}$
20	0	[a] 0.07[2]	[c] 1.112 [d] 1.048		0.997
20	0	[b] .068		[e] 1.106 [d] 1.046	.997
20	0.5	[a] .24	[c] 1.027 [d] 1.011		.997
20	.5	[b] .25		[e] 1.024 [d] 1.010	.997
30	0	[a] .08[9]	[c] 1.097 [d] 1.042		.997
30	0	[b] .08[9]		[e] 1.084 [d] 1.037	.997
30	0.5	[a] .36	[c] 1.020 [d] 1.009		.998
30	.5	[b] .42		[e] 1.017 [d] 1.007	.998
50	0	[a] .09[6]	[c] 1.084 [d] 1.036		.997
50	0	[b] .12		[e] 1.064 [d] 1.027	.997
50	0.5	[a] .50	[c] 1.016 [d] 1.007		.997
50	1.0	[a] .89	[c] 1.008 [d] 1.003		.997
50	1.0	[b] .9[4]		[g] 1.009 [d] 1.004	.997
60	0	[a] .08[3]	[c] 1.081 [d] 1.035		.997

[a] Source *a*.
[b] Source *b*.
[c] Using 7 cm wide collector in 20 to 100 kV chamber.
[d] Using 3 cm wide collector in 20 to 100 kV chamber.
[e] Typical values at ambient temperature and pressure, 60 cm from source.
[f] Typical values at ambient temperature and pressure, 66 cm from source.
[g] Typical values at ambient temperature and pressure, 33 cm from source.

of measurements. A separate study showed that these four temperature indicating devices agreed to within 0.04 percent. When compared to a calibrated thermometer, the thermistor had a constant error of −0.11 °C, and the thermometers each had a constant error of −0.2 °C, for which a correction was made.

4. Computations

According to the definition of exposure, one obtains the number of roentgens from the quotient of the ion charge in electrostatic units produced by the electrons that are generated per 0.001293 g of air. However all practical measurements are made under conditions of electronic equilibrium and for a free-air chamber the mass of gas is defined by the area of the defining aperture and the length of the collecting region. In addition, small corrections to the actual measurement are required for: (a) lack of saturation, (b) attenuation of photons between the defining aperture and the collecting region, (c) distortion of the collecting field defining the length of the collection region, (d) loss of electrons which have not dissipated all of their energy in the air, (e) gain of some ionization from the electrons generated by the photons scattered within the air of the chamber, (f) leakage of radiation through the lip of the defining aperture, (g) leakage of radiation through the front face of the chamber, and (h) the presence of water vapor in the air. Equation (1) gives the exposure rate in roentgens per second.

$$\frac{\Delta X}{\Delta t}=\frac{C\dfrac{\Delta V}{\Delta t}\cdot 2.9979\cdot 10^{9}}{L\cdot A}\cdot K_a\cdot K_f\cdot K_s\cdot K_l\cdot K_p\cdot K_h \left(\frac{100}{100-K_e+K_{sc}}\right)\left(\frac{T}{273.2}\right)\left(\frac{760}{P}\right), \quad (1)$$

where A is the area of the defining aperture in cm²,
L is the collector width in cm,
K_{sc} is the correction for ionization produced by scattered photons in percent,
K_e is the correction for loss of ionization from secondary electrons because of inadequate plate separation in percent,
K_s is the correction for lack of saturation,
K_a is the correction for air attenuation between the entrance aperture and the collecting region of the free-air chamber,
K_f is the correction for field distortion,
C is the capacitance in farads of the capacitor used for determining the charge collected from the free-air chamber,
T is the temperature of the collecting volume air in degrees absolute,
P is air pressure in mm of mercury,
$(\Delta V/\Delta t)$ is the rate of change of potential in volt/sec on the capacitor used with the free-air chamber,
K_l is the correction for radiation leaking through the front of the chamber,
K_p is the correction for radiation penetration of the aperture border, and
K_h is the correction for water vapor in the air.

Independent measurements and calculation have indicated that K_l and K_p are equal to one for both chambers for the range of qualities used here. If subscript R refers to the 20 to 100 kV chamber and subscript G to the 10 to 60 kV chamber, then one obtains

$$\frac{\left(\frac{\Delta X}{\Delta t}\right)_R}{\left(\frac{\Delta X}{\Delta t}\right)_G}=\frac{C_R}{C_G}\cdot\frac{L_G\cdot A_G}{L_R\cdot A_R}\cdot\frac{(100-K_e+K_{sc})_G}{(100-K_e+K_{sc})_R}\cdot\frac{(K_s)_R}{(K_s)_G} \cdot\frac{(K_a)_R}{(K_a)_G}\cdot\frac{(K_f)_R}{(K_f)_G}\cdot\frac{(T)_R}{(T)_G}\cdot\frac{(P)_G}{(P)_R}\cdot\frac{\left(\frac{\Delta V}{\Delta t}\right)_R}{\left(\frac{\Delta V}{\Delta t}\right)_G} \quad (2)$$

where K_h is assumed to be the same for both chambers in a given comparison. This equation is applicable to all comparisons with source *b*.

When a monitor is used with source *a*, the ion current in the monitor is proportional to the air

pressure in the monitor and to the area of the defining diaphragm for each free-air chamber and inversely proportional to the absolute temperature of the air in the monitor. As the monitor current (corrected to STP) per unit area of the defining diaphragm should be the same for both chambers one obtains

$$1=\frac{(C_m)_G(\Delta V_m/\Delta t)_G\cdot(T_m)_G/(A_G\cdot(P_m)_G)}{(C_m)_R(\Delta V_m/\Delta t)_R\cdot(T_m)_R/(A_R\cdot(P_m)_R)} \qquad (3)$$

where P_m and T_m are the pressure and temperature respectively in the monitor chamber, and C_m is the capacitance in the monitor current measuring circuit.

If one multiplies eq (2) by eq (3) one obtains

$$\frac{\left(\frac{\Delta X}{\Delta t}\right)_R}{\left(\frac{\Delta X}{\Delta t}\right)_G}=\frac{C_R}{C_G}\frac{L_G}{L_R}\frac{(100-K_e+K_{sc})_G}{(100-K_e+K_{sc})_R}\frac{(K_s)_R}{(K_s)_G}\frac{(K_a)_R}{(K_a)_G}\frac{(K_f)_R}{(K_f)_G}$$

$$\frac{(T)_R}{(T)_G}\frac{(T_m)_G}{(T_m)_R}\frac{(C_m)_G}{(C_m)_R}\frac{(\Delta V/\Delta V_m)_R}{(\Delta V/\Delta V_m)_G} \qquad (4)$$

by assuming that P_G is equal to $(P_m)_G$ and that P_R is equal to $(P_m)_R$ for a given comparison. This equation applies to all comparisons made with source *a*.

Many of the factors in eqs (2) and (4) were determined in advance of the comparisons. The same capacitor was used for both free-air chambers, and the capacitor used with the monitor chamber was the same for all comparisons made using source *a*. Therefore, the ratio C_R/C_G in eqs (2) and (4), and the ratio $(C_m)_G/(C_m)_R$ in eq (4) are both equal to one. The ratios of observed effective collector widths and observed aperture areas were obtained from the data in table 1. Values of the corrections for electron loss and scattered photon contribution, K_e and K_{sc}, vary slowly with the quality of the radiation so interpolated values were obtained from the data of Ritz [1959]. Values of the correction for lack of saturation, K_s, for each chamber were determined from experimental data obtained with each chamber and extrapolation according to the method given by Scott and Greening [1961, 1963]. Data for the air attenuation correction, K_a, were obtained by the experimental method used by Day and Taylor [1949]. For the softer qualities of radiation this factor was so large that it was not only a function of distance but also of air pressure and temperature.

Values of the field distortion correction, K_f, might differ from one because of space charge and distortion of the electric collecting field due to the proximity either of other electrodes or of the exit and entrance apertures and because of lack of coplanarity of the guard and collector electrodes. According to Boag [1963], space-charge effects causing a lack of saturation should give differences in the collected current for the two polarities of collecting potential. Differences of as much as 0.12 percent for the 20 to 100 kV chamber and of 0.02 percent for the 10 to 60 kV chamber were noted but the interpretation of the amount of field distortion caused by this difference is difficult. Experimental and theoretical data from Kemp and Barber [1958] indicated that distortion because of the proximity of other electrodes should be negligible for the 10 to 60 kV chamber. Comparative measurements with the 3 cm and 7 cm wide collectors of the 20 to 100 kV chamber indicated that such distortion was also negligible for this chamber. Separate experiments likewise indicated that the apertures had no effect on the collected current except as already noted for the 1 cm wide collector in the 20 to 100 kV chamber. The small lack of coplanarity in the collector-guard plate systems of the two chambers was also assumed to have a negligible effect on the field distortion. Thus $(K_f)_R/(K_f)_G$ was considered to be one for the present comparison. Table 2 gives typical values used for some of the other factors in eqs (2) and (4).

5. Results

The results of the comparisons are summarized in table 3 and are shown as a function of half value layer (mm Al) in figure 2. Table 3 and figure 2 show the average observed ratio of exposure rates determined by each chamber for each quality of radiation and with the two radiation sources. The ratios tabulated include combined results obtained with the 3 cm wide collector and with the 7 cm wide collector in the 20 to 100 kV chamber because there seemed to be no systematic difference between the two sets of results. The deviations shown below each observed ratio (table 3) indicate the maximum deviation from the average. It is seen that the 20 to 100 kV chamber always reads less than the 10 to 60 kV chamber. On the average this difference is about 0.2 or 0.3 percent. It may also be noted that the maximum amount that the observed exposure rate differs from one is about 0.4 percent with either source.

6. Analysis of Uncertainties and Errors

An estimate of the limits of disagreement to be expected in the comparison of the two free-air chambers was made by a detailed analysis of possible inaccuracies associated with all the various factors in eqs (2) and (4) as well as those associated with factors that do not appear explicity in these equations.

The same capacitor was used to measure the ionization current in the two free-air chambers. This capacitor was calibrated before, during, and after the results were obtained for this experiment. The calibration technique was such that a change in the value of the capacitance of less than 0.01 percent could not be observed. The observed value of the capacitance appeared to vary over a range of 0.03 percent for a period of 38 months. In view of this relatively slow change in the observed value of the capacitance and the fact that the ionization current measurements immediately followed one another, it

TABLE 3. *Summary of comparisons of 20 to 100 kV and 10 to 60 kV chambers*

	kV	20	20	30	30	50	50	50	60
Source *a*	Added filtration (mm Al) [a]	0	0.5	0	0.5	0	0.5	1.0	0
	Half value layer (mm Al)	.072	.24	.086	.36	.090	.50	0.89	.085
	Number of comparisons	7	4	6	4	8	4	4	4
	20 to 100 kV chamber exposure rate	0.998	0.996	0.998	0.996	0.998	0.997	0.999	0.999
	10 to 60 kV chamber exposure rate	+.003	+.001	+.004	+.000	±.002	±.001	±.001	±.001
		−.002	−.002	−.002	−.001				
Source *b*	Half value layer (mm Al)	0.068	0.25	0.089	0.42	0.12	----	0.94	----
	Number of comparisons	4	2	4	4	2	----	2	----
	20 to 100 kV chamber exposure rate	0.998	0.998	0.997	0.998	0.996	----	0.999	----
	10 to 60 kV chamber exposure rate	+.000	±.000	+.000	+.000	±.000	----	±.001	----
		−.001	----	−.001	−.001	----	----	----	----

[a] Added to an inherent filtration of 0.25 mm Be.

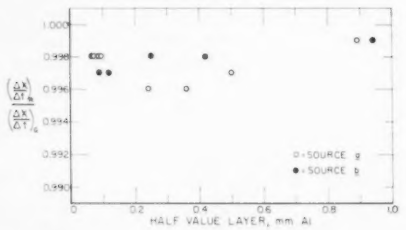

FIGURE 2. *Ratio of exposure rate versus half value layer, in mm of Al.*

seems reasonable to assume that the bias in the observed ratio of capacitances, C_R/C_G, is negligible.

The observed effective widths of the 7 and 3 cm collector plates of the 20 to 100 kV chamber and the 1 cm collector plate of the 10 to 60 kV chamber are calculated from single measurements at three different places along the collector height, at the middle, near the top and near the bottom. The measuring device used for these measurements is claimed to be accurate to within ±0.02 percent. In the absence of more measurements and in view of past experience with similar measurements, it is estimated that the standard deviation of a measurement is no more than 0.02 percent. Thus, the uncertainty in the ratio of observed effective widths is estimated to be no more than ±0.11 percent, based on a standard deviation of 0.02 percent and an allowance of ±0.02 percent for systematic error for each width.

The observed average area of each defining aperture was determined from 24 to 26 measurements of their diameters using devices claimed to be accurate to within 2 parts in 10,000. The apparent variation in the observed diameters of the apertures resulted largely from the irregularities of the aperture surfaces and from out-of-roundness. The standard error of the observed average areas of the apertures, due to imprecision in measuring any given diameter and to the variation in diameter with position, was computed to be 0.004 percent and 0.021 percent for the 20 to 100 kV and 10 to 60 kV free-air chamber apertures respectively. The standard error of the observed ratio of average areas (estimating A_G/A_R), based on the propagation of error formula, is thus 0.021 percent. The uncertainty of the ratio of average areas is taken to be ±0.063 percent (three times the standard error). The relative areas were also determined ionometrically, on three separate occasions, with one of the free-air chambers. The average value of the ratio of ionizations obtained with this ionometric technique fell within the range of three times the standard error of the observed ratio of average areas computed from measurements of the diameters of the apertures.

Values of the electron loss and scattered photon contribution corrections for each chamber were calculated according to the method described in NBS Handbook 64 [1957] from data of Ritz [1959]. As seen in table 2 the ratio of corrections for each chamber, as they appear in eqs (2) and (4) $(100-K_e+K_{sc})_G/(100-K_e+K_{sc})_R$, differ from 1 by only about 0.3 percent. Of this 0.3 percent, much less than one-third was due to electron loss, K_e. Data for computation of the scattered photon contribution correction, K_{sc}, have also been obtained experimentally by Allisy and Roux [1961]. Differences in the computed ratio due to differences in these two sets of data amounted to a maximum of 0.04 percent. Since the correction for electron loss was so small, the maximum difference of 0.04 percent in the scattered photon correction computed from the two sets of data was used as an estimate of the error in the scattered photon, electron loss correction for each chamber. Thus, the maximum error is the ratio $(100-K_e+K_{sc})_G/(100-K_e+K_{sc})_R$ is about ±0.03 percent.

As indicated earlier, the correction for lack of saturation in either chamber amounted to not more than 0.03 percent. However, even if the theory used for such extrapolation is not exact (and there is no experimental evidence for this) one would expect the correction for the lack of saturation of the two chambers to be similar because the diaphragm areas and the collecting field strengths are similar. Therefore it is estimated that the error in the ratio of $(K_s)_R/(K_s)_G$ could not be more than ±0.01 percent.

The observed ratio of the air attenuation correction for each chamber, $(K_a)_R/(K_a)_G$, was determined on 2 to 3 separate occasions for each of the qualities of radiation used in the comparisons for the difference in air absorption path lengths indicated in table 1, and normalized to the same air density. The standard deviation of the average of two to three observed ratios, based on 10 sets of two observations and 14 sets of three observations, is 0.05 percent. The uncertainty in this ratio is taken to

be three times the standard deviation of the average, or ± 0.15 percent.

The ratio of the correction for field distortion in each chamber, $(K_f)_R/(K_f)_G$, could be uncertain because of lack of coplanarity of the collector and guard plate for each of the chambers and because of field distortion caused by the proximity of either other electrodes or the entrance and exit apertures. According to Ritz [1960] the guard strips in the 20 to 100 kV chamber would cause an error of less than 0.1 percent in the widths of the collecting region. The width of the collecting region in the 10 to 60 kV chamber should not be influenced by more than a few hundredths of 1 percent by the proximity of other electrodes. However because of possible space charge effects, which are difficult to evaluate at this time, it was assumed that this ratio had a maximum uncertainty of ± 0.20 percent.

The error in the observed ratio of temperatures, T_R/T_G, is due to disagreement between the temperature indicating devices at the same temperature (which includes a possible reading error of no more than 0.02 percent), the temperature indicating device acting as a heat source or sink (important for the 10 to 60 kV chamber only) and a possible temperature gradient between the collecting region air volume and the temperature indicating device (20 to 100 kV chamber only). The devices appeared to agree with one another to within 0.04 percent. In subsequent investigations, it was found that placing the thermometer or thermistor into the 10 to 60 kV chamber collecting region air volume before and after an exposure might lead to an error in the determination of T_G during exposure of as much as ± 0.05 percent. The error in T_R, due to the possible temperature gradient mentioned above, is estimated to be no more than ± 0.03 percent since the rate of change of the temperature of the air volume is small. The total systematic error in the observed ratio T_R/T_G is assumed to be 0.04 percent and the total random error is assumed to be 0.06 percent. The total uncertainty in the observed ratio, T_R/T_G, is therefore ± 0.22 percent.

The same pressure indicating device was used to measure both P_G and P_R during any given comparison. The maximum observed change in pressure during any one set of comparisons was 0.04 percent. The maximum error in reading the pressure was estimated to be no more than ± 0.02 percent. The error in the observed ratio of pressure P_G/P_R was taken to be that due to reading error, ± 0.03 percent.

Since, for comparison measurements made with source *b* with any given chamber, the value of the change in potential for that chamber, ΔV, is held constant while the time interval, Δt, is observed, the error in the observed ratio of the rate of change of potential depends on constant errors in the ΔV's and Δt's plus random errors in the Δt's. The constant errors in the ΔV's are about ± 0.015 percent. The constant errors in the Δt's are estimated to be about ± 0.02 percent. The standard deviation of the average ratio of Δt's, based on 60 sets of three observations, is as much as 0.04 percent. The total uncertainty in the observed ratio $(\Delta V/\Delta t)_R/(\Delta V/\Delta t)_G$ is assumed to be ± 0.19 percent.

Since the same temperature indicating device was used to determine the observed temperature of the monitor in all comparison measurements, the source of error in the observed ratio $(Tm)_G/(Tm)_R$ is a reading error estimated to be not more than about ± 0.02 percent for each temperature measurement, which results in an estimated error of ± 0.03 percent in the ratio. The total uncertainty of the observed ratio is taken to be ± 0.09 percent.

The same capacitor was used for determining the monitor chamber current for each free-air chamber. This capacitor was also calibrated before, during and after the results were obtained for this experiment. The calibration technique was such that a change in the value of the capacitance of less than 0.01 percent could not be observed. The observed value of the capacitance appeared to vary over a range of 0.02 percent for a period of 38 months. In view of this relatively show change in the observed value of the capacitance and the fact that the ionization current measurements immediately followed one another, it seems reasonable to assume that the bias in the observed ratio of capacitances, $(C_m)_G/(C_m)_R$, is negligible.

The observed ratio of changes of potential $(\Delta V/\Delta V_m)_R/(\Delta V/\Delta V_m)_G$, (source *a*) has an error that is composed of four possible biases and four random errors due to reading the potentiometers. The biases in each of the ΔV's is about ± 0.015 percent. The random error of the individual ΔV's cannot be determined since the output of the source was not stabilized. However, since the value of the change of potential observed with the free-air chamber relative to that observed with the monitor should be approximately constant for any one comparison measurement, one can obtain an approximate measure of the standard deviation of the observed individual ratios, $(\Delta V/\Delta V_m)_R$ and $(\Delta V/\Delta V_m)_G$, from their ranges. Using the propagation of error formula, the average standard error of the observed ratio $(\Delta V/\Delta V_m)_R/(\Delta V/\Delta V_m)_G$ was computed to be 0.06 percent based on 117 sets of four observations and 23 sets of three observations. Thus the total uncertainty in this ratio is assumed to be ± 0.24 percent.

One must also consider the degree of unreliability of other possible factors not explicitly included in the equations which might influence the uncertainty of a comparison. In this category are the constancy of x-ray output and inaccuracy of positioning of the two chambers.

As indicated earlier, the relative position of each chamber could be adjusted to within 0.005 cm. At the source-to-chamber distances used with source *a* an error of ± 0.005 cm in positioning either chamber should have caused no error in the comparisons. However, at the shorter source-to-chamber distances used with source *b*, an error of ± 0.005 cm in positioning either chamber would have led to an error of about ± 0.03 percent in the comparisons.

TABLE 4. *Components of maximum uncertainty in comparison*

Factor	Uncertainty (percent)	
	Source *a*	Source *b*
C_R/C_G		
L_G/L_R	±0.11	±0.11
A_G/A_R		±.06
$(100-K_s+K_{sc})_G/(100-K_s+K_{sc})_R$	±.03	±.03
$(K_s)_R/(K_s)_G$	±.01	±.01
$(K_a)_R/(K_a)_G$	±.15	±.15
$(K_f)_R/(K_f)_G$	±.20	±.20
T_R/T_G	±.22	±.22
P_G/P_R		±.03
$(\Delta V/\Delta t)_R/(\Delta V/\Delta t)_G$		±.19
$(T_m)_G/(T_m)_R$	±.09	
$(C_m)_G/(C_m)_R$		
$(\Delta V/\Delta V_m)_R/(\Delta V/\Delta V_m)_G$	±.24	
Positioning		±.03
Output constancy		
Square root of sum of squares	0.44	0.41
Sum of absolute values	1.05	1.03

A measure of the x-ray output constancy (important only for source *b*) may be obtained from a comparison of the exposure rate obtained with one chamber before and after measurement obtained by the other. The maximum difference obtained for all comparisons with source *b* amounted to 0.1 percent. However, this apparent difference could be due also to the random and possible biases in P, $\Delta V/\Delta t$, T and positioning of the chamber. The square root of the sum of the squares of the errors in these four factors is 0.29 percent. Thus the observed variation in output is less than the random errors and biases in the four separate factors, so no additional uncertainty is attributed to output variation.

The components of the maximum uncertainty of the comparisons are summarized in table 4. The square roots of the sums of squares are seen to be 0.44 percent for source *a* and 0.41 percent for source *b*. If in the worst possible situation it is assumed that all of the uncertainties are in the same direction, then one obtains the maximum uncertainty by adding the absolute values of all the uncertainties associated with the various factors in eqs (2) and (4) plus those due to positioning and to output constancy. For this sum, one obtains 1.05 percent for comparisons with source *a* and 1.03 percent with source *b*.

7. Uncertainty of Exposure Rate Determinations With the 10 to 60 kV Chamber

It is also of interest to estimate the uncertainty of exposure rate measurements with the new chamber and to speculate as to how this can be reduced. It is convienient to consider separately the uncertainties of each of the factors contained in eq (1) and then obtain their sum as an indication of the maximum uncertainty to be expected in the determination of exposure rate. As many of the factors will depend upon the distance of the defining aperture from the x-ray focal spot and upon the quality of radiation, values for these must be assumed before considering numerical uncertainties in the components. This chamber will often be used for the calibration of Grenz-ray chambers. Therefore a distance of about 25 cm together with an x-ray voltage of about 10 or 15 kV will be assumed for the present discussion. The uncertainties of many of the components in eq (1) will be maximized by such a choice, so that the actual uncertainties for harder qualities and at larger distances may be somewhat less.

The calibration report of the capacitance C indicated a maximum uncertainty of ±0.05 percent. During the course of this investigation it was found that the drift in the value of the capacitance amounted to less than 0.01 percent in several months for some capacitors. Therefore it seems reasonable to indicate a maximum uncertainty of ±0.05 percent for the capacitance C.

The uncertainty of the observed ratio $\Delta V/\Delta t$ has been considered in the previous section. There it was indicated that the total uncertainty in the observed ratio is assumed to be ±0.19 percent. This of course assumes that the voltage measuring device has been recently calibrated and that, with the present equipment, Δt is 20 sec or more.

As indicated above, the standard deviation of a measurement of the effective width of the collector is assumed to be no more than 0.02 percent, and an allowance of ±0.02 percent is made for systematic error. Thus the total uncertainty of the observed effective collector width is assumed to be ±0.08 percent. The measurements of the aperture area were indicated previously to have a standard deviation of 0.02 percent. To be conservative, the maximum uncertainty in the area is taken to be three standard deviations, or ±0.06 percent.

At 10 or 15 kV and minimum filtration the value of the air attenuation correction factor is considerably larger than that considered during the comparison of the two chambers. Preliminary data indicates that the value of K_a for the 3.9 cm air absorption path is approximately 1.2. The standard deviation of the average of three observed values of K_a in this quality region, based on 8 sets of three observations and normalized to the same air density, is 0.10 percent. The uncertainty in K_a is taken to be three times the standard deviation of the average, or ±0.30 percent.

It was pointed out earlier that field distortions due to the proximity of other electrodes in this 10 to 60 kV chamber would be minimal. However, because of the possible space charge effects, it is assumed that the inaccuracy of K_f is about ±0.1 percent.

It is also difficult to assign an absolute uncertainty to the value of the correction for lack of saturation, K_s. If one assumes that the theory developed by Scott and Greening is correct, then the actual correction for lack of saturation is only about 0.01 percent for the useful range of this instrument. Thus, if one assumes that the theory is correct, the uncertainty is most likely less than 0.01 percent for this factor.

One can compute the transmission of radiation

through the front wall of the new chamber, or one can plug up the aperture and experimentally determine the value of K_l. In either case it can be shown that the contribution due to transmission of radiation through the front wall of this chamber is negligible compared to the total reading.

One may also compute the amount of radiation penetrating the aperture border. It may also be shown that the amount transmitted is negligible compared to that defined by the aperture.

It may be shown that for any reasonable value of temperature, pressure and water vapor in the air, the correction for humidity is not more than about 0.50 percent. The magnitude of this factor of course depends upon our knowledge of the average energy required to produce an ion pair in water vapor compared to air and the relative stopping power for electrons in water vapor and dry air. These errors should not cause an inaccuracy of more than ± 0.05 percent in K_h.

For the chamber and qualities of radiation being considered here, the value of the electron loss correction is estimated to be less than 0.01 percent and the value of the scattered photon contribution correction is the order of 0.4 percent. Ritz (1959) indicated an uncertainty of about ± 0.1 and ± 0.2 percent, respectively, for these two quantities. Therefore the uncertainty of the factor $(100/100-K_e+K_{se})$ is assumed to be ± 0.03 percent.

The chamber has since been fitted with a thermistor device for indicating the temperature. This has been placed on the guard plate and found to follow quite accurately the temperature of the air inside of the chamber. Therefore, in the future use of this chamber the maximum inaccuracy which could be expected in the temperature is ± 0.03 percent.

The maximum error in reading the observed pressure is estimated to be no more than ± 0.02 percent. It is assumed that a correction will be made to the indicated pressure reading for the systematic error of the device determined from recent calibrations. Therefore, the overall uncertainty of the observed pressure is taken to be three times the standard error of ± 0.02 percent, or ± 0.06 percent.

The position of the chamber can be adjusted to ± 0.005 cm. At a distance of 25 cm, an error of ± 0.005 cm in positioning the chamber could cause an uncertainty of ± 0.05 percent in the exposure rate determination.

We might also consider the uncertainty introduced because of variation in the x-ray tube output. However, as indicated before no extra allowance needs to be made for such an uncertainty. The components of the maximum uncertainty of an exposure rate determination using the 10 to 60 kV chamber are summarized in table 5. The square root of the sum of squares is seen to be 0.50 percent. If in the worst possible situation it is assumed that all of the uncertainties are in the same direction, then one obtains the maximum uncertainty by adding the absolute values of all the uncertainties associated with the various factors in eq (1) plus those due to positioning and output constancy. For this sum one obtains 1.27 percent.

TABLE 5. *Components of maximum uncertainty expected with 10 to 60 kV chamber*

Factor	Uncertainty
	Percent
C	± 0.05
$\Delta V/\Delta t$	$\pm .19$
L	$\pm .08$
A	$\pm .06$
K_a	$\pm .30$
K_f	$\pm .10$
K_e	
K_l	
K_p	
K_h	$\pm .05$
$(100/100-K_e+K_{se})$	$\pm .30$
T	$\pm .03$
P	$\pm .06$
Constancy of output	
Positioning	$\pm .05$
Square root of sum of squares	0.50
Sum of absolute values	1.27

8. Possible Future Increase in Accuracy of Exposure Rate Determinations With the 10 to 60 kV Chamber

One can see that the major contributors to the inaccuracy of exposure rate determinations with the 10 to 60 kV chamber are the uncertainties associated with the corrections for: (a) electron loss, K_e, (b) scattered photon contribution, K_{se}, (c) field distortion in the collecting region, K_f, and (d) air attenuation, K_a. The uncertainty in K_a could be reduced somewhat by more measurements. The field distortion uncertainty is a more difficult problem and it would probably require considerable effort in order to make a major reduction in this uncertainty. It might also be worthwhile to determine K_e and K_{se} more accurately. Here again a major effort would be required in order to appreciably reduce the uncertainty in these factors. Thus it appears that one might reduce the maximum inaccuracy of a measurement of 10 to 15 kV x-rays with this chamber by a few tenths of a percent with some extra effort but reducing it by as much as a factor of two would require a major effort. Such a major effort might be worthwhile to reduce possible disagreement between national standards but there is a real question as to whether the effort is necessary for calibration of clinical x-ray measuring instruments. If there is a medical requirement for greater accuracy in this quality range, x-ray sources of greater stability and clinical instruments capable of better reproducibility than are generally available will be required. In the meantime the new chamber seems adequate for present needs.

The authors thank Churchill Eisenhart, Harry Ku, and David Hogben for their help with the statistical analysis of the results of this experiment.

9. References

Allisy, A. and A. M. Roux (1961), Acta Radiologica **55,** 57.
Attix, F. H., L. R. DelaVergne, and V. Ritz (1958), J. Res. NBS **60,** 235 RP2842.
Boag, J. W. (1963), Phys. Med. Biol. **8,** 461.
Day, F. and L. S. Taylor (1949), Radiol. **52,** 239.
Greening, J. R. (1960), Brit. J. Radiol. **33,** 239.
Kemp. L. A. W. and B. Barber (1958) Phys. Med. Biol. **3,** 123
Ritz, V. (1959), Radiol. **73,** 911.
Ritz, V. (1960), J. Res. NBS **64C** (Eng. and Instr.) No. 49.
Scott, P. B. and J. R. Greening (1961), Brit. J. Radiol. **34,** 791.
Scott, P. B. and J. R. Greening (1963), Phys. Med. Biol. **8,** 51.
Wyckoff, H. O. and F. H. Attix (1957), NBS Handb. 64.

(Paper 69C1–184)

JOURNAL OF RESEARCH of the National Bureau of Standards—C. Engineering and Instrumentation
Vol. 69C, No. 1, January-March 1965

A Compensated Solenoid Giving a Uniform Magnetic Field Over a Large Volume

Chester Snow* and Raymond L. Driscoll

(October 7, 1964)

The magnetic field anywhere inside a long solenoid with two symmetrically placed auxiliary windings is expressed in terms of zonal harmonics. Formulas are given that enable one to compute the size and position of the auxiliary windings that make the field most uniform at points in the neighborhood of the center of the solenoid.

Inquiries from workers in the field of nuclear resonance have indicated their need of a region of uniform magnetic field of considerable volume. The field at any point in a solenoid can be calculated with an accuracy consistent with one's knowledge of its geometry and current but the uniformity of field inside ideal coils of reasonable length is not sufficient over the volume required to develop a satisfactory nuclear resonance signal at the 10 G level.

The following analysis shows how the variable part of the field near the center of a solenoid can be nearly compensated by two symmetrically placed auxiliary windings. This method of compensation has been suggested and used by others [1] but a detailed analysis does not appear to have been published.

The solenoid is treated as a current sheet made up of N turns of tape winding per unit length. The tape carries the current I, and the space between the turns of tape is assumed to be zero. The two equal and symmetrically placed auxiliary coils as shown in figure 1 with traces at T_1, $\overline{T}_1$, and T_1', $\overline{T}_1'$ are treated as current filaments carrying the current I_1 each, where $I_1=N_1I$ and N_1 is a disposable constant. The winding channels of the two auxiliary coils must each have linear dimensions of its axial section, say b and d, such that b^2/a_1^2 and d^2/a_1^2 are so small compared with unity as to be negligible to the precision desired in the magnetic field. The radius a_1 of each auxiliary coil and its axial position are to be determined so as to make the magnetic field most uniform near the origin. The equivalent filament that carries the current I_1 will have a trace that may be taken as the geometric center T_1 of the axial section of the winding channel.

The points T_1 and $\overline{T}_1$ are traces of a current filament of radius $a_1=r_1 \sin \theta_1$ in the plane $x_1=r_1 \cos \theta_1$. With spherical coordinates r, θ, ϕ and cylindrical coordinates x, ρ, ϕ the only component of the vector potential is $A(r, \theta)=A_\phi(r, \theta)$ and this is independent of the longitude ϕ. The spherical components of the magnetic field are

$$H_r(r,\theta)=\frac{1}{r \sin \theta}\mathcal{D}_\theta[A(r,\theta)\sin\theta]$$

$$H_\theta(r,\theta)=\frac{-1}{r}\mathcal{D}_r[rA(r,\theta)].$$

From these the cylindrical components are found by

$$H_x=H_r\cos\theta-H_\theta\sin\theta$$

$$H_\rho=H_r\sin\theta+H_\theta\cos\theta.$$

*Retired, present address: 2520 Harrison Blvd., Ogden, Utah.

[1] T. A. Heddle, Brit. J. Appl. Phys. **3**, 95 (1952); B. Lewis, Brit. J. Appl. Phys. **1**, 238 (1950); M. W. Garrett, J. Appl. Phys. **22** 1091 (1951), M. E. Gardner, J. A. Jungerman, P. G. Lichtenstein, and C. G. Patten, Rev. Sci. Instr. **31**, 929 (1960).

The vector potential at $P(r, \theta)$ due to a cgs unit circular current with trace at $T_1(r_1, \theta_1)$ is given by

$$A(r,\theta)=2\pi \sin\theta \sin^2\theta_1 \sum_{n=1}^{\infty}\left(\frac{r}{r_1}\right)^n \frac{P'_n(\cos\theta)P'_n(\cos\theta_1)}{n(n+1)} \text{ if } 0\leq r\leq r_1;$$

$$=2\pi \sin\theta \sin^2\theta_1 \sum_{n=1}^{\infty}\left(\frac{r_1}{r}\right)^{n+1} \frac{P'_n(\cos\theta)P'_n(\cos\theta_1)}{n(n+1)} \text{ if } r\geq r_1,$$

where $P_n(u)$ is Legendre's polynomial and $P'_n(u)$ denotes $\frac{d}{du}P_n(u)$.

The effect of the two symmetrically placed equal filaments each with current I_1 is found from the first of these expansions, by superposition and noticing that in reckoning the effect of the filament on the left, the term $P'_n(\cos\theta_1)$ must be replaced by $P'_n(\cos(\pi-\theta_1))=P'_n(-\cos\theta_1)$ $=(-1)^{n+1}P'_n(\cos\theta_1)$.

The vector potential at $P(r, \theta)$ of both current filaments is therefore

$$A^{(1)}(r,\theta)=4\pi I_1 \sin\theta \sin^2\theta_1 \sum_{n=1}^{\infty}\left(\frac{r}{r_1}\right)^{2n-1} \frac{P'_{2n-1}(\cos\theta)P'_{2n-1}(\cos\theta_1)}{2n(2n-1)} \text{ when } 0\leq r\leq r_1$$

which applies therefore at points inside the solenoid near the origin.

By use of $\frac{d}{du}[(1-u^2)P'_\nu(u)]=-\nu(\nu+1)P_\nu(u)$ it is found that the field components are

$$H_r^{(1)}=4\pi I_1 \frac{\sin^2\theta_1}{r} \sum_{n=1}^{\infty}\left(\frac{r}{r_1}\right)^{2n-1} P_{2n-1}(\cos\theta)P'_{2n-1}(\cos\theta_1);$$

$$H_\theta^{(1)}=-4\pi I_1 \sin^2\theta_1 \frac{\sin\theta}{r} \sum_{n=1}^{\infty}\left(\frac{r}{r_1}\right)^{2n-1} \frac{P'_{2n-1}(\cos\theta)P'_{2n-1}(\cos\theta_1)}{2n-1}.$$

To obtain from these the expressions for the cylindrical components H_z and H_ρ it is necessary to make use of the two relations

$$(1-u^2)P'_\nu(u)+\nu u P_\nu(u)=\nu P_{\nu-1}(u)$$

and

$$uP'_\nu(u)-\nu P_\nu(u)=P'_{\nu-1}(u).$$

We find

$$\left.\begin{aligned} H_z^{(1)}(r,\theta)&=\frac{4\pi I_1 \sin^2\theta_1}{r_1}\left[1+\sum_{n=1}^{\infty}\left(\frac{r}{r_1}\right)^{2n} P_{2n}(\cos\theta)P'_{2n+1}(\cos\theta_1)\right] \\ H_\rho^{(1)}(r,\theta)&=\frac{-4\pi I_1 \sin^2\theta_1 \sin\theta}{r_1} \sum_{n=1}^{\infty}\left(\frac{r}{r_1}\right)^{2n} \frac{P'_{2n}(\cos\theta)P'_{2n+1}(\cos\theta_1)}{2n+1}. \end{aligned}\right\} \quad (1)$$

The vector potential of the current I (cgs units) in the current sheet with N turns per cm is found by integration to be

$$A^{(2)}(r,\theta)=4\pi NIr \sin\theta\left[\frac{1}{2}\cos\alpha-\sin^2\alpha \sum_{n=1}^{\infty}\left(\frac{r}{c}\right)^{2n} \frac{P'_{2n+1}(\cos\theta)P'_{2n}(\cos\alpha)}{2n(2n+1)(2n+2)}\right]$$

at a point $P(r, \theta)$ inside the current sheet.

From this we find

$$\left.\begin{aligned} H_z^{(2)}(r,\theta)&=4\pi NI\left[\cos\alpha-\sin^2\alpha \sum_{n=1}^{\infty}\left(\frac{r}{c}\right)^{2n} \frac{P_{2n}(\cos\theta)P'_{2n}(\cos\alpha)}{2n}\right] \\ \text{and} \\ H_\rho^{(2)}(r,\theta)&=4\pi NI \sin^2\alpha \sin\theta \sum_{n=1}^{\infty}\left(\frac{r}{c}\right)^{2n} \frac{P'_{2n}(\cos\theta)P'_{2n}(\cos\alpha)}{2n(2n+1)} \end{aligned}\right\} \quad (2)$$

For the case where the filament currents and solenoidal current circulate in the same sense around the x axis we place $N_1 I = I_1$ in eq (1) and add eq (2).

The resultant magnetic field inside the solenoid has the components

$$H_x(r,\theta) = 4\pi NI \left\{ \cos\alpha + C_0 \sin^2\alpha - \sin^2\alpha \sum_{n=1}^{\infty} \left(\frac{r}{c}\right)^{2n} \frac{P_{2n}(\cos\theta) P'_{2n}(\cos\alpha)}{2n} \left(1 - \frac{C_0}{C_{2n}}\right) \right\} \tag{3a}$$

$$H\rho(r,\theta) = 4\pi NI \sin^2\alpha \sin\theta \sum_{n=1}^{\infty} \left(\frac{r}{c}\right)^{2n} \frac{P'_{2n}(\cos\theta) P'_{2n}(\cos\alpha)}{2n(2n+1)} \left(1 - \frac{C_0}{C_{2n}}\right) \tag{3b}$$

where

$$C_0 \equiv \frac{N_1 \sin^2\theta_1}{N r_1 \sin^2\alpha} \tag{4a}$$

$$C_{2n} \equiv \left(\frac{r_1}{c}\right)^{2n} \frac{P'_{2n}(\cos\alpha)}{2n P'_{2n+1}(\cos\theta_1)} \text{ for } n = 1, 2, 3, \ldots . \tag{4b}$$

Also we may place here for reference

$$\left.\begin{aligned} P'_2(u) &= 3u \\ P'_4(u) &= \frac{5u}{2}(7u^2 - 3) \\ P'_3(u_1) &= \frac{3}{2}(5u_1^2 - 1) \\ P'_5(u_1) &= \frac{15}{8}(21u_1^4 - 14u_1^2 + 1) \end{aligned}\right\}. \tag{5}$$

For brevity, also let

$$\lambda \equiv \frac{r_1}{c},\ u = \cos\alpha, \text{ and } u_1 = \cos\theta_1 \tag{6}$$

where all three are positive (since θ_1 refers to the filament on the right in fig. 1).

The variable part of H_x is the series in (3a). If the first two terms corresponding to $n=1$ and $n=2$ are made to vanish, then the first two terms in the series (3b) for H_ρ will also vanish. Therefore the approximately uniform resultant field near the origin will be in the axial direction.

The two equations $C_2 = C_0$ and $C_4 = C_0$ are

$$\frac{\lambda^3 P'_2(u)}{2P'_3(u_1)} = \frac{N_1(1-u_1^2)}{cN(1-u^2)} = \lambda C_0 > 0, \tag{7}$$

and

$$\frac{\lambda^5 P'_4(u)}{4P'_5(u_1)} = \frac{N_1(1-u_1^2)}{cN(1-u^2)}. \tag{8}$$

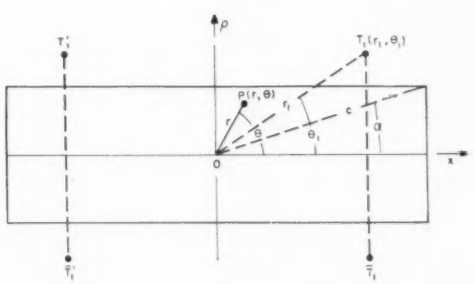

FIGURE 1. *Axial section of current sheet.*

c = the semi-diagonal of the section.
α = the semi-aperture of its end-circle viewed from O.
N = number of turns per cm (tape-winding).
I = the current circulating.
The points (T_1, $\bar{T}_1$ (and) T'_1, $\bar{T}'_1$) are traces of the compensating filaments.

Dividing the members of eq (7) by the corresponding members of eq (8) gives

$$\lambda^2=\frac{2P_2'(u)P_5'(u_1)}{P_4'(u)P_3'(u_1)}$$

or, in view of eq (5),

$$\frac{r_1}{c}=\lambda=3\sqrt{\frac{(u_1^2-1/3)^2-4/63}{5(u^2-3/7)(u_1^2-1/5)}} \tag{9}$$

which must be real. We consider only the case of a relatively long solenoid in which $u=\cos\alpha>\sqrt{\frac{3}{7}}=0.6547$ or $0<\alpha<49°6'$. In order that λ be real it is necessary that the value of $u_1(=\cos\theta_1)$ to be found shall be such that

$$\frac{(u_1^2-1/3)^2-4/63}{(u_1^2-1/5)}>0.$$

The zeros of the numerator of this fraction are

$$\frac{1}{3}\left(1+\frac{2}{\sqrt{7}}\right)=0.5853$$

and

$$\frac{1}{3}\left(1-\frac{2}{\sqrt{7}}\right)=0.08136.$$

Since in eq (9), u_1 occurs in even powers only let

$$Z=u_1^2. \tag{10}$$

Equation (9) may be written

$$\frac{r_1}{c}=\lambda=3\sqrt{\frac{(z-0.5853)(z-0.08136)}{5(u^2-\frac{3}{7})(z-0.20)}}. \tag{11}$$

If the value of z to be found makes λ real, this will correspond to the case that was adopted above in placing $I_1=+N_1I$ so the current filaments circulate around the x axis in the same sense as the current I in the solenoid. If values of z are found that make λ imaginary, a solution of the problem may still be found corresponding to $I_1=-N_1I$, which is equivalent to reversing the sign of C_0 so that λ will then be real. If λ as given by eq (11) is inserted in eq (7), and the relations of eq (5) employed, then

$$(1-z)P_3'(u_1)=\frac{15}{2}(1-z)(z-0.20)=\frac{cN(1-u^2)P_2'(u)\lambda^3}{2N_1}$$

$$=\frac{3^4cN(1-u^2)u}{2N_1}\left[\frac{(z-0.5853)(z-0.08136)}{5(u^2-\frac{3}{7})(z-0.20)}\right]^{3/2}. \tag{12}$$

Squaring eq (12) gives the following equation to determine z (which also applies to the case in which λ is imaginary):

$$(1-z)^2(z-0.20)^5=B[(z-0.5853)(z-0.08136)]^3 \tag{13}$$

where

$$B=3\left(\frac{3}{5}\right)^5\left(\frac{cN}{N_1}\right)^2\frac{u^2(1-u^2)^2}{(u^2-\frac{3}{7})^3}. \tag{13a}$$

Hence B is a positive constant if $u^2>\frac{3}{7}$ (or $\alpha<49°6'$). The numerical solution of eq (13) may be found without difficulty when B is given, that is, when the constants c, N, N_1, and $u=\cos\alpha$ are given.

If we let

$$F(z) \equiv \frac{[(z-0.5853)(z-0.08136)]^{3/5}}{(1-z)^{2/5}} \tag{14}$$

and

$$M = B^{-1/5} = \frac{5(u^2-\frac{3}{7})^{3/5}}{3^{6/5}\left[\frac{CNu(1-u^2)}{N_1}\right]^{2/5}} \tag{15}$$

equation (13) is equivalent to

$$M(z-0.20) = F(z) \text{ where } z = \cos^2 \theta_1. \tag{16}$$

The roots of this equation between zero and one are the abscissas of the points of intersection of the curve $y=F(z)$ and the straight line $y=M(z-0.20)$. The curve $F(z)$ could be plotted once for all, since the constants α and c of the solenoid enter only in the positive slope M of the straight line. The general nature of the curve $y=F(z)$ is indicated in figure 2. A fairly accurate plot of $F(z)$ and $M(z-0.20)$ versus z is helpful in getting a starting point for an accurate evaluation of the roots by successive approximation. If Z_1 is a root, the corresponding value of r_1 is, by eq (12),

$$\lambda^3 = \left(\frac{r_1}{c}\right)^3 = \left[\frac{5N_1}{cNu(1-u^2)}\right](1-Z_1)(Z_1-0.20) \tag{17}$$

which must be positive. There will be two roots of eq (16): Z_1 in the interval $0.5853 < Z_1 < 1$, Z_2 in the interval $0.08136 < Z_2 < 0.20$. The latter is inadmissible when $I_1 = +N_1 I$.

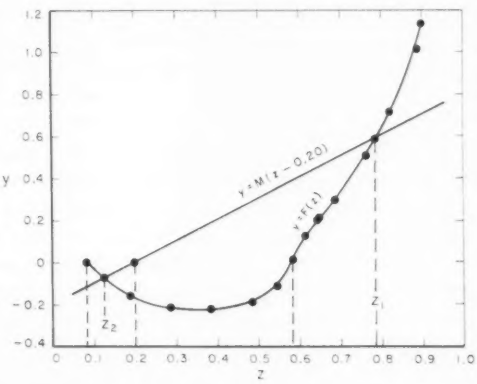

FIGURE 2. *The curves* y=F(z) *and* y=M(z−1/5) *plotted as a function of* z.

The root Z_1 gives the only value for $\cos^2 \theta_1$ permitted when the currents in the filament circulate around the x-axis in the same sense as the solenoidal current I. If in the opposite sense, Z_2 would be indicated. When the solenoid and the value of the constant N_1 are arbitrarily chosen, this solution gives the best radius and position of the two current filaments in order to produce a uniform field in a sphere with center at 0. When the first two terms are thus annulled in the series of eqs (3a) and (3b), the next term ($n=3$) will indicate the principal remaining nonuniformity of field near the center by comparison with the constant term ($\cos \alpha + C_0 \sin^2 \alpha$) in eq (3a).

The foregoing analysis has been applied to the compensation of a solenoid designated as NBS 58080. The constants of this solenoid at 25 °C are $N=9.99915$ turns per cm, $c=51.9138_7$ cm, and $\cos \alpha = 0.963064$. For several assumed values of N_1 the constants of the required auxiliary windings have been found and listed in table 1. For each value of N_1, the relative contribution of the compensating windings to the field at the center of the solenoid is shown in the column headed $C_0 \sin^2 \alpha / \cos \alpha$. With the terms $n=1$ and 2 removed from eqs (3a) and (3b), the value of r, at which the term $n=3$ reaches one part per million (ppm) relative to the constant term ($\cos \alpha + C_0 \sin^2 \alpha$) in (3a) will be found in the table under "compensated radius."

TABLE 1. *Constants of auxiliary windings for solenoid NBS 58080*

Condition: $I_1 = +N_1 I$

N_1	M	Z_1	λ	r_1	$r_1 \cos\theta_1$	$r_1 \sin\theta_1$	$\frac{C_0 \sin^2\alpha}{\cos\alpha}$	Comp. radius
				cm	*cm*	*cm*		*cm*
49	0.9946	0.7903	0.9423	48.91	43.5	22.4	0.022	7.5
16	.6356	.693	.6938	36.02	30.0	20.0	.014	5.8
1	.2097	.602	.2805	14.56	11.3	9.2	.003	3.1
0.25	.1204	.592	.1767	9.17	7.1	5.9	.001	2.3

TABLE 2. *Constants of auxiliary windings for solenoid NBS 58080*

Condition: $I_1 = -N_1 I$

N_1	M	Z_2	λ	r_1	$r_1 \cos\theta_1$	$r_1 \sin\theta_1$	$\frac{C_0 \sin^2\alpha}{\cos\alpha}$	Comp. radius
				cm	*cm*	*cm*		*cm*
−49	0.9946	0.1139	0.8017	41.6	14.05	39.2	−0.108	5.4
−16	.6356	.1006	.5823	30.2	9.59	28.7	−.059	4.6
−1	.2097	.0852	.2438	12.7	3.69	12.1	−.0075	2.7
−0.25	.1204	.0829	.1547	8.03	2.31	7.7	−.0029	2.0

Corresponding values for the condition $I_1 = -N_1 I$ have been found and are listed in table 2. There appears to be nothing in favor of the latter case, unless the relatively close spacing of the auxiliary windings is especially appropriate to an experiment. To give an idea of the expected improvement over the uncompensated solenoid, we calculate the term $n=1$ in the series of H_z (eq (2)) relative to the constant term cos α, and find that it reaches 1 ppm at $r=0.16$ cm.

We assume in what follows that the solenoid construction is accurate to 1 ppm. When deciding upon a design, one has to consider the accuracy required in the construction of the auxiliary coils in order to realize a given accuracy in the combination. If an accuracy of, say, 1 ppm is desired and an experiment requires a uniform region whose volume has a radius of 7.5 cm the required accuracy in the compensating coils ($N_1=49$) is about 1 part in 20,000, a rather severe requirement. On the other hand, a uniform region with 2 cm radius ($N_1=0.25$) can be had for an accuracy of only 1 part in 1,000 in the construction of the auxiliary windings. Obviously it does not pay to compensate over a region larger than necessary.

(Paper 69C1–185)

JOURNAL OF RESEARCH of the National Bureau of Standards—C. Engineering and Instrumentation
Vol. 69C, No. 1, January–March 1965

Evaluation of a Microwave Phase Measurement System

Doyle A. Ellerbruch

(August 27, 1964)

The best phase measurement sensitivity and accuracy are attained in a dual-channel balanced bridge type system. Two similar dual-channel systems are discussed in this report; these being the homodyne system and the modulated subcarrier. Both require low-frequency amplitude modulation in one of the channels; however, the homodyne system uses a balanced modulator. The difference in system theory due to the amplitude modulation difference is discussed, and the advantages of each are pointed out.

The standard phase shifter considered for these systems consists of a modified reflectometer terminated in a sliding short circuit. The requirements for a noncontacting short circuit are established, and its theoretical and experimental design data are given.

An error analysis is included, so the total error for any given system can quickly be determined. The maximum error can be derived by calculating the limits of the individual errors and adding them together. Equipments and tuning techniques that have been developed to reduce many errors to a minimum are discussed.

It is shown that either of these measurement systems are readily adaptable to automation. Samples of phase data that were taken from a few commercial components are included.

1. Introduction

A relative phase measurement system that will be utilized by the NBS Electronic Calibration Center for offering relative phase calibration services on most passive microwave devices has been investigated. The purpose of this report is to present the results of this investigation.

All experimental and theoretical data contained in this report were obtained using WR–90 waveguide. A discussion of the principles of operation of two similar measurement techniques is presented, the differences between these two techniques and relative advantage of each being pointed out in the section on modulation.

Development of the standard phase shifter for use with either of the measurement systems is discussed. This is followed by a discussion of the error sources which are the same for both measurement techniques.

It will be shown that the systems discussed in this report are readily adaptable to automated calibration services, which would reduce calibration time and provide continuous rather than point-by-point data. Data on various commercial microwave devices are included.

2. System

The basic circuit configuration used in measuring relative microwave phase shift is shown in figure 1. Microwave power is generated by a single source and divided between the bridge arms. One arm contains a reference phase shifter, while the other contains an amplitude modulator and the device, the phase shift of which is to be measured. The microwave signal

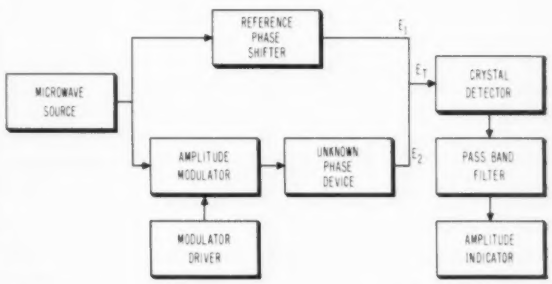

FIGURE 1. *The basic phase measurement bridge circuit.*

propagating through the arm containing the unknown is amplitude-modulated at a convenient low frequency.

The signals from the two arms are recombined in a crystal detector. When pure sine wave modulation is impressed, a band pass filter tuned to the fundamental modulation frequency is included as a harmonic rejector. The second harmonic arising through recombination of the carrier and modulated subcarrier is blocked by the filter, and the fundamental frequency component is allowed to proceed to the amplitude indicator.

Because the microwave signals traversing the two arms are coherent, the resultant signal present in the detector can be expressed by the use of the law of cosines. From the vector diagram shown in figure 2a, it is seen that

$$|E_t|^2=|E_1|^2+|E_2|^2-2|E_1|\ |E_2|\cos\phi, \qquad (1)$$

where E_1 is the amplitude of the component that reaches the detector through the standard phase

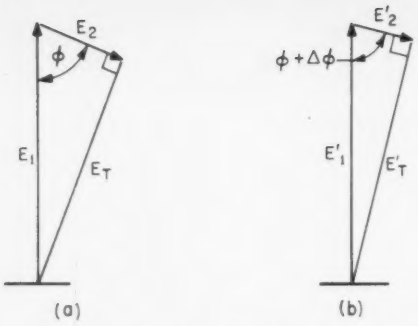

FIGURE 2. *Change of angle φ at bridge null due to a change in E_2/E_1.*

shifter, E_2 is the amplitude of the component that reaches the detector through the modulator and phase shifter under calibration, and E_T is the resultant amplitude incident on the detector. The power out of the square law detector is then proportional to E_T^2. Only those terms in (1) which contribute to the fundamental modulation frequency need be considered from here on. We have, therefore, only to consider the last two terms. This equation will be discussed in detail in the section on modulation; at this point, a general consideration of the equation is sufficient.

Considering the last two terms of (1), it can be seen that the magnitude of the modulation signal varies from zero to a maximum as the angle ϕ is varied. Proper bridge balance is arbitrarily assumed when the magnitude of the modulation signal is zero. This choice is made because maximum bridge sensitivity is attained at the null condition.

A change of microwave phase shift through either arm of the microwave bridge will cause a change at the detector ϕ and, hence, in the measured amplitude. The phase device to be calibrated (relative phase) is inserted into the system, and the reference phase shifter is adjusted to produce a null at the indicator. Then, any phase advance or retardation in the wave emerging from the unknown can be exactly counteracted by an identical change of phase in that wave through the standard. The change of phase through the unknown device is, then, exactly equal to the change of phase through the reference phase shifter.

2.1. Modulator

Double sideband, pure amplitude modulation, with or without carrier suppression, may be employed in this system. Either of these types of modulation is satisfactory; however, certain distinguishable characteristics must be considered when determining the type of modulation to be used.

Utilization of double sideband with unsuppressed carrier, or simple amplitude modulation, results in the modulated subcarrier phase measurement system. The theory for this system has been presented in reference [1].[1] As mentioned in the previous section, only the last two terms of (1) contribute to the power into the detector at the modulation frequency. The other terms either contain no modulation frequency component or are amplitude modulated at twice the fundamental rate. Assuming square-law detection, the modulation frequency component of the voltage from the detector, V_0, is proportional to E_T^2; i.e.,

$$V_0 \propto 2mE_2(E_2 - E_1 \cos \phi) \cos \omega_m t, \qquad (2)$$

where m is the modulation index at angular frequency ω_m. According to this equation, an amplitude null occurs when $E_1 \cos \phi = E_2$. It follows that the angle ϕ at which the null occurs is entirely dependent upon the relative magnitudes of E_1 and E_2. The angle ϕ at which a null occurs for various magnitude ratios has been tabulated [1] and is reproduced in this report as table 1. It can be seen in figure 2b, that, if known magnitude ratio changes occur during the phase calibration, the corresponding angle change, $\Delta\phi$, must be appropriately entered in the measurement data or this data will be in error by the amount $\Delta\phi$ plus the other system errors. A procedure for averaging out any error due to ratio changes during measurement is outlined in reference [1]. When that measurement procedure is used, it is not necessary to determine the ratio change.

TABLE 1. *Angular relationship at null for various relative signal levels*

$20 \log_{10} (E_c/E_{sc})$	Angle ϕ at null, degrees
0	0.00
10	71.56
20	84.26
30	88.19
40	89.43
50	89.82
60	89.94
70	89.98
80	89.99
90	90.00

Use of double sideband modulation with suppressed carrier, i.e., use of a balanced modulator in the system, results in a homodyne measurement technique discussed in reference [2]. When this type of modulation is used, only the last term in (1) contributes to the fundamental modulation frequency, whose amplitude can be given as

$$V_0 \propto -2E_1E_2m \cos \omega_m t \cos \phi. \qquad (3)$$

The angle ϕ is the angle between the two signals shown in figure 2. From this equation, it can be seen that a null occurs when $\phi = 90°$. Further, the angle ϕ is not dependent upon the relative magnitudes of the signal out of each arm. Therefore, it can be seen that the advantage of an ideally balanced modulator is that the calibration data need not be corrected for changes of the amplitude ratio. This advantage is never fully enjoyed, however, because no ideally balanced modulators exist. Some residual carrier is always present from the modulator, and this residual carrier combines with the other signals as shown in figure 3. For this condition, the tabu-

[1] Figures in brackets indicate the literature references at the end of this paper.

lated data for the relative magnitude ratio presented in table 1 applies, where the magnitude E_{sc} now refers to the magnitude of the residual carrier. Failure to take this angle change into account results in an error identical to that for the modulated subcarrier system, which can be corrected using the averaging process for the modulated subcarrier system [1].

A balanced modulator has been constructed [3] which is capable of suppressing the carrier to a level 45 dB or more below the signal incident at the modulator. If equal powers were delivered to the detector through each bridge arm, the relative phase relationship for the system would be that shown in figure 3b, where the angle ϕ is the angle in table 1 corresponding to the relative magnitude ratio of 45 dB. If, however, the signal incident on the detector through the unknown arm remains 20 dB or more below that from the reference channel, the magnitude ratio is increased to 65 dB or more making any phase changes due to the residual carrier level change negligible as can be seen from table 1.

2.2. Standard

The standard or reference phase shifter is a device which introduces the required relative phase change at the required accuracy of measurement. The standard phase shifter selected for this system is a precision waveguide section terminated by a sliding short circuit as proposed by Magid [4] and is shown in figure 4. The reasons for this choice are its broadband capability, small output signal level variation with changes of relative phase, and the good accuracy attainable when properly constructed and tuned. The symbol λg on figure 4 represents the precision waveguide wavelength, and Δl is the short circuit displacement within the waveguide.

Because the position of the short circuit within the waveguide is frequently adjusted during the course of measurement, it was suggested that a noncontacting type short circuit be developed to eliminate excessive wear on the precision section. The initial requirements set up for this short circuit were a constant reflection coefficient magnitude and constant reference plane with respect to motion along the precision section. A dumbbell, or cylindrical slug type arrangement, was selected on the basis of its reported behavior [5]. Because it is extremely difficult to analyze the configuration shown in figure 5 analytically, laboratory data were collected to justify its use.

The first test was to determine the variation of reflection coefficient magnitude with frequency for fixed diameter cylinders of variable length. This was accomplished by inserting a single cylinder in a swept frequency reflectometer system. The results of this test are shown in figure 6.

The next test series was designed to determine the separation of multiple cylinders so that the overall reflection coefficient would be optimum. Results of this test series indicated that $\lambda g/4$ is optimum where λg is the wavelength in the empty waveguide.

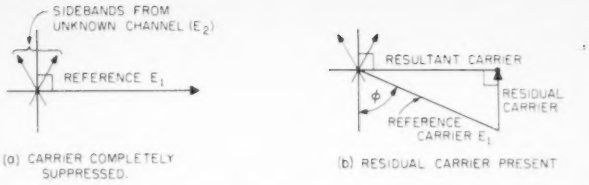

FIGURE 3. *Effect of residual carrier on the relative phase angle.*

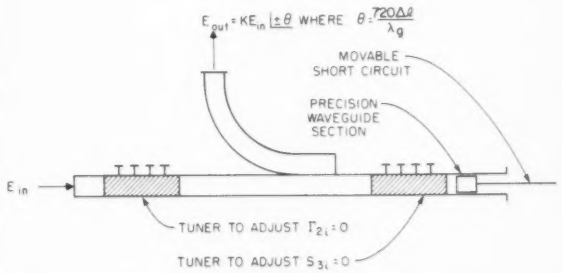
$E_{out} = KE_{in} \angle \pm\theta$ WHERE $\theta = \frac{720\Delta\ell}{\lambda g}$
MOVABLE SHORT CIRCUIT
PRECISION WAVEGUIDE SECTION
E_{in}
TUNER TO ADJUST $\Gamma_{2L} = 0$
TUNER TO ADJUST $S_{3L} = 0$

FIGURE 4. *Standard phase shifter.*

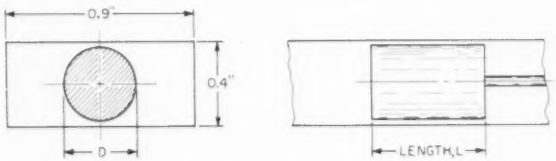

FIGURE 5. *Short circuit cylinder waveguide configuration.*

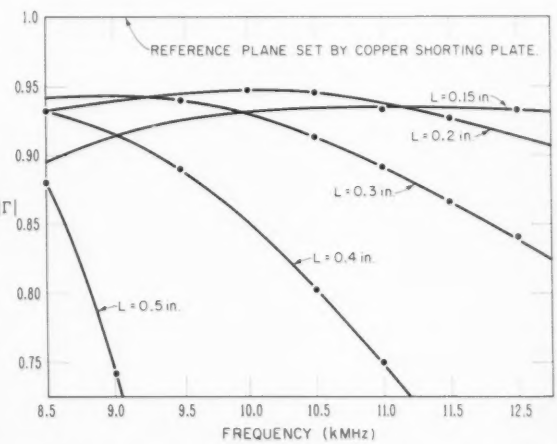

FIGURE 6. *Reflection coefficient versus frequency for a single brass slug 0.35 in diameter.*

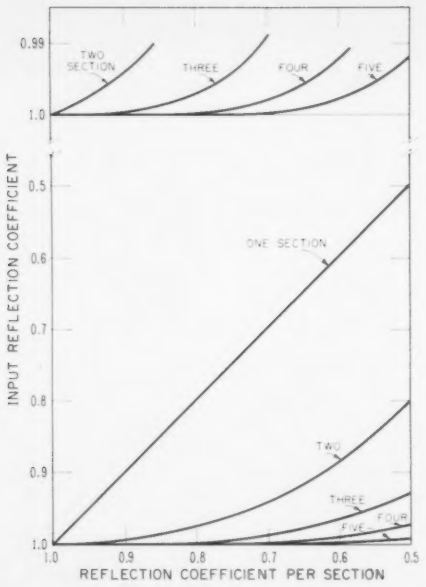

FIGURE 7. *Input* $|\Gamma|$ *versus* $|\Gamma|$ *per section for multiple section short circuit.*

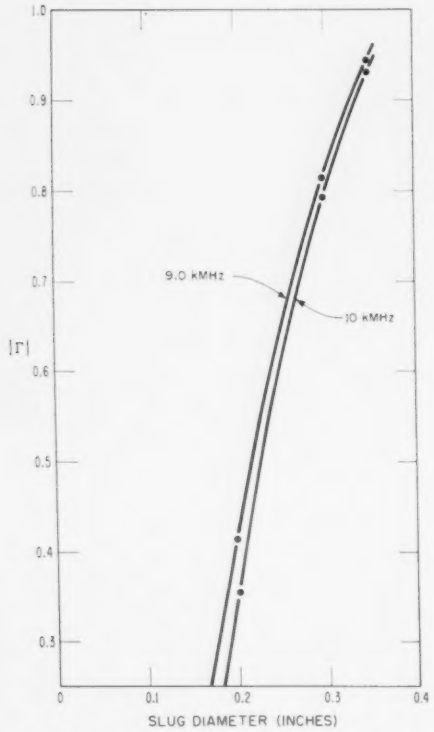

FIGURE 8. *Reflection coefficient versus slug diameter for a single brass slug 0.30 in. long.*

A theoretical curve is plotted in figure 7, showing the reflection coefficient that can be expected by cascading a number of cylinders. It was assumed that all cylinders have the same individual reflection coefficient and that the spacing between adjacent cylinders is optimum. The family of curves at the top of the figure is the same as those at the bottom; however, the input reflection coefficient scale has been changed to better show the high reflection characteristics.

The reflection coefficient of a single section as a function of cylinder diameter is shown in figure 8, this data having been obtained experimentally. Cylinder length was constant at 0.3 in.

The final test series was conducted to determine the change of the plane of reflection, as the lateral position of the cylinder combination is changed within the precision section. The result of this test is shown in figure 9, where the position of the cylinders within the waveguide was changed along the narrow dimension. The phase error introduced by this effect has been reduced to a negligible amount by using Teflon spacers between adjacent cylinders. The final version of the short circuit is then shown in figure 10.

Other areas of concern associated with the construction of an acceptable standard phase shifter include the dimensional tolerances of the precision section, ability to measure the relative position of the short circuit within the waveguide, and phase errors introduced by the reflectometer setup. The magnitudes of all these errors will be discussed in the error analysis section, but methods that were used to reduce these errors are discussed here.

Several types of precision waveguide constructions have been used in this system, including commercially available sections and some of special design. The best section used to the present time is shown in figure 11. It is of a four-piece construction with a cam assembly to permit adjusting of one side wall with respect to the other. This construction is easily seen in the view of a similar section in figure 12. The object of the adjustable wall is to allow for reduction of the waveguide width variation to a minimum throughout its entire length.

Different techniques of measuring the relative position of the short circuit have also been tried. The most suitable consists of a microscope-standard scale combination.

Figure 13 is a photograph of the completely assembled standard phase shifter resulting from this study.

3. Error Analysis

There are many sources of phase error introduced into the measurement from various parts of the overall system. These are divided into the following general categories.

3.1. Errors From the Standard Phase Shifter

The limits of error associated with the tuning, short circuit positioning, and precision waveguide

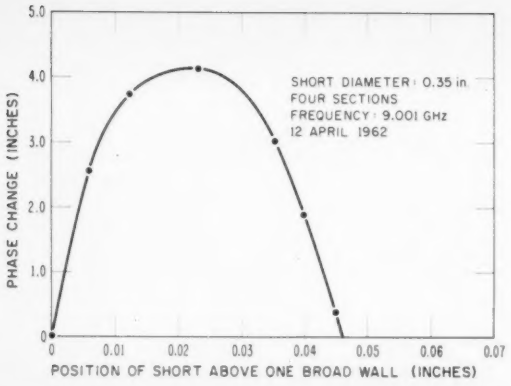

FIGURE 9. *Change of relative phase versus position of dumbbell short in the precision guide.*

FIGURE 10. *Complete short circuit.*

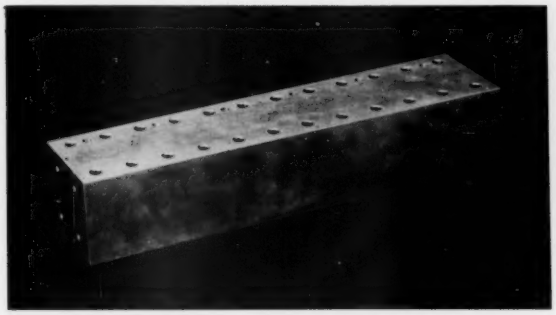

FIGURE 11. *Adjustable waveguide section.*

width tolerances have been calculated and presented in graphical form [6]. The influence a reduction of the reflection coefficient to a constant value below unity has upon these errors can be determined from the mathematical results, as given by (10) and (11) in reference [6].

The error introduced in the modulated subcarrier system by a standard phase shifter, yielding attenuation changes as well as phase changes, can be determined from table 1 of this report. This error can be eliminated through use of the measurement procedure outlined in [1]. The error introduced by standard phase shifter attenuation changes in a system using a balanced modulator, where the carrier is not fully suppressed, can also be determined from table 1. The error, in each case, is related to the magnitude ratio change of the signal emerging from the arm containing the standard phase shifter to the residual carrier, as discussed in the modulation section of this report. These errors may also be eliminated through use of the measurement procedure outlined in [1].

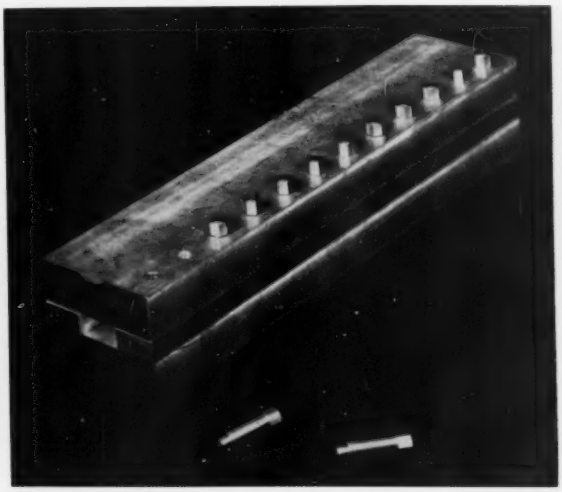

FIGURE 12. *Construction detail of adjustable waveguide section.*

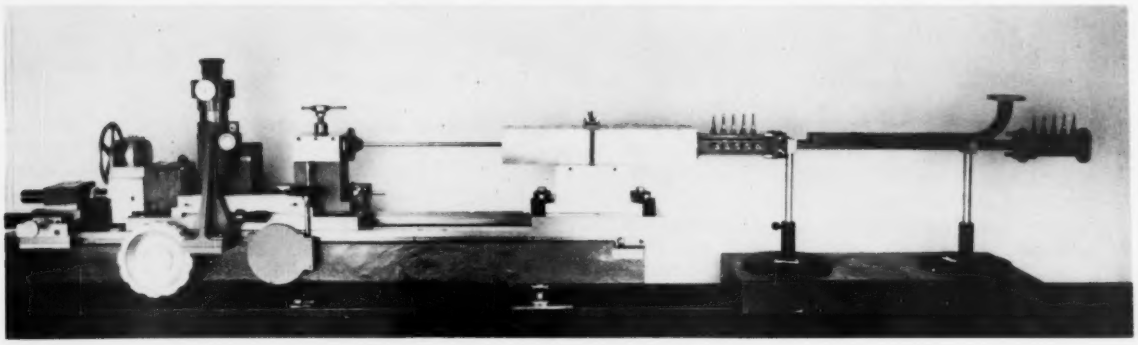

FIGURE 13. *Standard phase shifter.*

Because the standard phase shifter relates the phase shift produced to a measured length in waveguide wavelengths, the frequency stability of the source must be considered. If the change of phase of an ideal phase shifter [6] is

$$\psi=\frac{720l}{\lambda g}\text{ degrees,} \tag{4}$$

then the phase error introduced by frequency instability is

$$\frac{\Delta\psi}{\psi}=\frac{\frac{\partial\psi}{\partial F}\Delta F}{\psi}=\left(\frac{\lambda g}{\lambda}\right)^2\frac{\Delta F}{F}\frac{\text{degree error}}{\text{degree phase shift}}, \tag{5}$$

where F is the nominal frequency of the source and λ and λg are the free space and waveguide wavelengths. A graphical presentation for this error for WR–90 waveguide is shown in figure 14.

Changes in the laboratory environment affect the dielectric constant of the air in the standard phase shifter and will, therefore, introduce a measurement error. The use of (4) and the relation

$$\lambda g=\frac{1}{\sqrt{F^2\mu\epsilon-\frac{1}{(2a)^2}}} \tag{6}$$

gives the following error:

$$\frac{\Delta\psi}{\psi}=\frac{\frac{\partial\psi}{\partial\epsilon}\Delta\epsilon}{\psi}=\left(\frac{\lambda g}{\lambda}\right)^2\frac{\Delta\epsilon}{2\epsilon}\frac{\text{degree error}}{\text{degree phase shift}} \tag{7}$$

where $\epsilon=\epsilon_0\epsilon_r$.

An approximate dielectric constant for air in the laboratory environment can be calculated through the use of an equation for the radio refractive index of air [7].

$$N=\frac{77.6}{T}\left(P+\frac{4810e}{T}\right), \tag{8}$$

where

$$N=\frac{(\epsilon-1)10^6}{2}$$

ϵ=the dielectric constant,

P=partial pressure of air in millibars,

e=partial pressure of water vapor in millibars, and

T=absolute temperature, ° K.

Bean [7] has shown that changes in N, and thus ϵ, due to small changes in temperature, pressure, and vapor pressure may be evaluated from the partial derivatives of (8).

$$\Delta N=\frac{\partial N}{\partial T}\Delta T+\frac{\partial N}{\partial e}\Delta e+\frac{\partial N}{\partial P}\Delta P$$

$$=\frac{77.6}{T}\left(\Delta P+\frac{4810\Delta e}{T}-\frac{P\Delta T}{T}-\frac{9620e\Delta T}{T^2}\right). \tag{9}$$

Figure 15 is a graph of the limits of phase error for a variation in dielectric constant.

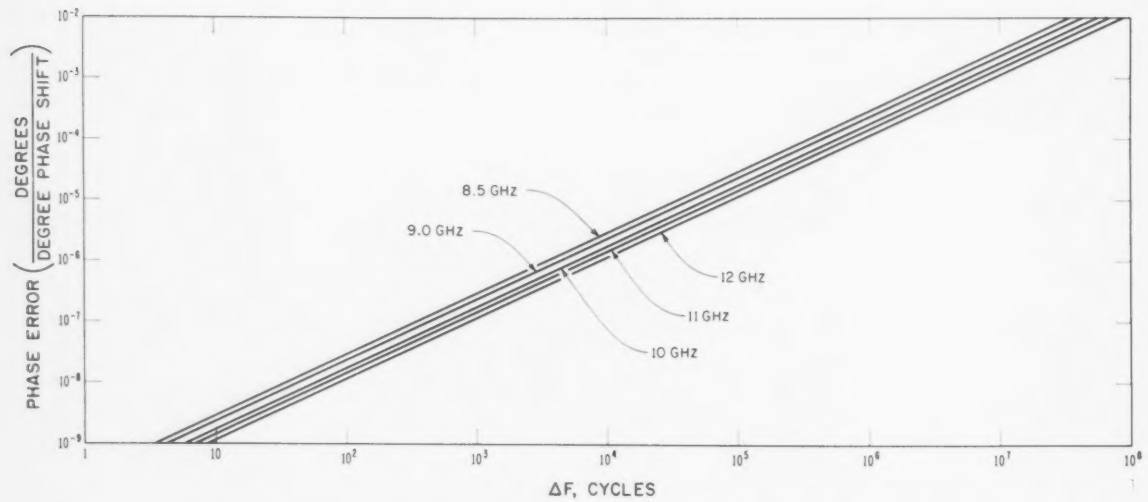

FIGURE 14. *Phase error versus frequency instability for the standard phase shifter.*

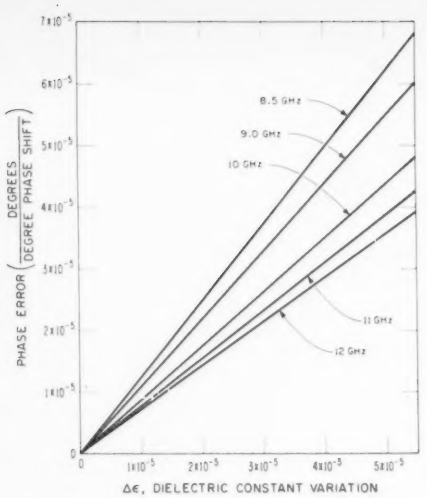

FIGURE 15. *Phase error versus dielectric constant variation.*

3.2. Other Errors

a. Mismatch Errors

The phase error introduced by mismatch of the unknown, when inserted into the system, has been analyzed and presented in reference [8].

b. Microwave Frequency Instability Effects

The microwave signal out of a source is propagated to the detector through two electrical paths. The physical length of these two paths will never be exactly equal in the systems discussed in this report, because the sliding short circuit will always be repositioned, thus changing the length of the reference arm.

The change of phase of the signal at the detector relative to the generator is

$$\varphi_1=\frac{360l_1}{\lambda g} \text{ degrees through path one,}$$

$$\varphi_2=\frac{360l_2}{\lambda g}\text{ degrees}=\frac{360l_1}{\lambda g}+\frac{360l'}{\lambda g}$$

degrees through path two, (10)

l_1 being the length of path one and λg being the average wavelength through path one, where l_2 is the total path length through channel 2 and l' is the difference in length of arms one and two. The phase difference at the detector is then

$$\Phi_0=\varphi_2-\varphi_1=\frac{360l'}{\lambda g}. \tag{11}$$

Only the phase difference, Φ_0, needs to be considered here, because if $\Phi_0=0$, then the paths are of the same length and the relative phase remains constant with changes in frequency.

The change of phase Φ_0, with changes in frequency, can be found by determining the partial derivative of (11).

$$\Delta\varphi_0=\frac{\partial\Phi_0}{\partial f}\Delta f=360\left(\frac{\lambda g}{\lambda^2}\right)l'\frac{\Delta f}{f}\text{ degrees.} \tag{12}$$

A graph of the phase change described by (12) is presented in figure 16.

c. Dissimilar Changes in the Microwave Bridge Arms

Inhomogeneous temperature variations within the laboratory, particularly those affecting the microwave bridge arms, can introduce phase differences of appreciable magnitude. An expression for the error introduced by this effect can be derived through the use of (10):

$$\varphi_1=\frac{360l_1}{\lambda g},$$

$$\varphi_2=\frac{360l_2}{\lambda g}.$$

Assume that the total effective bridge characteristic change occurs in arm two of the microwave bridge circuit. Then, the following relationship can be used:

$$\varphi_2=\frac{360l_2}{\lambda g}=\frac{360l_2\sqrt{1-\left(\frac{\lambda}{2a}\right)^2}}{\lambda}, \tag{13}$$

φ_2 being the total phase change throughout the length of the arm.

Inspection of (13) reveals that temperature effects upon the bridge arm can change the total phase shift through the arm and, thus, the measured relative phase shift either by changing the length l_2 or the width of the guide. It would be an extremely difficult task to determine theoretically the the amount of error introduced by each variable. The sensitivity of the system analyzed in this report to changes of this type is readily seen in figure 17.

4. Automation

The system described in this report, using either of the two types of modulation discussed above, is readily adaptable for automated measurements. The objective of automation, in view of the nature of this system and the type of data that will be collected from it, is to provide for continuous monitoring of the modulation frequency component out of the detector and adjusting of the microwave phase from the reference channel to reduce the modulation frequency fundamental to zero, thus maintaining bridge balance at all times. A suitable indicator device will then display phase changes in the signal emerging from the reference phase shifter. Hence, if phase changes occur in the signal traversing

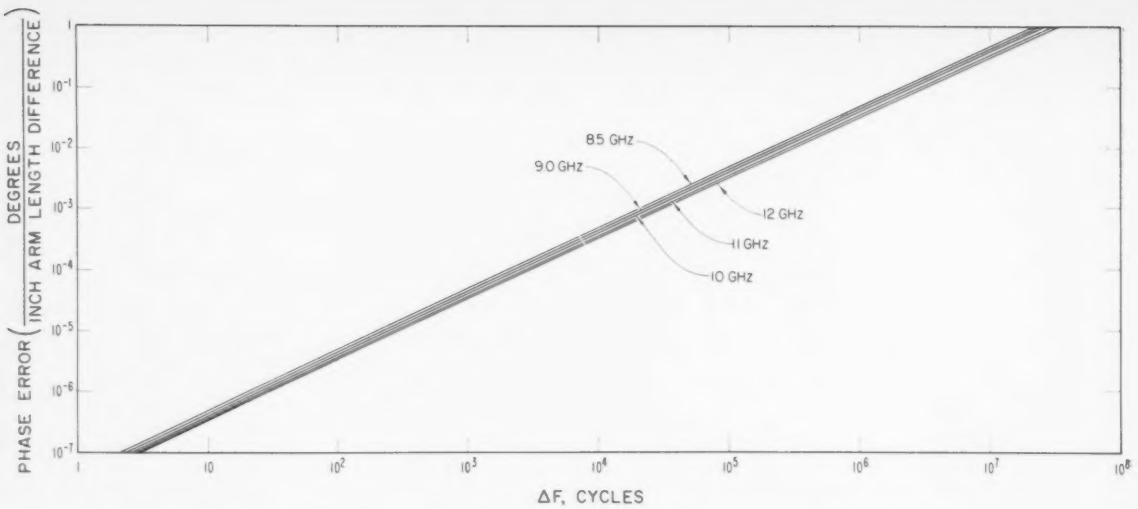

FIGURE 16. *Phase error versus frequency instability for bridge arms of unequal length.*

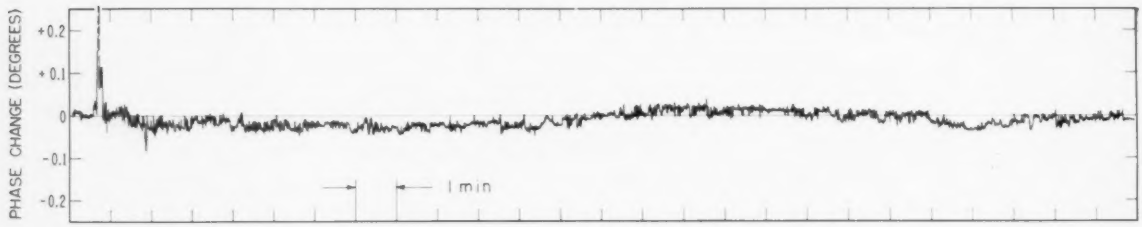

FIGURE 17. *Phase stability of the entire system in a normal laboratory environment.*

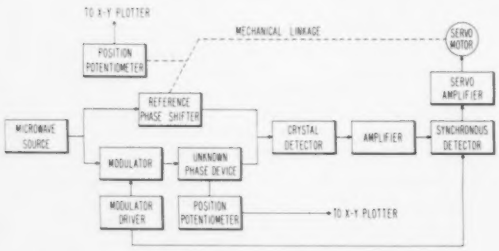

FIGURE 18. *Block diagram of automation system.*

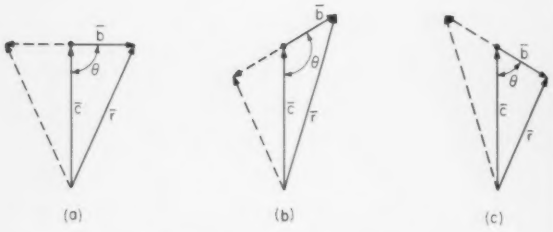

FIGURE 19. *Derivation of servo error signal.*

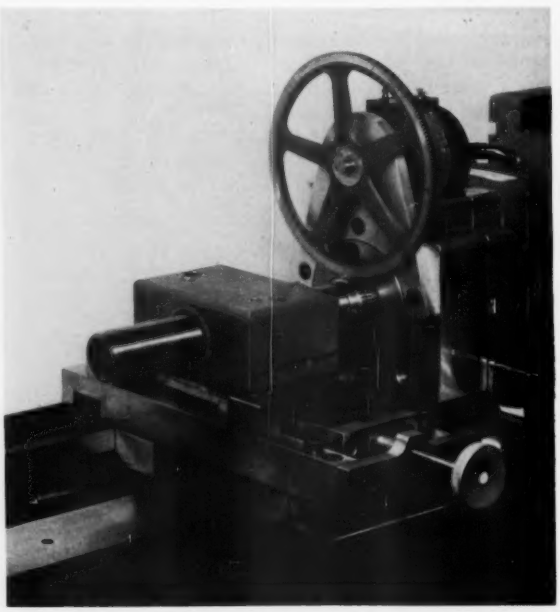

FIGURE 20. *Position potentiometer mechanical linkage.*

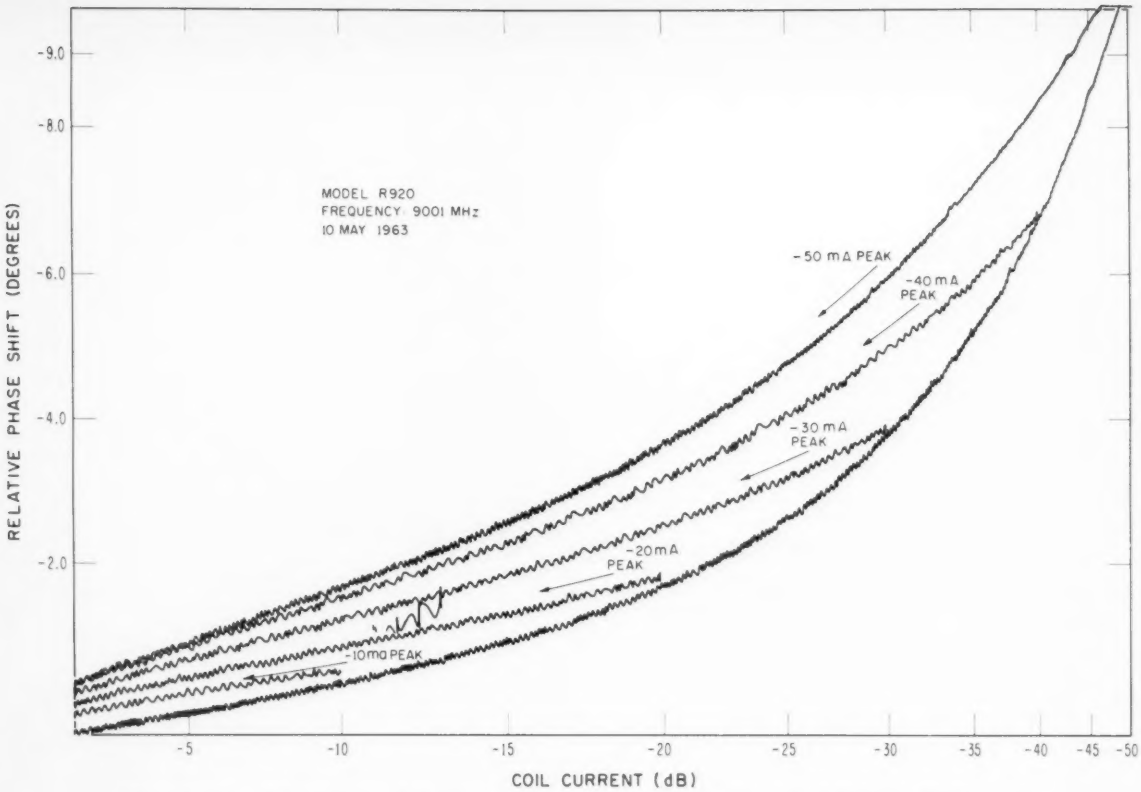

FIGURE 21a. *Relative phase shift versus coil current for low attenuation side of Gyraline Model R920.*

the channel containing the device under calibration, this change will be detected and automatically balanced out by a change of relative phase in the reference signal. The change of phase shift through the unknown will then exactly equal the change of phase shift through the reference phase shifter, as displayed by the indicator, to within the limits set by the measurement error.

An automatic phase tracking system capable of fulfilling this requirement has been constructed and is shown in figure 18. The error signal used to actuate the servo system is derived in a manner which is explained vectorially in figure 19 for the balanced modulation system.

Here, $\overline{c}$ is the vector representing the unmodulated component, and $\overline{b}$ is the vector representing the modulated (suppressed carrier) component, during the positive half-cycle of the modulation. The vector $\overline{r}$ is the resultant of $\overline{c}$ and $\overline{b}$. The dotted vectors depict the situation during the negative half-cycle of the modulation. Note that in (a), where $\theta=90°$, the resultant contains a second harmonic, but no fundamental of the modulation frequency. In (b) and (c), the fundamental is present, increasing in (b) with positively increasing $\overline{b}$, and decreasing in (c) with positively increasing $\overline{b}$. Hence, as the phase angle between the modulated and unmodulated components decreases from greater than 90°, through 90°, to less than 90°, the fundamental component of $\overline{r}$, decreases in magnitude to zero, reverses sign (or phase), and increases in magnitude with the new sign (or phase).

With the modulated subcarrier system a similar result is derived as the phase between carrier and subcarrier passes through the value such that the phase angle between the subcarrier and the resultant is 90°. In either case, the component of the resultant having the frequency of the fundamental modulation is selected by the synchronous detector and used to actuate the servo system to drive the reference phase shifter to effect a fundamental modulation frequency null in the resultant. The direction of the servo is opposite for opposite phases of the error signal, so that the reference phase shifter is always repositioned to restore the fundamental modulation frequency null illustrated by the vector relationship of figure 19a. The relative positions of both the reference phase shifter and an unknown device can be indicated automatically, in some manner. In the system used for this evaluation, linear position potentiometers are employed, their outputs being fed to an *X-Y* plotter, which provides a direct presentation of the calibration data. Figure 20 shows the coupling

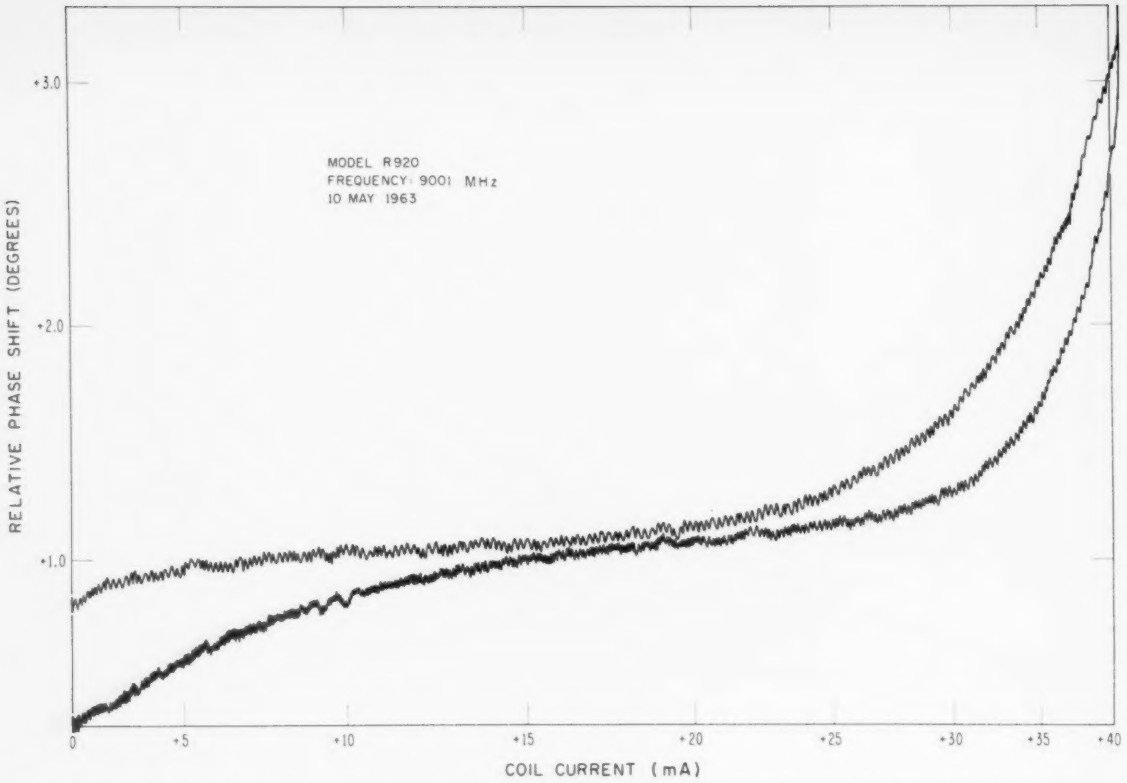

FIGURE 21b. *Relative phase shift versus coil current for high attenuation side of Gyraline Modulator Model R920.*

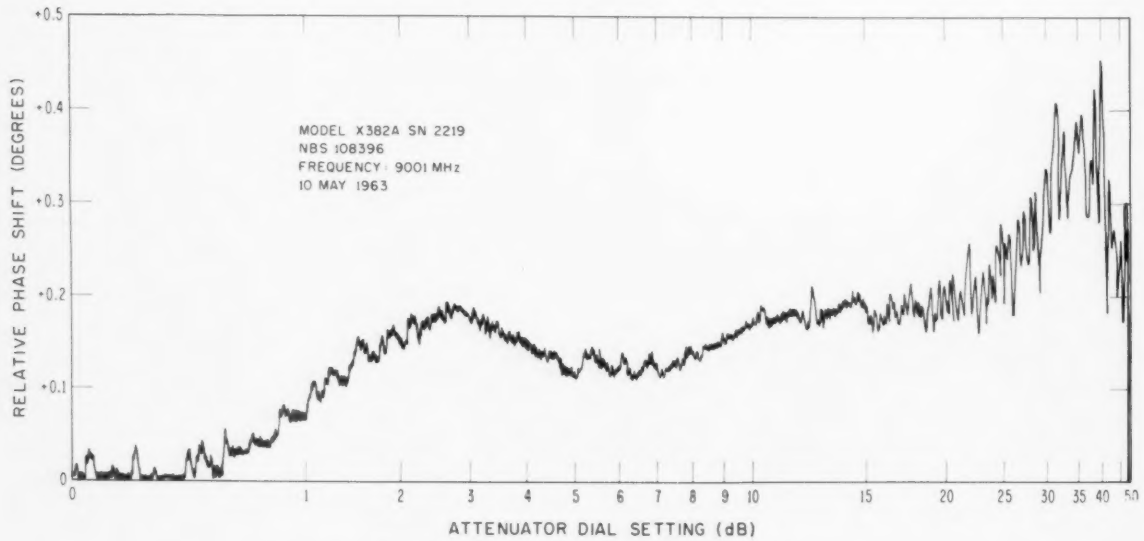

FIGURE 22. *Relative phase shift of a Rotary Vane Attenuator.*

between the standard phase shifter and position potentiometer.

5. System Measurement Capability

Phase data were collected on several commercial microwave components. Figure 21 is a plot of the relative phase characteristics of a gyraline modulator. Because the attenuation characteristics vary with coil current, the servo-loop gain was set at maximum at the beginning of the run. This was done to insure maximum sensitivity of the servo system.

Because of the maximum gain, the servo system was overdriven and broke into oscillation about the null, as is evidenced by the oscillations in figure 21. It can be seen that these oscillations resulted in a peak-to-peak microwave phase variation of approximately 0.075 deg. The actual phase shift of the device is, then, the average of this oscillation. The maximum error for this data is 0.117 deg.

Figure 22 is the phase characteristic for a commercial rotary-vane attenuator. Again the servo system was overdriven to insure maximum system sensitivity. The maximum error for this data was found to be 0.110 deg.

6. References

[1] G. E. Schafer (1960), A modulated subcarrier technique of measuring microwave phase shift, IRE Trans. on Instr. **I-9,** No. 2, 217–219.

[2] S. D. Robertson (1949), A method of measuring phase at microwave frequencies, Bell Tech. J. **28,** No. 1, 99–103.

[3] R. C. Mackey (1962), Some characteristics of microwave balanced modulators, IRE Trans. on MTT, **MTT-10,** No. 2, 114–117.

[4] M. Magid (1958), Precision microwave phase shift measurements, IRE Trans. on Instr. **I-7,** Nos. 3 and 4, 321–331.

[5] R. N. Assaly (Jan. 1961), The study of waveguide shorting plungers, Mass. Inst. Tech. Lincoln Lab. Rept. No. 315G–1, 35 pp.

[6] G. E. Schafer and R. W. Beatty (Oct.–Dec. 1960), Error analysis of a standard microwave phase shifter, J. Res. NBS **64C,** (Engr. and Instr.), No. 4, 261–265.

[7] B. R. Bean (1962), The radio refractive index of air, Proc. of the IRE, **50,** No. 3, 260–273.

[8] G. E. Schafer (1960), Mismatch errors in microwave phase shift measurements, IRE Trans. on MTT, **MTT-8,** No. 6, 617–622.

(Paper 69C1–186)

JOURNAL OF RESEARCH of the National Bureau of Standards—C. Engineering and Instrumentation
Vol. 69C, No. 1, January–March 1965

Polarographic Analysis of Titanium (IV)—EDTA Complex: Application to Paint Pigments

Harvey W. Berger and Barry C. Cadoff

(August 3, 1964)

The Ti^{+4}-EDTA complex, buffered at *p*H 4.7, has been found to give polarographic waves suitable for the analysis of TiO_2 in paint pigments. A linear relationship between diffusion current and concentration of Ti^{+4} for the range 2.8×10^{-5} to 8.4×10^{-3} *M* has been observed. The pigments analyzed have been either in the dry form or extracted from whole paint. The method gives results in good agreement with the more complicated and time-consuming standard wet chemical method.

Standard methods for the analysis of TiO_2 in paint pigments involve rather tedious and time-consuming procedures and are also subject to several interfering ions, such as iron, chromium, and arsenic [3,6].[1] In searching for a faster, simpler method, and one which would be comparatively free of interferences, polarography was investigated. A study of the literature revealed that a variety of supporting electrolytes have been used, such as tartrate, citrate, oxalate, ethylenediaminetetraacetic acid (EDTA). These methods have been reviewed by Codell [2]. More recently, Banerjee, Budke, and Miller reported the use of a sulfuric acid-potassium persulfate medium for the determination of titanium in ores [1].

Sinyakova [5] and Pecsok and Maverick [4] studied the chemistry of the Ti-EDTA complex and found that reversible waves could be obtained over a fairly wide *p*H range. The latter authors suggested that this could be adapted to analytical uses.

This paper reports the development of a polarographic method, employing EDTA as the complexing agent, that results in a rapid, accurate analysis of TiO_2 in dry pigments or pigments extracted from paint.

1. Experimental Detail

1.1. Apparatus and Reagents

A Sargent Model XV Polarograph with a dropping mercury electrode and an H-cell were used. The cell was placed in a constant temperature bath maintained at 25.0 ± 0.1 °C. Measurements of *p*H were made with a glass electrode *p*H meter.

Reagent grade titanium dioxide was used to determine the diffusion current constant (I_d). This standardization and calibration was checked with National Bureau of Standards Titanium Dioxide (Standard Sample No. 154).

[1] Figures in brackets indicate the literature references at the end of this paper.

1.2. Procedure

For pure samples of titanium dioxide a maximum of 0.2 g was weighed to 0.1 mg into a 100 ml beaker and 5.0 ml of concentrated H_2SO_4 and 1.0 g of $(NH_4)_2SO_4$ were added. The beaker was left uncovered, heated slowly at first and then rapidly, to fuming. After fuming for 5 min, the solution was cooled to room temperature and 15 ml of water was added very slowly with vigorous stirring. Two grams of the disodium salt of EDTA, dissolved in 15 ml of 7*M* NH_4OH, was then added to the sulfuric acid solution. The *p*H at this point was approximately 1.5 and 40 ml of 4*M* sodium acetate-acetic acid buffer was added to bring the *p*H to 4.7. The solution was diluted with water to a final volume of 250 ml. An aliquot was placed in the H-cell and purged with nitrogen for 10 min. A polarogram was then run. The graphical method described by Willard, Merritt, and Dean [7] was used to determine the wave heights.

The sulfuric-acid-insoluble components, such as white lead and silica, in titanium-containing pigments caused the formation of large aggregates which could not be adequately dispersed without prolonged heating. Therefore, it was necessary to modify the method for the preparation of solutions. After fuming for 5 min, the mixture was stirred thoroughly with a glass rod to break up any lumps of pigment. The mixture was then reheated to fuming for 1 min. The procedure for pure TiO_2 was then followed. It was found to be unnecessary to filter the mixture before running a polarogram.

2. Results and Discussion

2.1. Standardization

The data obtained for the analyses of reagent grade TiO_2 are shown in table 1. The I_d is independent of the concentration of titanium over the range 3×10^{-5} to 8×10^{-3} M. Although for the

purposes of pigment analysis it would be unnecessary to deal with concentrations at the lower end of the range, the method was investigated to these further limits to assess its potential for use as a general method of analysis which would be valid over a rather large concentration range.

The electrode reaction at *p*H 4.7 is [4]:

$$TiOY^{-2}+2H^{+}+e^{-}=TiY^{-}+H_2O$$

where Y represents the EDTA ligand. This equation is, in fact, valid for values of *p*H from about 2.5 to 8. Below *p*H 2.5 the electrode reaction is $TiY+e^{-}=TiY^{-}$. From calculations using the reported values for the equilibrium constants the concentrations of $TiOY^{-2}$ and TiY^{-} are equal at a *p*H of 2.4.

TABLE 1. *Polarographic analysis of titanium-EDTA complex using reagent grade* TiO_2

	T(IV) concentration mmoles/liter	Diffusion current $i_d(\mu A)$	Diffusion current constant I_d[1]
1	0.02804	0.0786	1.454
2	.06003	.1692	1.462
3	1.532	4.312	1.460
4	2.944	8.323	1.466
5	2.959	8.320	1.458
6	5.842	16.620	1.476
7	5.872	16.616	1.468
8	5.907	16.750	1.471
9	6.824	19.218	1.461
10	6.859	19.213	1.453
11	8.145	23.159	1.475
12	8.190	23.15	1.466
13	8.225	23.386	1.475
14	8.270	23.376	1.466
15	8.446	23.924	1.465
Average			1.465
Standard deviation			0.007₃

[1] $I_d = i_d/Cm^{2/3}t^{1/6}$.
C=concentration in mmoles/liter.
m=drop mass in mg/sec.
t=drop time in seconds.

The electrode reaction taking place below *p*H 2.5 was not used as the basis of an analytical procedure because the solubility of EDTA in such acidic solutions is below that which will permit the preparation of clear solutions containing 2 g of the disodium salt. In addition, at *p*H 2.5, three forms of EDTA are present: H_4Y, H_2Y^{-2} and primarily H_3Y^{-}. Between *p*H 3.5 and 5.5, essentially the only form present is H_2Y^{-2}. It is preferable that only one form of the ligand be involved in the complexation reaction. At *p*H 4.7, well defined, reversible polarographic waves are obtained which have low residual currents and flat plateau regions.

2.2. Effects of Supporting Electrolyte

The effect of sulfate ion concentration on the diffusion current (i_d) is shown in figure 1. With an excess of sulfate, added during the solution step, a wave appears at −0.7 V. versus the Saturated Calomel Electrode (S.C.E.), (curve C). This wave, attributed to a Ti-sulfate complex (curve A) [4], is formed at the expense of the Ti-EDTA complex and begins to appear at approximately 0.7 *M* SO_4^{-2}.

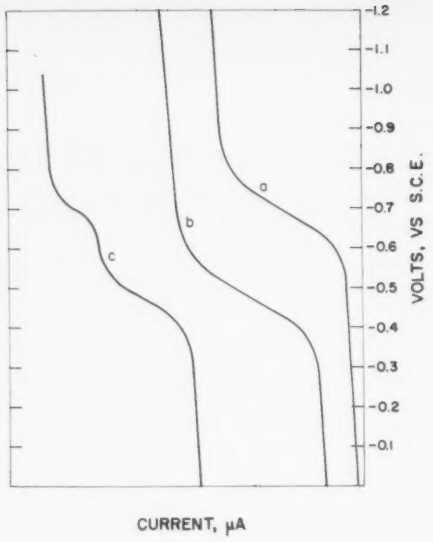

FIGURE 1. *Representative polarographic curves.*

a. H_2SO_4 solution of Ti(IV)−no EDTA 0.4 M SO_4^{-2} *p*H=4.5.
b. Same as above but with EDTA *p*H=4.7.
c. Same as b., but with 1*M* SO_4^{-2}.

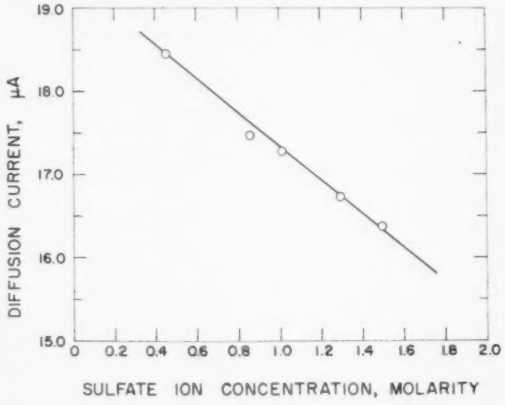

FIGURE 2. *Effect of sulfate ion concentration on the Ti(IV)–EDTA diffusion current.*

The addition of a large excess of EDTA does not achieve the complete removal of this wave. The Ti-EDTA reduction wave is shown in curve B. The effect of increasing sulfate concentration on the diffusion current of the Ti-EDTA complex is shown in figure 2. There is a linear decrease of i_d, and thus a decrease in the assay of titanium, with increase in the sulfate ion concentration and it is, therefore, necessary that the sulfate concentration be kept low and constant. In the routine preparation of solutions the concentration of sulfate can be sufficiently controlled to account for less than 0.1 percent change in the diffusion current. On the other hand, the Ti-EDTA diffusion current is

independent of the total concentration of EDTA over a range of 8 to 40 mM.

The order of addition of reagents has a pronounced effect upon the diffusion current. Addition of the buffer to the sulfuric acid solution prior to the addition of EDTA results in the formation of a different titanium complex which cannot be completely eliminated by the subsequent addition of EDTA.

2.3. Effect of Aging

Figure 3 illustrates the decrease of the diffusion current with time. About one week after the preparation of solutions a yellow color became noticeable and increased in intensity with time. Erratic results were obtained if solutions were left standing more than three days.

2.4. Effect of Temperature

The temperature dependency of the diffusion current was studied over the range of 20 to 30 °C. It was found that an increase of 1.4 percent in the diffusion current occurred for each degree rise in temperature.

2.5. Effect of Maximum Suppressor

No polarographic maxima were encountered in the analyses of the titanium-EDTA solutions and no maximum suppressors were used. When some other reducible cations are in solution, however, small maxima do occasionally occur. The effect of gelatin on the titanium-EDTA diffusion current was studied in the event that the simultaneous analysis of titanium and other cations might necessitate the presence of a maximum suppressor. The effect of gelatin on the diffusion current is shown in figure 4. Between 0.008 percent and 0.05 percent i_d decreases rapidly with increasing percentages of gelatin. Therefore, analyses should not be performed in this range. Lower percentages of gelatin are preferable if they succeed in eliminating maxima since maximum suppressors tend to change the values of the parameters in the Ilkovic equation, which is used to calculate I_d.

2.6. Interferences

A study was made of possible chemical interferences in the analysis. Weighed amounts of compounds were added in 1:1 molar ratios to the TiO_2 before dissolving in sulfuric acid. Al(III), Mg(II), Ca(II), Cr(III), Pb(II), Zn(II), and Fe(III) did not interfere in the analysis. Sb(III), however, did cause interference. In all of these determinations, it was necessary to have sufficient EDTA present to fully complex the foreign cations. For example, lead and zinc will compete for EDTA and, if those cations are added to a solution in which there is not sufficient EDTA available, the Ti-EDTA complex will dissociate so that the preferential lead and zinc complexes will form. In such cases, a titanium wave

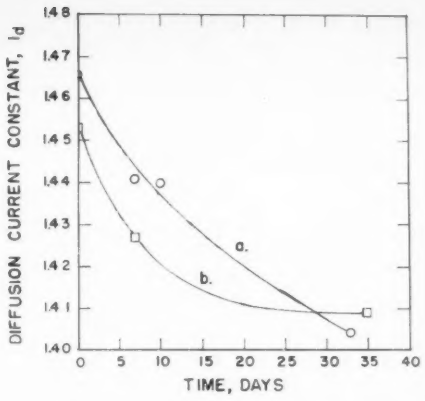

FIGURE 3. *Effect of time on the Ti(IV)–EDTA diffusion current constant.*

a. 0.1652 g. TiO_2/250 ml.
b. 0.1370 g TiO_2/250 ml.

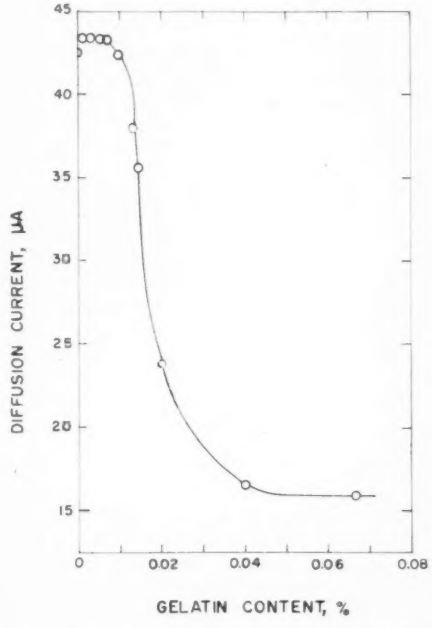

FIGURE 4. *Effect of gelatin on the Ti(IV)–EDTA diffusion current.*

attributable to the Ti-sulfate complex appears which cannot be completely removed on the further addition of EDTA.

2.7. Analysis of Pigments

Table 2 presents data on the analysis of pure TiO_2 as well as several pigments extracted from paint and a synthetic pigment extracted from a mixture of white lead, zinc oxide, titanium dioxide and bodied

linseed oil. The standard method referred to in the table utilizes the Jones reductor method for the titanium analysis [3]. The precision and accuracy of the polarographic method is seen to be comparable to the standard volumetric method. In addition, the polarographic method is considerably faster, less subject to interferences and requires smaller sample weights.

TABLE 2. TiO_2 *Assay of NBS standard paint pigments*

	Sample	Titanium dioxide content		Difference in methods
		% by Volumetric method	% by polarographic method	
1	Reagent grade	99.46±0.30 [4]	(1)	
2	NBS std.[5]	98.58±0.14	98.57±0.06	−0.01
3	Synthetic pigment	22.71±0.19	22.61±0.19	−0.10
4	TT–P–102 [3]	13.27±0.25	13.41±0.22	+0.14
5	TT–P–115	13.84±0.16	13.40±0.10	−0.44
6	TT–P–115 [2]	13.5₆±0.2₂		−0.16
7	TT–P–25	8.62±0.11	8.54±0.09	−0.08
8	TT–P–21	3.87±0.30	3.78±0.15	−0.09
	Average omitting run 5			0.10

[1] Reagent Grade TiO_2 used as standard material.
[2] Analysis of same pigment used in Run 5 by spectrophotometric method (Beckman D. U. Spectrophotometer) to check large difference between volumetric and polarographic results.
[3] Sample numbers refer to Federal Specification of the original paint from which pigment was extracted.
[4] Average of at least four determinations on all samples; precision is expressed as standard deviation.
[5] Standard Sample No. 154 certified as 98.7 percent TiO_2.

The authors express their appreciation to George Marinenko and John K. Taylor of the National Bureau of Standards for their help and encouragement throughout the course of this work.

3. References

[1] D. K. Banerjee, C. D. Budke and F. D. Miller, Anal. Chem. **31,** 1836 (1959).
[2] M. Codell, Analytical Chemistry of Titanium Metals and Compounds, p. 96 (Interscience Publishers, Inc., New York, 1959).
[3] Federal Test Method Standard No. 141, Method 7081 (GSA).
[4] R. L. Pecsok and E. F. Maverick, J. Am. Chem. Soc. **76,** 358 (1954).
[5] S. I. Sinyakova, Zh. Anal. Khim. **8,** 333 (1953).
[6] Standard Methods of Chemical Analysis, 6th ed. **II,** Part B, ch. 37 (D. Van Nostrand Company, Inc., Princeton, N.J., 1963).
[7] H. H. Willard, L. L. Merritt, Jr., J. A. Dean, Instrumental Methods of Analysis, p. 544 (D. Van Nostrand Company, Inc., Princeton, N.J., 1958).

(Paper 69C1–187)

JOURNAL OF RESEARCH of the National Bureau of Standards—C. Engineering and Instrumentation
Vol. 69C, No. 1, January–March 1965

Soil Resistivity as Related to Underground Corrosion and Cathodic Protection

W. J. Schwerdtfeger

(August 4, 1964)

Corrosion data discussed in this paper are based upon measurements made on about 4500 specimens of commonly used plain wrought ferrous materials which had been buried in back-filled trenches at 86 National Bureau of Standards sites for periods up to 17 years. The soils ranged in resistivity from 50 to 54,000 Ω-cm and in *p*H from 2.6 to 10.2.

Maximum pit depths at 5 years of exposure are taken from pit depth-time curves and the curves are also extrapolated to probable pit depths at 30 years for each of the 86 sites. Furthermore, data on the specimens are adjusted to maximum pit depths that might be expected on a larger area, equivalent to that of the exterior surface of a 20 ft length of 8 in. uncoated wrought ferrous pipe. Maximum penetration rates and pit depths are presented with respect to soil resistivity and *p*H.

Weight losses which resulted from about 2 years of underground exposure are converted to corrosion current densities and after this period of exposure current densities are calculated from the slopes of weight loss-time curves for each site. On the basis of ratios of protective current to corrosion current obtained from polarization curves on steel specimens underground and in soils in the laboratory, the corrosion current densities can be adjusted to approximate current densities necessary for cathodic protection.

1. Introduction

Between the years 1922 and 1952 the National Bureau of Standards exposed thousands of metallic specimens at numerous underground sites throughout the United States. Corrosion rates of over 300 varieties of protected and unprotected metals and alloys were evaluated about every 2 years for exposure periods as long as 17 years. The accumulated corrosion data were compiled by Romanoff [1].[1] The engineering significance of early NBS data pertaining to some commonly used wrought ferrous materials from the original 47 test sites was discussed in considerable detail by Logan [2]. The present paper is similar but includes data from about 40 additional sites and, based on the total available data, offers suggestions on the current densities probably required for cathodic protection.

In this paper, in addition to extrapolating the average maximum pit depths to 30 years as Logan [2] did, the weight losses of the specimens are converted to corrosion current densities. From these data the approximate current densities required for the cathodic protection of bare underground surfaces can be estimated. Although, based on NBS data, there is no precise relationship between the corrosivity and resistivity of soils, a general relationship is now revealed by the total accumulated data. This is also indicated by the data of Scott [3]. Recently, Schaschl and Marsh [4] discussed the effect of resistivity on the corrosion rates of steel in aqueous environments and showed that for resistivities above 400 Ω-cm, the corrosion rate bears an inverse relation to the resistivity of the electrolyte. Thus, a study is undertaken of the influence of soil resistivity, a measurement readily made in the field. The combined relation of *p*H and soil resistivity to corrosion rate was also investigated. The metals to which our data apply are confined to open-hearth iron, hand-puddled and mechanically puddled wrought irons, open-hearth and Bessemer steels, all without added alloying constituents.

[1] Figures in brackets indicate the literature references at the end of this paper.

2. Corrosiveness of Soils

The corrosiveness of a soil might be defined as its destructive or deteriorating effect on a metallic surface, as measured by weight loss and pit depth.

A soil can be potentially corrosive and yet have a negligible effect on plain ferrous materials. This was recently shown by Romanoff [5] as a result of his examination of steel pilings (pulled) exposed from 7 to 40 years in a variety of soils some of which had resistivities as low as 300 Ω-cm. No appreciable amount of corrosion was observed on pile surfaces adjacent to soils into which the piles had been driven below the water table, referred to as "undisturbed" soil. This type of exposure is in contrast to the soil exposure of metals in back-filled trenches, referred to as "disturbed" soil. On driven piling, the corrosion rate decreases rapidly as the initially available oxygen is depleted by the corrosion process and the accessibility of more is limited. In disturbed soils oxygen is more readily replenished and the soil is only very slowly restored to its natural state. This gives rise to differential aeration and then the corrosiveness of the soil depends largely on its physical and chemical properties. Properties of the soils to be considered have already been described [1].

The most severe corrosion usually takes place at low elevations in poorly drained disturbed soils, such as clays and tidal marshes, where, although also poorly aerated, the differential-aeration effects are large because of soil shrinkage. Then too, salts accumulate in these areas and increase the conduc-

tivity of the soil. The *p*H of such soils is usually neutral or in the alkaline range. In contrast, the least corrosive soils are well aerated, well drained and seem to be in areas of high annual precipitation which causes the salts to be washed away and increases the soil resistivity. The *p*H is usually between 4 and 7.

3. Effect of Area and Duration of Exposure

The data used in this paper are mostly for accumulated exposure periods of 12 and 14 years. In some soils the accumulated periods are 7 and 17 years. The exposed area of each specimen was about 0.4 ft^2.

It is of importance to know the effect of larger areas and longer periods of exposure. These variables have been considered by previous investigators [6,7]. Years ago, Scott [6] observed that pit depth is a function of the area of metal exposed. Based on National Bureau of Standards data and on data from pipelines, a linear relation was obtained when the logarithm of the average of the deepest pits (several specimens) on a given area was plotted against the logarithm of the area for increasing areas. Thus, for a modest extrapolation of the area, Scott suggested the empirical equation,

$$\log P = a \log A + \log b, \text{ or } P = bA^a, \qquad (1)$$

where P is the average maximum pit depth on the proposed area A, exponent a is the slope of the best linear plot, and b is the average maximum pit depth for a unit area. The useful form of this equation is,

$$P_2/P_1 = (A_2/A_1)^a \text{ or } P_2 = P_1(A_2/A_1)^a, \qquad (2)$$

where P_1 is the average maximum pit depth on a known area A_1, and P_2 is the extrapolated or calculated average maximum pit depth on some assumed area A_2 for the length of exposure time. Scott suggested as a standard area that of the exterior of a 20 ft length of 8 in. diam pipe which is about 45.16 ft^2. The values for the exponent, a, applicable to specimens in 47 soils have been given by Logan, Ewing, and Denison [7]. Based on their data, the average value of $a=0.15$ has been suggested for use with all soils, as the exponent is apparently not associated with any known soil property [8].

The effect of length of exposure time on rates of corrosion underground is better known than is the effect of area exposed. For example, it is well known that in some soils, after a few years, corrosion seems to cease. The effect of duration of exposure on corrosion rates depends on chemical and physical properties of the soils. Here again, it was observed that a linear relation appears to apply reasonably well between the logarithm of the average of maximum pit depths and the logarithm of the exposure period. This is expressed by the equation,

$$\log P = n \log T + \log k, \text{ or } P = kT^n, \qquad (3)$$

where P is the average maximum pit depth at some time T, n is the slope of the line of best fit, and k is the average maximum pit depth for a unit of time. Again, the useful form of the relation becomes,

$$P_2/P_1 = (T_2/T_1)^n \text{ or } P_2 = P_1(T_2/T_1)^n, \qquad (4)$$

where P_1 is the average maximum pit depth for the shorter period of exposure T_1, and P_2 is the average maximum pit depth at some longer time T_2. Logan, Ewing, and Denison [7] divided 47 NBS soil sites into 4 groups based on aeration and on drainage, ranging from well-aerated sands and sandy loams to tidal marshes. The exponent, n, was derived for each soil group and ranged from $n=0.19$ for soils having good aeration to $n=0.68$ for soils with very poor aeration, such as clays and tidal marshes. More recently, Scott [9] has proposed that the average rate of corrosion underground is inversely proportional to the square root of the duration of exposure time, that is, in eq (3), $n=0.5$.

4. Discussion of the Data

4.1. Maximum Pit Depths

The maximum pit depth data for 86 soil sites are given in table 1 and graphically presented with respect to soil resistivity and *p*H in figures 1 through 5. Figure 1 shows maximum pit depths on the specimens at 5 years taken from pit depth-time curves (not shown). On the average, pits are somewhat deeper in the soils with resistivities below 500 Ω-cm than in soils with higher resistivities but above 500 Ω-cm there appears to be no regular variation between pit depth and soil resistivity. However, the relationship looks different when the rate of maximum penetration after 5 years is plotted versus resistivity, as shown in figure 2. The data were calculated from the straight lines through points on the pit depth-time curves using rectangular coordinates. There now appears to be a definite trend to lesser pitting rates as resistivity increases. The effect of *p*H of the soil on maximum penetration rates is shown in figure 3. Note that the majority of very corrosive soils ($<$500 Ω-cm) are in the alkaline range ($>$ *p*H 7).

The effect on maximum penetration of increasing the area exposed from that of a specimen (about 0.4 ft^2) to a larger area (equivalent to that of a 20 ft length of 8 in. diam pipe) exposed to identical soil conditions, by calculations previously described, is shown in figure 4. Data pertaining to the effect of increased area are tabulated in table 1.

The estimated effect of increasing exposure time from 5 to 30 years is also shown in table 1, as based on linear extrapolation of data plotted on both rectangular and logarithmic coordinates. As would be expected, the pit depths extrapolated from log pit depth-log time curves are for the majority of soils somewhat smaller than the values from rectangular coordinates. Previous investigators, [7] whose work resulted in eq (3), favored the logarithmic relationship and their conclusions seem to be reasonable.

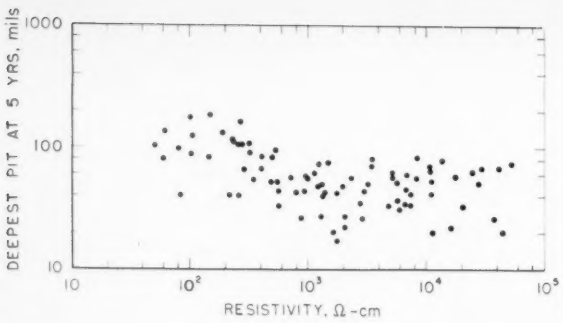

FIGURE 1. *Average of maximum pit depths on from 6 to 14 ferrous specimens buried in each of 86 underground soil sites.*
Pit depths are taken from the pit depth versus time curves at 5 years.

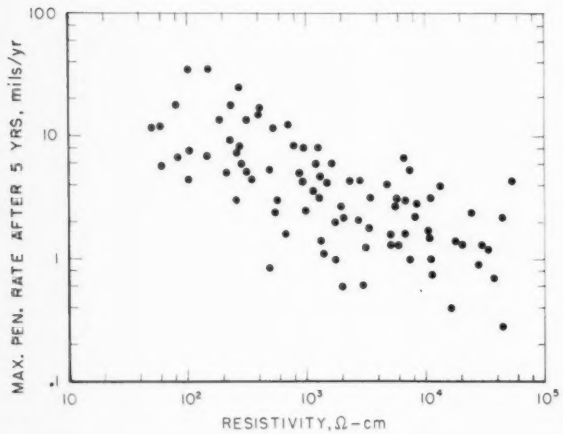

FIGURE 2. *Rates of penetration of the specimens (fig. 1), based on the maximum pit depth versus time curves, from 5 years to from 12 to 17 years (for the majority of the soils).*

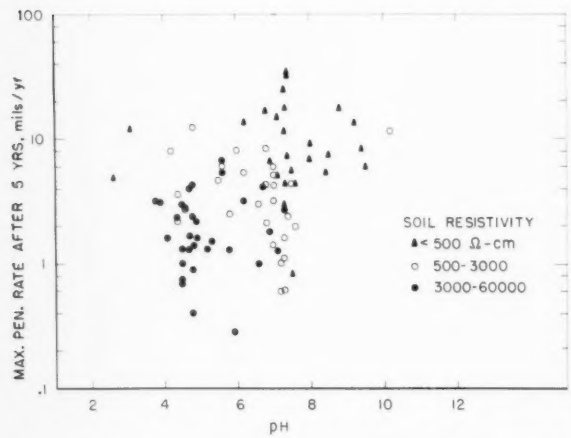

FIGURE 3. *Maximum rates of penetration (fig. 2) on specimens as related to* pH *for 3 ranges of soil resistivity.*

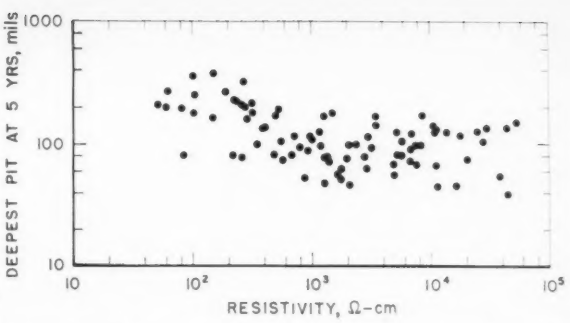

FIGURE 4. *Maximum pit depths at 5 years of underground exposure calculated for larger areas (equivalent to 20 ft of 8 in. diam bare pipe) from data on small pipe specimens (fig. 1).*

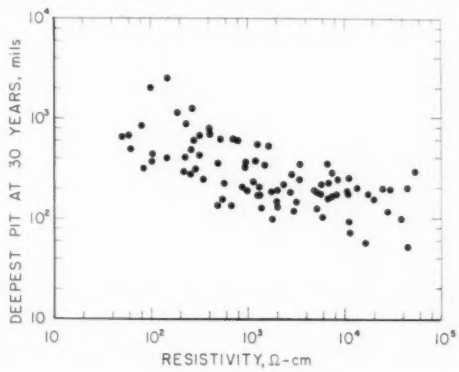

FIGURE 5. *Same as figure 4, except that the exposure time is extrapolated to 30 years.*

Data adjusted for the larger area shown in the last column table 1, are plotted against soil resistivity figure 5. Perforation of a pipe wall, ranging in thickness from 0.172 in. to 0.322 in. for 8 in. diam steel pipe, is predicted in almost all soils having resistivities less than 1000 Ω-cm. In some of these soils, many perforations would probably occur. For soils with resistivities over 2000 Ω-cm, and assuming the absence of stray currents or contact with more noble metals, the extrapolated data indicate that perforation of 8 in. diam (0.322 in. wall-thickness) steel pipe in 30 years is rather unlikely. However, the data definitely show the need for protective measures, such as coatings, cathodic protection or both, on wrought materials exposed to soils with resistivities less than 2000 Ω-cm and also even in some soils of higher resistivity, as indicated by predicted pit depths in a few of the soils shown above 25,000 Ω-cm, all depending on the hazard involved should a perforation occur.

Recent work by Scott [3, 9] has a direct bearing on the relation between soil resistivity and maximum penetration. Based on random measurements of soil resistivity in the field he found that a plot on log-probability coordinates of soil resistivity measurements for a given area versus estimated cumulative probability assumes a linear relationship in many

TABLE 1. *Maximum pit-depth* [a]

Soil site No. [b]	ρ [c]	pH	Internal drainage [d]	Time—5 yrs		Specimen pitting rate after 5 yrs [e]	Time—30 yrs		
				Specimen area A_1 [e]	Assumed area A_2 [f]		Specimen rectangular [h] co-ord	Specimen log-co-ord [i]	Assumed area A_2 [j]
	Ω-*cm*			*Mils*	*Mils*	*Mils/yr*	*Mils*	*Mils*	*Mils*
1	1215	7.0	P	48	96	6.0	198	190	378
2	684	7.3	P	44	82	1.6	84	72	134
3	30000	5.2	G	68	134	1.3	101	97	192
4	6670	5.6	F	34	72	6.7	202	165	351
5	1345	7.0	P	40	79	1.4	75	86	170
6	45100	5.9	G	20	39	0.28	27	26	52
7	2120	4.4	F	27	47	2.2	82	76	131
8	350	7.6	P	54	100	4.4	164	130	244
9	2820	6.8	P	35	79	2.1	88	82	185
10	7460	6.6	F	41	98	1.0	66	70	167
11	11000	5.3	G	64	124	1.5	102	90	174
12	3190	7.1	G	50	97	1.3	83	75	145
13	290	9.5	F	65	161	6.0	215	125	311
14	3520	6.2	F	80	169	3.2	160	165	348
15	489	7.5	P	52	83	0.84	73	84	134
16	8290	4.4	F	56	98	2.3	114	100	175
17	5980	4.5	F	31	56	1.3	64	57	103
18	1410	7.3	G	43	72	1.1	71	76	128
19	1970	4.6	G	48	77	2.7	116	92	148
20	2870	7.5	P	26	63	4.4	136	115	278
21	2370	6.2	F	56	103	4.4	110	120	220
22	5150	4.9	G	56	83	1.6	96	85	125
23	278	9.4	F	105	202	8.3	312	310	597
24	11400	4.5	G	20	45	0.75	39	32	72
25	1780	7.2	F	42	63	1.0	67	65	98
26	2980	7.3	G	60	114	0.61	77	67	118
27	570	6.6	VP	33	74	3.0	108	100	223
28	408	6.8	VP	83	137	17.0	508	420	693
29	1270	4.2	VP	73	169	8.1	276	235	545
30	1300	7.0	P	27	48	3.2	107	95	170
31	20500	4.7	G	33	75	1.3	66	69	156
32	5700	7.3	G	37	81	2.7	105	81	177
33	800	6.8	VP	43	95	8.4	253	270	598
34	4900	6.7	F	33	69	4.1	136	92	193
35	2060	7.3	G	22	99	0.60	37	43	193
36	11200	4.5	G	42	67	1.0	67	58	92
37	11200	3.8	P	53	131	3.2	133	103	254
38	38600	4.5	G	26	54	0.7	44	48	99
39	7440	5.6	F	34	69	5.4	169	140	284
40	970	6.0	P	58	115	8.1	261	185	365
41	1320	5.5	F	50	78	4.7	168	130	203
42	13700	4.7	F	79	125	4.0	179	135	214
43	60	3.1	VP	80	201	12.2	285	270	678
44	1000	5.8	G	55	111	2.5	118	95	191
45	263	7.4	P	40	78	7.3	223	240	469
46	1500	7.0	G	75	181	4.2	180	140	337
47	1770	7.6	P	17	52	2.0	67	60	183
51	190	6.2	VP	131	266	13.6	471	550	1117
53	17790	4.8	G	58	118	1.4	93	87	177
55	5210	5.8	G	62	126	1.3	95	90	183
56	406	7.1	VP	66	134	15.0	441	390	792
58	712	4.8	VP	57	116	12.6	372	305	619
59	1660	5.6	VP	28	57	6.0	178	260	528
60	218	2.6	P	40	81	5.0	165	145	294
61	943	6.8	P	44	89	4.3	152	160	325
62	6920	4.5	F	60	122	3.0	135	110	223
63	84	6.9	VP	40	81	6.7	208	155	314
64	62	7.5	F	134	272	5.7	277	240	487
65	148	8.0	G	82	166	6.9	255	195	396
66	232	8.0	F	112	228	6.0	262	200	406
52	234	8.8	VP	110	223	18.0	560	430	873
54	886	7.0	P	26	53	5.1	154	100	203
101	261	7.3	F	104	211	3.0	179	135	274
102	103	7.3	F	88	179	4.4	198	185	376
103	81	7.3	F	97	197	17.9	544	420	853
104	8500	4.6	G	84	171	2.8	154	120	244
105	28000	4.8	G	51	104	0.9	74	58	117
106	25000	4.8	G	63	128	2.4	123	98	199
107	54000	4.8	G	74	150	4.3	182	145	294
108	44400	4.8	G	68	138	2.2	123	100	203
109	497	8.4	P	83	169	5.4	218	175	355
110	531	10.2	P	95	193	11.7	388	300	609
111	51	7.3	P	102	207	11.8	397	320	650
112	149	7.4	P	185	375	35.0	1060	1250	2530
113	102	7.4	F	177	360	35.0	1052	1000	2030
114	320	7.1	VP	89	181	5.1	217	210	426
115	3450	6.9	G	70	142	1.8	115	120	244
116	320	9.2	F	107	217	13.7	450	330	670
117	106	8.5	P	123	250	7.6	313	215	437
118	273	7.3	F	160	325	25.4	795	610	1240
119	10800	4.7	G	70	142	1.7	113	93	189
121	16400	4.8	G	22	45	0.4	32	28	57
122	552	7.4	F	52	106	2.4	112	77	156
123	6840	4.1	P	45	91	1.6	85	78	158
124	1160	4.4	P	62	126	3.6	152	115	233
125	5770	3.9	P	52	106	3.1	130	110	223

[a] Average of the deepest pits on 6 to 14 specimens (area, approximately 0.4 ft²) for each soil.

[b] Romanoff [1], table 6.

[c] Soil resistivity, saturated soil at 60° F.

[d] Also aeration; G, good; F, fair; P, poor; VP, very poor.

[e] Romanoff [1], from pit depth-time curves using data in tables 13, 14, 15. There were from 6 to 14 specimens involved in each removal from a given soil and from 3 to 6 removals, the 3 removals being for the 100 series of soils.

[f] $A_2 = 45.16$ ft², equivalent to a 20 ft length of 8 in. pipe. See eq (2). For soils 1 through 47, used exponents a, from Logan, Ewing, and Denison [7]. For all other soils, used exponent $a = 0.15$, from Schwerdtfeger (8).

[g] Based on best straight line after 5 years on pit depth-time curves on linear coordinates.

[h] Extrapolated pit depth-time curves.

[i] Extrapolated pit depth-time curves.

[j] From log-coordinates (i) and use of eq (2).

areas and is therefore indicative of a uniform environment. Later, Scott offered a theoretical basis for his empirical relationship [10]. Soil resistivity measurements made by him along pipeline rights-of-way together with leak records on the pipelines show that leaks occur in the places of low resistivity and almost invariably at resistivities below the value shown by 50 percent probability on the log resistivity-probability curve.

4.2. Relation Between Weight Losses and Currents Required for Cathodic Protection

The weight losses on the specimens for which maximum penetration has been given were converted to corrosion current densities by applying Faraday's law and the usual assumptions that the iron was oxidized to the divalent state and the corrosion efficiency was 100 percent. The data tabulated in table 2 are based on weight losses measured at 2-year removal time and on removals after 5 years. The corrosion rates, expressed as current densities, plotted versus soil resistivity and pH are shown in figures 6, 7, and 8. The current densities calculated from the weight losses of specimens based on the first removals (approximately 2 years for most specimens) are shown plotted versus soil resistivity in figure 6. What was previously said about the significance of 500 Ω-cm as a dividing line for differences in maximum penetration during early exposure also seems to apply to the current densities associated with corrosion. The effect of soil resistivity in substantially reducing corrosion current densities for exposure beyond 5 years is illustrated by figure 7. These data are the result of straight lines on rectangular coordinates drawn through the weight losses after 5 years on the weight loss-time curves (not shown). The same data as related to soil pH are shown in figure 8.

These corrosion currents are primarily of interest in connection with current densities necessary for cathodic protection. The relationship between values of corrosion current and current required for cathodic protection depends on the type of control of the corrosion reaction. Theoretically, if the reaction is under strict cathodic control (no anodic polarization), the protective current is equal in magnitude to the corrosion current. This ideal situation is not usually realized with ferrous metals used underground, the protective current requirement being somewhat greater. For further information on this relationship and some data, the reader is referred to papers by the author [11,12] and other investigators [13,14,15]. Data obtained on steel pipe specimens exposed underground showed that the ratio, I_p/i_0, of protective current, I_p, to corrosion current, i_0, varied between 1 and 2, depending on the length of time the specimens were exposed and on the chemical and physical properties of the soil. For example, in the case of a specimen buried in a soil of 7500 Ω-cm resistivity, the ratio was about 1.3 during the first week of burial and around 2.0 at 6 months and thereafter for 16 months exposure when the specimen was removed [16]. For a similar specimen (area, 0.4 ft²) buried in a tidal marsh (300 Ω-cm, resistivity) for a period of 32 months, the corrosion reaction was under complete cathodic control during the first week of exposure; the I_p/i_0 ratio was 1.3 at 8 months, and about 1.6 at 32 months when the specimen was removed (fig. 9). The ratios are believed to be approximately correct because after the specimens were removed from the trenches they were cleaned, weighed and the actual weight losses were in reasonably good agreement with the weight losses calculated from the polarization data. Thus, after 32 months (fig. 9) the current density required for cathodic protection (based on I_p, area, 0.4 ft²) was about 8.2 mA/ft². Similar polarization data on steel specimens of the same size were obtained by Ardahl

TABLE 2. *Corrosion currents associated with weight losses of specimens* [a]

Soil site No.[b]	ρ [c]	Corrosion rate		Soil site No.[b]	ρ [c]	Corrosion rate	
		0–2 yr [d]	After 5 yr [e]			0–2 yr [d]	After 5 yr [e]
	Ω-cm	mA/ft²	mA/ft²		Ω-cm	mA/ft²	mA/ft²
1	1215	3.7	2.0	51	190	14.2	3.6
2	684	3.1	1.1	53	17790	5.0	0.50
3	30000	2.8	0.41	55	5210	4.4	0.41
4	6670	3.1	1.3	56	406	6.5	6.5
5	1345	1.8	1.1	58	712	5.2	3.4
6	45100	0.28	0.26	59	1660	2.5	1.6
7	2120	1.1	0.59	60	218	8.4	5.6
8	350	1.8	1.8	61	943	3.4	1.6
9	2820	2.3	1.0	62	6920	5.3	1.1
10	7460	2.9	1.1	63	84	4.7	2.5
11	11000	0.90	0.34	64	62	20.3	12.7
12	3190	1.3	0.81	65	148	9.4	1.4
13	290	5.6	3.6	66	232	12.5	2.8
14	3520	1.7	1.1	52	234	6.2	6.2
15	489	3.6	1.8	54	886	1.5	1.1
16	8290	3.6	1.7	101	261	7.0	2.2
17	5890	3.1	1.1	102	103	7.2	5.6
18	1410	1.2	0.56	103	81	6.9	6.6
19	1970	2.0	0.53	104	8500	4.6	1.5
20	2870	2.9	1.5	105	28000	5.3	0.31
21	2370	4.1	1.5	106	25000	3.9	1.9
22	5150	2.9	0.72	107	54000	3.6	1.0
23	278	11.2	4.7	108	44400	5.2	0.39
24	11400	0.62	0.22	109	497	8.7	2.6
25	1780	1.3	0.65	110	531	6.9	6.2
26	2980	2.2	0.68	111	51	9.2	5.9
27	570	2.0	1.6	112	149	11.9	7.5
28	408	5.9	5.5	113	102	13.5	9.9
29	1270	5.9	4.2	114	320	4.8	3.8
30	1300	2.8	1.2	115	3450	2.8	0.40
31	20500	1.6	0.56	116	320	10.1	4.6
32	5700	1.3	0.84	117	106	12.8	5.3
33	800	3.4	3.4	118	273	8.7	5.3
34	4900	2.9	1.1	119	10800	2.8	1.8
35	2060	1.3	0.12	121	16400	1.4	0.19
36	11200	1.7	0.40	122	552	3.1	1.4
37	11200	3.7	1.9	123	6840	4.8	2.0
38	38600	0.62	0.53	124	1160	9.0	1.4
39	7440	2.7	1.2	125	5770	5.6	1.3
40	970	3.4	1.6				
41	1320	2.0	0.91				
42	13700	4.5	3.0				
43	60	4.8	3.9				
44	1000	1.1	1.0				
45	263	3.1	2.8				
46	1500	2.3	2.0				
47	1770	1.0	0.97				

[a] Calculated from weight loss-time curves on data by Romanoff [1] using Faraday's law, assuming 100 percent corrosion efficiency and that the iron is divalent. For weight losses, see Romanoff [1], tables 13, 14, and 15.
[b] Romanoff [1], table 6.
[c] Soil resistivity, saturated soil at 60 °F.
[d] Based on first removal from soil, usually 1 to 2 years.
[e] Based on the best straight line on the weight loss-time curves after 5 years.

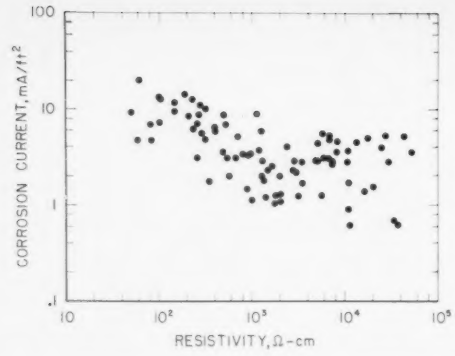

FIGURE 6. *Corrosion current densities calculated from the weight losses of the specimens (fig. 1) after removal from the underground sites upon 2 years of exposure.*

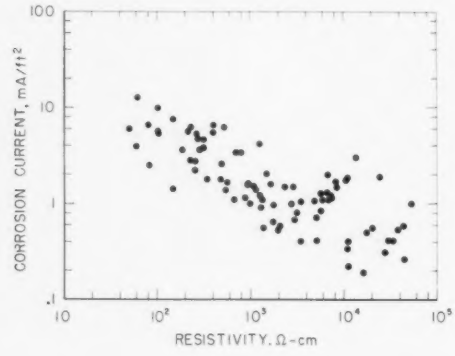

FIGURE 7. *Calculated corrosion current densities based on the rates of weight loss between 5 and 12, and between 5 and 17 years of exposure for the majority of soils.*

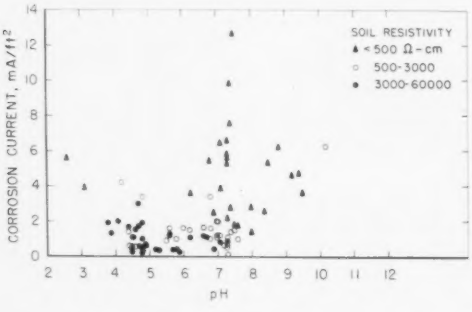

FIGURE 8. *Same as figure 7, except as related to* pH *for 3 ranges of soil resistivity.*

[17]. The writer analyzed these data and observed that after 2 years of underground exposure, in 2 soils with resistivities between 550 and 1000 Ω-cm, the I_p/i_0 ratio was between 1.1 and 1.8.

In higher resistivity soils (greater than 10,000 Ω-cm), the I_p/i_0 ratio is probably about 2 or more, depending

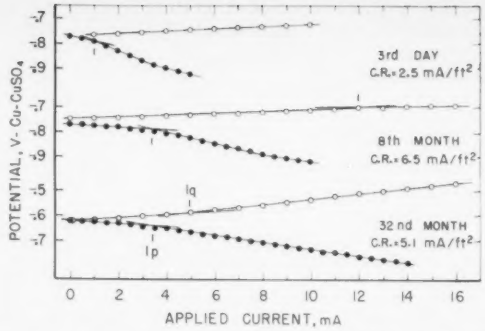

FIGURE 9. *Polarization curves on a plain steel specimen buried underground for 32 months in a tidal marsh.*

0 anodic ● cathodic

on soil properties and on duration of exposure. In a laboratory study, [18] a steel tube (area, 24 in.²) was exposed to a 20,000 Ω-cm sandy loam soil for 60 days. The current density necessary for cathodic protection was found to be about 3 times the value of current density associated with the weight losses of similar tubes which were permitted to corrode freely, that is, the I_p/i_0 ratio was about 3.

On the basis of the foregoing I_p/i_0 ratios, the corrosion current densities given in table 2 and in figures 6 and 7 might be increased accordingly and thus converted to values necessary for cathodic protection. This does not mean that current densities are substituted for polarization requirements as criteria [11] for cathodic protection. The protective current densities are presented to aid in estimating total current requirements in the design of underground cathodic protection systems. It would seem reasonable to multiply the corrosion current densities by 1.5 for soils having resistivities between 0 and 5000 Ω-cm. A factor of 2.0 might be used for soils with resistivities between 5000 and 10,000 Ω-cm. Above 10,000 Ω-cm, the I_p/i_0 ratio could be taken as being 3.0 and still result in relatively small protective current densities for most high resistivity soils.

A comparison of the corrosion current densities in the two columns (table 2) and of Figures 6 and 7 shows that it would be economically advisable, at least for uncoated underground structures, to allow about 2 years before designing the electrical requirements for cathodic protection. The current densities necessary for cathodic protection are considerably reduced after a few years of exposure, especially in the soils of high resistivity.

5. Conclusions

The maximum pit depths on commonly used wrought ferrous materials buried for periods up to 5 years in back-filled trenches are on the average deeper in soils with resistivities below 500 Ω-cm than in soils having higher resistivities while in the soils above 500 ohm-cm, there appears to be no regular pattern between maximum pit depth and soil resistivity. However, for periods of exposure in excess

TABLE 3. *Average values of maximum penetration rate and corrosion rate (current) on specimens for 3 ranges of soil resistivity after 5 years of exposure*

Soil resistivity	Number of soil sites	Maximum penetration rate [a]			Corrosion current [b]		
		Min	Avg	Max	Min	Avg	Max
Ω-cm		*mils/yr*			*mA/ft²*		
50 to 500	26	0.84	11.4	35.0	1.4	4.8	12.7
500 to 3000	28	.60	4.2	12.6	.12	1.6	6.2
3000 to 54,000	32	.28	2.2	6.7	.19	0.99	3.0

[a] Calculated from the specimen pitting rates after 5 years (table 1).
[b] Calculated from the corrosion rates (currents) after 5 years (table 2).

of 5 years, the rate of maximum penetration lessens as the soil resistivity increases beyond 500 Ω-cm. This is shown in table 3 where data from 86 soil sites are averaged for 3 ranges of soil resistivity. Based on an empirical equation, increasing the area exposed to that equivalent to a 20 ft length of 8 in. diam pipe (45.16 ft²) approximately doubles the maximum penetration rates shown in the table which apply to the actual specimens (0.4 ft²).

In soils with resistivities up to 500 Ω-cm, perforation of thick-wall (0.322 in.) bare wrought ferrous pipe is predicted in the majority of soils after 15 years of exposure. After 30 years of exposure, the same would be true probably in the majority of soils having resistivities to 1000 Ω-cm; in some of these soils many perforations would be likely to occur.

After the corrosion rates of the ferrous specimens became fairly well stabilized as shown by weight loss-time curves, the weight losses were converted to current densities. Corrosion current densities, averaged for three ranges of soil resistivity, are given in table 3. The current densities required for cathodic protection are greater than the current densities associated with the corrosion. By anticipating the type of corrosion control peculiar to the corrosive environment, corrosion current densities can be adjusted to current densities necessary for cathodic protection. A factor of 1.5 is suggested for soils with resistivities up to 5000 Ω-cm, a factor of 2.0 for soils from 5000 to 10,000 Ω-cm, and a factor of 3.0 for soils with resistivities above 10,000 Ω-cm. It is considered to be economically advisable to wait for about 2 years of exposure before measuring the current densities required for the cathodic protection of bare underground structures.

6. References

[1] Melvin Romanoff, Underground corrosion, NBS circ. 579, U.S. Government Printing Office, Washington, D.C. (1957).

[2] Kirk H. Logan, Engineering significance of National Bureau of Standards soil-corrosion data, J. Res. NBS **22,** 109 (1939) RP1171.

[3] Gordon N. Scott, The distribution of soil conductivities and some consequences, Corrosion **14,** 396t (August 1958).

[4] Edward Schaschl and Glenn A. Marsh, Some New Views on Soil Corrosion, Materials Protection **2,** 8 (November 1963).

[5] Melvin Romanoff, Corrosion of steel pilings in soils, J. Res. NBS **66C** (Eng. and Instr.) No. 3,223 (July–Sept. 1962).

[6] G. N. Scott, Adjustment of soil-corrosion pit depth measurements for size of sample, Proc. American Petroleum Institute **14,** No. 4, 204 (1933).

[7] K. H. Logan, S. P. Ewing, and I. A. Denison, Soil corrosion testing, Symposium on Corrosion Testing Procedures, ASTM (1937).

[8] W. J. Schwerdtfeger, Laboratory measurement of the corrosion of ferrous metals in soils, J. Res. NBS **50,** 329 (June 1953) RP2422.

[9] Gordon N. Scott, Distribution of soil conductivity and its relation to underground corrosion, Journal AWWA **52,** 378 (March 1960).

[10] Gordon N. Scott, A theory for the probability distribution of soil conductivity, Corrosion **18,** 251t (July 1962).

[11] W. J. Schwerdtfeger and O. N. McDorman, Potential and current requirements for the cathodic protection of steel in soils, J. Res. NBS **47,** 104 (August 1951) RP2233; Corrosion **8,** 391 (1952).

[12] W. J. Schwerdtfeger and O. N. McDorman, Measurement of the corrosion rate of a metal from its polarizing characteristics, J. Electrochem. Soc. **99,** 407 (1952).

[13] I. A. Denison, Electrolytic behavior of ferrous and nonferrous metals in soil-corrosion circuits, Trans. Electrochem. Soc. **81,** 435 (1942).

[14] Robert Pope, Cell currents and potentials, Corrosion **11,** 189t (April 1955).

[15] E. Schaschl and G. A. Marsh, The effect of dissolved oxygen on corrosion of steel and on current required for cathodic protection, Corrosion **13,** 243t (April 1957).

[16] W. J. Schwerdtfeger, A Study by polarization techniques of the corrosion rates of aluminum and steel underground for sixteen months, J. Res. NBS **65C** (Eng. and Instr.) No. 4, 271 (Oct.–Dec. 1961).

[17] E. H. Ardahl, Corps of Engineers, U.S. Army, Lower Mississippi Valley Division, Vicksburg, Miss. (private correspondence).

[18] W. J. Schwerdtfeger, Current and potential relations for the cathodic protection of steel in a high resistivity environment, J. Res. NBS **63C,** 37 (July–Sept. 1959); Corrosion **16,** 209t (May 1960).

(Paper 69C1–188)

JOURNAL OF RESEARCH of the National Bureau of Standards—C. Engineering and Instrumentation
Vol. 69C, No. 1, January-March 1965

Publications of the National Bureau of Standards*

Selected Abstracts

The 1962 He^3 scale of temperatures. I. New vapor pressure comparisons, S. G. Sydoriak and R. H. Sherman, *J. Res. NBS* **68A** (*Phys. and Chem.*), *No. 6, 547 (Nov.–Dec. 1964), 70 cents.*

A comparison of He^3 and He^4 vapor pressures (P_3, P_4), has been made in an apparatus designed to reduce the number and magnitude of corrections associated with the refluxing film in the He^4 pressure sensing tube and the attached bulb. The critical pressure of He^3 has been redetermined to be at 873.0 ± 1.5 mm Hg at 0 °C and standard gravity; the corresponding temperature as measured by a He^4 thermometer is 3.3240 ± 0.0018 °K on the 1958 He^4 scale. These (P_3, P_4) comparisons and the 1958 He^4 scale are the basis of the 1962 He^3 scale of temperatures derived and evaluated in the papers following this one.

Empirical interpolation equations containing only P_3 and P_4 are described by means of which existing P_4 measurements may be converted to an equivalent P_3. A comparison has been made between this interpolation and a conversion in which the 1958 He^4 and 1962 He^3 scales are used as parameters. Deviations between the two procedures are within the estimated errors of the (P_3, P_4) measurements.

In subsidiary experiments on techniques for He^4 thermometry a typical vapor pressure bulb arrangement was tested. It is shown that the refluxing film introduces a heat flux, $\dot{Q}_f$, and a resulting Kapitza temperature drop, ΔT_k, between the He II and its container, which may amount to many millidegrees.

The feasibility of calculating ΔT_k for a particular He^4 vapor pressure bulb was studied. The necessity of measuring $\Delta T_k/\dot{Q}_f$ at least once in situ is pointed out. In addition, it is necessary to redetermine the film-flow rate periodically at the same time that He^4 vapor pressure measurements are being made.

The 1962 He^3 scale of temperatures. II. Derivation. S. G. Sydoriak, T. R. Roberts, and R. H. Sherman, *J. Res. NBS* **68A** (*Phys. and Chem.*), *No. 6, 559 (Nov.–Dec. 1964), 70 cents.*
An Experimental Thermodynamic Equation (ETE) temperature scale valid from 0.2 to 2.0 °K has been calculated for He^3. The scale is based on new comparisons (P_3, P_4), of He^3 and He^4 vapor pressures above 0.9 °K; on the 1958 He^4 temperature scale; and on the best available data for several thermodynamic properties of He^3 from 0.2 to 2.0 °K.
The T_{62} Full-range Working Equation (FWE) scale,

$$P_3 = -2.49174/T + 4.80386 - 0.286001\,T + 0.198608\,T^2 - 0.0502237\,T^3 + 0.00505486\,T^4 + 2.24846 \ln T$$

fits the ETE scale and the (P_3, T_{58}– data and is therefore valid for use from 0.2 to the critical point 3.324 °K. The maximum deviation from the ETE scale is 0.4 mdeg and the standard deviation from the input data is 0.25 mdeg. The fit to the seven recalculated isotherms of Keller in the range of the 1962 He^3 scale can be determined by converting Keller's P_4's to equivalent P_3's, using direct P_4 to P_3 interpolation equations. The fit of the 1962 He^3 scale is as good as the fit of the 1958 He^4 scale to the same isotherms, the average displacements of the two scales both being 1.5 mdeg below the isotherms. The average standard deviations for ($T_{62} - T_{1\text{ISO}}$) and for ($T_{58} - T_{1\text{ISO}}$) are 1.2 and 1.0 mdeg, respectively, for these seven isotherms.

The 1962 He^3 scale of temperatures. III. Evaluation and status, T. R. Roberts, R. H. Sherman, and S. G. Sydoriak, *J. Res. NBS* **68A** (*Phys. and Chem.*), *No. 6, 567 (Nov.–Dec. 1964), 70 cents.*

In this third paper the 1962 He^3 Scale of Temperatures is evaluated both as to its precision and its deviations from the thermodynamic Kelvin Scale. Various thermodynamic quantities of He^3 consistent with the 1962 He^3 Scale are derived and listed. The correction to an observed vapor pressure for small amounts of He^4 is discussed and tabulated. A description is given of the method of multiple variable least squares analysis used for deriving the final scale equation and for reanalysis of isotherm data. Finally the present status of the 1962 He^3 Scale is discussed along with some considerations for the future.

The 1962 He^3 scale of temperatures. IV. Tables, R. H. Sherman, S. G. Sydoriak, and T. R. Roberts, *J. Res. NBS* **68A** (*Phys. and Chem.*), *No. 6, 579 (Nov.–Dec. 1964), 70 cents.*
The detailed tables of the 1962 He^3 Scale of Temperatures are presented. The vapor pressure of He^3 is tabulated in steps of 1 millidegree from 0.2 to 3.324 °K, the critical temperature. A table giving temperature, to 0.1 millidegree, as a function of pressure is included, as well as the temperature derivative of the vapor pressure.

Optical properties of thin films on transparent surfaces by ellipsometry; internal reflection for film covered surfaces near the critical angle, E. Passaglia and R. R. Stromberg, *J. Res. NBS* **68A** (*Phys. and Chem.*), *No. 6, 601 (Nov.–Dec. 1964), 70 cents.*

The application of ellipsometry to the determination of the optical properties of thin films on transparent substrates by the use of internal reflection and angles of incidence near the critical angle for total reflection is described and illustrated. Four cases are considered: 1. the angle of incidence, θ_i, is less than either the critical angle for total reflection between the substrate and the film, $\theta_c^{1,2}$, and the critical angle between the substrate and the surrounding medium, $\theta_c^{1,3}$; 2. $\theta_c^{1,3} > \theta_i > \theta_c^{1,2}$; 3. $\theta_c^{1,3} < \theta_i < \theta_c^{1,2}$; and 4. $\theta_c^{1,3} < \theta_i > \theta_c^{1,2}$. For case 1, at certain critical values of film thickness d and refractive index n_2, the reflected light may be polarized with its electric vector either entirely in or normal to the plane of incidence. Near these conditions the sensitivity of ellipsometric measurements is extremely high, but the intensity of the reflected light is very low. Except under these conditions the intensity is adequate for experimental measurements, as it is also in case 2. For case 1 it is always possible to determine n_2 and d by a single measurement; for case 2 this is possible only for thin films. For cases 3 and 4, and case 2 for thick films, only one of these may be determined. Under these conditions, however, the reflectivity is 100 percent.

Near infrared spectrophotometric method for the determination of hydration numbers, R. A. Durst and J. K. Taylor, *J. Res. NBS* **68A** (*Phys. and Chem.*), *No. 6, 625 (Nov.-Dec. 1964), 70 cents.*

The 970 mμ absorption band of water is employed in a new method for the determination of hydration numbers. The decrease in the concentration of "free" water is calculated from the change in absorbance resulting on the addition of an electrolyte. Data are given for chromic chloride and nitrate salts in H_2O-CH_3OH solutions, and an extrapolation is made to give the hydration number in pure water. The results obtained by this technique agree with the values reported using other methods.

Some elastic compliances of single crystal rutile from 25 to 1000 °C, S. Spinner and J. B. Wachtman, Jr., *J. Res. NBS* **68A** (*Phys. and Chem.*), *No. 6, 669 (Nov.-Dec. 1964), 70 cents.*
Young's modulus, as a function of temperature up to 1000 °C, was determined for eight rutile specimens of different crystallographic orientations. From these, the following four elastic compliances or combinations of them were determined as a function of temperature, s_{11}, s_{33}, $2s_{13}+s_{44}$, and $s_{11}-s_{12}-s_{66}/2$.

The method used was the same as had been used in a previous study for rutile at room temperature.

Steady-state response of silicon radiation detectors of the diffused P–N junction type to x rays. I: Photovoltaic mode of operation, K. Scharf and J. H. Sparrow, *J. Res. NBS* **68A** (*Phys. and Chem.*), *No. 6, 683 (Nov.-Dec. 1964), 70 cents.*

A relation is derived for the photocurrent produced by x rays in silicon radiation detector cells of the *p-n* junction type, giving the dependence of the generated photocurrent on exposure rate, photon energy, and electrical and geometrical parameters of the silicon wafer. Silcon radiation detector cells operated as photovoltaic cells are found to be more sensitive to x rays than silicon solar cells previously investigated, especially open-circuit voltages being several hundred times larger than those measured in solar cells. The short circuit current produced by x rays increases with increasing temperature by about 0.3 percent per °C at 25 °C cell temperature. Due to the high zero voltage junction resistance of silicon radiation detector cells, the temperature dependence of the photovoltaic output current increases with increasing load resistance at a smaller rate than that observed in silicon solar cells. The energy dependence of the short-circuit current produced by x rays, measured over a wide range of radiation qualities, is shown to be in good qualitative agreement with calculated values.

Intercomparison of high-energy x-ray intensity measurements J. S. Pruitt and S. R. Domen, *J. Res. NBS* **68A** (*Phys. and Chem.*), *No. 6, 703 (Nov.–Dec. 1964), 70 cents.*

This paper describes experimental comparison of the sensitivity of the NBS P2–4 ionization chamber and a replica of Wilson's Quantameter. The sensitivity ratios are used to compare calorimetric measurements of total x-ray beam energy made at the NBS and in the USSR between 20 and 90 MeV. The agreement is within the combined errors, but the source of an apparent 2 percent systematic difference has not been found.

Experiment on the constancy of the velocity of electromagnetic radiation, P. Beckman and P. Mandics, *Radio Sci. J. Res. NBS/USNC–URSI* **68D,** *No. 12, 1265 (Dec. 1964), $1.00.*

An experiment by Kantor, reporting results in sharp contradiction to Einstein's Second Postulate, was repeated using the coherent light of a laser. The results were found to be consistent with the Special Theory of Relativity. It is concluded that the ballistic hypothesis of light propagation disregarding the effect of air is incorrect. It is pointed out that the direct experimental evidence in favor of Einstein's Second Postulate is surprisingly meager and further experiments to confirm or reject the ballistic hypothesis are envisaged.

Standard x-ray diffraction powder patterns, H. E. Swanson, M. C. Morris, E. H. Evans, and L. Ulmer, *NBS Mono. 25, Sec. 3 (July 31, 1964), 40 cents.*

Standard x-ray diffraction powder patterns are presented for the following fifty-one substances: $3Al_2O_3{\cdot}2SiO_2$, (mullite); $(NH_4)_2BeF_4$; NH_4BF_4; Sb_2Se_3*; Sb_2Te_3*; As_2O_3*, claudetite; $BaBr_2{\cdot}H_2O$*; $BaSnO_3$; $BiPO_4$ (monoclinic); $BiPO_4$* (trigonal); $BiVO_4$* (tetragonal); $BiVO_4$* (monoclinic); Bi_2Te_3, (tellurobismuthite); Bi_2O_3, (bismite); $Cd(ClO_4)_2{\cdot}6H_2O$*; $CdSO_4$; CdTe; $Ca_5F(PO_4)_3$, (fluorapatite); $CeNbTiO_6$*, (eschynite); Cs_2CrO_4*; CsF; $CoSiF_6{\cdot}6H_2O$*; $Co(ClO_4)_2{\cdot}6H_2O$*; $CuSO_4$, (chalcocyanite); $DyAsO_4$*; $ErAsO_4$*; $EuAsO_4$*; GaAs*; $HoAsO_4$*; InAs; $LaAsO_4$*; $LaNbTiO_6$*; Li_3PO_4, (lithiophosphate) low form; Li_3PO_4 high form; $MgNH_4PO_4{\cdot}6H_2O$, (struvite); $KClO_3$; $KLiSO_4$*; K_2CrO_4*; $K_2Zn_2V_{10}O_{28}{\cdot}16H_2O$*; Rb_2CrO_4*; $AgSbTe_2$*; $NaMg_3Al_6B_3Si_6O_{27}(OH)_4$*, dravite; $Na_3P_3O_9$; $Na_3P_3O_9{\cdot}H_2O$; SnF_2*; $SrO{\cdot}B_2O_3$*; $TbAsO_4$*; $TlCrO_4$*; $TmAsO_4$*; TiO_2, brookite; and ZnTe. Twenty-one are to replace patterns already given in the X-ray Powder Data File issued by the American Society for Testing and Materials, and thirty patterns indicated by asterisks are for substances not previously included. The patterns were made with a Geiger counter x-ray diffractometer, using samples of high purity. When possible, the *d*-values were assigned Miller indices determined by comparison with calculated interplanar spacings and from space group extinctions. The densities and lattice constants were calculated, and the refractive indices were measured whenever possible.

An engineering method for calculating protection afforded by structures against fallout radiation, C. Eisenhauer, *NBS Mono. 76, (July 2, 1964), 20 cents.*

This report is a discussion of the technical assumptions underlying the methods currently recommended by the Office of Civil Defense (OCD) for calculating protection afforded by structures against fallout radiation. It discusses methods for calculating the contributions from radioactive sources on the roof and on the ground surrounding a simple one-storied building. It shows in detail how each technical chart in the OCD Professional Manual[1] is derived from basic data on radiation penetration developed by Dr. L. V. Spencer. Charts from the Professional Manual and relevant curves from Spencer's work are included in this report in order to make it self-contained.

Project FIST. Fault Isolation by Semi-automatic Techniques, G. Shapiro, O. B. Laug, G. J. Rogers, and P. M. Fulcomer, Jr., *NBS Mono. 83, (Sept. 17, 1964), 55 cents.*

The method of Fault Isolation by Semi-automatic Techniques developed at the National Bureau of Standards, to which the acronym FIST has been applied, creates a new field of metrology which permits the measurement of the dynamic performance of electronic circuits by unskilled personnel under field operating conditions. It is a diagnostic tool for rapidly isolating faults in modularized, non-computer type electronic equipment without removing the modules from the prime equipment.

The system consists of test points and associated circuitry which are built into the prime equipment, and a small, hand-carried, general-purpose test instrument. The test points are located on an easily accessible test panel and are arranged in an order which permits rapid checking of the modules in a logical sequence.

Fault isolation is accomplished by testing the dynamic performance of each module with a test instrument which is basically a device for comparing the peak-to-peak amplitudes of two periodic voltage waveforms. Since many circuit properties other than voltage must be measured, transformation networks are provided to convert the characteristic being measured to a periodic voltage which is within the range of the test instrument.

The tests are usually made while the module under test is performing its normal function with the normal inputs to the module providing the stimuli for the tests. When this is not possible, a stimulus generator is used to furnish the necessary signal or signals.

These techniques have been reduced to practice. This report described the hardware required and discusses practical ways in which the necessary circuitry can be built into the prime equipment. The simplicity of the programming and the speed with which a complex piece of electronic equipment can be checked are demonstrated. Finally, a prototype test instrument capable of simultaneously testing four characteristics of the module or of its stimuli is described in detail.

United States standard for the colors of signal lights, F. C. Breckenridge, *NBS Handb. 95, (Aug. 21, 1964), 25 cents.*

The standard provides in part I basic chromaticity definitions defining the chromaticities that are considered safe for use as representing the named colors. These are the basis for the selection of the national standard filters and for the tolerances given in part II for duplicating them. The procurement requirements of parts III and IV are based primarily on sets of these filters in combination with prescribed sources although provision is also made for procurement under the basic chromaticity definitions in cases in which it is impracticable to base the procurement on filters. Part V provides guidance in selecting signal colors for new uses, and part VI provides methods for special laboratory tests and serves as a technical interpretation of the practical tests prescribed in parts III and IV.

Shielding for high-energy electron accelerator installations, *NBS Handb. 97, (July 1, 1964), 30 cents.*

This report is intended to give a summary of the presently available data required to calculate the shielding for high-energy, high-intensity electron-accelerator installations. The

report is not intended to present specific, all-inclusive recommendations since it is not felt that at the present time the "state of the art" has progressed to the point where such recommendations are feasible. Rather the report is aimed at outlining the present state of our knowledge about the factors governing the shielding required in the vicinity of these accelerators. The recommendations that are made have to do primarily with a procedure to be followed in establishing the required amount of shielding.

Foreign-language and English dictionaries in the physical sciences and engineering. A selected bibliography 1952 to 1963, T. W. Marton, *NBS Misc. Publ. 258, (July 24, 1964), $1.25.*
The bibliography lists over 2800 unilingual, bilingual, and polyglot dictionaries, glossaries and encyclopedias in the physical sciences, engineering and technology published during the past twelve years. The majority of the titles cited have English as the source or target language, or are dictionaries giving definitions in English. The bibliographic entries are arranged in 49 subject classes; within each subject, the entries are listed alphabetically by language, and within each language group by author. Forty-seven foreign languages are represented in the compilation. Lists of abbreviations and reference sources, and detailed author, language, and subject indexes complement the publication.

Selection of camera filters for color photography, C. S. McCamy, *NBS Misc. Publ. 259, (June 26, 1964), 5 cents.*
This chart provides a quick and easy way to select the right filter for almost any combination of light source and color film. A straightedge laid across the three scales so that it connects the light source and the color film will cross the center line at a point corresponding to the proper filter. Notations consisting of a series of filter designations (e.g., 80B+82c+82a) mean that *all* these filters should be used at once for proper correction. When color correcting filters are used, the exposure must be increased by the "filter factor" assigned by the filter manufacturer.

Standard reference materials: Preparation of NBS white cast iron spectrochemical standards, R. E. Michaelis and L. L. Wyman, *NBS Misc. Publ. 260–1, (June 19, 1964), 30 cents.*
Several methods have been investigated for the preparation of cast iron spectrochemical standards and a satisfactory procedure has been devised. The method involves casting the molten metal into a grid type of mold on a massive water-cooled copper plate. The method has been applied to the preparation of eight NBS white cast iron spectrochemical standards containing a graded concentration range for some 20 elements, of which the following 10 initially have been certified: C, Mn, P, S, Si, Cu, Ni, Cr, V, and Mo. Details of the planning and preparation are given with particular emphasis on the problems peculiar to standards for cast materials.

Average power dissipated in a diode swept along its reverse characteristic, H. A. Schafft, *NBS Tech. Note 240, (Apr. 30, 1964), 20 cents.*
The commonly used method of sweeping to a fixed power in order to compare the reverse characteristics of a group of similar diodes is found lacking under conditions for which an average temperature is meaningful. It is shown how a determination may be made of the average power dissipation in a diode (or in any device with a similarly shaped characteristic) when it is swept along its reverse characteristic by a full-wave rectified sinusoidally varying voltage in series with a resistive load. The uncertainty in the determination due to the variability of the characteristic is for most cases less than $\pm 5\%$ if the ratio of the maximum voltage drop across the current limiting resistor to the maximum voltage across the device is larger than or equal to two. Errors introduced by small uncertainties in the pertinent parameters are also presented. Finally it is shown how the reverse characteristics of similar diodes can be examined under relatively equivalent heating conditions.

Calculations for comparing two-point and four-point probe resistivity measurements on rectangular bar-shaped semiconductor samples, L. J. Swartzendruber, *NBS Tech Note 241, (June 1, 1964), 25 cents.*
Fortran codes are given which enable the calculation of four-point probe correction factors for use with bar-shaped samples. Samples with either plated or unplated ends are considered. The errors that arise due to probe misplacement, inaccurate sample size and shape, and nonuniform end plating are also considered. Use of the results permits accurate comparison of two-point and four-point probe resistivity measurements. The codes are in Fortran II language and were written for an IBM 7090 computer.

A helicopter battery service simulator, W. G. Eicke, Jr., *NBS Tech. Note 244, (Aug. 28, 1964), 20 cents.*
A semi-automatic helicopter battery service simulator is described in detail. The simulator consists of a programing unit and operational unit for charging and discharging the battery, and peripheral equipment for furnishing charging current and recording data. The design of the program unit is based on the use of stepping switches and is capable of selecting any minute of a week uniquely. The programer is designed to handle a large number of programs but only 8 control units were installed. The capacity of the complete simulator is 3 batteries. The design is such that the simulator can be made fully automatic by the addition of certain data recording equipment.

Factors influencing the design of original-document scanners for input to computers, *NBS Tech. Note 245, (Aug. 19, 1964), 35 cents.*
This report considers some of the factors involved in the design and implementation of scanners capable of reading data from documents in their original form rather than from microfilm. The scanner is assumed to be part of a transcribing information processor such as the FOSDIC (Film Optical Scanning for Direct Input to Computers) type of machine. Advantages and disadvantages of microfilm as against original document scanning are discussed. Factors considered include the types of forms that are to be handled, paper handling problems, available electronic and mechanical scanning techniques, problems of resolution and image defects, precision limitations, and overall system limitations. A set of general specifications for scanners for direct data input to computers is developed in qualitative terms.

An international comparison of voltage-transformer calibrations to 350 kv, F. K. Harris, W. C. Sze, N. L. Kusters, O. Petersons, and W. J. M. Moore, *IEEE Trans. Commun. Elec. No. 79, 13–19 (Jan. 1964).*
An international comparison is reported of voltage-transformer calibration tests at voltages to 350 kilovolts. Measurements of ratio and quadrature errors are reported by the High Voltage Laboratories of the U.S. National Bureau of Standards and the National Research Council of Canada, for a transformer having nominal voltage ratios from 1000/1 to 4000/1. Where the transformer ratio is adequately stable, the results from the two laboratories are in agreement within 20 ppm in the measurement of ratio error and 10 ppm in quadrature error.

The quest for design data, R. B. Stewart, *Symp. The Role Cryogenics Is Playing in Expanding Mechanical Engineering, Am. Soc. Refrigerating and Air Conditioning Engineers, New York, N.Y., Feb. 11–14, 1964, pp. 13–24 (1964).*
The acquisition of data for the design and analysis of cryogenic systems is representative of the quest that confronts the engineering profession in new fields of technology. The compilation of thermodynamic properties for the cryogenic fluids is used as an illustration of the problems of acquiring data. Authoritative tabulations of thermodynamic data are required, based on experimental data that have been subjected to critical evaluation in selecting the "best values" of the data.
Compilation groups, utilizing the data available in the scientific literature, can generally lead the determination of new experimental data by years. The demands of new developments in cryogenics still outpace these efforts, however, and

the design engineer often must perform data compilations within the scope of his immediate needs.
Some examples of compilation problems are included, which demonstrate techniques of data compilation that may be within the province of the engineer. These examples include (1) the extension of the oxygen property charts into the liquid range, (2) the generation of P-ρ-T data for neon from corresponding states theory, and (3) the determination of an equation of state for helium.

Absolute temperatures determined from measurements of the velocity of sound in helium gas, G. Cataland and H. H. Plumb, *Proc. Advisory Committee on Thermometry to the Intern. Bureau of Weights and Measures, 6th Session, p. 175 (Sept. 26-27, 1962).*
At 20 °K and below, the measurement of the speed of sound in helium gas appears to yield a more accurate determination of absolute temperatures than has been previously realized. In an ideal gas, the speed of sound is directly proportional to the square root of the absolute temperature; for a real gas, corrections must be made which involve virial coefficients of the gas expressed in a pressure expansion. Because these corrections increase with pressure, it is desirable that velocity measurements for absolute temperature determinations be conducted at the lowest practical pressures, where a real gas approaches the state of an ideal gas.
An acoustical interferometer has been used as a measuring instrument, and absolute temperature determinations at 2 °K and 20 °K have been investigated. The temperature, measured acoustically, at 2 °K is three millidegrees higher than the temperature associated with the T_{58} helium vapor pressure scale; at 20 °K, it is within 10 millidegrees of the equilibrium hydrogen vapor pressure-temperature scale of Woolley, Brickwedde, and Scott. The work is being continued to determine an absolute temperature scale below 20 °K.

Some results and problems in calibrating the NBS photoelectric pyrometer of 1961, R. D. Lee, *Proc. Advisory Committee Thermometry to the Intern. Bureau Weights and Measures, 6th Session, pp. 79–90 (Sept. 26–27, 1962).*
The realization of the International Practical Temperature Scale (IPTS) above 1063 °C has been accomplished in the past with a disappearing filament optical pyrometer. Photoelectric means of detecting the equality of spectral radiance along the same principles of the visual optical pyrometer have been demonstrated to be considerably more precise, and this increased precision has been accomplished with a narrower spectral bandpass.
In the past few years photoelectric pyrometers have been developed at the National Bureau of Standards (NBS) and at other national standards laboratories. Some progress has been made toward the realization of the IPTS with the NBS pyrometer. This paper reports on the preliminary results and problems observed in this work.

A coaxial adjustable sliding termination, W. E. Little and J. P. Wakefield, *IEEE Trans. Microwave Theory Tech.* **MTT–12,** *No. 2, 247–248 (Mar. 1964).*
The design of an adjustable sliding coaxial termination for use in modified reflectometer techniques is presented. Some results from the use of terminations made from the design procedures are also discussed.

Effect of blowing variables on durability of coating grade asphalts, S. H. Greenfeld, *Indust. and Eng. Chem. Prod. Res. & Devel.* **3,** *158–164 (June 1964).*
The effects of varying temperature, agitation and air-rate during the blowing of fluxes from California, Kansas, Tia Juana and Talco fields on the physical properties and resistance to accelerated weathering (durability) of the coating-grade products were studied. Although the durabilities of the asphalts produced from each source varied with the blowing conditions, the California and Talco fluxes were more sensitive to the variables than were the Tia Juana and Kansas fluxes. The durabilities of the asphalts produced from the California flux varied in the range of 39–68 days, inversely with blowing temperature and directly with air flow rate and agitation rate. The durabilities of the Talco asphalts varied in the range of 32 to 56 days inversely with the blowing temperature but were relatively independent of air rate and agitation. The durabilities of the Tia Juana asphalts were highest when they were blown at the lower temperatures and higher air rates with little or no agitation. They varied within the range of 46 to 60 days. The durabilities of the Kansas asphalts ranged from 65 to 87 days. The highest blowing temperatures and air rates produced the least durable Kansas asphalts. The ranges of variables covered were as follows: Temperature 430–530 °F; Air Rate: 38–150 cu ft/ton-min.; Agitation: 0–2200 rpm.
All three variables had pronounced effects on the blowing rates (change of softening point with time) of the four fluxes. However, the final penetrations of the Kansas and Tia Juana asphalts were insensitive to the blowing conditions. The penetrations of the California and Talco asphalts varied to a greater extent with blowing conditions. The California asphalts had lower penetrations than normally specified for coating-grade materials.
The solubility parameters of the asphaltenes and the asphaltene contents of the asphalts were related to the flux source, but did not vary appreciably with the blowing variables.

Q meter measurements up to 260 MHz, M. G. Broadhurst (*Proc. Conf. Electric Insulation*), *1963 Annual Report, Natl. Acad. Sci.-Natl. Res. Council Publ. 1141, pp. 77–80 (1964).*
A system is proposed for measuring the dielectric constant and loss of solid-disk specimens up to 260 MHz. The sample holder is a small two-terminal parallel plate capacitor to be used with the Boonton type 190A Q meter. Accuracy of $\pm 1\%$ for $\mathbf{c}'$ and $\pm 5\%$ for $\mathbf{c}''$ is expected using susceptance-variation methods. Preliminary calibrations and measurements will be described and modifications to permit low temperature measurements will be discussed.

The performance of point level sensors in liquid hydrogen, D. A. Burgeson, W. G. Pestalozzi, and R. J. Richards (*Proc. 1963 Cryogenic Eng. Conf. Univ. Colorado and National Bureau of Standards, Boulder, Colo., Aug. 19–21, 1963*), *Book, Advances in Cryogenic Engineering* **9,** *Paper G–5, 416–422 (Plenum Press Inc., New York, N.Y., 1963).*
Seventeen manufacturers' point sensors have been tested for repeatability and time response from one atmosphere to 13.6 atmospheres. An analysis of the results by type and operating principle is presented. A description of the test apparatus and and operating procedure is included. Possible application of point level sensors to space systems is summarized.

He-Ne laser with perpendicular end windows, K. D. Mielenz, K. F. Nefflen, and K. Gillilland, *J. Opt. Soc. Am. Letter to Editor* **3,** *No. 6, 785 (June 1964).*
An external-mirror He-Ne laser has been successfully operated in which the discharge tube is sealed with dielectrically coated end windows perpendicular to the tube. Unlike the Brewster-angle design, the new laser retains both fields of polarization. Thus, the power output is increased, and certain optical experiments are facilitated.

Functions for the calculation of entropy, enthalpy, and internal energy for real fluids using equations of state and specific heats, J. G. Hust and A. L. Gosman (*Proc. 1963 Cryogenic Eng. Conf. Univ. Colorado and National Bureau of Standards, Boulder, Colo., Aug. 19–21, 1963*), *Book, Advances in Cryogenic Engineering* **9,** *Paper D–8, 227–233 (Plenum Press Inc., New York, N.Y., 1964).*
General functions for the determination of entropy, enthalpy, and internal energy are derived. In the first part of this paper the integration path is taken to be on the real gas surface thus yielding one set of equations. In the latter part of this paper the integration path is defined such that ideal gas specific heats and reference properties are introduced. The latter set of functions are applied to a particular equation of state resulting in algebraic expressions for the entropy, enthalpy, and internal energy.

On the measurement of random chain scission by stress relaxation, H. Yu, *Polymer Letter* **2,** *631–635 (1964).*
In enumerating the number of random chain scissions by the method of stress relaxation of a network, an inprovement

over the treatment by Bueche, and by Berry and Watson is proposed. The lower limit of the average length of the network chains where the treatment fails to account correctly for the number of scissions is computed.

Electrical resistances of wires of low temperature-coefficient of resistance useful in calorimetry (10°K –380°K), G. T. Furukawa, M. L. Reilly, and W. G. Saba, *Rev. Sci. Instr.* **35,** *No. 1, 113–114 (Jan. 1964).*
Measurements of the electrical resistance in the range 10° to 300°K were made on constantan, manganin, "Evanohm", and "Karma" wires in the course of a search for alloy wires with low temperature-coefficient of resistance for use as calorimeter heaters. Above 250°K, all four wires have comparable low temperature-coefficients of resistance suitable for calorimeter heaters; below this temperature, both "Evanohm" and "Karma" wires have significantly lower temperature-coefficients of resistance than constantan or manganin wire. The total resistance change in the range of the measurements was 0.9 percent for "Evanohm" and "Karma" as compared with 6 and 10 percent for constantan and manganin wires, respectively.

Intense resonance line sources for photochemical work in the vacuum ultraviolet region, H Okabe, *J. Opt. Soc. Am.* **54,** *No. 4, 478–481 (Apr. 1964).*
A simple, completely sealed, discharge resonance lamp operated by a 2450 Mc/sec microwave power is described which emits atomic lines of sufficient intensity to be useful as a photochemical light source.
When a water impurity is present in the lamp, many emission lines appear in the region of wavelength from 1500 to 200 Å. These impurity lines can be effectively removed by means of a getter or by a suitable cold trap. The pressures of pure Xe or Kr in the resonance lamp, required to give maximum intensity (approximately 5×10^{14} quanta/sec), are 0.7 and 1.0 mm, respectively. The presence of a CO impurity does not affect the intensity of the resonance lines. After passing through a 1-mm LiF window, the intensity of the Xe resonance line at 1295 Å is about 2% of that at 1470 Å and the intensity of the Kr line at 1165 Å is about 28% of that at 1236 Å. A mixture of the rare gas and He gives more intense light than the pure gas. The lifetime of the rare-gas resonance lamps is approximately 10 h. Lyman alpha (1216 Å) line from excited atomic hydrogen and a group of lines at 1743–45 Å from excited atomic nitrogen may be used as a photochemical light source.

Techniques for using the air-gap method for the precise determination of the dielectric constant and loss angle of solid disk specimens, A. H. Scott, (*Proc. Conf. Electric Insulation*), *1963 Annual Report, Natl. Acad. Sci.-Natl. Res. Council Publ. 1141, p. 74–76 (1964).*
Improved techniques in the use of the air-gap method of measuring the dielectric constant and dissipation factor are described and some typical results are given. It is concluded that this method can be used to determine the dielectric constant to 0.1% and the dissipation factor to $1\times10^{-5}+1\%$ or better.

Constants of the interpolation formula for platinum resistance thermometers, J. L. Riddle, *Proc. Advisory Committee Thermometry to the Intern. Bureau Weights and Measures, 6th Session, pp. 198–201 (Sept. 26–27, 1962).*
Values of the constants in the interpolation formula for a large number of thermometers recently submitted to the National Bureau of Standards for calibration are summarized. All thermometers suitable as standards which were received over a period of about one year during 1959 and 1960 are included. Limitations on such constants can serve either to make the International Practical Temperature Scale (IPTS) more precisely defined or to reduce the number of calibration points required for application over limited temperature ranges.

Separation and determination of zirconium in zirconia-yttria mixtures by precipitation with cupferron, E. J. Maienthal and J. K. Taylor, *Anal. Chem.* **36,** *1286–1287 (June 1964).*
A method is described for the determination of zirconium in zirconia-yttria mixtures which is simple, accurate, and applicable to concentrations of zirconia ranging from 4 to 97%. For 11 determinations within this range, the mean error was 0.05%; the maximum, 0.15%. Previous literature indicates that precipitation with cupferron yields a zirconia precipitate contaminated with yttria, but quantitative separation is achieved by a double cupferron precipitation.

Analysis of the frost phenomena on a cryo-surface, R. V. Smith, D. K. Edmonds, E. G. F. Brentari, and R. J. Richards, (*Proc. 1963 Cryogenic Eng. Conf. Univ. Colorado and National Bureau of Standards, Boulder, Colo., Aug. 19–21, 1963*), *Book, Advances in Cryogenic Engineering* **9,** *Paper B–7, 88–97 (Plenum Press Inc., New York, N.Y., 1964).*
An expression is presented for heat and mass transfer at the frost-air interface for frost formed by forced convection on a surface near liquid nitrogen temperatures. The results of this expression are compared with data obtained experimentally using a liquid-nitrogen-cooled cylinder in a cross-flow of air with air temperature, velocity, and humidity as controlled variables.
Expressions and correlations are presented to provide design information regarding the frost mass, thickness, density, and thermal conductivity.

The operating characteristics of Zener reference diodes and their measurements, W. G. Eicke, Jr., *ISA Trans.* **3,** *No. 2, 93–99 (Apr. 1964).*
A measurement technique with an accuracy in terms of the saturated standard cell of 20 ppm and capable of 2 to 4 ppm accuracy for making stability studies is described. Typical stability data are presented on several diodes. Results of a study of the effect of current and temperature on the output voltage are given including an equation relating the three variables. The effect of alternating-current components on the direct current output is discussed and a cause for this effect is suggested. Also the electrical noise generated by the diode is discussed.

The correlation of thermodynamic properties of cryogenic fluids, R. B. Stewart and K. D. Timmerhaus, (*Proc. 1963 Cryogenic Eng. Conf., Univ. Colorado and National Bureau of Standards, Boulder, Colo., Aug. 19–21, 1963*), *Book, Advances in Cryogenic Engineering* **9,** *Paper A–3, 20–27 (Plenum Press Inc., New York, N.Y., 1964).*
To provide tabulations of thermodynamic properties for cryogenic systems design, the staff of the Cryogenic Data Center of NBS has undertaken the correlation and selection of the pertinent experimental data. Tables and graphs of properties, as well as analytical functions for computer programming, are now available for several of the cryogenic fluids. These tabulations are intended to provide the engineer with comprehensive and consistent sets of data which are hopefully the best representation of the existing experimental data.
These compilations have also served to define the limitations of the existing data and to define the needs for new measurements. This paper summarizes the experimental data for the several cryogenic fluids and outlines some of the procedures utilized in providing the various sets of thermodynamic property values.

Modern methods of analysis for the design of cryogenic equipment and processes, T. R. Strobridge and D. B. ann, *Symp. The Role Cryogenics Is Playing in Expanding Mechanical Engineering, Am. Soc. Refrigerating and Air Conditioning Engineers, New York, N.Y., Feb. 11–14, 1963, pp. 26–37 (1964).*
Interest in cryogenic processes and equipment has developed rapidly over the past few years. Exotic rocket fuels and oxidizers, cryogenic magnets, masers and infrared detectors are but a few of the applications of low temperature technology. With this increased interest it is necessary to design and develop systems of high efficiency and dependability. Accurate real gas thermodynamic property data for use in low temperature process optimization and analysis and experimental data reduction are essential to the study of these problems.

At the National Bureau of Standards-Cryogenic Engineering Laboratory, high speed digital computers are being used to investigate refrigeration and liquefaction equipment and processes. Rather complex real gas state equations are developed in order to describe broad regions of the pressure-density-temperature surface. The reduction of these state equations to thermodynamic property tables is made practical only with the use of computers. These tabulated data for such refrigerants as helium, normal and para hydrogen, neon and nitrogen are used as input data for the computer. Performance of refrigeration and liquefaction systems incorporating unique or experimental components are investigated "on paper" by the computer before fabrication, thus saving time and reducing cost. After fabrication, test data is reduced, analyzed, and compared to the "on paper" predictions.

The calorimeter and its influence on the development of chemistry, G. T. Armstrong, *J. Chem. Educ.* **14,** *297 (June 1964).*
Compared to many techniques of current interest in physical chemistry, the measurement of heat is quite old. Some very early calorimeters are described, and some steps in the development of highly sophisticated modern calorimeters from these early instruments are outlined. The calorimetric laws of Hess and of Petit and Dulong are discussed in terms of the data available at the times of their formulation, and the effects of subsequent measurements on the validity of these laws. Current needs for calorimetric measurements are described, as related to development of theories of interaction energies of atoms and of the need by chemists in various pure and applied fields for thermodynamic data.

A new steady-state calorimeter for measuring heat transfer through cryogenic insulation, D. R. Beck, F. Kreith, and R. H. Kropschot, *(Proc. 1963 Cryogenic Eng. Conf., Univ. Colorado and National Bureau of Standards, Boulder, Colo., Aug. 19–21, 1963), Book, Advances in Cryogenic Engineering* **9,** *Paper B–4, 64–70 (Plenum Press Inc., New York, N.Y., 1964).*
A guarded cylindrical calorimeter, using evaporation techniques for heat flux measurement, is described. The apparatus can be used to measure the thermal conductivity of the same, undisturbed, sample over wide temperature limits to an accuracy of better than 3 percent. The conductivity of one sample of SiO_2 plus aluminum powder is reported.

A preliminary study of the orifice flow characteristics of liquid nitrogen and liquid hydrogen discharging into a vacuum, J. A. Brennan, *(Proc. 1963 Cryogenic Eng. Conf., Univ. Colorado and National Bureau of Standards, Boulder, Colo., Aug. 19–21, 1963), Book, Advances in Cryogenic Engineering* **9,** *Paper E–6, 292–303 (Plenum Press Inc., New York, N.Y., 1964).*
The storage and handling of liquid propellants on board vehicles in space presents many problems. Flow characteristics of the propellants through holes made in the tank walls by meteoroid puncture is one such problem and is the subject of this work. Overall discharge coe cients for small-diameter, thick-plate orifices were determined as a function of discharge pressure using liquid nitrogen and liquid hydrogen. Discharge pressures from 3 mm Hg to slightly above the triple point were investigated.
Flow characteristics appear to be sensitive to discharge pressure and the condition of the liquid upstream of the orifice. The condition of the liquid was, of course, dependent on the heat transfer to the containing vessel. A marked difference in flow pattern was observed that depended on whether the liquid was nearly saturated or if two phase flow existed. If the liquid was nearly saturated and no gas phase passed through the orifice the flow could be very nearly predicted by the adiabatic, incompressible flow equations. When gas phase was present upstream of the orifice it appeared that solid formation could take place in the orifice itself and thereby retard the flow.
In addition to the orifice discharge coefficients a general discussion of observed flow patterns is presented.

Sieve techniques for obtaining small amounts of narrowly classified particles, C. M. Hunt and A. R. Woolf, *Mater. Res. Std. Tech. Note* **4,** *No. 7, 364 (July 1964).*
Methods are described for obtaining small amounts of particles of narrow size distribution in individual sizes ranging from about 5 microns to 75 microns or possibly larger. One use to which such narrowly classified particles have been put is calibration of a Coulter Counter. By using narrowly classified particles, the number of microscopic measurements required to establish the distribution of the calibration sample are greatly reduced. The procedure is described partly because it is timely for Coulter Counter users, and partly because there may be other applications for small amounts of narrowly classified particles.

Tooth fluorometer, A. F. Forziati, J. Kumpula, and J. J. Barone, *J. Am. Dental Assoc.* **67,** *No. 5, 663–669 (Nov. 1963).*
A fluorometer for the measurement of the fluorescence of teeth in the mouth has been designed and constructed. The fluorometer consists of a medium pressure mercury vapor lamp (as a source of ultraviolet radiation), a filter passing only U. V. radiation in the 365 $m\mu$ region of the spectrum, a lens for focusing the radiation onto the specimen, an annular lens to collect the emitted fluorescence, another filter (passing only visible radiation), and a photomultiplier radiation detector. The signal from the photomultiplier is fed into a direct current amplifier, equipped with attenuation and sensitivity controls, and then to a recorder. The fluorometer has been used to record the fluorescence of natural teeth, artificial teeth and other materials.

NBS microcopy resolution test chart, B. H. Fouquet, *Proc. Natl. Microfilm Association Meeting, San Francisco, Calif., Apr. 30–May 13, 1963, pp. 67–74 (1963).*
The National Bureau of Standards supplies resolution charts for measuring the resolving power of microfilming systems. Recently, the master negatives used in the production of the charts were completely remade. This presented the opportunity to make certain desirable changes in the interest of standardization and efficiency of production. Since all principal design features have been retained, the new chart is applicable in every instance where the previous chart was used.
Measurements of the negatives and the resulting charts indicate that an accuracy of two percent is obtained in pattern line width and frequency.
The use of the chart is reviewed and the instructions issued with the charts are appended.

Studies at NBS of the platinum-6% rhodium vs. platinum-30% rhodium thermocouple—A preliminary report, G. W. Burns, Proc. *SAE Meeting, Sept. 23–27, 1963, Los Angeles, Calif., Preprint 750B (1963).*
The National Bureau of Standards is developing a reference table for the platinum-6% rhodium vs platinum-30% rhodium thermocouple. Thermocouples from three American manufacturers and one European manufacturer have been tested in the 0 to 1600 °C range. The paper discusses the choice of materials and briefly describes the methods of testing used in this work. The results of the tests are compared with a reference curve used in Europe for the thermocouple.

Medical applications of refrigeration, E. F. G. Brentari and R. V. Smith, *ASHRAE Guide and Data Book, ch. 68, 773–778 (Am. Soc. Heating, Refrig. Air Conditioning Engrs., Inc., New York, N.Y., 1964).*
The medical applications chapter reviews refrigeration applications in biological systems.

Measuring the directivity of a directional coupler using a sliding short-circuit and an adjustable sliding termination, R. W. Beatty, *IEEE Trans. Microwave Theory Tech.* **MTT–12,** *No. 3, 283 (May 1964).*
A modification of an earlier method for measuring the directivity of a directional coupler is described. A sliding short-circuit and an adjustable sliding termination are employed. In the earlier method one observed the average value of the

side arm output as the short-circuit was slid in the waveguide attached to the main waveguide of the directional coupler. In the modified method, the tuner connected to the input waveguide of the directional coupler is adjusted for the condition of constant side arm output as the short-circuit slides.
This results in an improvement of the technique and simplifies the error treatment.
Graphs are presented for making a correction to the observed data for the effect of coupling, and for estimating the limits of error due to the main waveguide VSWR of the directional coupler.

Magnetically retained evaporation mask, F. E. Jones and A. B. Castle, Sr., *Rev. Sci. Instr.* **34**, *No. 9, 1055 (Sept. 1963).*
This note describes a method of masking for vacuum deposited films. The method involves the use of a metal mask magnetically held against a substrate or a film on a substrate during the deposition of a film in a pattern established by the mask. The fabrication of the mask is described in detail including a special forming fixture for the mask.

Thermal Degradation of Organic Polymers, *Book,* S. L. Madorsky, *Interscience Publ. Inc., New York, N.Y. (1964).*
The book represents a critical review of the techniques employed and of the results obtained in studies on the thermal degradation of organic polymers during the past fifteen years or so, at the National Bureau of Standards and elsewhere. The topics covered pertain primarily to relative thermal stability of the polymers, the chemical nature of the degradation products, and the kinetics involved in the chemical reactions. The discussion degradation of polymers in vacuum and neutral apmospheres in the temperature range of about 200° to 1200° C.

Frequency and time standards, G. E. Hudson, *Electronic World* **72**, *20–23 (Aug. 1964).*
A review of the work of the Institute of Basic Standards, of the National Bureau of Standards, in the area of atomic frequency standards and atomic time scales. Some theoretical notions concerning accuracy of measurements, are included, as well as a description of the U.S. frequency standard and the NBS–A time scale and their dissemination via WWVB, WWVL, and WWV.

Recognition of clauses in machine translation of languages, F. L. Alt, *Proc. Intern. Conf. Machine Translation of Languages and Applied Language Analysis, Teddington, England, Symp. No. 13, pp. 126–142 (Her Majesty's Stationery Office, London, England, Sept. 1961).*
In analyzing the syntactic structure of a sentence in the course of machine translation, it is necessary to decompose the sentence into its constituent clauses. In the machine translation scheme under development at the National Bureau of Standards, it is efficient to do this as a separate step, preceding the main portion of the syntactic analysis. Further, it is advantageous to identify prepositional, participial and other phrases simultaneously with the separation of clauses. The present paper lists the types of clauses and phrases which can be recognized, and the indicators which the computing machine can use in their identification.

X-ray study of a cadmium borate glass, S. Block, J. Molin, and J. Piermarini, *J. Am. Ceram. Soc.* **46,** *557 (1963).*
The electron radial distribution function of $40CdO:60B_2O_3$ (mole %) glass is presented and an interpretation of the distribution maxima is given.

Transequatorial reception of a very-low-frequency transmission, C. J. Chilton, A. Diede, and S. Radicella, *J. Geophys. Res.* **69,** *No. 7, 1319–1328 (Apr. 1, 1964).*
A comparison is made between the phase and amplitude of the 18 kc/s signal NBA (Balboa, Panama) recorded at Boulder, Colorado in the northern hemisphere and Tucuman, Argentina in the southern hemisphere. Although these two propagation paths are essentially the same length the difference between the two paths in the diurnal change in phase height is approximately 5 km and the estimated field strength appears to be significantly lower at Tucuman than at Boulder. It is suggested that the cause of these experimentally observed differences is the variation in cosmic ray ionization with latitude.

Tomorrow's facilities for standards and measurement, H.F. Wollin, *Scale J.* **50,** *No. 6, 2 (Mar. 1964).*
Over the 60 years of its existence the National Bureau of Standards has constantly examined itself, its mission, and its responsibilities, and has reshaped its program to meet the needs of the nation. During the past several years, such reevaluation has been intensified and is bringing about significant changes in the Bureau's physical plant and in its organizational structure.
Elaborate new facilities involving 20 major buildings are now under construction at Gaithersburg, Maryland. Occupancy of the new facilities is expected by 1967.
The organizational structure of NBS recently underwent a major change. Under the new organization four institutes have been established. They are the Institute for Basic Standards, the Institute for Materials Research, the Institute for Applied Technology, and the Central Radio Propagation Laboratory. The new organization was created to permit more effective management, and to more closely identify NBS activities with the specific needs of science, industry, and commerce.

Review of recent developments of high temperature thermocouples, P. D. Freeze, *Am. Soc. Mech. Engrs., Paper No. 63–Wa, 212, 16 (Nov. 1963).*
Some of the results obtained by recent investigators in the development of thermocouples for measurement of high temperatures are reviewed. Of particular interest are the thermocouple combinations which can be used in the range of 1000° to 2400°C.
Base-metal thermocouples are used up to 1000°C, but this temperature is near their maximum for continuous use. Investigators are seeking to extend their operating range and improve their resistance to oxidation and reducing atmospheres.
When temperatures in the range 1000° to 2160°C are to be measured accurately, and conditions of chemical attack and oxidation arise, the use of noble metals becomes mandatory. A variety of thermocouple combinations of noble metals such as those of platinum-rhodium alloys and of iridium-rhodium alloys against iridium are discussed.
Temperatures above 2000°C generally require the use of refractory metals. Progress in development of thermocouples made from tungsten and rhenium and their alloys is discussed. Comparisons of results of various investigators are given for thermocouple calibrations, atmospheres, thermoelectric outputs, estimated maximum errors, temperature ranges, and mechanical and thermoelectric stabilities.

Correction to "a method for measuring the directivity of directional couplers," G. E. Shafer and R. V. Beatty, *IEEE Trans. Microwave Theory Tech.* **MMT–12,** *No. 3, 361 (May 1964).*
Correction to Equations (18) and (19) of "A Method for Measuring the Directivity of Directional Couplers."

Inline waveguide attenuator, W. Larson, *IEEE Trans. Microwave Theory Tech. Corres. Sec.* **MMT–12,** *No. 3, 367–368 (May 1964).*
A new inline attenuator fabricated in the manner of the common multi-hole directional coupler has qualities for use as an interlaboratory standard. Calibrations of one model of this attenuator, and experiments with conventional waveguide components indicate improvements in calibration results with simplified calibration procedure.

Improved transducer for external recording of arterial pulse waves, M. Davis, B. Gilmore, and E. Freis, *IEEE Trans. Bio-Med. Elec.* **BME–10,** *No. 4, 173–175 (Oct. 1963).*
This paper describes a new instrument with excellent low-frequency response for recording arterial pulse-waveforms. It uses a fluid-filled chamber and a stiff diaphragm to which a set of semi-conductor strain gages are cemented.

Physical properties of cements, based on zinc oxide hydrogenated rosin, *o*-ethoxybenzoic acid and eugenol, S. Civijan and G. M. Brauer, *J. Dental Res.* **43,** *No. 2, 281–299 (Mar.–Apr. 1964).*

Previous studies in this laboratory showed that addition of *o*-ethoxybenzoic acid (EBA) improved the properties of zinc oxide-eugenol cements. The physical properties of two formulations containing *o*-ethoxybenzoic acid (EBA)-eugenol liquid and zinc oxide-hydrogenated rosin powder were investigated and compared with those of zinc oxide-eugenol and zinc phosphate cements.

With the exception of their higher coefficient of thermal expansion, the EBA cements had much better physical properties than zinc oxide-eugenol cement and showed compressive, tensile, and shear strengths that approached those of zinc phosphate cements.

Addition of heat-treated fused quartz to the powder improved the dimensional stability and strength of the EBA cements. The materials appear promising as improved sedative bases and as pulp-capping and cementing media.

The characterization of large single crystals by high-voltage X-ray Laue photographs, H. S. Peiser and E. P. Levine (*Proc. 11th Ann. Conf. Applications of X-ray Analysis, Aug. 1962), Book, Advances in X-ray Analysis* **6,** *158–163 (Plenum Press Inc., New York, N.Y., 1963).*

Large single crystals can be examined by conventional X-ray diffraction procedures only at their surface or by destructive sectioning. With the limitations inherent in polychromatic X-ray photography, high-voltage Laue pictures are shown to give some information on the internal quality of large crystals.

Asterism in conventional Laue photographs is contrasted with streaks due to geometric effects in Laue patterns of large crystals. Detail within the streaks reveals sub-grain structure. A primary extinction effect can be used as striking proof of good crystals being capable of scattering coherently over large distances.

The anomaly in the response of semiconductor detectors at low temperatures, W. R. Dodge, S. Domen, D. Hopper, and A. Hirshfeld, *IEEE Trans. Nucl. Sci.* **NS–11,** *1–14 (June 1964).*

Investigation of the response to photons and beta particles of silicon solid state detectors cooled to temperatures below 77 °K has led to the discovery of an anomaly in the pulse height distribution which is a function of the detector temperature. The pulse height distribution from a detector exposed to a Bi^{207} source between 40 ° and 77 °K has the normal appearance; however, between 30 ° and 40 °K the apparent charge collection efficiency decreases by a factor of 2/3 and the resulting spectrum shows no clearly resolved structure. This response anomaly persists for lithium-drifted silicon detectors to at least .8 °K. Preliminary investigations indicate that at constant temperature below the anomalous region the maximum observable pulse increases slowly for electric field strengths in the intrinsic region up to 3200 volts/cm, attaining about ½ the value characteristic of temperatures above 40 °K. At higher electric field strengths (up to 4200 volts/cm) little change in the shape or maximum pulse height of the spectrum occur. Measurements indicate that the transition region from the anomalous low temperature spectrum to the well resolved (10 Kev FWHM) high temperature spectrum is less than 5 °K in width. Measurements of the behavior of the response anomaly as a function of detector resistivity, barrier type, bias voltage, and ionization density of the incident radiation will be presented. Similar data will also be presented for lithium-drifted germanium detectors.

A new high voltage calibration facility at the National Bureau of Standards, Boulder, W. W. Scott, *ISA 1963 Proc. Paper No. 7.2.63.*

The paper describes a newly constructed high voltage calibration facility located at NBS Boulder, Colorado, and presents a discussion of standards, calibration procedures, instrument protection circuits, and operator safety devices. The facility performs steady state calibrations up to 50 kv with an uncertainty less than ±0.01% at dc and up to 13.2 kv with an uncertainty less than 0.2% at 60 or 400 cps. Ratio and phase angle measurements are also performed on potential transformers with an uncertainty less than ± 0.05% at 60 or 400 cps and ±2 minutes at 60 cps or ±5 minutes at 400 cps.

A low input VSWR coaxial diode switch for the UHF band, W. L. Ecklund, *IEEE Trans. Microwave Theory Tech. Corres. Sec.* **MTT–12,** *No. 3, 359 (May 1964).*

A unique SPDT coaxial diode switch has been developed at the Boulder Laboratories of the National Bureau of Standards. By using a system of outer conductor reducers, special blocking capacitors, and a series of tuning screws, an input VSWR of less than 1.07 is achieved over a broad frequency band centered at 1000 Mc. The characteristic impedance of the switch is 50 ohms; the isolation in one arm is greater than 63 db; the insertion loss is about 1.5 db; the switching time is 20 nanoseconds; and it has a power handling capability of 3 watts CW.

Suggested practices for establishing sampling and sample preparation techniques in spectrochemical analysis, R. E. Michaelis, *Book, Methods for Emission of Spectrochemical Analysis, 4th Edition, pp. 256–259 (American Society for Testing Waterials, Phila., Pa., Feb. 1964).*

The requirements necessary to establish suitable spectrochemical sampling and sample preparation techniques in spectrochemical analysis are emphasized. Factors are considered which dictate how a material should be sampled and prepared to yield reliable, accurate spectrochemical results.

The large 50 Mc/s dipole array at Jicamarca Radio Observatory, G. R. Ochs, *Digest of the 1963 IEEE Professional Group on Antennas and Propagation, p. 237 (July 1963).*

A vertically directed antenna having a square aperture of 84,000 square meters has been constructed near Lima, Peru, for electron density measurements of the ionosphere and exosphere. It consists of two superimposed arrays of half-wave dipoles at right angles to each other, placed 0.3 wavelength above a reflecting screen of poultry netting. The half-power beamwidth of the antenna is 1.06°. It will accept maximum input power levels of 0.8 megawatt average of 16 megawatts peak. The measured on-axis gain is 0.63 that of a perfect uniformly illuminated aperture of this size.

Numerical analysis of the thermal environment of occupied underground spaces with finite cover using a digital computer, T. Kusuda and P. R. Achenbach, *ASHRAE Trans.* **6,** *No. 6, 99–105 (June 1964).*

A rectangular parallelepiped underground cavity at finite depth was used as a mathematical model for the heat transfer phenomena associated with the thermal environment in occupied fallout shelters in a study sponsored by the Office of Civil Defense. Finite difference time-iteration formulae corresponding to the three-dimensional transient heat conduction equation were programmed for the digital computer. Simultaneous exchange of heat and water vapor inside the cavity among the occupants, ventilation air, and surfaces were included in the boundary conditions, as well as the solar radiation and convective heat exchange at the earth's surface above the cavity. Computed values for shelter air temperature and relative humidity, shelter surface temperature, and surface heat flux were compared with observed data available from two experimental fallout shelters. The computed data followed the pattern of observed values very closely, and the majority of the calculated shelter air temperatures and relative humidities agreed with observed values to within 2° F and 5%, respectively, at the end of a 14-day occupancy test. The digital computer technique based on the finite-difference method appears promising from the standpoint of calculation speed, economy, and accuracy.

Emission spectrometry, B. F. Scribner and M. Margosnes, *Anal. Chem.* **36,** *No. 5, 329–343R (1964).*

This chapter is to be included in the treatise, Part I, Section E–3, Optical Methods of Analysis. The chapter is concerned with the fundamental theory and application of optical emission spectroscopy to the analysis of materials. The

major topics discussed are excitation of spectra, spectrographs and detectors, accessory equipment, qualitative analysis, quantitative analysis, semi-quantitative methods of analysis, and sources of information.

Polarography as an analytical tool, J. K. Taylor, *J. Assoc. Offic. Agri. Chem.* **47,** *No. 1, 21–27 (Jan. 1964).*
The precision and sensitivity of polarographic methods of analysis are discussed. Modified polarographic techniques developed to provide increased sensitivity or to minimize analytical interferences are reviewed.

Optically pumped magnetometers and related experiments in high magnetic fields, P. L. Bender, *Book, Quantum Electronics, Ed. P. Grivet and N. Bloembergen,* **III.** *I, 263–273 (Columbia University Press, New York, N.Y., 1964).*
Some considerations on optically pumped magnetometers are given. Related experiments in high magnetic fields giving alkali nuclear moments and departures from the Breit-Rabi formula are suggested.

The units and standards of electrical measure, F. K. Harris, *Electron World* **72,** *No. 2, 29–32 (Aug. 1964).*
The historical background of the electrical units and their experimental realization are discussed, together with the present status of our National reference standards for electrical measurement. State-of-art capabilities in some of the d-c and low-frequency areas of electrical measurement are briefly considered.

Internal friction in rutile containing point defects, J. B. Wachtman, Jr., and L. R. Doyle, *Phys. Rev.* **135A,** *276 (1964).*
The type of point defect which is introduced into rutile by reduction caused by heating in vacuum is not firmly established although both oxygen vacancies and titanium interstitials have previously been suggested. Symmetry arguments are used to determine the orientation dependence of internal friction for both. A peak with activation energy of 23.5 kcal/mole with a computed standard error of 1 kcal/mole was observed with stress along the [100] direction which is forbidden for isolated oxygen vacancies with the full symmetry of the oxygen sites; oxygen vacancies of lower symmetry might cause this peak, but would also cause another peak which was not observed. The observed peak is permitted for titanium interstitials. Such interstitials should also cause a peak for stress directed along [110], but no such peak was observed. Full agreement with the present experimental results can be obtained by assuming that titanium interstitials are associated in pairs over the temperature range of the peak. This interpretation may not be the only way of explaining the data, particularly since we have not considered the effect of chemical impurities in association with point defects or more complicated phenomena. The evidence strongly suggests that the predominant point defect in vacuum reduced rutile is neither a simple oxygen vacancy nor a simple titanium interstitial as is frequently assumed.

Review of static seals for cryogenic systems, R. F. Robbins and P. R. Ludtke, *J. Spacecraft* **1,** *No. 3253–259 (May-June 1964).*
A review of cryogenic static seals is given, with particular emphasis on seals for propellant systems and high vacuum. Categories described are gasket seals, O-ring seals, pressure actuated seals, and temperature actuated seals. The review does not include information on welded or brazed joints, sealant materials, or dynamic seals.

Dose fields from plane sources using point source data, J. H. Hubbell, *Nucleonics* **21,** *No. 8, 144–148 (Aug. 1963).*
Six currently-used analytic point source buildup factor formulas are summarized, all of which lead to analytic solutions for a variety of distributed source problems with rotational symmetry about a source-detector axis. The use of these formulas may be extended to include other distributed source problems, such as the dose-rate from a rectangular source or off-axis from a circular disk source. This is done by expanding the buildup factor as a power series

$$\exp(+\rho_0 r)\sum_{n=0}^{\infty} b_n \cdot (-\mu_0 r)^n/n!$$

(a generalization of the Leshchinskii formula) in which $\mu_0 r$ is the mean free path distance between point source and detector, and the b_n coefficients are easily generated from parameters given for any of the above analytic buildup factor formulas. The power series formulation is applied to give:
(1) a comparison with dose-rates measured by a detector separated from a Co–60 rectangular plaque food irradiator by a layer of steel and a layer of water and
(2) dose-rate profiles at constant heights across cleared circular areas in a Co–60 infinite plane source in air.

Hall generators: what, why, and how much? S. Rubin, *1964 IEEE Intern. Convention Record, Part 8, p. 74 (Mar. 1964).*
A brief tutorial introduction to the galvanomagnetic effects, the Hall effect and the magnetoresistive effect is presented. The characteristics of the Hall effect of interest in engineering applications are outlined, and a list of applications is given. Standards of terminology and measuring methods being evolved, both internationally under the auspices of the IEC, TC–47, and nationally under the Department of the Navy, Bureau of Naval Weapons, are noted. Several of these are outlined in detail, and three are discussed at length.
The concept of linearity error as the departure of the actual characteristic of a device from the straight line graph that would characterize a perfectly linear device, expressed as a percent of the ordinate magnitude at a particular point of the straight line, as opposed to a percent of the full scale ordinate magnitude, is fully discussed. An example of its application in a magnetic induction measuring application is given.
The common sensitivity index for Hall generators, the product sensitivity, is discussed, and two additional indices, the current and magnetic sensitivities, are introduced. The relations between the three and the advantages of each are considered. Equations are presented which allow the derivation of either one of the other two, if one of the three indices is known.

The half-life of carbon-14: Comments on the mass-spectrometric method, E. E. Hughes and W. B. Mann, *Intern. J. Appl. Rad. Isotopes* **15,** *No. 1, 97–100 (Jan. 1964).*
An assessment has been made of the mass-spectrometer results in the recent NBS determination of the half-life of carbon-14. Evidence is presented to show that the uncertainties due to effusive separation and the dependence of the sensitivity constant on the isotopic abundance of carbon-14 are small. It is proposed, however, to reduce the value of the half-life of carbon-14 determined by Mann, Marlow, and Hughes (1961) to 5740 ± 50 years.

A recalibration of the National Bureau of Standards tritiated water standards by gas counting, W. B Mann, R. W. Medlock, and O. Yura, *Intern. J. Appl. Rad. Isotopes* **15,** *No. 6, 351–361 (1964).*
The National Bureau of Standards hydrogen-3 standards were prepared in the winter of 1954–55 using microcalorimetric measurements. They have now been re-calibrated by means of the National Bureau of Standards length-compensated internal gas counters. The new value for their activity is 1.96% lower than that previously measured, but this difference also involves uncertainties in the half-life and the average beta energy for hydrogen-3. A value for the ratio of the combined evaporation and reaction rates with zinc, for HTO and H_2O, equal to 0.92 has been obtained.

Electronic scanning for large radiotelescopes, T. A. Clerk, *Digest 1963 IEEE Prof. Group Antennas and Propagation, pp. 242-246 (July 1963).*
This paper describes a means by which a large radio-telescope can be electronically scanned in one dimension, and a simple scheme for producing a variable phase shift by purely elec-

tronic means. The paper concludes with a proposed Mills Tee array which can be electronically scanned in declination for use in ionospheric and radio-astronomical studies at a frequency near 10 Mc/s. The basic phase sweeping scheme involves the use of traveling-wave feeds and variable conversion oscillators to effect a net phase change along a transmission line.

Electron microscopy and diffraction of aluminum oxide whiskers, D. J. Barber, *Phil. Mag.* **10,** *No. 103, 75–94 (July 1964).*
Whiskers of $\alpha-Al_2O_3$ have been grown by the condensation and oxidation of aluminium on an alumina substrate, and examined by transmission electron microscopy and diffraction. Unbroken whiskers invariably terminate in a small globule of aluminum and have a "drumstick" form. The most perfect whiskers are ribbons with their principal surfaces parallel to the (0001) planes; the majority of these have a $<1120>$ growth direction. With intense heating in the electron beam, such ribbons can be thermally etch-pitted. Many drumsticks are tubular rather than ribbon-like and drumsticks containing axial dislocations have also been seen. The effect of intense heating on these whiskers has been investigated. Occasionally, the aluminium globules melt and react with the carbon support film in the microscope to give crystalline Al_4C_3. Alternatively, a globule may explode to form many small globules that immediately develop stems; thus, new whiskers are formed in the microscope. The relevance of these observations to proposed mechanisms for the growth of drumstick whiskers is discussed.

Theory of operation of the rotary positive displacement meter, C. T. Collett (*Proc. 23d Annual Gas Measurement Short Course, Aug. 20, 1963*), *West Virginia Univ. Tech. Bull.* **70,** *48–53 (1963).*
The fundamental theory of the operation of the rotary positive displacement meter is developed. The general principles of idealized multi-lobed gear meters are compared with actual characteristics of manufactured two-lobed impeller meters.

The establishment and maintenance of the unit of voltage at the NBS Boulder Laboratories, B. A. Wickoff, *ISA 1963 Proc. Paper No. 28.2.63 (1963).*
This paper describes the methods and techniques used with saturated cells to establish a unit of voltage at NBS Boulder. This group of cells is one of two groups both known as National Working Standards that are directly related to the National Reference Group. Also presented is a discussion of (1) the problems involved, (2) calibration facilities and procedures used to disseminate the unit of voltage, and (3) future plans for the unit of voltage maintained at Boulder.

Four-point probe measurement of non-uniformities in semiconductor sheet resistivity, L. H. Swartzendruber, *Solid State Electronics* **7,** *413–422 (1964).*
Equations and graphs are presented to aid in the evaluation of resistivity non-uniformities when measured by use of the four-point probe. Both the in-line and square array four-point probes are considered. To enable a circular disc to be probed for non-uniformities, correction factors for a displaced probe are given for an in-line array displaced with points on a diameter, for an in-line array displaced with points perpendicular to a diameter, and for a displaced square array.

Discrepancy in conversion of early melting-point temperatures, S. J. Schneider, *J. Am. Ceram. Soc.* **46,** *No. 7, 354–355 (1963).*
The assumption that the melting points of Al_2O_3 and other refractories reported in the early 1900's were based on a scale identical with the International Temperature Scale of 1927 is pointed out to be false. A positive correction generally must be applied when converting the earlier data to equivalent values on the International Practical Temperature Scale of 1948.

Relationship between intensity of carbon arc and asphalt oxidation, J. R. Wright, P. G. Campbell, and T. L. Fridinger, *ASTM Spec. Tech. Publ. No. 247, pp. 3–20 (May 1964).*
Films of two air-blown asphalts were exposed to the carbon arc at different intensities to determine the effect of radiant energy intensity on the rate of asphalt oxidation. The oxidation rates were established by measuring the changes in infrared absorption in the carbonyl band as a function of exposure time. The intensity of the radiant energy was varied by the voltage adjustment switch on the accelerated weathering machine or by moving the samples closer to the arc. The intensity was monitored by power consumption and the incident flux by chemical dosimetry. It was found that: (1) the asphalt oxidation rate increased with the intensity of the carbon arc; (2) the radiant energy output of the accelerated weathering machine tends to level off at the higher voltage settings; and (3) at the maximum voltage setting of the accelerated weathering machine, the incident radiant flux does not equal or exceed that which can be absorbed by asphalt. Monitoring the incident radiant energy is recommended as a part of the accelerated weathering procedure for asphalt.

Standard potential of the Ag-AgCl electrode in 5% aqueous manitol, R. Gary and R. A. Robinson, *J. Chem. Eng. Data* **9,** *No. 3, 376–378 (July 1964)*
The standard potential of the Ag-AgCl electrode from 0° to 60° has been determined by e.m.f. measurements on the cell:

$$Pt\text{-}H_2/HCl\ (m),\ \text{mannitol (5 wt. \%)},\ H_2O/AgCl\text{-}Ag$$

From these data and from data on the same cell containing no mannitol, the relative partial molal quantities $\Delta G°$, $\Delta H°$ and $\Delta S°$ for the change in solvent are calculated. The value of $\Delta G°$ for HCl in 5% mannitol at 25° is found to be 54 j. $mole^{-1}$. There is a small but significant change in the e.m.f. of the cell if mannitol is replaced by its diastereoisomer, sorbitol.

Summary of symposium on recent research on bituminous materials, S. H. Greenfeld, *ASTM Spec. Tech. Publ. No. 347, pp. 108–111 (May 1964).*
Eight papers were presented in the Symposium on Recent Research on Bituminous Materials sponsored by Committee D–8 on Bituminous and Other Organic Materials for Roofing, Waterproofing, and Related Building or Industrial Uses of the American Society for Testing and Materials. This summary includes the reasons for having the symposium and the important contributions of the eight papers.

Report on standard samples, reference samples, and high-purity material for spectrochemical analysis, R. E. Michaelis, *ASTM Spec. Tech. Publ. No. 58–E (1963).*
A revision of the survey on available samples, reference samples, and high-purity materials has been prepared. Included in the revision are new sources of these materials from this country and foreign countries as well. The report lists 2851 standard samples, about 1200 reference samples, and more than 1000 materials having a claimed purity of 99.9 percent or higher. This represents an increase of about 1650 entries for the three-year period between revisions.

Standard electromotive force of the hydrogen-silver chloride cell and the thermodynamics of solutions of hydrochloric acid in 50 wt. % methanol from 10 to 40° C, M. Paabo, R. A. Robinson, and R. G. Bates, *J. Chem. Eng. Data* **9,** *No. 3, 374–376 (July 1964).*
The standard electromotive force of the cell Pt/H_2 (g., 1 atm.): HCl (m) in 50 wt. % methanol-water: AgCl/Ag has been determined at seven temperatures from 10 to 40 °C. The activity coefficients of hydrochloric acid in 50% methanol for molalities in the range 0.005 to 0.1 have been derived from the e.m.f. measurements. From the variation of the activity coefficient with temperature, the relative partial molal enthalpy of hydrochloric acid at 25° was calculated for comparison with the value in the aqueous medium.

Gallium-palladium alloys as dental filling material, R. M. Waterstrat and R. W. Longton, *Public Health Rept. 79, No. 7, pp. 638–642 (July 1964).*
Alloys of gallium and palladium may be prepared for use as dental filling materials by mixing a liquid gallium-tin eutectic solution together with palladium powder in a manner analogous to the present methods used for mixing dental amalgam alloys.

The mechanical properties of these alloys depend to a great extent upon the particle size of the metal powders and they may be controlled over a rather wide range of values. When compared with dental amalgam, the gallium alloys frequently have a greater strength and are more resistant to flow. They permit a greater retention of room temperature strength at mouth temperature and possess a thermal expansion coefficient closer to that of human teeth. In addition the gallium alloys possess the remarkable ability to "wet" the tooth structure.

At the present time the use of gallium alloys as dental filling materials is prevented by an inadequate knowledge of their stability in the oral environment. A considerable latitude exists for alloying palladium with other noble metals in order to improve the properties of the gallium alloys.

Thermodynamics of aqueous solutions of hydriodic acid from electromotive force measurements of hydrogen-silver iodide cells, H. B. Hetzer, R. A. Robinson, and R. G. Bates, *J. Phys. Chem.* **68,** *No. 7, 1929–1933 (1964).*

Electromotive force measurements of the cell $Pt;H_2(g)$, HI(m), AgI;Ag have been made at 11 temperatures from 0 to 50°. The standard e.m.f. ($E°$) is given within 0.05 mv. by the equation $E° = -0.15242 - 3.19 \times 10^{-4}(t-25) - 2.84 \times 10^{-6}(t-25)^2$, where t is the temperature in degrees Celsius. These values are in excellent agreement with those obtained by Owen from studies of borax-buffered KI solutions at 5, 10, 30, 35, and 40° but differ by 0.14 to 0.17 mv. at 15, 20, and 25°. The activity coefficient ($\gamma \pm$) of HI at molalities (m) from 0.005 to 0.9 has been derived. The relative partial molal enthalpy ($\bar{L}_2$) of HI at 25° was calculated and compared with that for HCl and HBr. At 25° and m=0.1, $\gamma \pm$ is 0.811 and $\bar{L}_2$ is 130 cal. mole^{-1}.

Electrode potentials in fused systems. VII. Effect of ion size on membrane potentials, K. H. Stern and J. A. Stiff, *J. Electrochem. Soc.* **III,** *No. 8, 893–897 (Aug. 1964).*

Concentration cells exhibiting glass membrane potentials have been measured for the AgBr–NaBr, AgCl–KCl, and AgCl–CsCl systems. Only for the first of these can the bulk composition be used to calculate cation transport numbers in the membrane. For the latter two the sodium ion impurities in the melt appear to be potential determining. In the sodium-containing systems the anions appear to be transported as part of a cationic silver complex.

Analysis of rotation errors of a waveguide rotary-vane attenuator, W. Larson, *IEEE Trans. Instr. Meas.* **IM–12,** *No. 2, 50–55 (Sept. 1963).*

In the Microwave Calibration Services Section of the NBS Radio Standards Laboratory, Boulder, Colo., and analysis of calibration data obtained from measurements made on a rotary-vane type attenuator reveals that the vane alignment produces an inherent vane-angle error. It is found that the standard deviation of the measured values of attenuation is correlated with the vane-angle error. Approximately two-thirds of the attenuators calibrated were in error by less than 50 per cent of the manufacturer's stated specifications of accuracy.

The treatment of the errors of a rotary vane attenuator is extended to cover the vane-angle error, resettability error, and mismatch error. The method of analysis is applicable to all attenuation values and vane-angle errors of this sample. Graphs are used to estimate the limits of these errors. Several representative cases are given using the deviation from the "estimated vane-angle error" to establish limits in the correction of vane-angle error.

A modified rotary-vane attenuator with a resolution equal to 30 times the resolution of the attenuators comprising the sample was used to verify calculated vane-angle error at various values of attenuation. Inherent vane-angle error can be reduced by increasing the dial resolution and by a technique of precise vane alignment at zero dial setting.

Other NBS Publications

Journal of Research 68A (Phys. and Chem.), No. 6 (Nov.–Dec. 1964), 70 cents.

The 1962 He^3 scale of temperatures. I. New vapor pressure comparisons. S. G. Sydoriak and R. H. Sherman. (See above abstracts.)

The 1962 He^3 scale of temperatures. II. Derivation. S. G. Sydoriak, T. R. Roberts, and R. H. Sherman. (See above abstracts.)

The 1962 He^3 scale of temperatures. III. Evaluation and status. T. R. Roberts, R. H. Sherman, and S. G. Sydoriak. (See above abstracts.)

The 1962 He^3 scale of temperatures. IV. Tables. R. H. Sherman, S. G. Sydoriak, and T. R. Roberts. (See above abstracts.)

Absolute isotopic abundance ratio and the atomic weight of a reference sample of copper. W. R. Sheilds, T. J. Murphy, and E. L. Garner.

Absolute isotopic abundance ratio and the atomic weight of bromine. E. J. Catanzaro, T. J. Murphy, E. L. Garner, and W. R. Sheilds.

Optical properties of thin films on transparent surfaces by ellipsometry; internal reflection for film covered surfaces near the critical angle. E. Passaglia and R. R. Stromberg. (See above abstracts.)

On the second-order transition of a rubber. E. A. DiMarzio.

Ionization constants and reactivity of isomers of eugenol. G. M. Brauer, H. Argentar, and G. Durany.

Near infrared spectrophotometric method for the determination of hydration numbers. R. A. Durst and J. K. Taylor. (See above abstracts.)

Franck-Condon factors for the ionization of H_2, HD, and D_2. M. E. Wacks.

Calculation of the geometrical structure of some AH_n molecules. M. Krauss.

Preparation and heat of formation of a magnesium oxysulfate. E. S. Newman.

Heat capacity of potassium borohydride (KBH_4) from 15 to 375 °K thermodynamic properties from 0 to 700 °K. G. T. Furukawa, M. L. Reilly, and J. H. Piccirelli.

Heat of combustion and heat of formation of aluminum carbide. R. C. King and G. T. Armstrong.

Some elastic compliances of single crystal rutile from 25 to 1000 °C. S. Spinner and J. B. Wachtman, Jr. (See above abstracts.)

Energy dependence of the D–D reaction cross section at low energies. J. G. Brennan and J. J. Coyne.

Steady-state response of silicon radiation detectors of the diffused P–N junction type to x rays. I: Photovoltaic mode of operation. K. Scharf and J. H. Sparrow. (See above abstracts.)

Intercomparison of high-energy x-ray intensity measurements. J. S. Pruitt and S. R. Domen.

Journal of Research 68B (Math. and Math. Phys.), No. 4 (Oct.–Dec. 1964), 75 cents.

Hydrodynamic fluctuations and Stokes' Law friction. R. Zwanzig.

Equivalence of certain inequalities complementing those of Cauchy-Schwarz and Hölder. J. B. Diaz, A. J. Goldman, and F. T. Metcalf.

Weak generalized inverses and minimum variance linear unbiased estimation. M. Zelen and A. J. Goldman.

Improvement of bounds to eigenvalues of operators of the form T^*T. N. W. Bazley and D. Fox.

The greatest crossnorm. R. Schatten.

Radio Sci. J. Res. NBS/USNC–URSI 68D, No. 1 (Jan. 1965), $1.00

Some problems of ionospheric nonlinearities. D. H. Menzel.

Some nonlinear phenomena in the ionosphere. V. A. Bailey.

An experimental study of gyro interaction in the ionosphere, at oblique incidence. F. H. Hibberd.

On some nonlinear phenomena in the ionospheric plasma. P. Caldirola and O. De Barbieri.

Ionospheric cross modulation: a microscopic theory. D. Layzer and D. H. Menzel.

VLF noise bands observed by the Alouette I satellite. J. S. Belrose and R. E. Barrington.

Excitation of optical radiation by high power density radio beams. L. R. Megill.

Alteration of the electron density of the lower ionosphere with ground-based transmitters. P. P. Lombardini.

Collision effects in hydromagneto-ionic theory. H. K. Sen and A. A. Wyller.

Electromagnetic wave reflection from an oscillating, collision-free magneto-ionic medium. O. E. H. Rydbeck.

Nonlinear propagation of electromagnetic waves in magnetoplasmas. II. (An invited abstract) M. S. Sodha and C. J. Palumbo.

Radio Sci. J. Res. NBS/USNC–URSI 68D, No. 12 (Dec. 1964), $1.00.

Experiment on the constancy of the velocity of electromagnetic radiation. P. Beckmann and P. Mandics. (See above abstracts.)

Measurement of the phase velocity of VLF propagation in the earth-ionosphere waveguide. F. K. Steele and C. J. Chilton.

Wave hop theory of long distance propagation of low-frequency radio waves. L. A. Berry.

Wave propagation in a compressible ionosphere. Part I. S. R. Seshadri.

Wave propagation in a compressible ionosphere. Part II. S. R. Seshadri.

Spatial properties of the amplitude fading of continuous HF radio waves. J. Ames.

Physical properties of the polar winter mesosphere obtained from low-frequency propagation and partial reflection studies. J. S. Belrose, L. R. Bodé, and L. W. Hewitt.

Reply to the "Remarks by Donald H. Menzel With Reference to Bailey's Comments on Solar Electric Fields." V. A. Bailey.

Line parameters and computed spectra for water vapor bands at 2.7μ, D. M. Gates, R. F. Calfee, D. W. Hansen, and W. S. Benedict, NBS Mono. 71, (Aug. 3, 1964), $2.00.

Tables of electron radial functions and tangents of phase shifts for light nuclei (Z–1 through 10), C. P. Bhalla, NBS Mono. 81 (Aug. 6, 1964), $3.25.

Examination of farm milk tanks. A manual for weights and measures officials, M. W. Jensen, NBS Handb. 98 (May 22, 1964), 35 cents.

Hydraulic Research in the United States 1964, Ed. H. K. Middleton, NBS Misc. Publ. 261 (Aug. 14, 1964), $1.25.

Water-repellent preservative non-pressure treatment for millwork, CS262–63 (Dec. 31, 1963), 10 cents.

Quarterly radio noise data March, April, May 1963, W. Q. Crichlow, R. T. Disney, and M. A. Jenkins, NBS Tech. Note 18–18, (July 25, 1964), 50 cents.

Absolute photometry of the light of the night sky. The zenith intensity of Haleakala (latitude N 20.7°) and at Fritz peak (latitude N 39.9°), F. E. Roach and L. L. Smith, NBS Tech. Note 214 (June 29, 1964), 35 cents.

Survey of multiply charged ions, F. L. Mohler, NBS Tech. Note 243 (May 27, 1964), 10 cents.

Radiochemical analysis: Activation analysis, instrumentation, radiation techniques, and radioisotope techniques, Ed. J. R. DeVoe, NBS Tech. Note 248 (Aug. 21, 1964), 50 cents.

Metastable levels in the continuum and the independent particle model, F. Prats and U. Fano, Proc. IIIrd Intern. Conf. Physics of Electronic and Atomic Collisions, London, England, p. 600–605 (July 22–26 1963).

Satellite scintillation observations at Boulder, Colorado, J. L. Jespersen and G. Kamas, J. Atmospheric Terrest. Phys. **26,** 457–473 (1964).

The reaction of methyl radicals with dimethylmercury, R. E. Rebbert and P. Ausloos, J. Am. Chem. Soc. **86,** No. 10, 2068–2069 (May 20, 1964).

On associated ions in polyelectrolytes and trapped Browian trajectories, J. L. Jackson and S. R. Coriell, J. Chem, Phys. **40,** No. 5, 1460–1461 (Mar. 1, 1964).

Approximations to the pair correlation function for a hard-sphere fluid, M. Klein, Phys. Fluids **7,** No. 3, 391–410 (Mar. 1964).

Physical processes in the *D* region of the ionosphere, G. C. Reid, Rev. Geophys. **2,** No. 2, 311–333 (May 1964).

Observation of FeO in absorption by flash heating and kinetic spectroscopy, A. M. Bass, N. A. Kuebler, and L. S. Nelson, J. Chem. Phys. **40,** No. 10, 3121–3122 (May 15, 1964).

Computer simulation of traffic on nine blocks of a city street, M. C. Stark, (Proc. 41st Annual Meeting Highway Research Board, Jan. 8–12, 1962), Highway Res. Board Bull. 356, Publ. 1051, p. 40 (Natl. Acad. Sci.-Natl. Res. Council, Wash, D.C., 1962).

One man's opinion—a common language (nomenclature for rubbers), R. D. Stiehler, Rubber World **148,** No. 3, 119 (June 1963).

Long-lived effects in the *D* region after the high-altitude nuclear explosion of July 9, 1962, A. H. Brady, D. D. Crombie, A. G. Jean, A. C. Murphy, and F. K. Steele, J. Geophys. Res. **69,** No. 9, 1921–1924, (May 1, 1964).

Some remarks concerning non-reciprocity in radio propagation, J. R. Wait, IEEE Trans. Ant. Prop. **AP–12,** No. 3, 372–373 (May 1964).

Synthesis of diatomic radicals, H. E. Radford, J. Chem. Phys. **40,** No. 9, 2732–2733 (May 1, 1964).

The effective area of a guarded electrode, J. I. Lauritzen, Jr., (Proc. Conf. Electric Insulation) 1963 Annual Report, Natl. Acad. Sci.-Natl. Res. Council Publ. 1141, pp. 67–73 (1964).

The listing of sudden ionospheric disturbances, J. V. Lincoln, Planet Space Sci. **12,** 419–434 (1964).

Evidence of a stratified echoing region at 150 kilometers in the vicinity of the magnetic equator during daylight hours, B. B. Balsley, J. Geophys. Res. **69,** No. 9, 1925–1930 (May 1, 1964).

Effect of pressure in the radiolysis and photolysis of methane, P. Ausloos, R. Gordon, Jr., and S. T. Lias, J. Chem. Phys. **40,** No. 7, 1854–1860 (Apr. 1, 1964).

Introduction, V. J. Johnson, Am. Soc. Refrigerating and Air Conditioning Engineers, Symp., The Role Cryogenics is Playing in Expanding Mechanical Engineering at the semi-annual meeting of the Am. Soc. of Heating, Refrigerating and Air-Conditioning Engineers, New York, N.Y., Feb. 11–14, 1963, pp. III–IV (1964).

Measurement of the cross section for elastic scattering of slow electrons by hydrogen atoms, W. L. Wiese, VIth Intern. Conf. Ionization Phenomena in Gases I, 5–8 (Paris, 1963).

Mass spectrometric study of the isotopic exchange rate of oxygen atoms with O_2, NO, and NO_2 J. T. Herron and F. S. Klein, J. Chem. Phys. **40,** No. 9, 2731 (May 1, 1964).

Growth twins and branching of electrodeposited copper dendrites, F. Ogburn, J. Electrochem. Soc. **11,** No. 7, 870–872 (July 1954).

Ultrasonically induced nuclear spin transitions in antiferromagnetic $KMnF_3$ A. B. Denison, L. W. James, J. D. Currin, W. H. Tantilla, and R. J. Mahler, Phys. Rev. Letters **12,** 244–245, (1964).

Low-temperature infrared study of intermediates in the photolysis of HNCO and DNCO, M. E. Jacox and D. E. Milligan, J. Chem. Phys. **40,** No. 9, 2457–2460 (May 1, 1964).

N_2+ oscillators strength from arc spectroscopic measurements using an analog computer, J. B. Shumaker, Jr., (Proc. Sixth Intern, Symp. Ionization Phenomena in Gases VII, No. 15, 311–313 (1963).

Ixiolite and other polymorphic types of $FeNbO_4$, R. S. Roth and J. L. Waring, Am. Mineralogist **49,** 242–246 (Mar.–Apr. 1964).

Free subgroups and normal subgroups of the modular group, M. Newman, Ill. J. Math. **8,** No. 2, 262–265 (June 1964).

Four critical fields in superconducting indium lead alloys, S. Gygax, J. L. Olsen, and R. H. Kropschot, Phys. Letters **8,** No. 4, p. 228–230 (1964).

Survey of current NBS work on properties of parahydrogen, R. D. Goodwin, D. E. Diller, W. J. Hall, H. M. Roder, L. A. Weber, and B. A. Younglove (Proc. 1963 Cryogenic Eng. Conf., Univ. Colorado and National Bureau of Standards, Boulder, Colo., Aug. 19–21, 1963), Book, Advances in Cryogenic Engineering **9,** Paper D–9, 234–242 (Plenum Press Inc., New York, N.Y., 1964).

Presidential address before the Electrochemical Society meeting, Toronto, Canada, May 5, 1964, W. J. Hamer, J. Electrochem. Soc. **III,** No. 7, 145C–147C (July 1964).

Precise determination of the area of guarded electrodes for accurate dielectric measurements on solid-disk specimens, W. P. Harris (Proc. Conf. Electric Insulation) 1963 Annual Report, Natl. Acad. Sci.-Natl. Res. Council Publ. 1141, p. 71 (1964).

Open-probe thermocouple control of radio-frequency heating, A. W. Ruff, Jr., Rev. Sci. Instr. **35,** No. 6, 760–761 (June 1964).

Surface currents in type II superconductors, S. Gygax and R. H. Kropschot, Phys. Letters **9,** No. 2, 91 (Apr. 1, 1964).

Preliminary thermodynamic properties of neon, R. D. McCarty and R. B. Stewart (Proc. 1963 Cryogenic Eng. Conf. Univ. Colorado and National Bureau of Standards, Boulder, Colo., Aug. 19–21, 1963), Book, Advances in Cryogenic Engineering **9,** Paper D–1, 161–167 (Plenum Press Inc., New York, N.Y., 1963).

Thermodynamic representation of high-pressure vapor-liquid equilibria, J. M. Prausnitz, Chem. Eng. Sci. **18,** 613–630 (1963).

Nuclear magnetic relaxation of the impurity nucleus in dilute ferromagnetic alloys, R. L. Streever, Phys. Rev. **134,** No. 6A, A1612–A1617 (June 15, 1964).

Metastable transitions in mass spectra of methane and the deuteromethanes, V. H. Diebeler and H. M. Rosenstock, J. Chem. Phys. **39,** 1326 (1963).

Electron distribution in the ionosphere, J. W. Wright, Proc. URSI XIVth General Assembly, Sept. 1963, Tokyo, Japan XIII, pp. 206–222 (1964).

Studies of photodissociation of molecular ions, G. H. Dunn, Book, Atomic Collision Processes, pp. 997–1005 (North-Holland Publ. Co., Amsterdam, The Netherlands, 1964).

Spread-*F* observations by the Alouette topside sounder satellite, W. Calvert and C. W. Schmid, J. Geophys. Res. **69,** No. 9, 1839–1852 (May 1, 1964).

Spectral distribution of typical daylight as a function of correlated color temperature, D. B. Judd, D. L. MacAdam, and G. Wyszecki, J. Opt. Soc. Am. **54,** No. 8, 1031–1040 (Aug. 1964).

Mechanical and dielectric relaxation of crystalline polymers in relation to degree of crystallinity and morphology, E. Passaglia, Soc. Plastics Engrs., pp. 169–177 (July 1964).

Mass spectrometric study of the photoionization of acetylene and acetylene-d_2, V. H. Dibeler and R. M. Reese, J. Chem. Phys. **40,** No. 7, 2034–2035 (Apr. 1, 1964).

Low-temperature infrared studies of the chemistry of free radicals, M. E. Jacox and D. E. Milligan, Appl. Opt. **3,** 873 (July 1964).

Characteristics energy losses of electrons in solids, Marton, Book, Actions Chimiques et Biologiques Des Radiations, Chapt. IV, pp. 260–281 (Masson et Cie Editeurs, Paris, France, 1964).

Isotopic fractionation of uranium related to roll features in sandstone, Shirley Basin, Wyoming, J. N. Rosholt, E. N. Harshman, W. R. Shields, and E. L. Garner, Econ. Geology **59,** 570 (1964).

Solid state detector for beta-ray spectroscopy below 4.2°, K. J. Chin, A. T. Hirshfeld, and D. D. Hoppes, Rev. Sci. Instr. **34,** No. 12, 1258–1259 (Nov. 1963).

Simple derivation of the Faxen solution to the Lamm equation, G. H. Weiss, J. Math, Phys. **5,** No. 5, 675–676 (May 1964).

Should the convention definition of mismatch loss be abandoned? K. A. Norton, Proc. IEEE **52,** 710 (June 1964).

World days program, A. H. Shapley, IQSY Notes **5,** 27–30 (Dec. 1963); **6,** 27–32 (Mar. 1964); **7,** 13–15 (May 1964).

Weights and measures and aerosols, M. W. Jensen, Proc. 50th Annual Meeting of Chemical Specialties Manufactures Association, pp. 33–35 (Dec. 9–12, 1963).

Unitary symmetry in photoproduction and other electromagnetic interactions, C. A. Levinson, H. J. Lipkin, and S. Meshkov, Phys. Letters **7,** No. 1, 81–84 (Oct. 15, 1963).

Effects of magnetic disturbance as noted on oblique incidence ionograms, V. Agy and K. Davies, AGARDograph **59,** The effect of disturbances of solar origin on communications, Ed. G. J. Gassmann, pp. 167–176 (Pergamon Press, Inc., London, England, 1963).

Editorial, R. W. Beatty, IEEE Trans. Microwave Theory Tech. **MTT–12,** No. 3, 274 (May 1964).

Comparison calibration of inductive voltage dividers, R. V. Lisle and T. L. Zapf, ISA 1963 Proc. Paper 7.1.63 (1963).

Ionospheric absorption in conjugate regions and possible oscillation of the ionosphere, H. J. A. Chivers and J. K. Hargreaves, Nature **202,** 891–893 (May 30, 1964).

Initial preparation and metastable transitions in mass spectra, H. M. Rosenstock, V. H. Dibeler, and F. N. Harllee, J. Chem. Phys. **40,** No. 2, 591–594 (Jan. 15, 1964).

Infrared spectroscopy of weak charge-transfer absorption spectra of NO in Kr and CH_3OH solutions, E. E. Ferguson and H. P. Broida, J. Chem. Phys. **40,** 3715 (1964).

Index to Journal of Association for Computing Machines, W. W. Youden, J. Assoc. Comp. Mach. **10,** No. 4, 583–646 (Oct. 1963).

Inelastic electron scattering from rare gases, determination of oscillator strengths in the continuum, C. E. Kyuatt and J. A. Simpson, Proc. Third Intern. Conf. Physics of Electronic and Atomic Collisions, London, England, 1963, pp. 191–200 (North Holland Publ. Co., Amsterdam, The Netherlands, 1964).

Physical properties of cements, based on zinc oxide hydrogenated rosin, *o*-ethoxybenzoic acid and eugenol, S. Civijan and G. M. Brauer, J. Dental Res. **43,** No. 2, 281–299 (Mar.–Apr. 1964).

A study of geomagnetic effects associated with auroral zone electron precipitation observed by balloons, W. H. Campbell, J. Geomagnetism and Geoelectricity **11,** No. 1, 37–57 (June 1964).

The calculations of autoionization probabilities, J. W. Cooper, Proc. Third Intern. Conf. Physics of Electronic and Atomic Collissions, London, 1963, pp. 595–599 (North Holland Publ. Co., Amsterdam, The Netherlands, 1964).

The basis of the functional assumption in the theory of the Boltzmann equation, M. S. Green and R. A. Piccirelli, Phys. Rev. **132,** No. 3, 1388 (Nov. 1963).

On the constitution of the topside ionosphere, R. W. Knecht, H. Rishbeth, and T. E. VanZandt, (Proc. of NATO Advanced Study Inst., April 17–26, 1963, Skeikampen, Norway), Book Electron Density Distribution in Ionosphere and Exosphere, pp. 348–350 (North Holland Publ. Co., Amsterdam, The Netherlands, 1964).

On a problem of G. Sansone, M. Newman, Ann. Mat. **LXV,** 27–34 (1964).

A time-varying model of the ionospheric *F*2 layer, H. Rishbeth, J. Atmospheric Terrest. Phys. **26,** No. 6, 657–685 (June 1964).

A theoretical study of the Martian ionosphere, R. B. Norton, Book, Advances in the Astronautical Science Exploration of Mars **15,** 533–542 (Western Periodicals, California, 1963).

Energy dependence for the photodetachement of I⁻near threshold, B. Steiner, M. L. Seman, and L. M. Branscomb, Proc. Third Intern. Conf. Physics of Electronic & Atomic Collision, London, England, 1963, pp. 537–542, (North Holland Publ. Co., Amsterdam, The Netherlands, 1964).

S-wave hyperon-nucleon interactions and SU_3 symmetry, P. D. DeSouza, G. A. Snow, and S. Meshkov, Phys. Rev. **135,** 565 (1964).

Synthesis of higher ketoses by aldol reactions, II. Unsubstituted heptuloses, R. Schaffer, J. Org. Chem. **29,** 1471–1475 (June 1964).

Excess entropy at glass transformation, A. B. Bestul and S. S. Chang, J. Chem. Phys. **40,** 3731 (1964).

The ionosphere and radio propagation in the lower frequencies (a report of an AGU session by the same title), T. N. Gautier, Science **143,** No. 3611, 1197–1199 (Mar. 13, 1964).

Nuclear magnetic resonances of ^{69}Ga and ^{71}Ga in gallium-substituted yttrium iron garnet, R. L. Streever and G. A. Uriano, Phys. Rev. Letters **12,** No. 22, J516 1–3—J516 3–3 (June 1, 1964).

A diffusive model for the initial phase of a solar proton event, G. C. Reid, J. Geophys. Res. **69,** 2659–2667 (June 1964).

Elementary derivation of time-correlation formulas for transport coefficients, R. Zwanzig, J. Chem. Phys. **40,** No. 9, 2527–2533 (May 1964).

A complete description of the normal subgroups of genus one of the modular group, M. Newman, Am. J. Math., **86,** 17–24 (1964).

Abbreviated Calendar record, January–February 1964, A. H. Shapley, IQSY Notes **7,** 19–25 (May 1964).

Evidence for a cooperative intramolecular transition in poly-L-proline, F. Gornick, L. Mandelkern, A. F. Diorio, and D.E. Roberts, Am. Chem. Soc. **86,** No. 13, 2549–2555 (July 1964).

The isomerization of D-manno-3-heptulose by alkali, R. Schaffer, J. Org. Chem. **29,** 1471–1475 (June 1964).

Insertion loss concepts, R. W. Beatty, Proc. **IEEE 52,** 663–671 (June 1964).

Reaction rates for the formation of He_2+ and Ne_2+, E. C. Beaty and P. L. Patterson, Book, Comptes Rendus de la VI^e Conference Internationale sur les Phenomenes D'Ionisation dans les Gaz, Ed. P. Hubert and E. Cremieu-Alcan III, pp. 289–293 (S. E. R. M. A. Publ. Co., Paris, France, 1963).

Ranking laboratories and evaluating methods of measurement in round-robin tests, T. W. Lashof, Mater. Res. Std. **4,** No. 8, 397–407 (Aug. 1964).

Projection X-ray microscopy of roofing materials, S. B. Newman and S. H. Greenfeld, Mater. Res. Std. **3,** No. 11, 893–898 (Nov. 1963).

Polymorphism of ABO_3-type rare earth borate solid solutions, R. S. Roth, J. L. Waring, and E. M. Levin (Proc. Third Rare Earth Research Conf., Apr. 2–24, 1963), Book, Rare Earth Research, ch on Structure of Rare Earth Compounds, pp. 1030–1055 (Gordon & Breach Science Publishers, Inc., New York, N.Y. 1964).

Polar-cap absorption, D. K. Bailey, Planetary Space Sci. **12,** 495–541 (May 1964).

Polymorphism in isopropyl alcohol, G. S. Ross, H. L. Dixon, L. Frolen, and D. J. Termini, Science **141,** No. 3585, 1043–1044 (Sept. 1963).

Changes in relation between refractive index and Young's modulus as the result of successive heat treatment, E. H. Hamilton, J. Am. Ceram. Soc. **47,** No. 4, 167–170 (Apr. 1964).

Characteristics of programs for KWIC and other computer-produced indexes, W. W. Youden, (Proc. American Documentation Institute Annual Meeting, Oct. 1963) Book, Automation & Scientific Communication, pp. 331–332 (H. T. Luhn, Am. Documentation Inst., 1963).

Plastics, G. M. Klein, The 1964 Americana Annual, p. 5321 Americana Corp., Chicago, Ill.

Oxygen atom reactions with condensed olefins, M. D. Scheer and R. Klein, Science **144,** No. 3623, 1214 (Apr. 1964).

Bound states in a Debye-Hueckel potential, C. R. Smith, Phys. Rev. **134,** A1235–A1237 (June 1964).

Tetragonal phases of the general type $10M_2O_5{\cdot}90M_2O_5$ apparently isostructural with $Ta_2O_5{\cdot}2Nb_2O_5$, J. L. Waring and R. S. Roth, Acta Cryst. **17,** 455–456 (1964).

Ionizing radiation and constitution of the atmosphere, T. E. VanZandt, Proc. URSI XIVth General Assembly, Sept. 1963 Tokyo, Japan **XIII,** 158–164 (1964).

Interpretation of frequency shifts due to electron exchange collisions, P. L. Bender, Phys. Rev. **134,** No. 5A, A1174-A1180 (June 1, 1964).

International Geophysical Calendar for the years of the Quiet Sun 1964–1965, A. H. Shapley and J. V. Lincoln, J. Radio Res. Lab., Japan **10,** 185–192 (Mar. 1963); IUGG Chronicle **50,** 171–174 (July 1963); URSI Inform. Bull. **139,** 64–71 (July–Aug. 1963); IGY Bull. **74,** 15–18 (Aug. 1963); Weatherwise **16,** 160–161 (Aug. 1963); J. Geophys Res. **68,** 5318–5323 (Sept. 1963); Trans. Am. Geophys. Union **44,** 821–824 (Sept. 1963); J. Atmospheric Terrest. Phys. **26,** No. 1, 151–157 (Jan. 1964); Nature **201,** 11–13 (Jan. 4, 1964).

International Geophysical calendar 1963, A. H. Shapley and and J. V. Linclon, IQSY Notes **4,** 34 (Sept. 1963).

Instant color correction, C. S. McCamy, Modern Photo. **28,** No. 1, 66–67 (Jan 1964).

Resurgence of solar and geomagnetic activity in September and October 1963, A. H. Shapley, IQSY Notes **5,** 10 (Dec. 1963).

Diurnal and seasonal variations of the atomosphere near the 100-kilometer level, J. W. Wright, J. Geophys. Res. **69,** 2851–2853 (June 1964).

D-region electron density profiles during auroras, G. M. Lerfald, C. G. Little, and R. Parthasarathy, J. Geophys. Res. **69,** 2857–2860 (June 1964).

Binary error probability due to an adaptable fading model, M. Nesenbergs, IEEE Trans. Comm. Systems **CS12,** No. 1, 64–73 (Mar. 1964).

An X-ray determination of the Debye temperature of silver iodide, G. Burley J. Phys. Chem. Solids **25,** 629 (1964).

Hydrogen atom addition to solid four-carbon olefins, R. Klein and M. D. Scheer, J. Phys. Chem. **67,** 1874–1877 (Sept. 1963).

HF propagation characteristics in equatorial latitudes, A. Barghausen, G. Jacobs, and D. Lillie, Program & Digest of IEEE Trans. Ant. Prop. Intern. Symp. July 9–11, 1963, Boulder, Colo., p. 37042 (IEEE, New York, N.Y. 1963).

A unitary symmetry selection rule and its application to new resonances, C. A. Levinson, H. J. Lipkin, and S. Meshkov, Il Nuovo Cimento **32,** Ser. X, 1376-1379, (1964).

Anomalous transmission of rare gases for electrons of sub-excitation energies, J. A. Simpson, (Proc. Third Intern. Conf. Physics of Electronic and Atomic Collisions, London, England 1963), pp. 128–134 (North Holland Publ. Co., Amsterdam, The Netherlands, 1964).

The guided propagation of ELF and VLF radio waves between the earth and the ionosphere, D. D. Crombie and A. G. Jean, Proc. URSI XIVth General Assembly, Sept, 1963, Tokyo, Japan **XIII,** 195–206 (1964).

The excitation of the 2P state of hydrogen by electrons of near-threshold energy, G. E. Chamberlain, S. J. Smith, and D. W. O. Heddle, Phys. Rev. Letters **12,** No. 23, 647–649 (June 8, 1964).

The zeros of infrapolynomials with prescribed values at given points, J. L. Walsh and O. Shiska, J. Math. Anal. Appl. **7,** No. 2, 176–182 (Oct. 1963).

The crystal structure of 1-ethyldecaborane, A. Perloff, Acta. Cryst. **17,** 332 (1964).

Optically observed inner shell electron excitation in neutral Kr and Xe, K. Codling and R.-P. Madden, Phys. Rev. Letters **12,** No. 4, 106–107 (Jan. 1964).

On the production of the $Z^-(\Omega^-)$ Baryon, H. J. Lipkin, C. A. Levinson, and S. Meshkov, Phys. Letters **7,** No. 2, 159–161 (Nov. 1, 1963).

On the implication of diurnal, seasonal and geographical variations in composition of the high atmosphere from F-region measurements, J. W. Wright, J. Geophys. Res. **68,** No. 19, 5413–1520 (Oct. 1, 1963); Book, Electron Density Distribution in Ionosphere and Exosphere (Proc. of NATO Advances Study Institute, April 17–26, Sheikampen, Norway), pp. 105–115 (North Holland Publ. Co., Amsterdam, The Netherlands, 1963).

On the effect of heterogeneity in molecular weight on the sedimentation equilibrium second virial coefficient of polymers in good solvents, I. H. Billick, J. Phys. Chem. **68,** No. 7, 1798–1800 (July 1964).

A symmetry group containing both the Lorentz group and SU_3 A. O. Barut, Il Nuovo Cimento **32,** 234–236 (Apr. 1964).

The use of dual-polarized broad beam antennas to determine the extraterrestrial intensity of the cosmic radio noise at high frequencies, C. G. Little, G. M. Lerfald, and R. Parthasarathy, Digest of the 1963 IRE Professional Group on Antennas and Proagation, pp. 9–15 (July 1963).

The solid state of rare gases, G. L. Pollack, Rev. Mod. Phys. **36,** No. 3, 748–792 (July 1964).

The present and future of astrophysics and its effects on industry in Colorado, L. M. Branscomb, Book, Colorado and the New Technological Revolution: Proceedings of the University-Industry Liaison Conference 1963, Ed. W. H. Miernyk, pp. 55–64 (Bureau of Economic Research, Institute of Behavioral Science, Univ. of Colorado, Boulder, 1964).

A simplified freezing point apparatus, G. S. Ross and A. R. Glasgow, Jr., Anal. Chem. **36,** No. 3, 700 (Mar. 1964).

Autoionization in helium using a synchrotron light source, R. P. Madden, and K. Codling, Proc. VIth Intern. Conf. of Ionization Phenomena in Gases, Paris, France, 1963, **1,** 139–143 (1963).

Radiowave scattering in the ionosphere, K. L. Bowles, Book, Advances in Electrons and Electron Physics **19,** 55–176 (1964).

Radio, the ionosphere, and IQSY, R. W. Knecht, Proc. URSI XIVth General Assembly, Sept. 1963, Tokyo, Japan **XIII,** 169–180 (1964).

Pseudopentagonal twins in electrodeposited copper dendrites, F. Ogburn, B. Paretzkin, and H. S. Peiser, Acta Cryst. **17,** 774–775 (1964).

Dielectric polarizability of fluid parahydrogen, J. W. Stewart, J. Chem. Phys. **40,** 3297–3306 (June 1964).

Conduction-cooled, concentric sphere glass trap, S. Ruthberg, J. Vacuum **14,** No. 1, 11 (Jan. 1964).

Conductance of potassium chloride in highly purified *n*-methylpropionamide from 20 to 40°, T. B. Hoover, J. Phys. Chem. **68,** No. 14, 876–879 (Apr. 1964).

Field measurements of air infiltration in ten electrically heated houses, C. W. Coblentz, and P. R. Achenbach, ASHRAE J. **5,** No. 7, 69 (July 1963).

Relation of solar active regions at central meridian passage to ionospheric disturbance, C. S. Warwick and J. V. Lincoln, AGARDograph **59,** The Effect of Disturbances of Solar Origin on Communications, Ed. G. J. Gassmann, pp. 229–233 (Pergamon Press Inc., London, England, 1963).

Report of committee E–2 on emission spectroscopy, R. E. Michaelis, Am. Soc. Testing Mater. Proc. 63, 456 (1963).

Evidence for field-aligned ionization irregularities between 400 and 1000 km above the earth surface, T. E. VanZandt, W. Calvert, R. W. Knecht, and G. B. Goe, Book, Space Research, Ed. W. Priester, III, 271–273 (North Holland Publ. Co., Amsterdam, The Netherlands, 1963).

Experimental predictions from unitary symmetry (SU_3), C. A. Levinson, H. V. Lipkin, and S. Meshkev, (Proc. 1963 Intern. Conf. Nucleon Structure, Stanford Univ., Calif.), Book, Nucleon Structure, p. 309 (University Press, Stanford, Calif., Aug. 1963).

First results in NASA topside sounder satellite, R. W. Knecht, S. Russell, and J. E. Jackson, Book, Advances in Astronautical Sciences **11,** 61–85 (Western Periodicals Co., Calif., 1963).

Reaction rates for the formation of He_2^+ and N_e^+, E. C. Beaty and P. L. Patterson, Book, Comptes Rendus de la VI^e Conf. Intern. sur les Phenomenes d'Ionisation dans les Gaz, Ed. P. Hubert and E. Cremieu-Alcan III, pp. 289–293 (S.E.R.M.A. Publ. Co., Paris, France, 1963).

Comparisons of experimental reaction cross sections with various relations obtained from SU_3, S. Meshkov, Proc. Conf. Symmetry Principles at High Energy, Coral Gables, Fla., Jan. 1964, pp. 104–126 (1964).

Very-low-frequency radio waves and the ionosphere, D. D. Crombie, Science **142,** No. 3591, 508–510 (Oct. 25, 1963).

Standardization of dimensions of packages for self-service selling, A. T. McPherson and A. S. Best, THE PACKET, Packaging Professional **2,** No. 3, 4–5 (Packaging Inst., 1964).

Response characteristics of a 4π neutron detector, H. Gerstenberg, Bull. Am. Phys. Soc. **9,** Pt. 2, 421 (Apr. 28, 1964).

Geomagnetic and solar data, J. V. Lincoln, J. Geophys. Res. **69,** No. 13, 2841 (July 1, 1964).

Spectroscopic investigations of fluorescence and chemiluminescence in gases (collection of papers), T. Carrington, Aero-Space Research Laboratory Report No. 64–51 (Mar. 1964).

Fractionation of uranium isotopes and daughter products in weathered granite and uranium-bearing sandstone, Wind River basin region, Wyoming, J. N. Rosholt, E. L. Garner, and W. R. Shields, U.S. Geol. Surv. Prof. Paper 501–B, pp. 884–887 (1964).

Some results of a new method for obtaining ionospheric N(h) profiles with a bearing on the structure of the lower *F* region, J. W. Wright and A. K. Paul, J. Geophys. Res. **68,** No. 19, 5413–5420 (Oct. 1, 1963); Proc. NATA Advanced Study Institute, Skeikampen, Norway (Apr. 17–26, 1963), Book, Electron Density Distribution in the Ionosphere and Exosphere, pp. 105–115 (North Holland Publ. Co., Amsterdam, The Netherlands, 1963).

Error analysis of Miller's recurrence algorithm, R. W. J Olver, Math. Comp. **18,** No. 85, 65–74 (Jan. 1964).

Sr^{87}/Sr^{86} ratios in Hawaiian lavas, P. Lessing and E. J. Catanzaro, J. Geophys. Res. **69,** No. 8, 1599–1601 (Apr. 15, 1964).

Optical investigations of film formation and removal on gold anodes in acidic oxalate solutions, W. E. Reid and J. Kruger, Nature **203,** No. 4943, 402 (July 25, 1964).

The spheroidal method for satellite orbits, J. P. Vinti, Proc. Intern. Symp. Use of Artificial Satellites for Geodesy, pp. 12–16 (North Holland Publ. Co., Amsterdam, The Netherlands, 1963).

Opening angles of electron-positron pairs, H. Olsen, Phys. Rev. **131,** No. 1, 406–415 (July 1, 1963).

Some impulse sparkover voltages for a 200 cm sphere gap, H. N. Cones, IEEE Component Parts Conf. Paper No. CP 63–929 (June 1963).

Determination of optical thickness gradients from a far distance, J. R. Meyer-Arendt, R. B. Herrick, and C. B. Emmanuel, J. Opt. Soc. Am. **53,** 1344 (1963).

Solar particles and interplanetary fields, C. S. Warwick, Book, Advances in the Astronautical Sciences **13,** 666–681 (Western Periodicals, Calif., 1963).

Vaporization of uranium monophosphide, K. A. Gingerick, P. K. Lee, and J. E. Efimenko, Nature **200,** No. 4908, 774–776 (1963).

A radio-meteorological study, B. R. Bean, E. J. Dutton, V. R. Frank, J. A. Lane, and W. B. Sweezy, Program and Digest 1963 IEE Prof. Group Antennas and Propagation Symp. Space Telecommunications, July 9–11, 1963, Boulder, Colo., pp. 56–60 (1963).

The interaction of 350 keV polarized neutrons with oriented Ho^{165} nuclei, H. Marshak, R. Wagner, P. P. Miller, and T. Tamura, Physics Letters **10,** No. 3, 316 (June 15, 1964).

Systematic atmospheric refraction errors of baseline type radio tracking systems and methods of their correction, G. D. Thayer and B. R. Bean, Proc. First Space Congress, Cocoa Beach, Florida (Apr. 1964).

Error bounds for asymptotic expansions in turning-point problems, F. W. J. Olver, Soc. Ind. Appl. Math. **1,** No. 1, 200–214 (Mar. 1964).

Summary of session I and II of the symposium on X-ray and electron probe analysis, R. E. Michaelis, ASTM Spec. Tech. Publ. No. 349 (Dec. 1963).

Prebunching in electron linacs, J. E. Leiss, Proc. Conf. Proton Linear Accelerators, Yale Univ., New Haven, Conn., pp. 267–273 (Oct. 1963).

Phase diagrams for ceramists, Book, E. M. Levin, C. R. Robbins, and H. F. McMurdie, American Ceramic Society, Inc., Columbus, Ohio (1964).

Transverse propagation of electromagnetic waves in a cylindrically stratified plasma, J. R. Wait, Proc. Radio Physics Symp., University of California, Los Angeles, Aug. 7–9, 1963, Ed. J. Brandstatter (Holden-Day, Inc., San Francisco, Calif., 1964).

Variations in phase path of man-made one-hop whistler mode signals at 18.6 kilocycles per second, D. D. Crombie, F. A. McNeill, and G. M. Allcock, J. Geophys. Res. **68,** No. 23, 6229–6235 (Dec. 1, 1963).

Recently discovered autoionizing states of krypton and xenon in the λ 380–600A, R. P. Madden and K. Codling, J. Opt. Soc. Am. **54,** No. 2, 268–269 (Feb. 1964).

Fluorometric demonstration of tryptophan in dentin and bone protein, K. C Hoerman and S. A. Mancewicz, J. Dental Res. **43,** No. 2, 276–280 (Mar.–Apr. 1964).

The calibration of inductive voltage dividers and analysis of their operational characteristics, T. L. Zapf, ISA Trans. **2,** No. 3, 195–200 (July 1963).

Nighttime variations of *F*-region electron density profiles at Puerto Rico, T. Shimazaki, J. Geophys. Res. **69,** No. 13, 2781–2797 (July 1, 1964).

Obscurities of oscillator noise, L. Fey, W. R. Atkinson, and J. Newman, Proc. IEEE Letter **52,** 104–105 (Jan. 1964).

The *F*-region seasonal anomaly, J. W. Wright, J. Geophys. Res. **68,** No. 14, 4379–4381 (July 15, 1963).

Coherent Raman effect in the off-axis Raman resonator, H. Takuma and D. A. Jennings, Appl. Phys. Letters **4,** No. 11, 185–186 (June 1964).

Effects of composition and irradiation on the glass transition temperature of methyl methacrylate-styrene copolymers, M. S. Parker, V. J. Krasnansky, and B. G. Acchammer, J. Appl. Polymer Sci. **8,** 1825–1838 (1964).

"U-spin equalities" and octet symmetry breaking, S. Meshkov, G. A. Snow, and G. B. Yodh, Phys. Rev. Letters **13,** No. 6, 212–217 (Aug. 10, 1964).

The scope of electrochemistry, W. J. Hamer, J. Electrochem. Soc. **110,** No. 6, 115C (June 1963).

Report on sugars and sugar products, E. J. McDonalds, J. Assoc. Official Agri. Chem. **46,** 35 (1963).

Thermal conductivity and viscosity of simple fluids, J. V. Sengers, Am. Chem. Soc. **9,** No. 4, C–57–C–70 (Sept. 1964).

Some recent developments in noble metal thermocouples, L. O. Olsen, Am. Soc. Auto. Engrs. Paper No. 750A, p. 10 (Sept. 1963).

Minutes of the meeting at the Ohio State University, Columbus, Ohio, of the Triple Commission for Spectroscopy, June 13, 1963, C. E. Moore, J. Opt. Soc. Am. **54,** No. 3, 425–432 (Mar. 1964).

High frequency microvolt measurements, F. X. Ries, ISA Preprint, pp. 37.2.63–1—37.2.63–5 (Sept. 1963).

Comparison of a new SU_3 prediction with experiment, S. Meshkov, G. A. Snow, and G. B. Yodh, Phys. Rev. Letters **12,** No. 3, 87–92 (Jan. 20, 1964).

Measurement of photochemical degradation in certain plastics by color reactions with phenylenediamines, V. E. Gray and J. R. Wright, J. Appl. Polymer Sci. **8,** No. 4, 1505–1519 (1964).

On Rayleigh's non-linear vibration equation, A. Ghaffari, Proc. Intern. Symp. Non-Linear Vibration II, 130–133 (Sept. 1961).

An unmodulated twin channel microwave attenuation measurement system, D. H. Russell, ISA Preprint, pp. 37.3.63–1—37.3.63–17 (Sept. 1963).

Beam loading and beam blowup in electron linacs, J. E. Leiss, Proc. Conf. Proton Linear Accelerators, Yale Univ., New Haven, Conn., pp. 74–95 (Oct. 1963).

Residual range and range rate errors due to the troposphere, E. C. Barrows, Proc. Conf. Tropospheric Refraction (Dec. 1963).

Tropospheric refraction and attenuation of radio waves, B. R. Bean, Book, Advances of Radio Research, pp. 53–155 (Academic Press Inc., New York, N.Y., June 1964).

Kikuchi pattern from a silicon wedge, H. A. Fowler, Acta Cryst. **17,** No. 7, 869–871 (July 1964).

On line data handling system for the National Bureau of Standards LINAC, J. Leiss, J. Broberg, R. Schrack, and J. M. Wyckoff, IEEE Trans. Nuclear Sci. **NS–11,** No. 3, 331–337 (June 1964).

Long-term characteristic for air-ground propagation in band nine, R. S. Kirby, Program and Digest 1963 IEEE Prof. Group Antennas and Propagation Symp. Space Telecommunications, July 9–11, 1963, Boulder, Colo., pp. 43–47 (1963).

Measurement of effective temperatures of microwave noise sources, J. S. Wells, W. C. Daywitt, and C. K. S. Miller, IEEE Trans. Instr. Meas. **IM–13,** No. 1,17–28 (Mar. 1964).

The turbulent characteristics of the radio refractive index near the ground, B. R. Bean and R. E. McGavin, Program and Digest 1963 IEE Prof. Group Antennas and Propagation Symp. Space Telecommunications, July 9–11, 1963, Boulder, Colo., pp. 60–64 (1963).

Use of high-strength ceramics in vibration transducers, E. Jones, J. Acoust. Soc. Am. **36,** No. 6, 1215–1216 (June 1964).

Phase instability in a tropospheric relay link, E. C. Barrows, Program and Digest 1963 IEEE Prof. Group. Antennas and Propagation Symp. Space Telecommunications, July 9–11, 1963, Boulder, Colo., pp. 52–55 (1963).

The radio thermal noise properties of the lower atmosphere, B. R. Bean, Program and Digest 1963 IEEE Prof. Group. Antennas and Propagation Symp. Space Telecommunications, July 9–11, 1963, Boulder, Colo., pp. 30–31 (1963).

On the identity of three generalized master equations, R. Zwanzig, Physica **30,** 1109–1123 (1964).

The oxide films formed on copper single crystal surfaces in water. III. Effect of light, J. Kruger and J. P. Calvert, J. Electrochem. Soc. **III,** No. 9, 1038–1041 (Sept. 1964).

**Publications for which a price is indicated are available by purchase from the Superintendent of Documents, U.S. Government Printing Office, Washington, D.C., 20402 (foreign postage, one-fourth additional). Reprints from outside journals and the NBS Journal of Research may often be obtained directly from the authors.*

U.S. GOVERNMENT PRINTING OFFICE:1965

UNIVERSITY MICROFILMS INC
EDITORIAL DEPARTMENT
313 NORTH FIRST ST
ANN ARBOR MICH

UNITED STATES
GOVERNMENT PRINTING OFFICE
DIVISION OF PUBLIC DOCUMENTS
WASHINGTON, D.C. 20402

OFFICIAL BUSINESS

PENALTY FOR PRIVATE USE TO AVOID PAYMENT OF POSTAGE, $300 (GPO)

JOURNAL OF RESEARCH of the National Bureau of Standards — Vol. 69C, No. 1 — January–March 1965
C. Engineering and Instrumentation

Contents

	Page
Two picnometers of increased convenience and precision. Arnold Johnson.	1
Construction of a Michelson interferometer for Fourier spectroscopy. Howard N. Rundle.	5
The National Bureau of Standards gas thermometer II. Measurement of capacitance to a grounded surface with a transformer ratio-arm bridge. L. A. Guildner and R. E. Edsinger.	13
An adiabatic calorimeter for the range, 10 to 360 °K. K. F. Sterrett, D. H. Blackburn, A. B. Bestul, S. S. Chang, and J. Horman.	19
A rugged null-type pressure transducer of high reproducibility for accurate gas phase PVT measurements. Meyer Waxman and William T. Chen.	27
Detection and damping of thermal-acoustic oscillations in low-temperature measurements. David A. Ditmars and George T. Furukawa.	35
NBS free-air chamber for measurement of 10 to 60 kV x rays. P. J. Lamperti and H. O. Wyckoff.	39
A compensated solenoid giving a uniform magnetic field over a large volume. Chester Snow and Raymond L. Driscoll.	49
Evaluation of a microwave phase measurement system. Doyle A. Ellerbruch.	55
Polarographic analysis of titantium (IV)—EDTA complex: application to paint pigments. Harvey W. Berger and Barry C. Cadoff.	67
Soil resistivity as related to underground corrosion and cathodic protection. W. J. Schwerdtfeger.	71
Publications of the National Bureau of Standards.	79

Library of Congress Catalog Card Number: 62–3900

For sale by the Superintendent of Documents, U.S. Government Printing Office, Washington, D.C., 20402. Price 75 cents (single copy). Subscription price: $2.25 a year; 50 cents additional for foreign mailing.
UNITED STATES GOVERNMENT PRINTING OFFICE, WASHINGTON : 1965